



HAL
open science

Neurogenesis regulation and homeostasis: role of Pax6 signalling and mathematical modelling

Yi Cui

► **To cite this version:**

Yi Cui. Neurogenesis regulation and homeostasis: role of Pax6 signalling and mathematical modelling. Neurons and Cognition [q-bio.NC]. Sorbonne Université, 2018. English. NNT : 2018SORUS309 . tel-02864832

HAL Id: tel-02864832

<https://theses.hal.science/tel-02864832>

Submitted on 11 Jun 2020

HAL is a multi-disciplinary open access archive for the deposit and dissemination of scientific research documents, whether they are published or not. The documents may come from teaching and research institutions in France or abroad, or from public or private research centers.

L'archive ouverte pluridisciplinaire **HAL**, est destinée au dépôt et à la diffusion de documents scientifiques de niveau recherche, publiés ou non, émanant des établissements d'enseignement et de recherche français ou étrangers, des laboratoires publics ou privés.



THÈSE DE DOCTORAT DE L'UNIVERSITÉ PARIS VI
ÉCOLE DOCTORALE CERVEAU-COGNITION-COMPORTEMENT

**Neurogenesis regulation and homeostasis:
role of Pax6 signalling and mathematical modelling**

Présentée par CUI Yi

Soutenance le 21 Décembre 2018

Composition du jury

Dr. Hugues Berry	Rapporteur
Dr. Frédéric Causeret	Rapporteur
Dr. Sylvie Schneider-Maunoury	Examinatrice
Dr. Fiona Francis	Examinatrice
Pr. Philip Kumar Maini	Examineur
Dr. Alessandra Pierani	Examinatrice
Pr. Alain Prochiantz	Directeur de thèse
Dr. Jonathan Touboul	Directeur de these

Summary

The cerebral cortex is the largest region of the cerebrum in the mammalian brain. It controls higher-order brain functions such as sensory perception, cognition, motor commands and language. Thus, a tight control of the organization of the cerebral cortex is vital for most species. Understanding the regulatory mechanisms supporting these processes is an important endeavor in developmental biology. Here, we focused on the processes taking place during neurogenesis of the cerebral cortex, and took a multi-disciplinary approach combining biological experiments and mathematical models.

For the mathematical modelling of neurogenesis, we start with a model describing the probability of progenitor divisions sequence as a function of time during the neurogenesis. It is parsimonious, but sufficient to explain and draw predictions on the phenotype observed in *Lhx2* conditional knock-out mutant that precocious neurogenesis affected cortical surface and thickness. Moving one step further, we relaxed the constraints prescribing the timing of division probability in the model, and designed a model with intrinsic clocks whereby the progenitors undergo a sequence of divisions as they progress along a fixed profile, much like the movement of a particle descending a tilted potential with wells, in response to two parameters: ‘force’ and ‘noise’. Thus, the switches from different type of divisions are modeled as an intrinsic property, so that the timing is generated by the cells themselves. The new model not only can explain the microcephaly, but also explain the ‘force’ and ‘noise’ together influence cortex thickness and neuron layer proportion in different cortical areas, especially in detail the timing of piriform cortex and entorhinal cortex generation.

The first part of the thesis presents our works in this domain, and is organized as follows. In Chapter I, we introduce the basic notions of the cerebral cortex organization and the characteristics of neocortex (and neocortical different functional areas), piriform cortex and entorhinal cortex. We discuss in more detail dorsal telencephalon neural progenitor proliferation and differentiation to produce neurons of the pallium. In Chapter II, the first model and the application of explain *Lhx2* conditional knock-out mice microcephaly phenotype is explained in the publication I. Then we describe the second model and its application.

The second topic we studied is how the brain compensates cell death to maintain homeostasis during development. In two mutant mouse models with neuronal death between embryonic days 11 to 14, different compensation phenotypes are observed: in one mutant, around 30% reduced volume is observed but deep layer and upper layer neuron proportions remain untouched. In the other mutant, normal neuron number per unit was kept with abnormal neuron layer proportions, 30% reduction of deep layer neurons and 20% increase of upper layer neurons. Here, we develop a unified mathematical model that reconciles those two opposite observations. This model is based on two fundamental compensation mechanisms, each supported by biological evidence, and that can, alone, explain both phenotypes: 1) an increase in the probability and maximal number of intermediate progenitor proliferative divisions; 2) a delay in the switching time between upper- and deep-layer neurons generation by a maximum of 24h. In the last section of Chapter I, we introduce the different progenitor types, types of division of progenitors and their cell cycle duration. In the introduction part of Chapter III, we discuss a selection of papers on neuronal death during development and the possible biological regulatory mechanism of neuronal homeostasis after cell death. In the publication II, we applied the compensation model to one of the cell death mutant mice model showing that increased intermediate proliferation is a powerful compensation mechanism. Then we adapted the model and added the second mechanism for a comprehensive understanding of homeostasis and compensation of neuron death during brain development.

The third topic we studied is the role of extracellular Pax6 on neurogenesis. Pax6, as classical transcriptional factor, is one of the master regulators of neuronal progenitor proliferative division and differentiation. Meanwhile, with its homeodomain, it can transfer between cells and exert non-cell autonomous activities. We showed that an overexpression of extracellular Pax6 at Cajal-Retzius neurons source inhibits their generation. In contrast, blocking extracellular Pax6 by electroporation switches pyramidal neuron progenitors generating Cajal-Retzius neurons ectopically in the dorsal region. Similarly blocking extracellular Pax6 by genetic approach at cortical hem induces Cajal-Retzius neurons generation in ventricular zone of neighboring region. This ectopic induction of Cajal-Retzius neurons is timing- and region-specific. Basic mechanisms reported in the literature on the generation and migration of

Cajal-Retzius neurons and their role in cortical development is summarized in Chapter I. The role of Pax6 in dorsal telencephalic development is described in the neocortical regionalization section of Chapter I and detailed with extracellular function of homeoproteins in the introduction part in Chapter IV. The result section in Chapter IV is the topic of a publication in preparation on the role of extracellular Pax6 on neurogenesis.

Acknowledgements

I would like to thank the honored members of my thesis committee for having accepted to be part of this board of examiners, especially Dr. Frédéric Causeret and Dr. Hugues Berry, for taking time to read and evaluate my thesis.

To Pr. Alain Prochiantz and Dr. Jonathan Touboul for starting this collaboration and having given me the opportunity to work on these exciting projects. Also for their patient supervision, and for encouraging me during the research. Their keen and vigorous academic observations have helped me throughout last past four years and have provided a thread for my future.

To Dr. Alessandra Pierani for hosting me to perform the experiments and having all the fruitful scientific discussions and encourage.

To Dr. Shen-Ju Chou for sharing the experiment results and ideas to start the modelling project.

To all the people in the lab I have closely worked with: Dr. Hadhemi Kaddour for working together on Pax6 project. Dr. Betty Freret-Hodara for working together on compensation of neuron loss. Dr. Yoko Arai for tutoring and help with experiments. Dr. Iffat Sumia for being my best lunch friend.

To all current and former members of the Prochiantz, Touboul and Pierani team, for making work in the lab a real pleasure.

To my parents and Xu, for their love and permanent support.

Chapter I: Introduction.....	1
1. Cerebral cortex organization	1
1.1 Neocortex	2
1.2 Piriform cortex.....	4
1.3 Entorhinal cortex.....	5
2. Neocortical arealization.....	5
3. Cajal-Retzius cell generation and migration and role in cortical development	8
3.1 Cajal-Retzius cell generation and migration	8
3.2 Role of Cajal-Retzius cell	10
4. Development of the pallium	13
4.1 Origin of excitatory neurons.....	13
4.2 Cortical progenitors cell cycle duration.....	16
5. Mathematical modelling of brain development.....	20
Chapter II: Modeling the neurogenesis	22
1. Results/Publications.....	22
1.1 Mathematical of neurogenesis based on progenitor divisions	22
1.2 Publication I.....	23
1.3 Theoretical calculation of the model.....	29
1.4 Mathematical of neurogenesis based on progenitor potential drop.....	49
2. Discussion	57
Chapter III: Modeling the cell death and neurogenesis homeostasis	60
1. Introduction.....	60
1.1 Cell death during development.....	60
1.2 Regulation of neuronal homeostasis after cell death by feedback from post-mitotic neurons	62
1.3 Several predictions of mathematical model of compensation	63
2. Methods	64
3. Results	68
3.1 Publication II.....	68
3.2 Basic response mechanisms to cell death	86
3.3 Compensation breakdown in mutant models	88
3.4 Homeostasis and compensation of mild to severe neuronal death.....	90

3.5	Programmed and abnormal cell death, homeostasis and its breakdown.....	93
4.	Discussion	96
4.1	Possible biological compensation mechanisms	96
4.2	A universal mathematical model of compensation	97
4.3	Compensation capacity of the model.....	97
4.4	Prenatal ethanol exposure induced neuron loss triggers both of the compensation mechanisms	98
Chapter IV: Role of homeoprotein Pax6 diffusion in cortical development.....		100
1.	Introduction.....	100
1.1	Role of homeoproteins during development.....	100
1.2	Homeoprotein transfer	102
1.3	Role of Pax6 during cortical development.....	103
2.	Materials & Methods.....	105
3.	Results	108
3.1	Neutralizing extracellular Pax6 induces ectopic generation of neurons	108
3.2	Induction of CR neurons generation by blocking ePax6 is time and region specific.	111
4.	Discussion	115
Bibliography		117

Chapter I: Introduction

The cerebral cortex is the largest region of the cerebrum in the mammalian brain. It controls higher-order brain functions such as sensory perception, cognition, motor commands and language. The size of cerebral cortex has undergone a strong expansion during evolution. The mammalian cerebral cortex comprises the neocortex, the hippocampus and the piriform cortex. Both the hippocampus and the piriform cortex conserve common characteristics with the three-layered general cortex of reptiles, while the neocortex is organized in six layers. The neocortex is composed of with highly connected excitatory (~80%) and inhibitory (~20%) neurons.

Neurogenesis is the process during development by which neural stem cells generate neurons of the central nervous system, followed by migration of neurons, formation of dendrites and axons and synaptogenesis. After neurogenesis, the stem cells that generated the neurons also participate in the generation of glial cells (astrocytes and oligodendrocytes) during a phase called gliogenesis.

The first neurons to be generated during cortical development are the Cajal-Retzius cells (CRs) and the subplate cells that form the preplate (Allendoerfer & Shatz, 1994; Luskin & Shatz, 1985). The preplate is split into superficial marginal zone and the deeper subplate by the excitatory pyramidal neurons generated from pallium progenitors forming the cortical plate (CP) in between. The CP of the neocortex is composed of six layers of neurons that migrate in an inside-out fashion, the first neurons generated are positioned in the deepest layer of CP and the last in the most superficial (Berry, Rogers, & Eayrs, 1964; Rakic, 1974). Inhibitory GABAergic neurons are generated by the sub-pallium progenitors and by tangential migration inserted into the pallium (Anderson, Eisenstat, Shi, & Rubenstein, 1997; Parnavelas, Barfield, Franke, & Luskin, 1991; Rakic, 1988).

1. Cerebral cortex organization

The structure of the cerebral cortex is not uniform throughout. Actually, an almost monotonic variation of its phenotype is immediately apparent when considering brain

atlases. In particular, substantial variation of thickness can be observed. According to cytoarchitectural differences in layer thickness and cell density, at the beginning of the 20th century, the pioneer histological work of Brodmann identified in the cortex 52 cortical areas (figure 1A) (Brodmann, 1909). Up to a two-fold expansion was observed between the thinnest of cortical regions Brodmann's area 3 on the posterior bank of the central sulcus (with an average thickness of less than 2 mm) and the thickest regions Brodmann's area 4 on the anterior bank (4mm) (Fischl & Dale, 2000). The relationship between cortical areas and cortical function was deduced from patients who lost a certain cognitive ability after a brain injury. Broca discovered that patients lost speaking ability due to single cortical region damage, demonstrating that this region was responsible for language processing (Broca, 1861). This theory was then confirmed by Penfield's electrical stimulation and ablation work. Each area is involved in the processing of specific information: motor, sensory or cognitive (Penfield, 1961).

1.1 Neocortex

The neocortex is composed of neurons and glial cells. It is organized in six layers segregated principally by cell type and neuronal connections. On several aspects the overall structure of the neocortex can be found relatively uniform. However, finer investigation reveals many exceptions to this uniformity, both globally and locally. Indeed, there is an important variation in thickness of neuron layers, along a gradient from a thick rostro-lateral region to a thinner caudo-medial region. At a more local scale, one can find also rapid variation in brain's organization; in primate for example, there is a sharp transition of cytoarchitecture between the area 17 and area 18 (primary and secondary visual areas): the layer 4 in area 17 is much thicker and complex compared to the same layer in area 18 (figure 1B) (O'Leary & Nakagawa, 2002).

Neurons in the neocortex are connected in an intricate network with subcortical structures (Mayhew, 1991). Connections established by pyramidal neurons can be divided into two groups: intracortical (commissural and associative) projections and corticofugal (subcortical and subcerebral) projections neurons (figure 1C). Neurons located in the superficial layers (2,3 and 4) establish mainly intracortical connections.

They can extend their axons to the opposite hemisphere, thus forming the contralateral connections crucial for synchronization and integration of bilateral connections. They also form ipsilateral connections with other neurons in the same hemisphere. Ipsilateral connections are also observable within the same hemisphere. This is the case of the pyramidal neurons of the layer 4 which project their axons over short distances (Migliore & Shepherd, 2005; Molyneaux, Arlotta, Menezes, & Macklis, 2007). The neurons of the deep layers (5 and 6) send their axons to non-cortical brain areas, thus forming corticofugal connections. Layer 6 neurons will establish corticothalamic connections while those in the layer 5 will mainly send their axons long distances out of the cortex to different targets such as the brainstem and spinal cord creating subcerebral connections (S. Lodato, Shetty, & Arlotta, 2015b) (figure 1C). The cytoarchitecture of the different cortical areas serves specific functions. For example, layer 4, which is the primary target for thalamic sensory afferents, is much more developed in primary sensory areas than in motor areas. The layer 5, composed of pyramidal neurons that send their axons to the level of subcortical structures, is considerably developed in the motor region. This specificity is established at early stages of cortical development but will be refined with individual experience during the postnatal period via afferents joining the cortex (Alfano, Magrinelli, Harb, Hevner, & Studer, 2014).

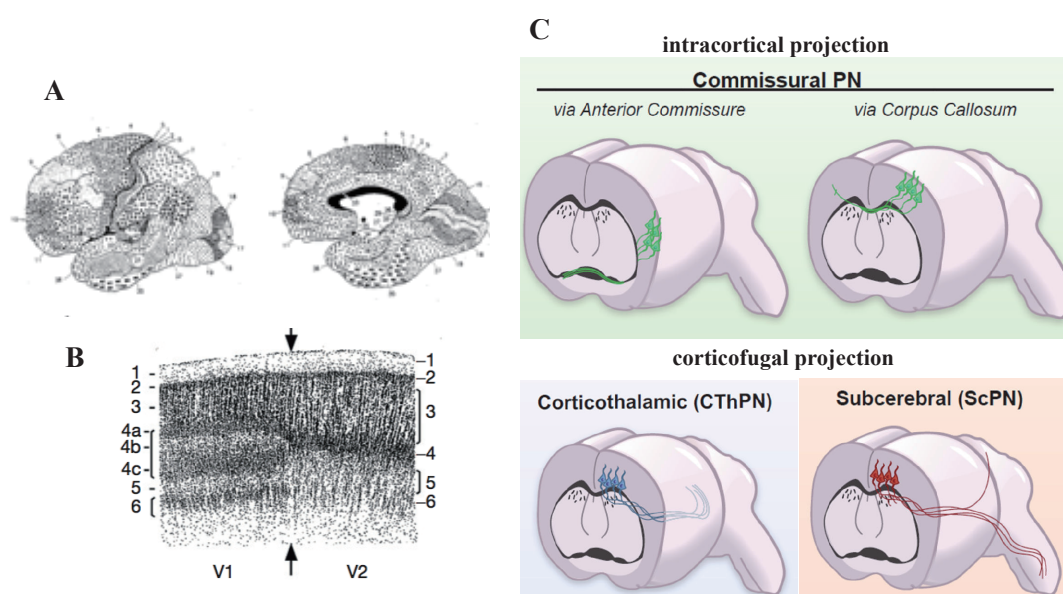


Figure 1. Regionalization in cortex and diversity of cortical projection neurons and

their connections. (A) Map of the 52 cortical areas in humans according to Brodmann. (B) The sharp transition of cytoarchitecture between the area 17 and area 18 primary and secondary visual areas in primate. The layer 4 in area 17 is much thicker and complex than in area 18. (C) The neurons of the superficial layers (2, 3 and 4) establish intracortical connections. Neurons can project on the contralateral hemisphere via commissural connections or in the same hemisphere via associative connections. The neurons of the deep layers (5 and 6) establish corticofugal connections which can be towards the thalamus: corticothalamic connections or towards the brainstem and the spinal cord in particular: subcerebral connections. Adapted from M. A. Lodato et al., 2015a; O'Leary & Nakagawa, 2002.

1.2 Piriform cortex

The piriform cortex is located in the ventrolateral part of the telencephalon. Its function is to contribute to odor coding and representation. Anatomically, it is thinner than the neocortex (Srinivasan & Stevens, 2017), and presents a simpler layer structure: it is composed of three layers, a characteristic feature of allocortical structures. The most superficial layer of the piriform cortex is the lateral olfactory tract (LOT) formed by the axons receiving the input from the olfactory bulb. Underneath the LOT cells layer, layers 1a and 1b are both primarily neuropil with axodendritic synapses from the LOT and cortico-cortical association axons respectively (Haberly, Hansen, Feig, & Presto, 1987). Neurons in layer 2 are divided into 2 subtypes: semilunar and superficial pyramidal cell forming a compact band of projection neurons. The deepest layer III includes a low density of so-called deep pyramidal cells. Inhibitory neurons are distributed throughout all three layers (Aboitiz, Montiel, Morales, & Concha, 2002; Shipley & Ennis, 1996).

Moreover, unlike the “inside-out” pyramidal neuron generation order in the neocortex, the relation between order of excitatory neuron generation and layer distribution is more complicated in piriform cortex. The neurogenesis duration of the piriform cortex is premature and abbreviated compared with the neocortex, starting from E10 and ending around E15. It has been demonstrated that the deeper layer 3 neurons are generated before layer 2, showing a temporal canonical “inside-out” pattern. However, within the piriform layer 2, neurons in the superficial layer 2a are formed earlier than

deep layer 2b, exhibiting an inverse “outside-in” temporal neurogenic pattern. Due to the shorter duration of neurogenesis time window in the piriform cortex, neurons born at the same time are less well separated between layers in the piriform cortex compared with neocortex (Martin-Lopez, Ishiguro, & Greer, 2017). Neuron layer markers expressed in the neocortex, including *Cux1*, *Barhl1*, *Tle4*, *Foxp2* and *Fezf2*, are also expressed in piriform cortex, but in different layer organization (Diodato et al., 2016).

1.3 Entorhinal cortex

The entorhinal cortex is an area of the brain located at the caudal end of the temporal lobe in rodents. It functions as a hub in a widespread network for memory, navigation and the perception of time (Hafting, Fyhn, Molden, Moser, & Moser, 2005; Tsao et al., 2018). Entorhinal cortex principal cells divide into pyramidal neurons (mostly calbindin positive) and dentate gyrus-projecting stellate cells (Tang et al., 2014). Stellate cells are generated first starting before E11 and pyramidal cells start appearing from E13. At E16, more than 90% of new born neurons are pyramidal cells. Stellate cells exhibit an orderly birthdate-dependent distribution along the dorso-ventral axis. Early born stellate cells are prevailing on the dorsal regions, whereas later born neurons were found at progressively more ventral positions. Similar to the case of the piriform cortex, the canonical inside-out generation of neuron is not observed in the piriform cortex: the pyramidal cells are distributed randomly in the layers irrespective of their birthdate (Donato, Jacobsen, Moser, & Moser, 2017).

2. Neocortical arealization

The neocortex has four primary areas. Three of those are sensory: the primary visual (V1), somatosensory (S1), and auditory (A1) cortices, respectively processing information received from the retina, body, and cochlea. The fourth primary area of the neocortex is the motor (M1) area, which controls voluntary movement of body parts (figure 2). In the adult, the transition from one neocortical area to another is typically abrupt, with borders that can be sharply defined by area differences in

architecture, and in some instances by the distributions of projection neurons, input projections, or gene expression patterns. For example, SVZ progenitors proliferate more in V1 resulting a major increase in the numbers of superficial layer neurons compared to adjacent higher order visual areas (Dehay & Kennedy, 2007). In the primate brain, between these primary areas, there appears an increasing number of higher level areas (O'Leary & Nakagawa, 2002; Sur & Rubenstein, 2005).

The specification and differentiation of neocortical areas are controlled by an interplay between intrinsic mechanisms and extrinsic mechanisms (figure 2). Intrinsic mechanisms correspond to the specific combination and concentration of transcription factors expressed in the associated cortical progenitors. Important evidence demonstrated the significance of the intrinsic genetic mechanisms regulating arealization, chiefly based on the finding that many of the differential transcription factor expression patterns appear before the thalamocortical axons input reach the cortex. Cell fate is indeed determined at very early stages in progenitors along the dorsoventral and anteroposterior axis (Campbell, 2003; Jessell, 2000; Miyashita-Lin, Hevner, Wassarman, Martinez, & Rubenstein, 1999; Schuurmans & Guillemot, 2002). Patterning centers, cortical hem (between cortical and choroidal fields), septum (at the rostromedial pole of the telencephalon) and antihem (at the pallial–subpallial boundary) lie at the borders of the telencephalon and participate in the arealization of the cortex. The morphogens and signaling molecules secreted from patterning centers and diffused on the developing cortex induced the graded expression of these transcription factors in cortical progenitors, such as *Emx2*, *Pax6*, *COUP-TFI*, and *Sp8* (figure 2). These transcription factors were shown to have direct and significant functions in arealization. The combination of the expression level of these different transcription factors provide positional information for the cortical progenitors to form different cortical areas (Arai & Pierani, 2014; Borello & Pierani, 2010; O'Leary & Sahara, 2008).

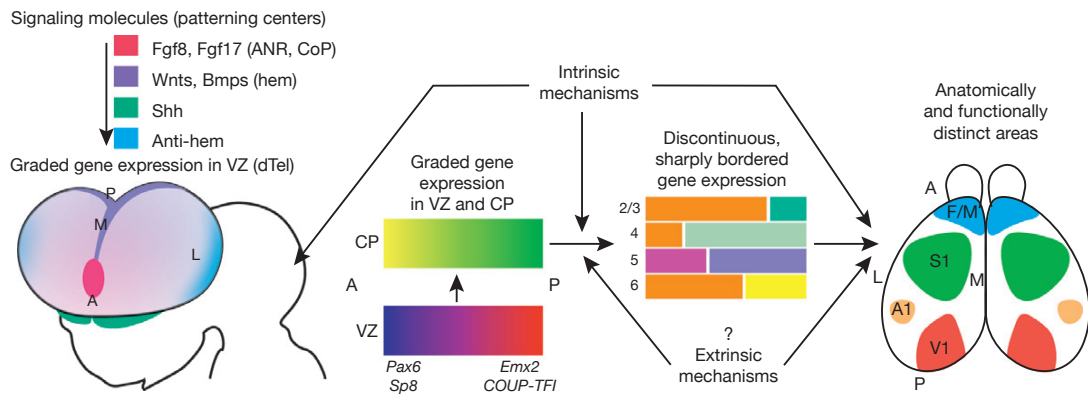


Figure 2. Patterning centers and graded transcription factors drive arealization of the neocortex. The initial, tangential gradients of transcription factors in the VZ are established by morphogens secreted from telencephalic patterning centers. The graded expression of certain TFs, such as Pax6, Emx2, COUP-TFI, and Sp8, imparts positional or area identities to cortical progenitors, which is transmitted to their neuronal progeny that form the CP. The CP also initially exhibits gradients of gene expression that are gradually converted to distinct patterns with sharp borders. Coincident with this process, distinct cortical layers (2–6), and the anatomically and functionally distinct areas seen in the adult, differentiate from the CP. Genes that are differentially expressed across the cortex are often expressed in different patterns in different layers, suggesting that area-specific regulation of such genes is modulated by layer-specific properties, and questions the definition of area identity. Adapted from O’Leary & Nakagawa, 2002.

Extrinsic mechanisms are just as crucial as the intrinsic. Arealization happens when signals from subcortical structures thalamocortical axons reach the cortex. The study of how extrinsic mechanisms influence cortical arealization dates back to the discovery of the emergence of the barrel field in the somatosensory cortex by in 1973. This indeed led the authors to later evidence that thalamocortical axons control the formation of the barrel field, and that the loss of a vibrissa results in the reorganization of the barrel field (Van der Loos & Woolsey, 1973; Woolsey & Wann, 1976).

3. Cajal-Retzius cell generation and migration and role in cortical development

3.1 Cajal-Retzius cell generation and migration

CRs are the first post-mitotic neurons migrating into the developing cortex between E10.5 and E12.5 in mice. They participate in the formation of the pre-plate and are located in the marginal zone during cortical development. It was first suggested that these neurons come from the pallial VZ, since they express pallial markers such as *Tbr2* (Hevner, Neogi, Englund, Daza, & Fink, 2003). However, various laboratories have shown that CRs are generated from multiple sources at signaling centers and migrate into the developing cortex (figure 3B). Using tracing and electroporation methods, Takiguchi-Hayashi and colleagues have showed that the reelin positive CRs originated at the cortical hem and joined the developing cortex by tangential migration in order to cover its entirety (Takiguchi-Hayashi et al., 2004). Since then, it has been reported that between 60% and 70% of CRs come from this region. One year after the publication of these results, Bielle in Pierani's team identified two other sources at the sulptum and pallial-subpallial border (PSB) as sources of CRs from *Dbx1*-expressing progenitors, using genetic tracing and ablation experiments in mice (figure 3A) (Bielle et al., 2005). Various proteins have been identified expressing in CRs and the generation of several transgenic lines gave the possibility of permanent tracing of the CRs migration. The transcription factor p73 was found in particular at the level of the hem in the mouse at E12.5. Tissir and colleagues generated the knock-in line *DeltaNp73Cre* to follow the CRs permanently until postnatal stage. This mouse lines allowed observing a distribution of CRs of the hem in the whole cortex: neocortex, median cortex and also in the hippocampus (Tissir et al., 2009).

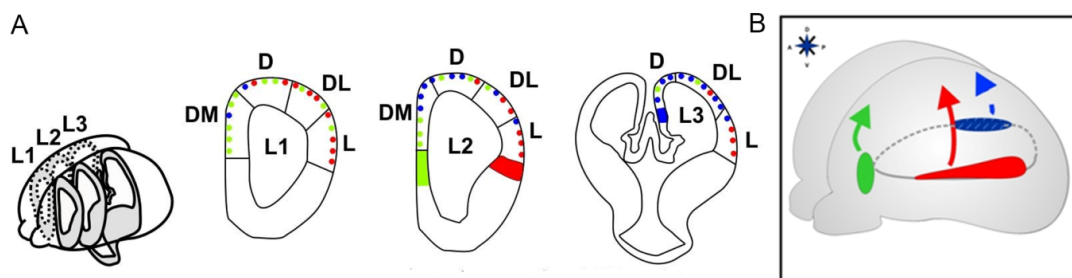


Figure 3. Sources of CRs in mice. (A) Schematic representation of the three CRs sources at coronal slices on the rostro-caudal axis (L1, L2, L3) in E 11.5 mice. The septum (in green) is found at the pallial-subpallial rostro-medial border (L1 section), the PSB (red) is found at the pallial-subpallial rostro-lateral border (L1 section), the hem (blue) is found at the pallial-subpallial medio-caudal border (L3 section). The color points correspond to the CRs of the different sources distributed in the dorsal cortex. DM: dorsomedian, D: dorsal, DL: dorso-lateral and L: lateral. (B) Side view of an E12.5 mouse brain with the three CRs sources represented by the same color code as in (A). Adapted from Griveau et al., 2010.

The migration of a CR cell depends on various elements: its origin, environment and its interactions with other CR cells. The meninges, especially the pia, are in contact with the CRs during migration. The pia mater is composed of blood vessels, meningeal cells and fibroblasts with a high secretory activity. A secreted factor in the extracellular matrix of meninges plays an important role in the correct positioning of CRs. In the study of chemokine CXCL12, a protein highly secreted by the meninges, and its receptors expressed by CRs: CXCR4 and CXCR7, researchers found that disturbing the expression of both the ligand and receptors causes ectopic distribution of CRs in CP, SVZ of the developing cortex. This ectopic distribution is found preferentially in the dorsolateral cortex (Trousse et al., 2014). Using time-lapse video microscopy technique, Villar-Cerviño and colleagues found that movement of CRs is regulated by repulsive interactions between themselves; CR cells perform repelled random walks and are eventually found throughout the whole cortical surface. They also have shown that this contact repulsion between CRs is mediated by Eph/ephrin interactions (Villar-Cerviño et al., 2013). Brain-derived neurotrophic factor and neurotrophin 4 are also involved in the control of CR cell migration. Ectopic over-expression of brain-derived neurotrophic factor prior to the onset of its endogenous expression down-regulates reelin and produces a polymicrogyric cortex with disorganized CRs and aberrant cortical lamination (Alcántara, Pozas, Ibañez, & Soriano, 2005).

For Pax6, its expression is opposite to the migration of CH-derived CR cells during

the early development of the nervous system. Implants of GFP-positive CR cells into Sey mutant mice at E11 and E12, compared with WT embryos, shows more cells that arise from the cortical hem and seem to migrate by unclear and expanded routes. A large number of cells lose their subpial position and appear at different levels of the neuroepithelial thickness, demonstrating that the absence of Pax6 has an effect on CR cells migration (Ceci, López-Mascaraque, & de Carlos, 2010).

Barber and colleagues have also shown that the VAMP1-3 protein family was necessary for the migration and positioning of CRs. One of the members of this family, VAMP3, is strongly expressed in septum derived CRs and hem derived CRs in contrast to VAMP1 and 2 expressed slightly in CRs. It is possible to invalidate this protein with the transgenic line Ibot, which allows the expression of the light chain of botulinum neurotoxin B to cleave and inactivate the VAMP1-3 proteins. In order to target only the septum derived CRs and hem derived CRs, the Ibot line was crossed with the DeltaNp73Cre line causing an increase in the migration speed of these two subpopulations as well as the ectopic distribution of septum CRs in the caudo-dorsal cortex and hem CRs in the rostro-dorsal cortex. In a non-cell autonomous manner, a dorsolateral expansion of the PSB CRs was also found, the total number of CRs remaining unchanged in this mouse model (Barber et al., 2015).

3.2 Role of Cajal-Retzius cell

Among the multiple function of CRs in the development of the cortex, the most known is their role in the establishment of cortical lamination through the secretion of reelin. The absence of reelin is found in the Reeler mutant mice first described by Falconer in 1951. This spontaneous mutant exhibits abnormal behaviors such as ataxia and tremors. The histological study of the mutant mouse brain reported aberrant lamination of the cortex, cerebellum and hippocampus due to lack of projection neuron migration (Falconer, 1951).

Only in 1995 the gene responsible for this phenotype has been identified and the protein named reelin. Using the *in situ* hybridization technique to detect reelin mRNA in mice, the expression of reelin has been identified in multiple brain areas such as cortex, olfactory bulbs, striatum and cerebellum. In mice developing cortex, only the CRs in layer 1 expressed reelin (D'arcangelo et al., 1995). This protein has therefore

become a marker of choice for studying CRs during embryonic development.

In order to study the involvement of CRs in cortical lamination, different teams performed ablations of CRs subpopulations using fragment A of diphtheria toxin leading to cell death. In each case, it was impossible to eliminate all populations of the CRs. Tissir et al by disabling the cortical hem CRs and septum CRs using the *DeltaNp73Cre* line; *Wnt3aCre: RosaDTA*; *Reelin +/-* showed that suppression of the majority (up to 75%) of CRs caused no cortical lamination defects (Tissir et al, 2009). These observations were also made during the suppression of only cortical hem CRs with the *Wnt3aDTA* line (Yoshida et al, 2005) and the suppression of septum CRs and PSB CRs with the *NesCre* line; *Dbx1DTA* (Bielle et al, 2005). In all the cases, the remaining CRs alone are enough to cover the whole cortex and modulate pyramidal neuron radial migration.

CRs also regulate cortical arealization. In 2010, Griveau and colleagues performed a specific ablation of septum CRs. Based on the *Reelin* staining, there were less CRs in the rostro-medial part of the cortex around E11. This depletion was accompanied by a decrease in the proliferation of underlying progenitors in VZ. At E12.5, a redistribution of hem CRs and PSB CRs filled this vacant space on the surface of the cortex. At this stage, no proliferation defects were observed in the underlying VZ. The ablation of septum CRs also influenced the early transcriptional factor gradients of the cortex such as *Pax6*, *Emx2* and *Sp8*, further, changing the arealization of cortex at postnatal stages (Griveau et al., 2010). In 2015, Barber and colleagues observed a small but significant modification of the primary area subregions and the establishment of secondary and associative areas in the mutant mice when CRs migration speed and distribution were disturbed (Barber et al., 2015).

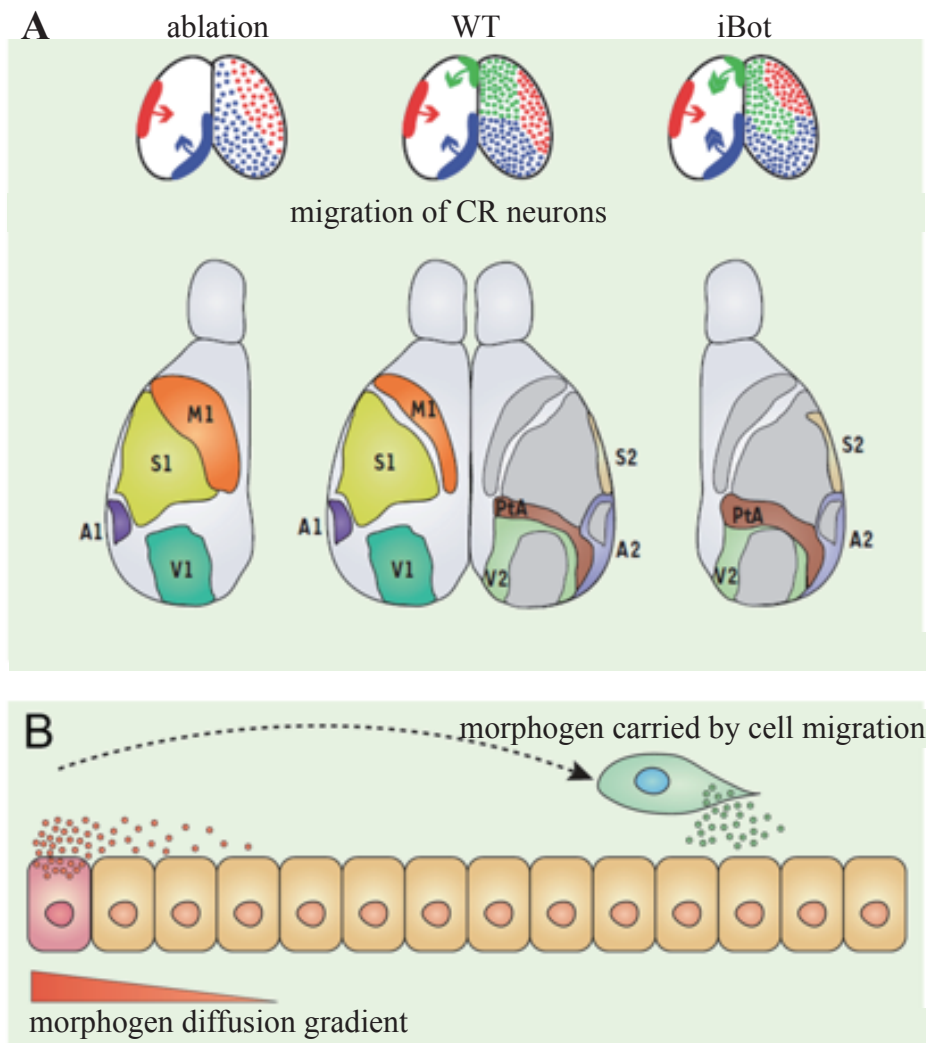


Figure 4. CRs control the regionalization of the cerebral cortex by their signaling activity. (A) Diagram showing dorsal views of mouse brains in the case of redistribution of PSB-CRs (red population) and CH-CRs (blue population) during ablation of S-CRs (green population) (scheme) top left) and when invalidating Vamp1-3 in the S-CRs and CH-CRs with the line *Np73Cre; Ibot* (Diagram at the top right). These redistributions are accompanied by a deformation of the cortical areas observed at P8. (B) Diagram illustrating the concept of CR as a mobile signaling center. The CR is represented in green and secretes various factors necessary for the early regionalization of the cortex away from its place of origin, the cell in pink represents a fixed source that will diffuse its factors in gradient from its position. Adapted from Causeret & Pierani, 2016.

4. Development of the pallium

4.1 Origin of excitatory neurons

In the beginning of mouse embryo development, the neuroepithelial cell (NECs) perform proliferative symmetric divisions, allowing the exponential growth of progenitor pool (Noctor, Martínez-Cerdeño, Ivic, & Kriegstein, 2004). Then NECs transform into radial glia progenitors (RGs) (figure 5) by losing tight junctions but maintaining adherents junctions and initiating the expression of astroglial cell markers (Hatakeyama et al., 2004). RGs are bipolar cells whose cell body is located in the ventricular zone (VZ) and fibers span the width of the cortex (Rakic, 1972). From E10.5, the first population of post-mitotic neurons, namely Cajal–Retzius (CR) cells, are generated from the border of neocortex, migrate through the marginal zone and give rise the layer I of the cortex (Bielle et al., 2005; Takiguchi-Hayashi et al., 2004; Valverde, De Carlos, & López-Mascaraque, 1995). Very soon after, around E11, the RGs start asymmetric divisions, keeping one progenitor in the VZ and generating one intermediate progenitor (IP) or one neuron (Noctor et al., 2004). IPs delaminate into the subventricular zone (SVZ) and divide at basal positions. IPs have limited proliferative potential. After a small number of proliferative divisions, IPs divide symmetrically and generate two neurons (figure5). In ferrets and primates, the vast majority of IPs perform proliferative divisions and they undergo multiple rounds of proliferative divisions before generating neurons (Betizeau et al., 2013; Fietz et al., 2010).

RGs through the indirect IPs pathway, transiently amplify the capacity of projection neurons production (Noctor et al., 2004; Wu et al., 2005). During evolution, the emergence of another type of progenitor, basal radial glial cells (bRGs) who keep one basal process and that they divide in the SVZ, contribute to the expansion of the neocortex in mammals. Unlike IPs, these basal progenitors with glial characteristics are capable of self-renewal, performing asymmetric divisions to maintain one bRGs and add one neuron or IP (Franco & Müller, 2013).

New born neurons either directly from RGs or indirectly through IPs or bRGs migrate radially along RGs fibers into the cortical plate (CP) (Noctor, Flint, Weissman, Dammerman, & Kriegstein, 2001; Rakic, 1972). At the end stage of neurogenesis,

once neuron radial migration is complete, RGs lose neurogenesis capacity and start producing oligodendrocytes or astrocytes (figure5) (Misson, Takahashi, & Caviness, 1991).

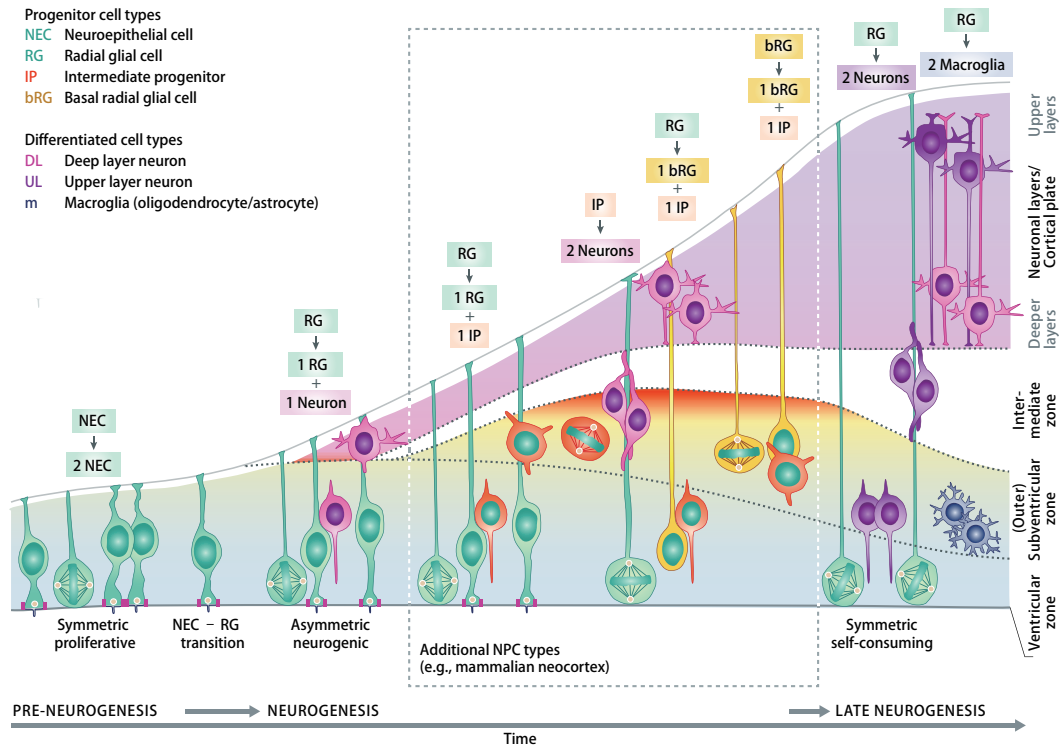


Figure 5. Progenitors and their divisions in cortical neurogenesis. The main types of neuronal progenitors: neuroepithelial cell, intermediate progenitors and basal radial glial cell are represented as well as differentiated cells from their division over time. Progenitors mainly found in primates are represented in the dashed rectangle. Adapted from Paridaen & Huttner, 2014.

The development starts from a monolayer of NECs in VZ that expand tangentially in surface and in thickness (Williams & Price, 1995). From E12 to E14 NECs differentiate into RGs initiating the expression of astroglial cell markers: Brain lipid-binding protein (BLBP) and Glast promoters (Hatakeyama et al., 2004). Within the cell cycle the nuclei of NECs and RGs undergo stereotyped movement called interkinetic nuclear migration. Their nuclei migrate radial away from the ventricular

surface during G1 phase, reach maximum movement at S phase and then move back to the apical side during G2 to divide at the ventricular surface (figure 8A) (Sauer, 1935)

There are two main types of progenitors in the SVZ: bRGs and IPs. The bRGs had first been identified in ferret and human (Fietz et al., 2010; D. V. Hansen, Lui, Parker, & Kriegstein, 2010). Soon after, several research groups also found them in rodents' developing cortices but with a much lower frequency (Shitamukai, Konno, & Matsuzaki, 2011; Xiaoqun Wang, Tsai, LaMonica, & Kriegstein, 2011). bRGs are generated from RGs losing the apical process, but keeping the basal process that reaches the pia membrane and retaining epithelial features characteristic. NECs, RGs and bRGs are self-renewable progenitors that express markers Pax6, Sox2 and Nestin (Fietz et al., 2010; D. V. Hansen et al., 2010). IPs show either multipolar shape in SVZ or 'short radial' in VZ (Kowalczyk et al., 2009). IPs divide symmetrically either into 2 IPs or 2 neurons. All types of IPs express marker Tbr2, while neurogenic IPs lose the expression of Pax6 (Figure6) (Noctor et al., 2004; Wu et al., 2005).

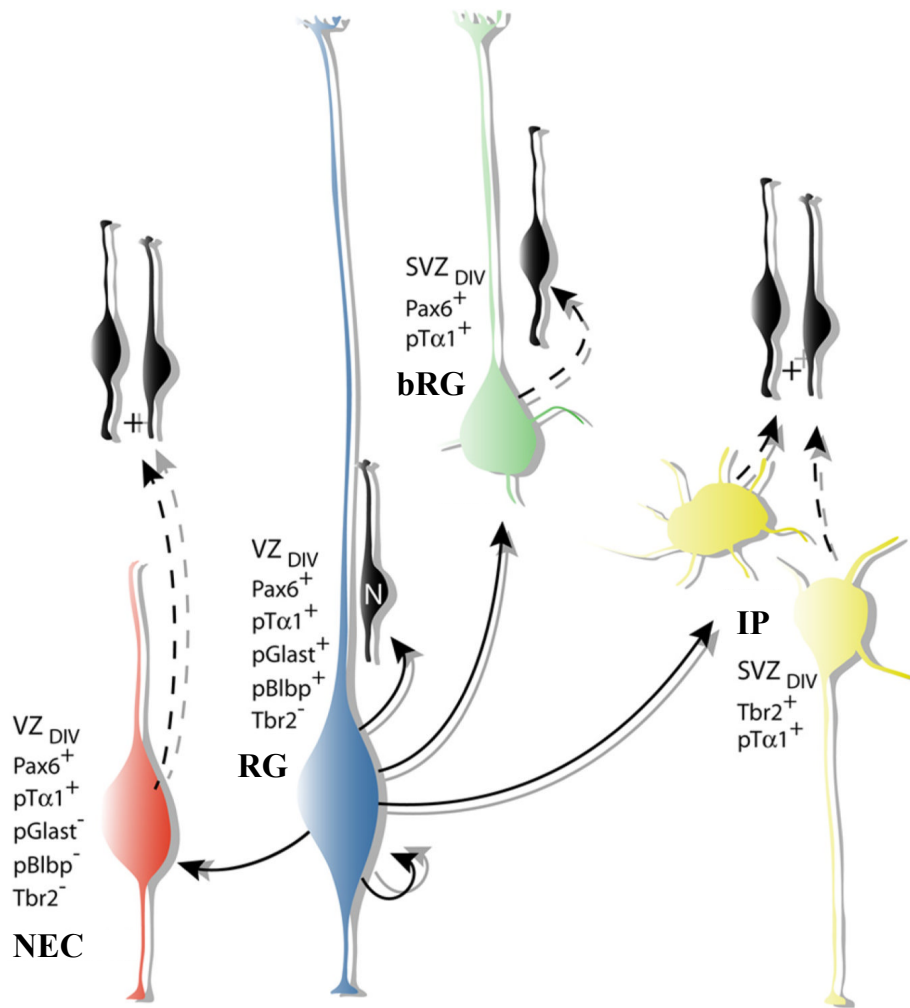


Figure 6. Molecular profiles and morphologies of different types of mouse cortical precursors and their lineage relationships. Adapted from Tyler & Haydar, 2013.

4.2 Cortical progenitors cell cycle duration

The cell cycle has long been considered identical in all different types of cortical progenitor cells (Cai, Hayes, & Nowakowski, 1997), however, more detailed studies of the cell cycle have identified that the duration of the cell cycle varies between the different progenitor types, but also, within a single progenitor population, as a function of time in development. In particular, the rapid division rate observed in early progenitors is attributed to a significantly short cell cycle caused by short G1 phase. This regulation of the cell cycle is limited in pluripotency progenitors and prevent differentiation (Lange & Calegari, 2010; Orford & Scadden, 2008; Singh &

Dalton, 2009; White & Dalton, 2005). Studies have shown that the cell cycle duration of RGs increases through the development (Calegari, Haubensak, Haffner, & Huttner, 2005; T. Takahashi, Nowakowski, & Caviness, 1995). Cell cycle duration enlarged after the switching from proliferative division to neurogenic division (Dehay & Kennedy, 2007; Salomoni & Calegari, 2010). Several studies have shown that the main contribution of this enlargement is longer G1 phase duration in a neurogenic division compared with in a proliferative division (Arai et al., 2011; Calegari et al., 2005; Lukaszewicz, Savatier, Cortay, Kennedy, & Dehay, 2002). Manipulations the duration of G1 phase in mouse influence the progenitors division preference: an increase in the G1 phase correlates with an increase in neurogenic divisions and, conversely, a reduction in the duration of the G1 phase, with an increase of proliferative divisions (Calegari & Huttner, 2003; Lange, Huttner, & Calegari, 2009; Pilaz et al., 2009).

Thanks to advances in experimental techniques of BrdU incorporation, the duration of each cycle phase of the main progenitor cells that populate VZ and SVZ in the mouse on E14.5 days has been established (figure 7) (Arai et al., 2011). This study has shown that APs have a shorter cell cycle time than BPs, in particular by reducing the length of the G1 phase. In addition, the duration of the S phase is greatly increased in progenitor cells that begin proliferative rather than neurogenic division.

	Cell-cycle phases (h)						Growth fraction (%±s.e.m.)
	T_c-T_s	T_s	T_c	T_{G2}	T_M	T_{G1}	
APs (Pax6+/Tbr2-)	14.1	5.0	19.1	1.6	0.9	11.6	98±1
Tis21-GFP-	14.1	8.3	22.4	1.6	1.1	11.4	98±1
Tis21-GFP+	14.0	1.8	15.8	1.6	0.7	11.7	99±0.5
BPs (Tbr2+/Tbr1-)	23.3	3.2	26.5	1.6	0.5	21.2	99±1
Tis21-GFP-	23.0	6.4	29.4	1.6	0.5	20.9	99±1
Tis21-GFP+	23.4	2.8	26.2	1.6	0.5	21.3	99±1
Tis21-GFP- NPCs		8.0	23.3	1.6	1.0	12.7	
Tis21-GFP+ NPCs		2.4	21.7	1.6	0.6	17.1	

Figure 7. Parameters of the cell cycle of progenitor cells at the peak of neurogenesis. The duration of the cell cycle and especially the G1 phase of apical progenitor cells is shorter than the basal progenitor cell cycle time. Within these populations, proliferating progenitor cells (Tis21-GFP-) have a longer S-phaseduration than neurogenic progenitor cells (Tis21-GFP+). Adapted from Arai et al., 2011.

Pyramidal neurons are generated sequentially from RGs in VZ or indirectly through IPs or bRGs in SVZ and migrate radially into CP successive waves. The earlier-born neurons will be placed at the level of the basal surface of the CP. The later-born neurons will cross this first layer of post-mitotic neuron to place themselves at the surface. This "inside-out" process evidenced by Angevine et al, in 1961 performing pulses of tritiated thymidine at different stages of mouse corticogenesis and by Rakic et al, in 1974 in rhesus macaque. Radioactive tritiated thymidine is incorporated by progenitors in S phase, will be inherited by their progeny and only remain undiluted in cells that have not undergone subsequent division thus labeling their birthdate (Jun & Sidman, 1961; Rakic, 1974).

Two mechanisms are involved in pyramidal neuron radial migration: somal translocation and glia-guided locomotion. Translocation alone is preferred during the early stages of cortical development when the migration distance is short and does not appear to require support. Neurons that use this mechanism have a long extension to the marginal zone. Their nuclei are translocated slowly and continuously to their final position. Neurons that move by locomotion have a very short extension and migrate freely along the basal processes of the radial glia (figure 8B) (Nadarajah & Parnavelas, 2002; Nadarajah, Brunstrom, Grutzendler, Wong, & Pearlman, 2001). This migration entails complex mechanisms. It is described into 4 steps: first, the neurons generated at the VZ move radially in the SVZ. Second, they become multipolar in SVZ. At this stage, the neurons do not seem to be attached to the guidance extension of the RGs and are still able to migrate tangentially. Then, neurons stretch and attach to the extension of the adjacent RGs to migrate toward the CP, using locomotion. Finally, the neurons get off the RGs and switch to soma translocation (figure 8C) (Azzarelli, Guillemot, & Pacary, 2015).

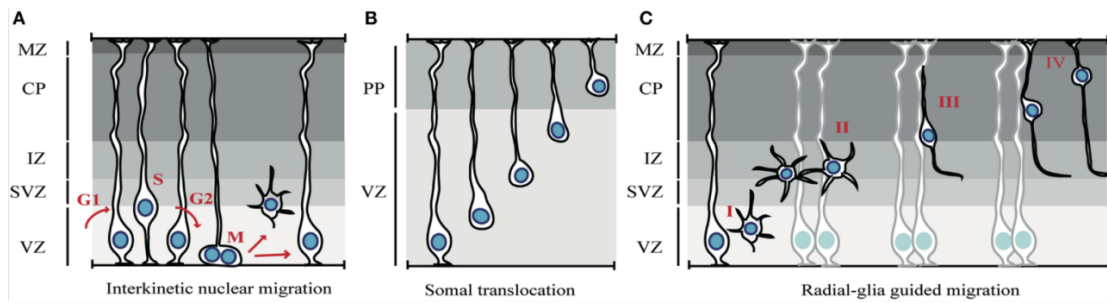


Figure 8. Modes of migration in the cortex. (A) Interkinetic nuclear migration. The nuclei of neuroepithelial cells or radial glia cells occupy different positions along the apical-basal axis depending on the phase of the cell cycle. (B) Somal translocation of early-born cortical neurons. Newborn neurons lose their apical attachment and reach the PP by translocation of the soma and progressive shortening of the basal process. (C) Glia-guided radial migration of cortical neurons. Four phases of radial migration can be distinguished. Newborn neurons leave the proliferative areas (I) and reach the SVZ/IZ, where they acquire a multipolar morphology (II). After pausing in the SVZ/IZ, cells migrate toward the CP, using locomotion (III). At the end of their migration, cortical neurons switch to soma translocation (IV). MZ, marginal zone; CP, cortical plate; PP, preplate; IZ, intermediate zone; SVZ, subventricular zone; VZ, ventricular zone. Adapted from Azzarelli et al., 2015.

5. Mathematical modelling of brain development

The history of mathematical models in morphogenesis, from shapes of organisms (D'Arcy Thompson, 1942) to the spots on the leopard skin (Murray, 1988) is remarkably rich and fruitful for both mathematics and biology. In the narrower domain of brain development also, a number of models have been very useful for a better understanding of the mechanisms supporting the development of brain morphology.

A large part of the mathematical modeling in brain development is concerned with the organization of the brain phenotype at a macroscopic scale (full brain or brain areas). In this domain, an important landmark in mathematical models of morphogenesis Alan Turing's 1952 celebrated article *The Chemical Basis of Morphogenesis* (Turing, 1952) describing how a uniform state could evolve into a non-uniform pattern during development. The latter reaction–diffusion theory of morphogenesis, has served as a basic model in theoretical biology, but also in brain macroscopic and functional phenotype (Lefèvre & Mangin, 2010; Striegel & Hurdal, 2009).

In the 1960s, Lewis Wolpert offered another conceptual definition of a morphogen and devised a model to describe basic pattern formation in development, the French Flag Model. In the French flag model, a morphogen diffuses between a source and a sink and cells decide on their "states" depending on the local morphogen concentration. Due to the existence of thresholds in the cell response, the states are discrete and in the simple model proposed by Wolpert, there are only three states represented by the different colors of the French flag (Wolpert, 1969). Homeoprotein diffusion was also studied using theoretical models, first using discrete-space models to derive mechanisms for gradient and boundary formation (Holcman, Kasatkin, & Prochiantz, 2007; Kasatkin, Prochiantz, & Holcman, 2008), and, few years after, combining Turing's models with spatial cues, Quiñinao, Prochiantz and Touboul (Perthame, Quiñinao, & Touboul, 2015; Quiñinao, Prochiantz, & Touboul, 2015) showed that slow diffusion of homeoproteins can stabilize and regularize boundaries between brain areas.

In this thesis, we are interested in models of brain development at a smaller scale, in terms of number of cells generated and of the layers they belong to. A number of

models have also considered this question in recent years. For instance, Slater and colleagues have developed a stochastic model of neurogenesis based cell lineage tree; their model emulates a single population of multipotent progenitors and their stochastic escape from symmetric divisions (Slater, Landman, Hughes, Shen, & Temple, 2009). Barbara Finlay and collaborators have built a model consider progenitor cell-cycle duration, cell death rate, and the probability to exit symmetric division, to explain how different parameters influence neuron number and the expansion through an evolutionary perspective (Cahalane, Charvet, & Finlay, 2014; Workman, Charvet, Clancy, Darlington, & Finlay, 2013).

The model we will present in this thesis was developed with the purpose of being simple enough to be easily implementable and parameterized, yet precise enough to be fitted to actual data. Compared to existing models in the literature, the model presented in Chapters II of this thesis emulates multiple cell populations and their divisions as a function of time, either within a prescribed program or through an intrinsic clock. With this model, we were able to draw quantitative predictions on the role of the switching time between proliferative and neurogenic divisions in microcephalies. Also, contrasting with previous studies, our model was directly applied to mutant mice models of microcephalies to better understand the regulation mechanisms at play in brain development.

Very recently, new developments in mathematical modeling of neurogenesis at cell populations scales were developed. In particular, Picco and colleagues proposed a deterministic model reproducing a similar sequence of divisions of progenitor cells, and concluded that this switch from proliferative and neurogenic divisions could be used to describe the diversity of cortical phenotypes in mammalian species (Picco, García-Moreno, Maini, Woolley, & Molnár, 2018). Delving at finer temporal scales, Postel and collaborators have developed a mathematical model considering both RGs and IPs divisions depending on the precise phase within the cell cycle of each cell. This model, fitted to experimental data of mouse embryos (cell numbers at different cortical development stages), was applied to a mutant mouse model with a shortening of the neurogenic period and an increased of number IPs (Postel et al., 2018).

Chapter II: Modeling the neurogenesis

1. Results/Publications

1.1 Mathematical of neurogenesis based on progenitor divisions

Mathematical models of neurogenesis can provide a new tool to understand the determinants of brain architecture and size. In collaboration with Shen-Ju Chou (Taipei), we developed a simple model of the sequence of divisions and differentiations of cells during neurogenesis, to explain her experimental data on microcephaly in mice.

In detail, *Nestin-cre; Lhx2* conditional knockout mice shows a significantly smaller and thinner cortex, which is associated with a precocious initiation of cortical neurogenesis. To demonstrate that this early neurogenesis can indeed account for the phenotype we observed in *Lhx2* cKO, we developed a parsimonious mathematical model that simulates the sequence of divisions of progenitors during cortical neurogenesis.

The model reproduces the four main types of divisions observed during corticogenesis; namely

- (i) symmetric division into two progenitors (proliferative phase);
- (ii) asymmetric division into a progenitor and an intermediate progenitor, itself generating two neurons;
- (iii) asymmetric division into a progenitor and a neuron (ii and iii are neurogenesis phase);
- (iv) loss of capacity to generate neurons (gliogenesis phase).

Moreover, neurons generated are considered to belong to a specific layer depending on the time at which the division of progenitors occurred, according to the classical radial inside-out migration of neurons to the distinct layers. All divisions and differentiations thus occur at rates (probabilities of occurrence) that vary in time.

Using that model, we first reproduced the smaller and thinner phenotype of the

Nestin-cre; Lhx2 conditional knockout mice. Also we analyzed the consequence of several possible timing shifts. The mathematical model provided us with further information that the duration of symmetric division (i) into two progenitors controls the number of progenitors (the cortical surface); the duration of neurogenic phase divisions (ii) and (iii) controls the number of neurons generated by each progenitor (the cortical thickness). Early initiation of gliogenesis division (iv) during the neurogenesis phase would lead to a more dramatic reduction of neuronal numbers in superficial layers than in deep layers. Together with the transition time point from deep to upper layer neurons, (iv) controls the proportion of deep and upper layer neurons numbers.

1.2 Publication I

Lhx2 regulates the timing of β -catenin-dependent cortical neurogenesis

Lea Chia-Ling Hsu^{a,b,c,1}, Sean Nam^{a,1}, Yi Cui^d, Ching-Pu Chang^a, Chia-Fang Wang^a, Hung-Chih Kuo^a, Jonathan D. Touboul^{d,e}, and Shen-Ju Chou^{a,b,c,2}

^aInstitute of Cellular and Organismic Biology, Academia Sinica, Taipei, 115, Taiwan; ^bMolecular Cell Biology, Taiwan International Graduate Program, Academia Sinica, Taipei, 115, Taiwan; ^cGraduate Institute of Life Sciences, National Defense Medical Center, Taipei, 114, Taiwan; ^dCollège de France, Centre for Interdisciplinary Research in Biology, CNRS UMR 7241, INSERM U1050, MemoLife Paris Science Lettres, 75231 Paris, France; and ^eInria Paris-Rocquencourt, Mycena Team, 78153 Le Chesnay, France

Edited by John L. R. Rubenstein, University of California, San Francisco, San Francisco, CA, and accepted by the Editorial Board August 18, 2015 (received for review April 12, 2015)

The timing of cortical neurogenesis has a major effect on the size and organization of the mature cortex. The deletion of the LIM-homeodomain transcription factor Lhx2 in cortical progenitors by *Nestin-cre* leads to a dramatically smaller cortex. Here we report that Lhx2 regulates the cortex size by maintaining the cortical progenitor proliferation and delaying the initiation of neurogenesis. The loss of Lhx2 in cortical progenitors results in precocious radial glia differentiation and a temporal shift of cortical neurogenesis. We further investigated the underlying mechanisms at play and demonstrated that in the absence of Lhx2, the Wnt/ β -catenin pathway failed to maintain progenitor proliferation. We developed and applied a mathematical model that reveals how precocious neurogenesis affected cortical surface and thickness. Thus, we concluded that Lhx2 is required for β -catenin function in maintaining cortical progenitor proliferation and controls the timing of cortical neurogenesis.

cortical neurogenesis | Lhx2 | β -catenin

Understanding how genetic mechanisms interact to set up a precise developmental timing is a fundamental issue in biology. In the cerebral cortex, excitatory neurons are generated by progenitor cells in the dorsal telencephalon (dTel) lining the lateral ventricle. During the early developmental stages, cortical progenitors undergo symmetric divisions, resulting in the proliferation of progenitors and thereby allowing expansion of the developing cortex. Soon after, cortical progenitors start generating distinct types of neurons through asymmetric differentiative divisions (1–5). The precise timing of the switch from proliferative division to differentiative division is crucial to determining the number of cortical neurons, and thus the cortical size.

The switch from proliferation to differentiation is reportedly regulated by the canonical Wnt signaling pathway, in which β -catenin (β -Cat) is the major downstream effector. In the absence of Wnt signaling, β -Cat is phosphorylated by glycogen synthase kinase 3 and targeted for proteasome degradation. Once Wnt ligands bind to the Frizzled-Lrp5/6 receptors, the activity of glycogen synthase kinase 3-Axin-APC (adenomatous polyposis coli) destruction complex is inhibited. As a consequence, β -Cat accumulates in the cytoplasm, translocates to the nucleus, and activates downstream gene transcription together with the lymphoid enhancer-binding factor (LEF)/T-cell factor (TCF) transcription factors (6). Overexpression of the stabilized, N-terminally truncated form of β -Cat in cortical progenitors during early neurogenesis promotes their overproliferation (7, 8), whereas inactivation of β -Cat in the cortex promotes neurogenesis (9, 10). However, stabilized β -Cat was also shown to promote cortical progenitor differentiation (11). Thus, it has been proposed that Wnt/ β -Cat signaling promotes proliferation and differentiation of cortical progenitors at early and late developmental stages, respectively (12). This raises the essential and largely open question of how Wnt/ β -Cat regulates cortical progenitor proliferation and differentiation.

The LIM-homeodomain transcription factor Lhx2 plays an important role in cortical development. In the neocortex, Lhx2 is

expressed by neocortical progenitors within the ventricular zone (VZ) of the dTel throughout cortical neurogenesis. Lhx2 was shown to play stage-specific roles determining the fate of cortical progenitors during early stages of corticogenesis (13–15). Further, the mutant mice with *Lhx2* deleted in the neural progenitors at embryonic day 11.5 (E11.5) by *Nestin-cre* exhibited a significantly smaller neocortex than WT mice (16). Overall, these previous studies showed that Lhx2 is important for the determination and maintenance of neocortical progenitors, although how Lhx2 regulates the proliferation and differentiation of cortical progenitors is unclear.

In this study, we identified a role for Lhx2 in regulating the function of the Wnt/ β -Cat signaling pathway in maintaining progenitor proliferation. The deletion of *Lhx2* in cortical progenitors leads to a temporal shift of neurogenesis. We found that by regulating how cortical progenitors respond to Wnt/ β -Cat signaling, Lhx2 regulates cortex size. By delaying neuronal differentiation and maintaining progenitor symmetric division, Lhx2 allows a suitable increase of the numbers of cortical progenitors needed to develop a proper cortex.

Results

Lhx2 Regulates the Timing of Sequential Cortical Neurogenesis. The deletion of *Lhx2* in the cortical progenitors at E11.5 by *Nestin-cre* in *Lhx2* conditional knockout (cKO, *Lhx2*^{fl/fl};*Nestin-cre*) leads to a significantly smaller and thinner cortex, although all six

Significance

The cerebral cortex is the most highly evolved structure in the human brain. Generating the correct number and types of neurons is crucial for brain function. We show a central role of the Lhx2 homeoprotein in this task: deleting Lhx2 in cortical progenitors leads to a temporal shift of neurogenesis initiation, resulting in a much smaller cortex with decreased numbers of neurons in all cortical layers. Further, we found that Lhx2 is required for the Wnt/ β -catenin pathway to maintain progenitor proliferation. Using a parsimonious mathematical model, we demonstrated that such disruptions of neurogenesis timing are enough to explain the cortical size and thickness modifications observed. Our findings enlighten how neurogenesis timing is regulated molecularly and how it affects cortical size and organization.

Author contributions: J.D.T. and S.-J.C. designed research; L.C.-L.H., S.N., Y.C., C.-P.C., C.-F.W., J.D.T., and S.-J.C. performed research; H.-C.K. contributed new reagents/analytic tools; L.C.-L.H., S.N., Y.C., and S.-J.C. analyzed data; and J.D.T. and S.-J.C. wrote the paper.

The authors declare no conflict of interest.

This article is a PNAS Direct Submission. J.L.R.R. is a guest editor invited by the Editorial Board.

¹L.C.-L.H. and S.N. contributed equally to this work.

²To whom correspondence should be addressed. Email: schou@gate.sinica.edu.tw.

This article contains supporting information online at www.pnas.org/lookup/suppl/doi:10.1073/pnas.1507145112/-DCSupplemental.

cortical layers were generated in the cKO, and the relative positions of cortical neurons in each were generally normal (16). To investigate the mechanisms for *Lhx2* to regulate cortical neurogenesis, we first examined the timing of neurogenesis by injecting BrdU into pregnant mothers when embryos were at different developmental stages and analyzing the distribution of BrdU-labeled neurons at postnatal day 7 (P7), when the six cortical layers are easily distinguishable. To define each cortical layer in WT (*Lhx2*^{fl/+} or *Lhx2*^{fl/fl}) and *Lhx2* cKO cortex, we analyzed the expression of cortical layer markers in P7 brains (17, 18). We found that in both WT and cKO cortex, the CTGF (connective tissue growth factor)-expressing subplate neurons were distributed in a single layer. We used *Brn2*, *Ctip2*, and the *Tbr1* expression domain to determine layers (L) 2/3, 5, and 6, respectively (Fig. 1 *A* and *A'*). We found that the number of cells in all layers all significantly decreased in cKO cortex (*SI Appendix*, Fig. S1). In WT cortices, almost all neurons generated at E11.5 contributed to the subplate, whereas most neurons generated at E13.5 and E15.5 contributed to the deep (L6, L5) and superficial (L2/3) layers, respectively (Fig. 1 *B* and *C*) (17). In cKO cortices, although the inside-out organization was maintained, we found that neuronal birth dates shifted to earlier points. For example, in the cKO brain, most neurons born at E11.5 contributed to layer 6, and most neurons born at E13.5 contributed to superficial layers. In cKO cortices, the number of neurons generated at E15.5 dramatically decreased relative to WT, and these neurons were located superficially in layer 2/3 (Fig. 1 *B'* and *C'*). BrdU birth dating analyses suggested that *Lhx2* deletion in cortical progenitors altered the timing of neurogenesis. To confirm this, we examined expression of neuronal markers at E13.5. We observed comparable numbers of Reelin-positive Cajal-Retzius cells in WT and cKO cortices, whereas the cortical plate, which is labeled by *Tbr1*, *Ctip2*, and *Satb2*, was relatively thicker in the cKO cortex (*SI Appendix*, Fig. S2). Overall, these findings confirmed that cortical neurons are produced earlier in *Lhx2* cKO.

Neurogenesis and Radial Glia Differentiation Initiate Earlier in *Lhx2* cKO. To demonstrate that the loss of *Lhx2* leads to increased neurogenesis during early cortical development, we analyzed the

production of divisions by cortical progenitors derived from E13.5 WT and cKO dTel. We cultured progenitors at clonal density for 24 h to allow them to divide once to form two-cell pairs. We observed significantly fewer two-cell pairs formed from cells from the cKO compared with WT dTel (Fig. 24). We also stained the two-cell pairs with antibodies against TuJ1 (neuron-specific class III b-tubulin) to label neurons and Sox2 (sex-determining region Y-related HMG box 2) to label progenitors. Pairs were identified as symmetric proliferative (P–P) divisions to form two Sox2-positive progenitors, symmetric neurogenic (N–N) divisions to form two TuJ1-positive neuronal cells, or asymmetric (P–N) divisions with one Sox2-positive and one TuJ1-positive cell. In WT and cKO cortices, the percentage of N–N pairs was comparable. In WT cortex, the majority of the two-cell pairs were P–P, indicating proliferative division of most progenitors at this stage. We found that in cKO cortex, the percentage of P–P and P–N pairs was significantly decreased and increased, respectively (Fig. 2*B*). This finding agreed with our previous report that *Lhx2* deletion by *Nestin*-cre enhances neurogenesis, with an increased number of cortical progenitors exiting cell cycle at early developmental stages (16).

To provide additional evidence to support that the deletion of *Lhx2* leads to increased neurogenic progenitors, we examined the expression of neurogenic progenitor markers, such as *Tis21* (*Btg2*) and *Hes6* (19–21), in E12.5 WT and cKO cortices. We found significantly increased expression of *Tis21* and *Hes6* in the dTel VZ in *Lhx2* cKO relative to WT (Fig. 2 *C*, *C'*, *D*, and *D'* and *SI Appendix*, Fig. S3), an effect consistent with increased neurogenesis in the cKO.

Our results suggested that neurogenesis initiates earlier in *Lhx2* cKO, and thus we further examined whether the differentiation of radial glia, the neurogenic progenitors, occurs earlier in cKO. In the developing dTel, we defined radial glial cells (RGCs) with RGC markers *Bblp* (brain lipid-binding protein; or *Fabp7*, fatty acid binding protein 7), *Glast* (glial high-affinity glutamate transporter; or *Slc1a3*, solute carrier family 1 member 3), and *TnC* (Tenascin-C) (22–27). We found that all these RGC markers are precociously up-regulated in the VZ of cKO dTel (Fig. 2 *E*, *E'*, *F*, and *F'* and *SI Appendix*, Figs. S3 and S4). The precocious

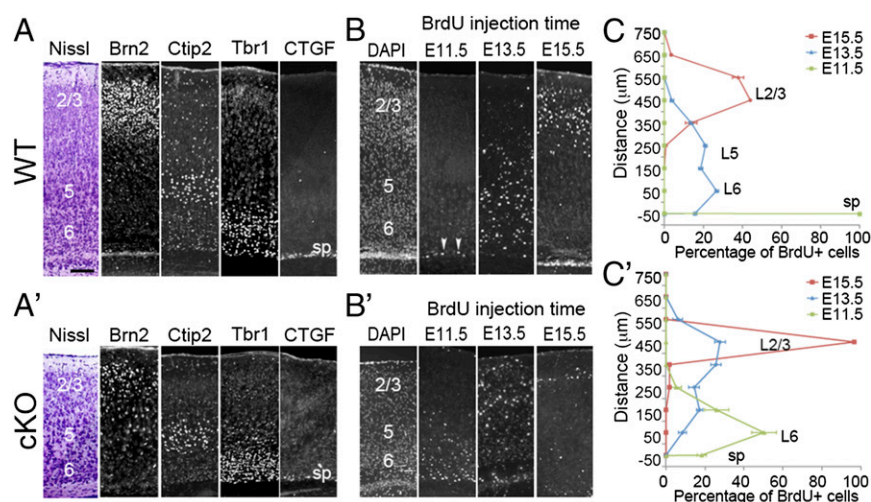


Fig. 1. *Lhx2* regulates the timing of sequential neurogenesis. (*A* and *A'*) Immunostaining for markers of specific cortical layers on coronal sections of P7 WT (*A*) and cKO (*A'*) cortices. In both WT and cKO samples, six neuronal layers are present, including the *Brn2*-expressing L2/3 (2/3), *Ctip2*-expressing L5 (5), *Tbr1*-expressing L6 (6), and CTGF-expressing subplate (sp). (*B* and *B'*) Immunostaining for BrdU on coronal sections of P7 WT (*B*) and cKO (*B'*) cortices. BrdU was injected into pregnant mothers at E11.5, E13.5, or E15.5. BrdU injected at E11.5 labeled neurons distributed in the subplate in WT mice (arrowheads), but BrdU-labeled cells were detected in layer 6 in cKO mice. BrdU injected at E13.5 labeled neurons concentrated in layer 6 in WT mice, but E13.5 BrdU-labeled cells were spread to L2/3 in cKO mice. BrdU injected at E15.5 labeled many neurons in L2/3 in WT, but only a few superficially in L2/3 in cKO. (*C* and *C'*) Quantification of results from *B* and *B'* indicating the location of BrdU-positive neurons in P7 WT and cKO cortices labeled at indicated times ($n = 3$). In a 100- μm -wide radial column, BrdU-labeled neurons were counted at 100- μm intervals from the subplate (defined as 0) to the pial surface. The percentage of BrdU-positive cells was calculated by determining the number of BrdU-positive cells in a 100 \times 100 μm box divided by the total number of BrdU-positive cells in the entire radial column. (Scale bar, 100 μm .)

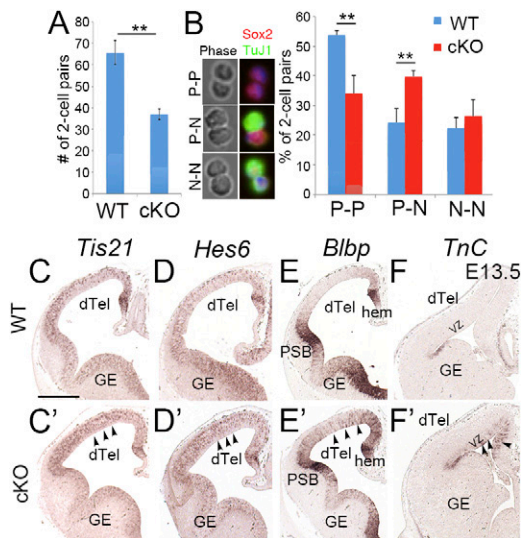


Fig. 2. *Lhx2* maintains proliferative division in progenitor cells and regulates the timing of radial glia differentiation. (A) Cortical progenitors from E13.5 WT and cKO dTel were cultured at clonal density for 24 h and then evaluated for cell pair formation. cKO formed significantly fewer pairs than WT ($n = 3$; $P < 0.01$). (B) Immunostaining of two-cell pairs for Sox2 and TuJ1. P-P, a pair with two Sox2-positive cells; N-N, a pair with two TuJ1-positive cells; and P-N pairs exhibit one of each. Quantitative results demonstrated that in the cKO cortex, the number of P-P pairs decreased significantly ($n = 3$; $P < 0.01$), and the number of P-N pairs increased significantly ($n = 3$; $P < 0.01$), whereas the number of N-N pairs is not significantly different ($n = 3$; $P = 0.3435$). (C-F) In situ hybridization for *Tis21*, *Hes6*, *Blbp*, and *TnC* on coronal sections of E12.5 (C-E) and E13.5 (F and F') WT and cKO dTel. (C-D') *Tis21* and *Hes6* expression in the dTel increased in the cKO cortex (arrowheads). (E and E') At E12.5, *Blbp* is expressed in the cortical hem (hem) and the pallial-subpallial boundary (PSB) in WT dTel. *Blbp* expression is increased in the cKO (arrowheads). (F and F') At E13.5, *TnC* expression is up-regulated in the cKO dTel VZ (arrowheads). (Scale bar, 200 μm .) GE, ganglionic eminence.

expression of radial glial marker genes suggested that the neurogenic RGCs are precociously generated in the *Lhx2* cKO. Together with the previous results, we concluded that the deletion of *Lhx2* in the cortical progenitors by *Nestin-cre* results in an earlier neurogenic RGC differentiation and an earlier initiation of neurogenesis.

The smaller cortex phenotype could alternatively be the consequence of increased cell death in the cKO cortices. To test this hypothesis, we examined whether the deletion of *Lhx2* causes increased cell death. We performed TUNEL analyses on E11.5, E12.5, E13.5, and E15.5 WT and cKO embryos. In general, very few apoptotic cells are present in the developing WT dTel, and we did not detect a measurable increase of apoptotic cells in the *Lhx2* cKO dTel (SI Appendix, Fig. S5). As the decreased cortical size is apparent by E13.5, we concluded that cell death is unlikely to account for the change in cortical size in cKO.

dTel of *Lhx2* cKO Mice Shows Misregulated β -Cat Transcriptional Activity. Canonical Wnt signaling reportedly governs whether cortical progenitors undergo proliferation or differentiation (28). To establish a readout for activity of canonical Wnt signaling, we crossed *Lhx2* cKO mice with the BAT-Gal reporter line, in which the β -Gal gene is regulated by TCF binding sites such that the reporter is activated by accumulated β -Cat in the nucleus (29). Given the stage-dependent function of β -Cat in inducing proliferation or differentiation, we examined BAT-Gal reporter expression at several stages from E11.5 to E13.5 in the WT and cKO cortices. In WT cortices, LacZ-positive cells were distributed in a high/medial to low/lateral gradient in the dTel VZ, which correlates with the location of Wnt-expressing cortical hem

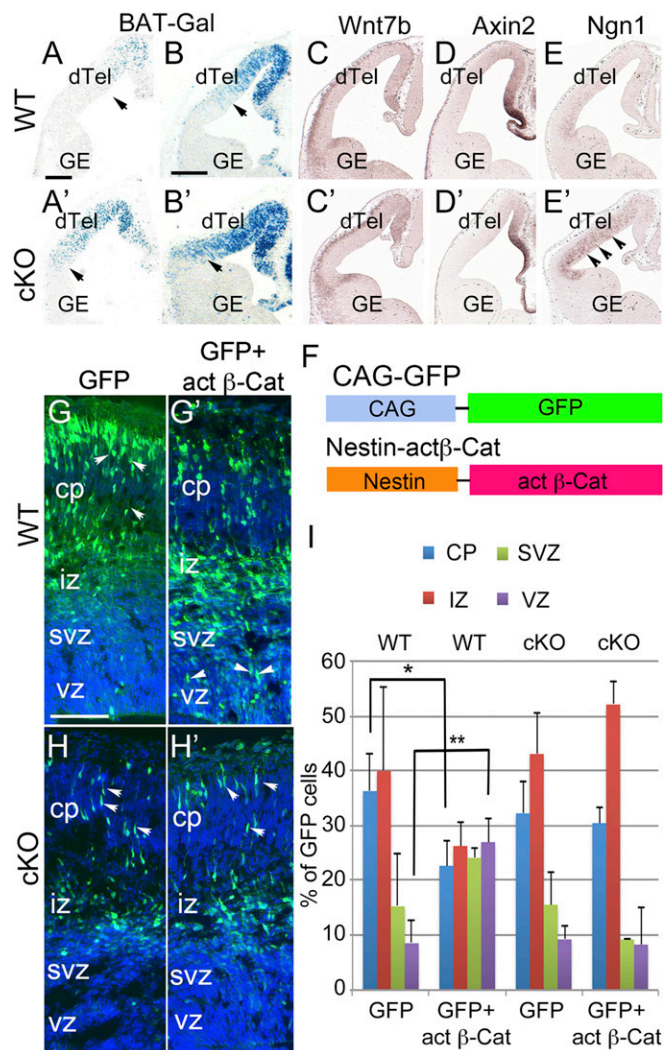


Fig. 3. Wnt/ β -Cat signaling is misregulated and fails to maintain progenitor proliferation in the dTel of *Lhx2* cKO mice. (A and B') LacZ staining of coronal sections from E11.5 (A and A') and E12.5 (B and B') WT and cKO cortices with the BAT-Gal reporter. In WT mice, β -Gal expression shows a high/medial to low/lateral gradient and is undetectable in lateral dTel. In cKO mice, β -Gal expression is greatly increased, especially in the lateral dTel. Arrowheads indicate the extent of the distribution of LacZ-positive cells. (C-E') In situ hybridization of *Wnt7b*, *Axin2*, and *Ngn1* on coronal sections of E12.5 WT and cKO cortices. The expression level and pattern of *Wnt7b* and *Axin2* are maintained in the cKO, whereas the expression of *Ngn1* is up-regulated in the cKO (arrowheads). (F) Constructs used for in utero electroporation. (Top) CAG-GFP contains a ubiquitously active CAG promoter and GFP. (Bottom) *Nestin-act β -Cat* contains a *Nestin* enhancer in front of the *Hsp68* promoter driving expression of the active form of β -Cat in the neural progenitor cells. (G and H') Immunostaining for GFP on coronal sections of E15.5 WT (G and G') and cKO (H and H') brains electroporated at E13.5 with CAG-GFP alone (G and H) or CAG-GFP together with *Nestin-act β -Cat* (G' and H'). (G) Most GFP-expressing cells are distributed in cortical plate (cp) (arrowheads) and the intermediate zone (iz) in brains transfected with CAG-GFP alone. (G') Many GFP-expressing cells remain in the ventricular zone (vz) (arrowheads) in CAG-GFP+*Nestin-act β -Cat*-cotransfected WT brains. (H and H') In either GFP alone (H) or CAG-GFP+*Nestin-act β -Cat* (H') transfected cKO brains, most GFP-expressing cells are distributed in the intermediate zone and cortical plate (arrowheads), rather than in the ventricular zone. (I) Histogram showing the percentage of GFP+ cells in cp, iz, svz, and vz in a 100- μm -wide column of dTel. When act β -Cat is transfected in the WT, GFP+ cells located in the cortical plate are significantly reduced ($n = 3$; $P < 0.05$), whereas GFP+ cells located in the ventricular zone are significantly increased ($n = 3$; $P < 0.01$). (Scale bars, 100 μm , A, A', G, H'; 200 μm , B-E'). GE, ganglionic eminence.

cells located in the most medial part of the cortex (30). The number of LacZ-positive cells increased in the cKO dTel VZ from E11.5 to E13.5, and these LacZ-positive cells were distributed throughout the entire VZ of the cKO dTel, even in the most lateral part (Fig. 3 A, A', B, and B' and SI Appendix, Fig. S6). Thus, with the BAT-Gal reporter, we found that the transcriptional activity of canonical Wnt signaling is dramatically increased in the *Lhx2* cKO. This is unexpected, given that the precocious neurogenesis we observed in *Lhx2* cKO is similar to the phenotype of β -Cat deletion (9, 10).

We then examined whether the deletion of *Lhx2* affects the expression of components in Wnt/ β -Cat signaling pathway in a similar way as the BAT-Gal reporter. We examined the expression of genes involved in Wnt signaling during early cortical development in the cKO, including Wnt ligands *Wnt3a* and *Wnt7b*; Wnt antagonists *Sfrp1* and *Sfrp2*; and Wnt downstream factors *Axin2*, *Lef1*, *CyclinD1*, and *Ngn1* (11, 31). We found no significant difference in the expression of most of these genes in the *Lhx2* cKO dTel compared with WT from E11.5 to E13.5 (Fig. 3 C, C', D, and D' and SI Appendix, Fig. S7). However, we did detect a dramatic up-regulation of *Ngn1* (Fig. 3 E and E'), a reported Wnt downstream target driving neuronal differentiation (11). Further, the expression of *Sfrp2* at the pallium-subpallium boundary is decreased in cKO at E13.5 (SI Appendix, Fig. S7). We found that in *Lhx2* cKO, the high level of Wnt/ β -Cat signaling transcriptional activity fails to increase the expression of many of the Wnt downstream genes, such as *Axin2* and *CyclinD1*. We thus hypothesized that *Lhx2* is required for the function of Wnt signaling.

Wnt/ β -Cat Signaling Fails to Maintain Cortical Progenitor in the dTel of *Lhx2* cKO Mice. To examine the requirement for *Lhx2* in the Wnt/ β -Cat signaling pathway to promote cortical progenitor proliferation, we compared the function of active β -Cat in WT and cKO cortical progenitors. We generated a *Nestin-act β Cat* construct, in which a stabilized β -Cat with first 47-amino acid truncation is driven by the *nestin* enhancer and the *hsp68* basal promoter (32) (Fig. 3F) to drive transcriptionally active β -Cat expression in VZ progenitors. In addition, we generated a CAG (CMV early enhancer/chicken β -actin promoter)-GFP construct, in which a GFP reporter is driven by a constitutively active CAG promoter (Fig. 3F). In E13.5 dTel, we electroporated the CAG-GFP construct with or without the *Nestin-act β Cat* construct and then analyzed distribution of GFP-expressing cells as the transfected cells at E15.5. In WT cortices transfected with CAG-GFP alone, most GFP-expressing cells were distributed in the intermediate zone and cortical plate, but not in the proliferative zone, VZ/SVZ (Fig. 3 G and I). However, after cotransfection with the *Nestin-act β Cat* construct in WT, a significantly increased number of transfected cells remained in the VZ and decreased number of transfected cells migrated to the cortical plate (Fig. 3 G' and I). To ensure that the increased number of the active β -Cat transfected cells in the VZ was not a result of migration defects of these cells, we stained them with a neuronal marker, TuJ1. We found that these VZ located cells do not express the neuronal marker (SI Appendix, Fig. S8). We thus concluded that the expression of active β -Cat in WT cortical progenitors maintains these progenitors in the proliferating zone.

We also electroporated CAG-GFP alone into the cKO dTel at E13.5, and we found, similar to in WT dTel, that most GFP-expressing cells were distributed in the intermediate zone and cortical plate at E15.5 (Fig. 3 H and I). When both CAG-GFP and *Nestin-act β Cat* constructs were electroporated into the cKO dTel, most GFP-labeled cells still migrated to the cortical plate and did not stay in the VZ/SVZ (Fig. 3 H' and I). Our results here showed that in the absence of *Lhx2*, the cKO cortical progenitors do not remain in the proliferating zone in response to active β -Cat.

Our results demonstrated that *Lhx2* is required for the function of β -Cat to promote cortical progenitor proliferation. We

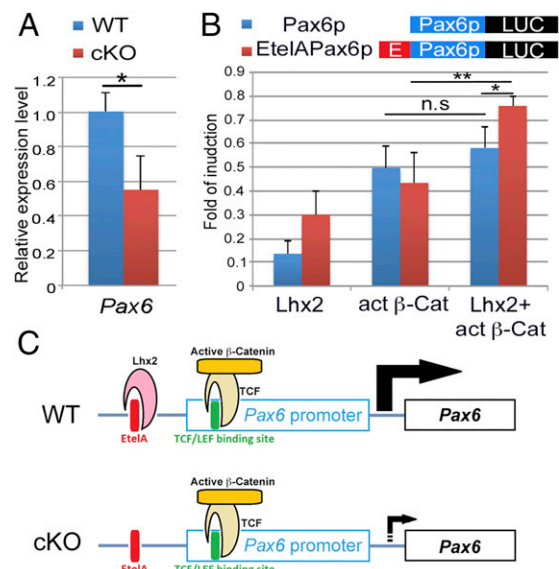


Fig. 4. *Lhx2* and β -Cat collaboratively induce *Pax6* expression. (A) Quantitative RT-PCR to compare the relative expression level of *Pax6* in E12.5 WT and cKO dTel. The expression of *Pax6* is significantly down-regulated in the cKO ($P < 0.05$; $n = 5$). (B) The reporter constructs, Pax6p-Luc (containing *Pax6* promoter) and EtelAPax6p-Luc (containing *Pax6* promoter and a *Pax6* enhancer, E, as indicated). Reporter activity without cotransfection of effectors was set as 1, and results are presented as fold of induction. The activity of Pax6p cannot be induced by *Lhx2*, but it can be induced by active β Cat, and there is no further induction when *Lhx2* and active β Cat were both added (n.s., not significant). EtelAPax6p-Luc activity can be induced by *Lhx2* and active β Cat, individually. *Lhx2* and active β Cat together can further induce the activity of EtelAPax6p ($P < 0.01$; $n = 3$). (C) Model for *Lhx2* and active β Cat collaboratively regulate *Pax6* expression.

hypothesized that *Lhx2* could act together with β -Cat to regulate the expression of genes governing progenitor proliferation. *Pax6* is likely to be one of such genes, as it is a key regulator for cortical progenitor proliferation and neurogenesis (33). Further, in cortical progenitors, the β -Cat/TCF complex was shown to activate *Pax6* transcription by binding to the *Pax6* promoter (34), and *Lhx2* was also reported to directly regulate *Pax6* expression by binding to its enhancers (35, 36). We first confirmed that *Pax6* is down-regulated in the cKO dTel at E12.5 (Fig. 4A). We then performed luciferase reporter assays to analyze the function of *Lhx2* and active β -Cat on regulating *Pax6* expression. We compared the induction level of *Lhx2*, active β -Cat or *Lhx2* and active β -Cat together on Pax6p, in which luciferase gene is under the control of the *Pax6* promoter containing a β -Cat/TCF binding site (34), and EtelAPax6p, in which luciferase gene is under the control of the *Pax6* promoter and a *Pax6* enhancer containing a *Lhx2* binding site (35). We found that EtelAPax6p can be induced by active β -Cat, as well as by *Lhx2*, while Pax6p can be induced by active β -Cat, but not by *Lhx2*. When both *Lhx2* and active β -Cat were cotransfected, EtelAPax6p can be further induced to reach a significantly higher level than Pax6p (Fig. 4B). These results suggested that *Lhx2* and active β -Cat could collaboratively induce *Pax6* expression (Fig. 4C).

Timing of Neurogenesis Affects the Cortical Size. Our experimental data reveal that the deletion of *Lhx2* leads to a significantly smaller cortex, which is associated with a precocious initiation of cortical neurogenesis. To demonstrate that this early neurogenesis can indeed account for the phenotype we observed in *Lhx2* cKO, we developed a parsimonious mathematical model that simulates the sequence of divisions of progenitors during cortical neurogenesis (see details in SI Appendix). The model reproduces the sequences of progenitor divisions during corticogenesis (2); namely (i) symmetric division into two progenitors (proliferative phase); (ii) asymmetric

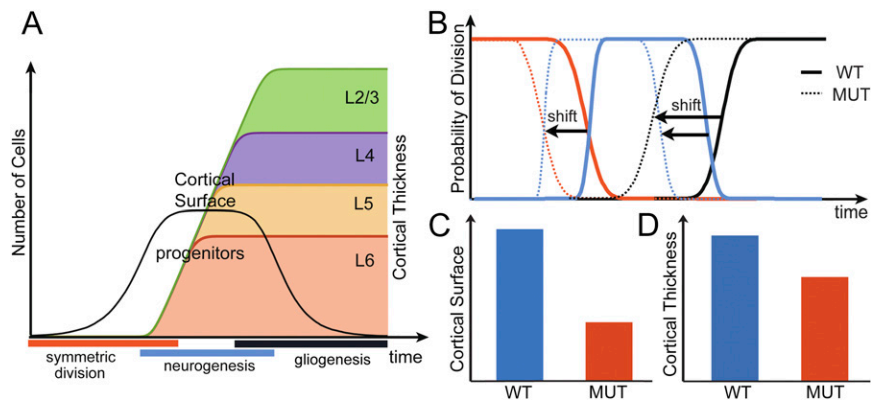


Fig. 5. Theoretically deciphering the effect of *Lhx2* deletion. (A) Evolution of the number of progenitors (black line) and number of neurons in each layer as a function of time. Symmetric division (red) duplicates the number of progenitors, neurogenesis (blue) gives rise to neurons, and gliogenesis (black) decreases the pool of progenitors. (B) Comparison between fitted models to WT and cKO (MUT, dotted lines). In cKO, the precocious end of symmetric division and neurogenesis leads to decreased cortical surface (C) and thickness (D).

division into a progenitor and an intermediate progenitor, itself generating two neurons; (iii) asymmetric division into a progenitor and a neuron (ii and iii are neurogenesis phase); and (iv) loss of capacity to generate neurons (gliogenesis phase). When a neuron is generated, it is considered to belong to a specific layer according to the classical radial inside-out migration of neurons to the distinct layers, depending on their generation time (17, 37). An example of the evolution of the number of progenitors and neuronal cells as a function of time in the model is provided in Fig. 5A.

We used the model to investigate the causal relationship of the smaller and thinner cortex and the temporal shift of neurogenesis program in *Lhx2* cKO (as shown in Fig. 1). The size of the cortical surface is directly related to the number of the progenitors lining the ventricular zone. As the number of progenitors is an exponential function of the duration of the proliferative phase, a shorter duration of the progenitor symmetric division period reduced the surface size of the cKO cortex (Fig. 5B and C and *SI Appendix*, Fig. S9). The thickness of the cortex is related to the number of neurons generated in a radial column and is governed by the duration of the neurogenesis phase (*SI Appendix*, Fig. S9). To generate a smaller and thinner cortex, we found that the durations of proliferative phase and the neurogenesis phases in *Lhx2* cKO are shorter (Fig. 5B, C, and D).

In addition, the mathematical model provided us with further information on how to generate a thinner cortex with a disproportional change in the thickness of deep and superficial layers, as in the cKO cortices (as shown in *SI Appendix*, Fig. S1). We found that an early initiation of gliogenesis during the neurogenesis phase would lead to a more dramatic reduction of neuronal numbers in superficial layers than in deep layers. We tested this prediction experimentally and confirmed that the gliogenesis indeed initiates earlier in the cKO (*SI Appendix*, Figs. S9 and S10).

Discussion

In this study, we uncovered biological mechanisms regulating the timing of neurogenesis. We found that *Lhx2* deletion by *Nestin*-cre leads to a shift of the sequential process of neurogenesis to an earlier time. We thus concluded that *Lhx2* maintains cortical progenitors in proliferative state and delays the initiation of neurogenic differentiation at early developmental stages. This finding is consistent with the fact that *Lhx2* expression in cortical progenitors decays during cortical development and that *Lhx2* is expressed in a pattern opposite to that of neurogenesis: it forms a high/medial to low/lateral and high/caudal to low/rostral gradient, whereas neurogenesis initiates from the rostrolateral cortex, where *Lhx2* is expressed at the lowest level (38).

Further, we identified that *Lhx2* is involved in the Wnt/ β -Cat signaling pathway. This pathway is known to play important roles in regulating cortical neurogenesis; however, it was shown to induce both progenitor proliferation and differentiation, two contradicting events (28). It has been difficult to analyze β -Cat function in knockout animals because mutants also show defects in cell adhesion and tissue integrity. Ectopic expression of *Dkk1*, a negative regulator of Wnt signaling pathway, in the developing cortex was used to reduce Wnt signaling activity while maintaining β -Cat function in cortical progenitors. It confirmed that Wnt signaling plays a positive role in the expansion of progenitors (39). Recently, the role of β -Cat in cortical development was studied elegantly by constructing a mutant form of β -Cat with normal cell-cell adhesion activity, but defective transcriptional activity (40). Interestingly, mice harboring this mutant form of β -Cat exhibited a phenotype similar to what we observe in *Lhx2* cKO, including a temporal shift of neurogenesis and fewer neurons in both deep and upper cortical layers (40).

As the deletion of *Lhx2* resembles the loss of Wnt/ β -Cat signaling activity, we expected to find decreased β -Cat transcriptional activity in *Lhx2* cKO. However, with BAT-Gal reporter, we found an increase in β -Cat transcriptional activity in *Lhx2* cKO dTel (Fig. 3). Interestingly, we observed a discrepancy between the expression of the BAT-Gal reporter, a faithful reporter for Wnt/ β -Cat signaling pathway in many systems (9, 29, 39, 41, 42), and the known Wnt/ β -Cat downstream genes, such as *Axin2* and *CyclinD1* (*SI Appendix*, Fig. S7). Only *Ngn1*, a neurogenic Wnt/ β -Cat downstream gene (28), is up-regulated in the *Lhx2* cKO (Fig. 3). We further confirmed that the loss of *Lhx2* impairs cortical progenitor self-renewal promoted by Wnt/ β -Cat signaling by showing that the expression of stabilized β -Cat maintains transfected cells in the ventricular zone in WT, but not in *Lhx2* cKO (Fig. 3). Thus, we proposed that *Lhx2* is involved in directing the activity of the Wnt/ β -Cat signaling pathway to promote progenitor proliferation, probably in a similar way as *Axin*, a component in the Wnt/ β -Cat signaling pathway, directing the proliferation or differentiation choice in the intermediate progenitors (43).

During cortical development, patterning centers express signaling molecules such as Fgfs and Wnts to establish expression patterns of transcription factors and regulate cortical neurogenesis and patterning. Several patterning transcription factors, including *Emx2* (empty spiracles homeobox 2), *COUP-TF1* (chicken ovalbumin upstream promoter transcription factor 1 or NR2F1), *Pax6* (paired box 6), and *Sp8* (trans-acting transcription factor 8), were shown to collaboratively regulate the proliferation and differentiation of cortical progenitors and cortical arealization

(44). In cortical progenitors, these transcription factors establish a regulatory network, such as the reciprocal regulation between COUP-TF1 and Sp8 (45), to coordinate multiple signaling pathways. For example, COUP-TF1 regulates progenitor proliferation and differentiation (46) and also plays an important role in regulating cortical areal patterning (47). Similar to these patterning transcription factors, Lhx2 controls multiple aspects of cortical development. It is likely these different functions of Lhx2 are coordinated in cortical progenitors by interacting with other transcription factors during cortical neurogenesis. Further studies of genetic machinery regulated by Lhx2 and the interactions between Lhx2 and other transcription factors are needed to understand the mechanisms of the temporal regulation of neurogenesis.

Cortical size expansion and the increase in cortical neuronal number suggest that regulation of neurogenesis has changed over evolution (48, 49). The mathematical model of cortical neurogenesis we developed provided insights on how the timing of different phases in neurogenesis affect the size and composition of the

cortex. Our findings suggested that the intricate interplay between Lhx2 and Wnt/ β -Cat signaling pathway, by modifying the timing of neurogenesis, appears to be a key regulatory mechanism in cortical evolution and may function in cortical developmental disorders, such as microcephaly.

Materials and Methods

The different mouse lines and antibodies used in this study, along with their sources and the detailed protocols for cell culture, luciferase reporter assays, and in utero electroporation, are described in *SI Appendix, Materials and Methods*. In situ hybridization and immunostainings were performed as described previously (14, 16).

ACKNOWLEDGMENTS. We thank Dr. Dennis O'Leary for providing the Lhx2 floxed allele, Nestin-cre, and BAT-Gal mouse lines; Dr. Paola Bovolenta for Axin2 and CyclinD1 in situ probes; and Dr. Chin-Ying Tai for stabilized β -cat constructs. We also thank Dr. Hwai-Jong Cheng for advice and members of the S.-J.C. laboratory for their help. This work was supported by NHRI-EX102, 103-10260NI (National Health Research Institutes), AS-104-TP-B09-2 (Academia Sinica), and the Institute of Cellular and Organismic Biology of Academia Sinica.

- Fishell G, Kriegstein AR (2003) Neurons from radial glia: The consequences of asymmetric inheritance. *Curr Opin Neurobiol* 13(1):34–41.
- Florio M, Huttner WB (2014) Neural progenitors, neurogenesis and the evolution of the neocortex. *Development* 141(11):2182–2194.
- Götz M, Huttner WB (2005) The cell biology of neurogenesis. *Nat Rev Mol Cell Biol* 6(10):777–788.
- Noctor SC, Martínez-Cerdeño V, Kriegstein AR (2008) Distinct behaviors of neural stem and progenitor cells underlie cortical neurogenesis. *J Comp Neurol* 508(1):28–44.
- Miyata T, Kawaguchi D, Kawaguchi A, Gotoh Y (2010) Mechanisms that regulate the number of neurons during mouse neocortical development. *Curr Opin Neurobiol* 20(1):22–28.
- Clevers H, Loh KM, Nusse R (2014) Stem cell signaling. An integral program for tissue renewal and regeneration: Wnt signaling and stem cell control. *Science* 346(6205):1248012.
- Chenn A, Walsh CA (2002) Regulation of cerebral cortical size by control of cell cycle exit in neural precursors. *Science* 297(5580):365–369.
- Wrobel CN, Mutch CA, Swaminathan S, Taketo MM, Chenn A (2007) Persistent expression of stabilized beta-catenin delays maturation of radial glial cells into intermediate progenitors. *Dev Biol* 309(2):285–297.
- Machon O, et al. (2007) A dynamic gradient of Wnt signaling controls initiation of neurogenesis in the mammalian cortex and cellular specification in the hippocampus. *Dev Biol* 311(1):223–237.
- Mutch CA, Schulte JD, Olson E, Chenn A (2010) Beta-catenin signaling negatively regulates intermediate progenitor population numbers in the developing cortex. *PLoS One* 5(8):e12376.
- Hirabayashi Y, et al. (2004) The Wnt/beta-catenin pathway directs neuronal differentiation of cortical neural precursor cells. *Development* 131(12):2791–2801.
- Inestrosa NC, Varela-Nallar L (2015) Wnt signalling in neuronal differentiation and development. *Cell Tissue Res* 359(1):215–223.
- Bulchand S, Grove EA, Porter FD, Tole S (2001) LIM-homeodomain gene Lhx2 regulates the formation of the cortical hem. *Mech Dev* 100(2):165–175.
- Chou SJ, Perez-Garcia CG, Kroll TT, O'Leary DD (2009) Lhx2 specifies regional fate in Emx1 lineage of telencephalic progenitors generating cerebral cortex. *Nat Neurosci* 12(11):1381–1389.
- Mangale VS, et al. (2008) Lhx2 selector activity specifies cortical identity and suppresses hippocampal organizer fate. *Science* 319(5861):304–309.
- Chou SJ, O'Leary DD (2013) Role for Lhx2 in corticogenesis through regulation of progenitor differentiation. *Mol Cell Neurosci* 56:1–9.
- Molyneux BJ, Arlotta P, Menezes JR, Macklis JD (2007) Neuronal subtype specification in the cerebral cortex. *Nat Rev Neurosci* 8(6):427–437.
- Leone DP, Srinivasan K, Chen B, Alcamo E, McConnell SK (2008) The determination of projection neuron identity in the developing cerebral cortex. *Curr Opin Neurobiol* 18(1):28–35.
- Arai Y, et al. (2011) Neural stem and progenitor cells shorten S-phase on commitment to neuron production. *Nat Commun* 2:154.
- Iacopetti P, et al. (1999) Expression of the antiproliferative gene TIS21 at the onset of neurogenesis identifies single neuroepithelial cells that switch from proliferative to neuron-generating division. *Proc Natl Acad Sci USA* 96(8):4639–4644.
- Gratton MO, et al. (2003) Hes6 promotes cortical neurogenesis and inhibits Hes1 transcription repression activity by multiple mechanisms. *Mol Cell Biol* 23(19):6922–6935.
- Hartfuss E, Galli R, Heins N, Götz M (2001) Characterization of CNS precursor subtypes and radial glia. *Dev Biol* 229(1):15–30.
- Anthony TE, Klein C, Fishell G, Heintz N (2004) Radial glia serve as neuronal progenitors in all regions of the central nervous system. *Neuron* 41(6):881–890.
- Feng L, Hatten ME, Heintz N (1994) Brain lipid-binding protein (BLBP): A novel signaling system in the developing mammalian CNS. *Neuron* 12(4):895–908.
- Hegedus B, et al. (2007) Neurofibromatosis-1 regulates neuronal and glial cell differentiation from neuroglial progenitors in vivo by both cAMP- and Ras-dependent mechanisms. *Cell Stem Cell* 1(4):443–457.
- Anthony TE, Heintz N (2008) Genetic lineage tracing defines distinct neurogenic and gliogenic stages of ventral telencephalic radial glial development. *Neural Dev* 3:30.
- Götz M, Bolz J, Joester A, Faissner A (1997) Tenascin-C synthesis and influence on axonal growth during rat cortical development. *Eur J Neurosci* 9(3):496–506.
- Bielen H, Houart C (2014) The Wnt cries many: Wnt regulation of neurogenesis through tissue patterning, proliferation, and asymmetric cell division. *Dev Neurobiol* 74(8):772–780.
- Maretto S, et al. (2003) Mapping Wnt/beta-catenin signaling during mouse development and in colorectal tumors. *Proc Natl Acad Sci USA* 100(6):3299–3304.
- Grove EA, Tole S, Limon J, Yip L, Ragsdale CW (1998) The hem of the embryonic cerebral cortex is defined by the expression of multiple Wnt genes and is compromised in Gli3-deficient mice. *Development* 125(12):2315–2325.
- Kato M (2008) WNT signaling in stem cell biology and regenerative medicine. *Curr Drug Targets* 9(7):565–570.
- Zimmerman L, et al. (1994) Independent regulatory elements in the nestin gene direct transgene expression to neural stem cells or muscle precursors. *Neuron* 12(1):11–24.
- Manuel MN, Mi D, Mason JO, Price DJ (2015) Regulation of cerebral cortical neurogenesis by the Pax6 transcription factor. *Front Cell Neurosci* 9:70.
- Gan Q, et al. (2014) Pax6 mediates β -catenin signaling for self-renewal and neurogenesis by neocortical radial glial stem cells. *Stem Cells* 32(1):45–58.
- Hou PS, et al. (2013) LHX2 regulates the neural differentiation of human embryonic stem cells via transcriptional modulation of PAX6 and CER1. *Nucleic Acids Res* 41(16):7753–7770.
- Shetty AS, et al. (2013) Lhx2 regulates a cortex-specific mechanism for barrel formation. *Proc Natl Acad Sci USA* 110(50):E4913–E4921.
- Greig LC, Woodworth MB, Galazo MJ, Padmanabhan H, Macklis JD (2013) Molecular logic of neocortical projection neuron specification, development and diversity. *Nat Rev Neurosci* 14(11):755–769.
- Suter B, Nowakowski RS, Bhide PG, Caviness VS (2007) Navigating neocortical neurogenesis and neuronal specification: a positional information system encoded by neurogenetic gradients. *J Neurosci* 27(40):10777–10784.
- Solberg N, Machon O, Krauss S (2008) Effect of canonical Wnt inhibition in the neurogenic cortex, hippocampus, and premigratory dentate gyrus progenitor pool. *Dev Dyn* 237(7):1799–1811.
- Draganova K, et al. (2015) Wnt/ β -catenin signaling regulates sequential fate decisions of murine cortical precursor cells. *Stem Cells* 33(1):170–182.
- Mutch CA, Funatsu N, Monuki ES, Chenn A (2009) Beta-catenin signaling levels in progenitors influence the laminar cell fates of projection neurons. *J Neurosci* 29(43):13710–13719.
- Ivaniutins U, Chen Y, Mason JO, Price DJ, Pratt T (2009) Adenomatous polyposis coli is required for early events in the normal growth and differentiation of the developing cerebral cortex. *Neural Dev* 4:3.
- Fang WQ, Chen WW, Fu AK, Ip NY (2013) Axin directs the amplification and differentiation of intermediate progenitors in the developing cerebral cortex. *Neuron* 79(4):665–679.
- O'Leary DD, Chou SJ, Sahara S (2007) Area patterning of the mammalian cortex. *Neuron* 56(2):252–269.
- Borello U, et al. (2014) Sp8 and COUP-TF1 reciprocally regulate patterning and Fgf signaling in cortical progenitors. *Cereb Cortex* 24(6):1409–1421.
- Faedo A, et al. (2008) COUP-TF1 coordinates cortical patterning, neurogenesis, and laminar fate and modulates MAPK/ERK, AKT, and beta-catenin signaling. *Cereb Cortex* 18(9):2117–2131.
- Armentano M, et al. (2007) COUP-TF1 regulates the balance of cortical patterning between frontal/motor and sensory areas. *Nat Neurosci* 10(10):1277–1286.
- Kaas JH (2013) The evolution of brains from early mammals to humans. *Wiley Interdiscip Rev Cogn Sci* 4(1):33–45.
- Kriegstein A, Noctor S, Martínez-Cerdeño V (2006) Patterns of neural stem and progenitor cell division may underlie evolutionary cortical expansion. *Nat Rev Neurosci* 7(11):883–890.

Supplementary material for Hsu et al.,

Lhx2 regulates the timing of β -catenin-dependent cortical neurogenesis

Lea Chia-Ling Hsu^{a,b,c,1}, Sean Nam^{a,1}, Yi Cui^d, Ching-Pu Chang^a, Chia-Fang Wang^a, Hung-Chih Kuo^a, Jonathan D. Touboul^{d,e}, and Shen-Ju Chou^{a,b,c,2}

^aInstitute of Cellular and Organismic Biology, Academia Sinica, Taipei, 115, Taiwan;

^bMolecular Cell Biology, Taiwan International Graduate Program, Academia Sinica, Taipei, 115, Taiwan;

^cGraduate Institute of Life Sciences, National Defense Medical Center, Taipei, 114, Taiwan;

^dCollège de France, Centre for Interdisciplinary Research in Biology, CNRS UMR 7241, INSERM U1050, MemoLife Paris Science Lettres, Paris, 75231, France;

^eInria Paris-Rocquencourt, Mycenae Team, Le Chesnay 78153, France

¹These authors contributed equally.

²Corresponding author

Shen-Ju Chou, schou@gate.sinica.edu.tw

Institute of Cellular and Organismic Biology, Academia Sinica

128 Academia Rd. Sec. 2, Taipei, Taiwan 115.

Including: Mathematical model and simulations, Materials and methods, Supplemental references and Figure S1-S10.

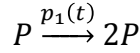
Mathematical Model and Simulations

In this section we provide the details of the mathematical model used to simulate the cortical development, and the algorithm used to perform the stochastic simulations.

System specification

The model only depends on the rate at which cortical progenitor cells divide (number of divisions per unit time) and how this rate depends on time and on the type of division. According to the previous studies, there are 4 main phases for cortical neurogenesis (S1):

- (i) *Symmetric division* of the progenitor cells that occur at early stages of cortical development, with a rate $p_1(t)$ (see Figure S9A)



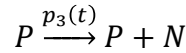
This is the unique phase associated with an increase of the number of progenitor cells. It constitutes the substrate upon which neurons and glia is formed, and therefore tightly regulates the size of the brain.

- (ii) *Asymmetric division* of a progenitor cell into IPC (intermediate progenitor cell, or basal progenitors) with a rate $p_2(t)$. IPCs subsequently divide and differentiate into two neurons



Neurons formed at time t migrate to layer $l \in \{6,5,4,2/3\}$ with a time-dependent probability $q_l(t)$.

- (iii) *Asymmetric division* of a progenitor cell into a progenitor and a neuron with a rate $p_3(t)$



Similar to phase (ii), the differentiation at time t gives rise to a neuron of layer l with probability $q_l(t)$.

- (iv) The last phase taking place in the process of cortical development is the loss of capacity to generate a progenitor or a neuron. This phase, occurring at a rate $p_4(t)$, either corresponds to the formation of glial cells or to apoptosis.

$$P \xrightarrow{p_4(t)} \emptyset$$

Parameters fit

As mentioned in the main text, the only parameters to fit are the initiation and end times of the different phases ($p_\varphi(t)$, $\varphi = 1 \dots 4$) as well as the probability for a neuron generated at time t to belong to layer l ($q_l(t)$, $l \in \{6,5,4,2/3\}$). We consider that the probabilities p_φ and q_l have a typical profile $\varphi(t_{start}, t_{end}, t)$ only parameterized by their initiation (t_{start}) and end (t_{end}) times, and thus the model is complete once adjusted the start and end time of each phase. The map $t \mapsto \varphi(t_{start}, t_{end}, t)$ is a smooth step function. Results do not tightly depend on the choice of the function, and we fixed in our simulations:

$$\varphi(t_{start}, t_{end}, t) = (1 + \text{erf}(t - t_{start})) \cdot (1 - \text{erf}(t - t_{end}))$$

We chose the start and end times of each phase so that the end state fits the cell counts obtained for the WT cortex (Figure S1). We then varied these parameters in mutant scenarios to uncover what type of disruption may be consistent with the *Lhx2* cKO phenotype.

Mutant Models

The *Lhx2* cKO mice shows a significantly smaller cortex with approximate halving of the number of neurons in superficial layers and a reduction of 40% in deeper layers (Figure S1). The reduction of the cortical size is the result of a shorter duration of progenitor symmetric division phase. We adjusted to the duration of progenitor symmetric division phase to reach the reduction of cortical size in *Lhx2* cKO (Figure 5). We fitted the parameters in order to recover the correct cell counts in a given column. We started with an initial pool of $P_0 = 50$ progenitor cells (note that this acts only as a scale parameter and does not change qualitatively the outcome of the system). The parameters of the WT model (and other mutant scenarios) are provided in Table S1.

In order to illustrate how the different timings affect the cortical thickness and composition of the different layers, we further provide the four conceivable

scenarios with different disruption during neurogenesis (see Figure S9A and Table S1):

- (i) Model M1: The switch from neurogenesis to gliogenesis is delayed (i.e. end of the neurogenesis and beginning of gliogenesis shifted by the same amount)
- (ii) Model M2: Similar as M1 except that the switch is advanced
- (iii) Model M3-M4: gliogenesis onset only is advanced (more dramatically in M4)

	End of symmetric division	Neurogenesis start	Neurogenesis end	Gliogenesis
WT	5	5	10	10
MUT	3	3	8	6
M1	5	5	12	12
M2	5	5	8	8
M3	5	5	10	8.5
M4	5	5	10	6

Table S1 Parameters used in Figure S9, The WT and MUT models are used in the main text (Figure 5).

The cortical thickness is evaluated as the number of neurons generated by a progenitor and it is thus proportional to the number of neurons produced: It increases when the duration of neurogenesis phase is longer (model M1) or decreases when the duration of neurogenesis is shorter (model M2). The cortical thickness t is also sensitive to the onset of gliogenesis: the earlier the gliogenesis, the thinner the resulting cortex (Fig. S9B). If both neurogenesis termination and onset of gliogenesis are shifted, the proportions of neurons in the different layers are unchanged (models M1 and M2, Fig. S9C), but as soon as gliogenesis is advanced during neurogenesis phase, the proportions of neurons in the superficial layers is reduced. The level of this phenomenon depends on how advanced gliogenesis is (only L2/3 for M3, both L4 and L2/3 for M4).

Simulation Algorithm

The simulations were performed using so-called the Doob-Gillespie algorithm (S2) for exact simulation of cell divisions. Given the rate of division of progenitor cells, it draws the time of the division, which is an exponential random variable with parameter given by the total rate of division $\Pi(t) = \sum_{i=1}^4 p_i(t)$ multiplied by the number of progenitors cells at time t , $P(t)$. Once the time of the next event is found, the division occurring is chosen with a probability equal to the ratio between the rate of this event and the total rate: $P_i(t)/\Pi(t)$, and if a neuron is created, it is attributed to layer I with probability $q_I(t)$. The simulations start with an initial pool of progenitors P_0 and are run until all progenitors have lost their capacity to generate neurons (or when neurogenesis is stopped). All simulations were performed in Matlab®, using a code that we developed for the purpose of this article.

Materials and methods

Animals

Timed pregnant mice were used in accordance with Academia Sinica institutional guidelines. The day of insemination and day of birth are designated as embryonic day 0.5 (E0.5) and postnatal day 0 (P0), respectively. Genotyping for the *Lhx2* floxed, *Nestin-cre* and the BAT-gal alleles was performed using the polymerase chain reaction (PCR), as previously described (20, 21).

Cell culture and Luciferase reporter assay

The 293T cell line was cultured in medium that contained DMEM (Life Technologies) supplemented with 10% fetal bovine serum. For luciferase assays, cells were plated in 12-well plates and transfected the next day with luciferase reporters and a *Renilla* luciferase vector to normalize transfection efficiency. The transfection was performed using Lipofectamine transfection reagent according to the manufacturer protocol (Life Technologies). The cells were harvested 48 h after transfection and processed using the Dual-Glo Luciferase Assay System (Promega). The data were obtained in from three independent experiments.

Histochemistry

For immunostaining and X-Gal staining, brains were fixed in 4% PFA in PBS, cryoprotected in 30% sucrose/PBS, cut in 20 μm sections, and stained as described (20, 21). Antibodies used were: rat anti-BrdU (Accurate), goat anti-Brn2 (Santa Cruz), rabbit anti-Ctip2 (Novus), EdU (Click-iT EdU Imaging kit, Life Technologies), mouse anti-GFAP (cell signaling), rabbit anti-GFP (Life Technologies), mouse anti-Reelin (Millipore), mouse anti-Satb2 (Abcam), rabbit anti-Sox2 (Millipore), rabbit anti-Tbr1 (Abcam) and mouse anti-TuJ1 (Covance). Cell counts were made on coronal section images at matching rostral-caudal and medial-lateral levels. Statistical comparisons of cell counts in mutant and control mice were made using a paired *t*-test. TUNEL (terminal deoxynucleotidyl transferase–mediated deoxyuridinetriphosphate nick end-labeling) assay was performed with In Situ Cell Death Detection Kit (Roche).

***In situ* hybridization**

Brains were fixed with 4% paraformaldehyde in PBS, cryoprotected with 30% sucrose in 0.1 M PBS, embedded in Tissue Tek OCT compound (Sakura Finetek) and cut in 20 μm sections on a cryostat. *In situ* hybridization using digoxigenin (DIG)-labeled riboprobes was undertaken as described (20, 21).

***In utero* electroporation**

Expression construct CAG-GFP was made by subcloning GFP into a pCAG vector containing the cytomegalovirus (CMV) early enhancer element and chicken β -actin promoter. Nes-act- β Cat was generated by subcloning the constitutively active β -catenin (chicken β -Cat with first 47 amino acid truncation) into the Nestin enhancer and hsp68 promoter containing vector. *In utero* electroporation was performed as described (S3). In short, E13.5 embryos were visualized through the uterus using a fiber optic light source. DNA solutions containing 0.25 $\mu\text{g}/\mu\text{l}$ pCAG-GFP +/- 0.75 $\mu\text{g}/\mu\text{l}$ Nestin-Act β Cat + 1% fast green (Sigma) were injected with a glass capillary into the ventricle of each embryo and electroporated with Paddle-type electrodes (CUY21 Electroporator: Nepa Gene) in a series of five square-wave current pulses (35 V, 100 ms \times 5). Electroporated embryos were allowed to develop until E15.5 and selected for further analyses by direct visualization of GFP expression.

The distribution of eGFP-expressing cells was assessed by immunostaining with anti-GFP antibody.

Pair-Cell Analysis

Clonal culture and pair-cell analysis were done as described previously (S4). Briefly, the cortices of WT or *Lhx2* cKO embryos at E12.5 were dissected and dissociated in single clones. Single cells were plated in poly-L-lysine coated 60-well Terasaki plates incubated. Pair cells were identified after 24 hours of incubation and were fixed with 4% PFA and stained with DAPI, TuJ1 and Sox2 antibodies.

Quantitative RT-PCR

Total RNA from the dTel of E12.5 WT and cKO brains was extracted using Trizol (Life Technologies). Reverse transcription was performed using Superscript III (Life Technologies). 1 µg of total RNA was reverse transcribed using random hexamers. Quantitative PCR (qPCR) was performed using the SYBR Green PCR Master Mix (Life Technologies). 18sRNA transcripts served as a normalizing control. All samples were tested in triplicate. For all qPCR analyses, RNA from three independent replicates for both WT and cKO dTel were examined. Error bars represent STDEV. Primers used for qPCR analyses were:

Lhx2	AAGCTCAACCTGGAGTCGGAA	TGAGGTGATAAACCAAGTCCCG
Tis21	GCGAGCAGAGACTCAAGGTT	CCAGTGGTGTTTGTAAATGATCG
Hes6	ATGAGGTGCACACGTTCCG	GCAGCGGCATGGATTCTA
Blbp	TAAGTCTGTGGTTCGGTTGG	CCCAAAGGTAAGAGTCACGAC
Tnc	GGGCTTTGACTGTAGTGAGAT	CATCACAGATACACATGCCATTC
Pax6	GCCCTTCCATCTTTGCTTGGGAAA	TAGCCAGGTTGCGAAGAACTCTGT
18sRNA	GAGGCCCTGTAATTGGAATGAG	GCAGCAACTTTAATATACGCTATTGG

Supplementary References

- (S1) Kwan, K.Y., Sestan, N, Anton, E.S., (2012). Transcriptional co-regulation of neuronal migration and laminar identity in the neocortex. *Development* 139, 1535-1546.
- (S2) Gillespie, D.T., (1977). Exact Stochastic Simulation of Coupled Chemical Reactions. *The Journal of Physical Chemistry* 81 (25): 2340–2361.

(S3) Li, H., Chou, S.J., Hamasaki, T., Perez-Garcia, C.G., O'Leary, D.D., (2012). Neuregulin repellent signaling via ErbB4 restricts GABAergic interneurons to migratory paths from ganglionic eminence to cortical destinations. *Neural development* 7, 10.

(S4) Sahara S & O'Leary DD (2009) Fgf10 regulates transition period of cortical stem cell differentiation to radial glia controlling generation of neurons and basal progenitors. *Neuron* 63(1):48-62.

Supplementary Figures

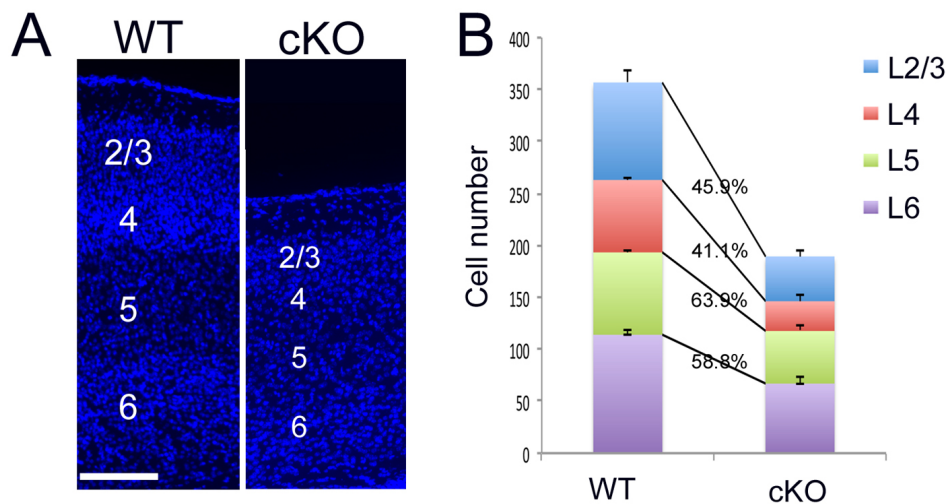


Figure S1 Comparison of the thickness of cortex and of each cortical layer in WT and cKO mice. (A) DAPI staining of coronal sections of P7 WT and cKO cortices. (B) Histogram showing the numbers of neurons in P7 WT and cKO cortices in a 100 μ m wide column. Relative to WT (layers (L)2/3, 93.7 \pm 12.9; L4, 69.7 \pm 4.9; L5, 79.3 \pm 1.5 and L6, 114.0 \pm 5.0; n=3), the number of cortical neurons in each layer in the cKO mouse is significantly decreased ($P < 0.05$ by an unpaired Student's *t*-test) (L2/3, 43.0 \pm 6.0; L4, 28.7 \pm 4.0; L5, 50.7 \pm 5.8 and L6, 67.0 \pm 6.1; n=3). The number of neurons in cKO (189.3, n=3) is 53.1% of that in the WT (356.7, n=3). The neuronal number in each cortical layer is differentially affected; the deep layers (L5 and L6) are less affected than the superficial layers (L2/3 and L4). Scale bar, 100 μ m.

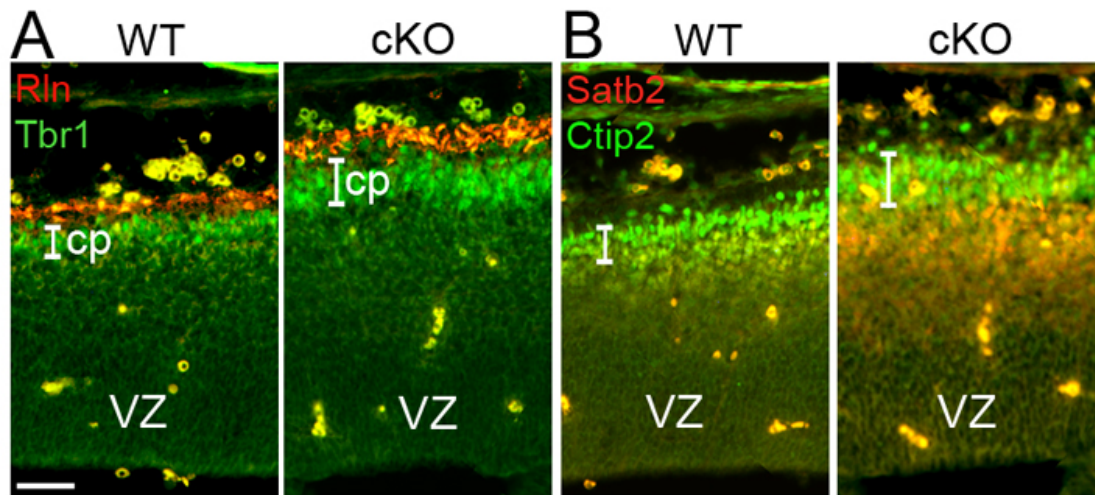


Figure S2 Precocious neurogenesis in *Lhx2* cKO mice. (A) Immunostaining for Reelin (Rln) and Tbr1 on coronal sections of E13.5 WT and cKO dTel. Reelin (red) labels Cajal-Retzius neurons in the marginal zone, and Tbr1 labels the cortical plate (cp). (B) Immunostaining for Ctip2 and Satb2 on coronal sections of E13.5 WT and cKO dorsal telencephalon. Ctip2 (green) labels newly born layer 5 neurons in the cortical plate. A greater number of Satb2-labeled superficial neurons are seen in the cKO relative to WT dTel. VZ, ventricular zone. Scale bar, 100 μ m.

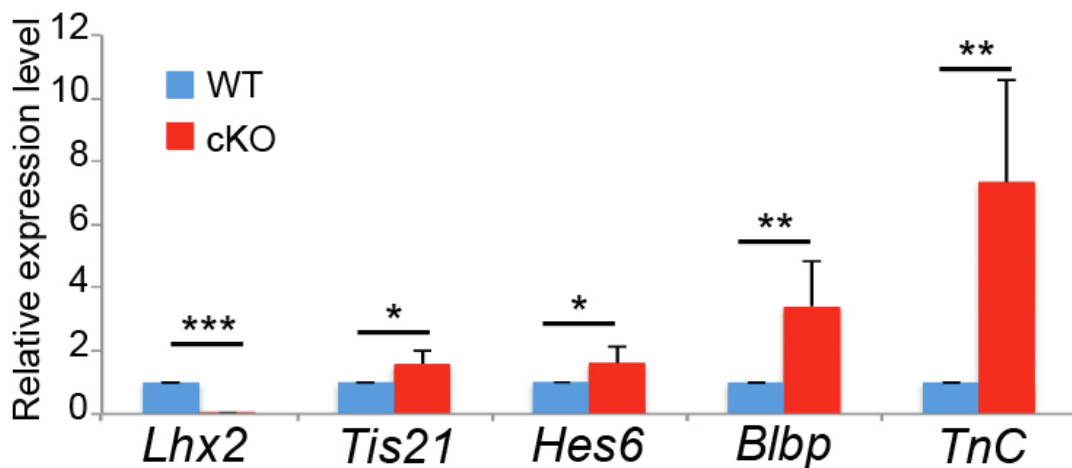


Figure S3. *Lhx2* regulates the timing of neurogenesis and radial glia differentiation. (G) Quantitative RT-PCR for *Lhx2*, *Tis21*, *Hes6*, *Blbp* and *TnC* to compare the relative expression levels of these genes in E12.5 WT and cKO dorsal telencephalon. The expression of *Lhx2* is significantly down-regulated in the cKO ($p < 0.001$, $n = 5$). *Tis21* ($p < 0.05$, $n = 4$), *Hes6* ($p < 0.05$, $n = 4$), *Blbp* ($p < 0.01$, $n = 5$) and *TnC* ($p < 0.01$, $n = 4$) are significantly up-regulated in the cKO.

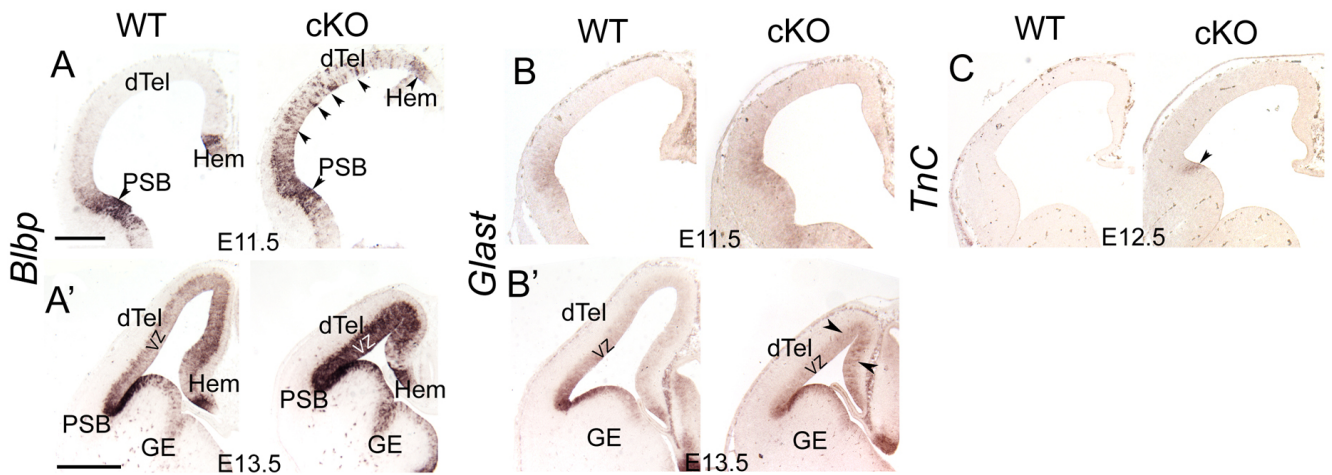


Figure S4. Expression of radial glial marker genes is up-regulated in the dorsal telencephalon of *Lhx2* cKO mice. *In situ* hybridization of *Blbp*, *Glact* and *TnC* on coronal sections from E11.5 to E13.5 WT and cKO cortices. The expression levels of *Blbp* is dramatically up-regulated (arrowheads) in the ventricular zone (vz) of dorsal telencephalon (dTel) in cKO at E11.5 (A) and E13.5 (A'). The expression level of *Glact* is similar in WT and cKO dTel at E11.5 (B), but is up-regulated (arrowheads) in cKO at E13.5 (B'). The expression of *TnC* is up-regulated in the cKO at the pallial-subpallial boundary (PSB) (arrowhead) at E12.5 (C). GE, ganglionic eminence. Scale bars, 200µm (A, B, C) and 500µm (A', B').

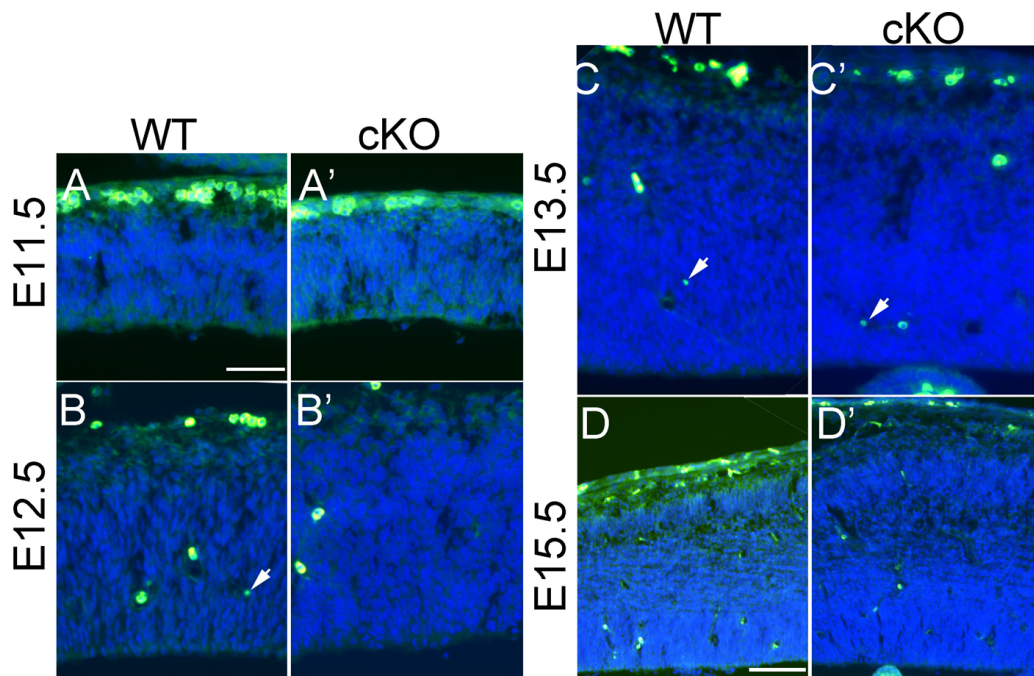


Figure S5 No detectable increase of apoptotic cells in *Lhx2* cKO dorsal telencephalon. TUNEL assays on coronal sections from E11.5 to E15.5 WT and cKO cortices. Very few apoptotic cells (arrowheads) are detected in the ventricular zone of dorsal telencephalon in WT or cKO from E11.5 to E15.5 Scale bars, 50µm (A-C') and 100µm (D, D').

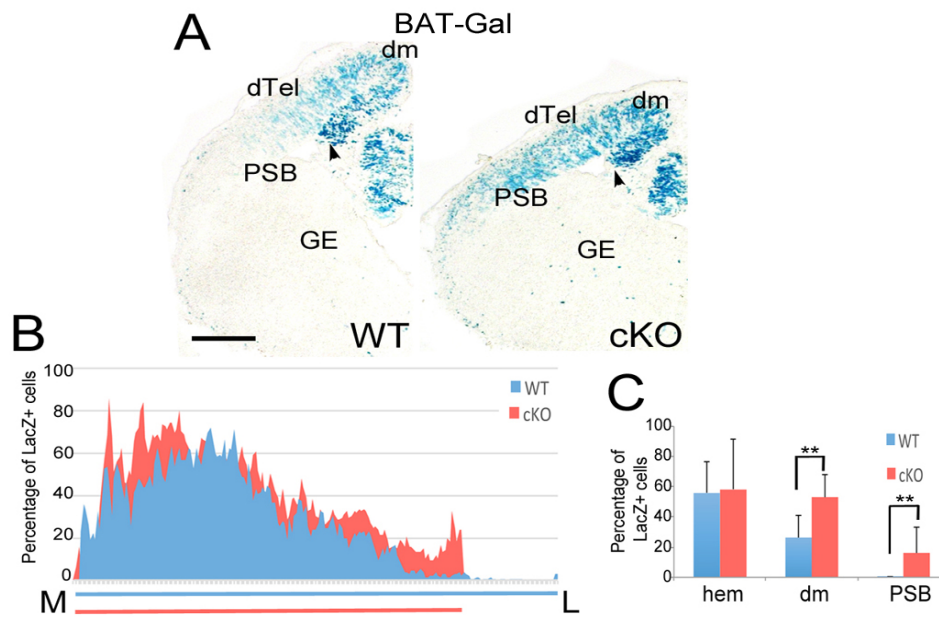


Figure S6. The β -catenin transcriptional activity is increased in *Lhx2* cKO. (A) LacZ staining of coronal sections from E13.5 WT and cKO cortex with the BAT-Gal reporter. In WT mice, β -Gal expression shows a high/medial-to-low/lateral gradient and is almost undetectable in the VZ of the most lateral dTel. In cKO mice, β -Gal expression is greatly increased, especially in the VZ of the lateral dTel. Scale bar, 250 μ m. Arrowheads indicate the location of cortical hem. (B) Percentage of LacZ-positive cells among total cells in 10 μ m wide columns from medial (M) to lateral (L) in dTel in WT (blue) and cKO (red) mice (n=3). Lines beneath the histogram represent the length of dTel from cortical hem (M) to the PSB (L) in WT (blue) and cKO (red) samples. Across the M-L axis, there was a greater number of LacZ positive cells in the cKO than in WT. (C) Comparison of relative numbers of LacZ-positive cells in WT and cKO cortex at the cortical hem or dorsal medial cortex (dm, as shown in A) or the PSB. The level of LacZ-positive cells at the hem is similar between WT and cKO samples, but a significantly larger number of LacZ-positive cells is detected in the cKO cortex at the dm and PSB relative to WT samples ($p < 0.01$; n=3).

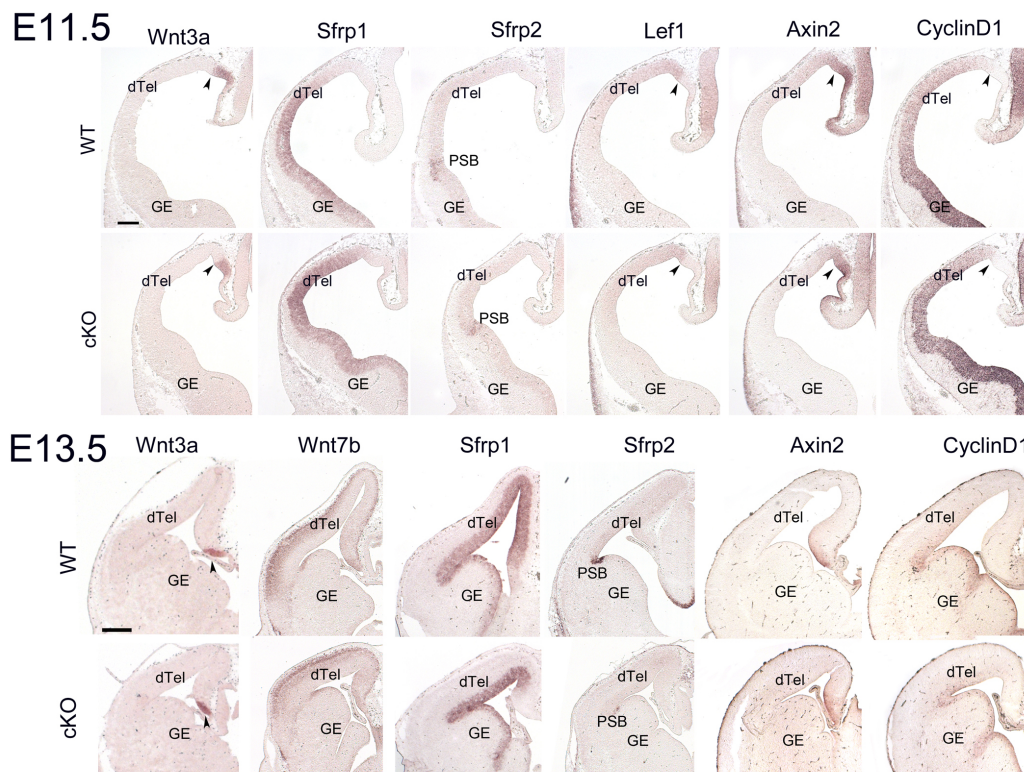


Figure S7. Expression of genes involved in Wnt signaling pathway is mostly unchanged in the dorsal telencephalon of *Lhx2* cKO mice. *In situ* hybridization of *Wnt3a*, *Wnt7b*, *Sfrp1*, *Sfrp2*, *Lef1*, *Axin2* and *CyclinD1* on coronal sections from E11.5 (Top) and E13.5 (Bottom) WT and cKO cortices. The spatial expression and levels of these genes are similar in WT and cKO at both E11.5 and E13.5. The only detectable difference is that the expression of *Sfrp2* in the pallial-subpallial boundary (PSB) is decreased in the cKO at E13.5 when compared with WT. dTel, dorsal telencephalon; GE, ganglionic eminence; arrowheads: cortical hem. Scale bars, 200 μm.

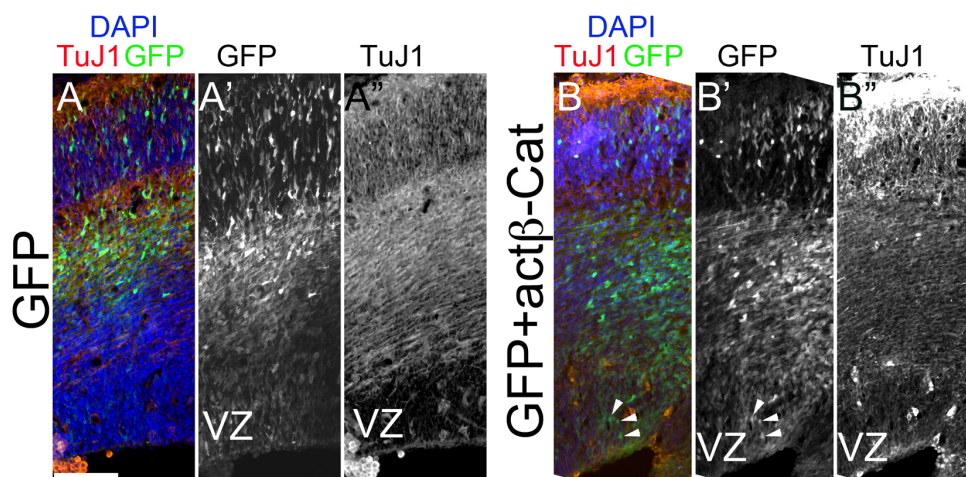


Figure S8 The expression of stabilized β -Cat maintains transfected cells in the ventricular zone in WT. Immunostaining for GFP (green) and TuJ1 (red) with DAPI staining (blue) on coronal sections of E15.5 WT and cKO dTel electroporated with GFP expression vector (A-A'') or GFP expression vector

together with *nestin*-active β -Cat (B-B''), as described in Figure 3). The electroporated cells are marked by GFP. The cells transfected with active β -Cat are maintained in the ventricular zone (VZ, arrowheads in B, B') and they do not express the neuronal marker, TuJ1. Scale bar, 100 μ m.

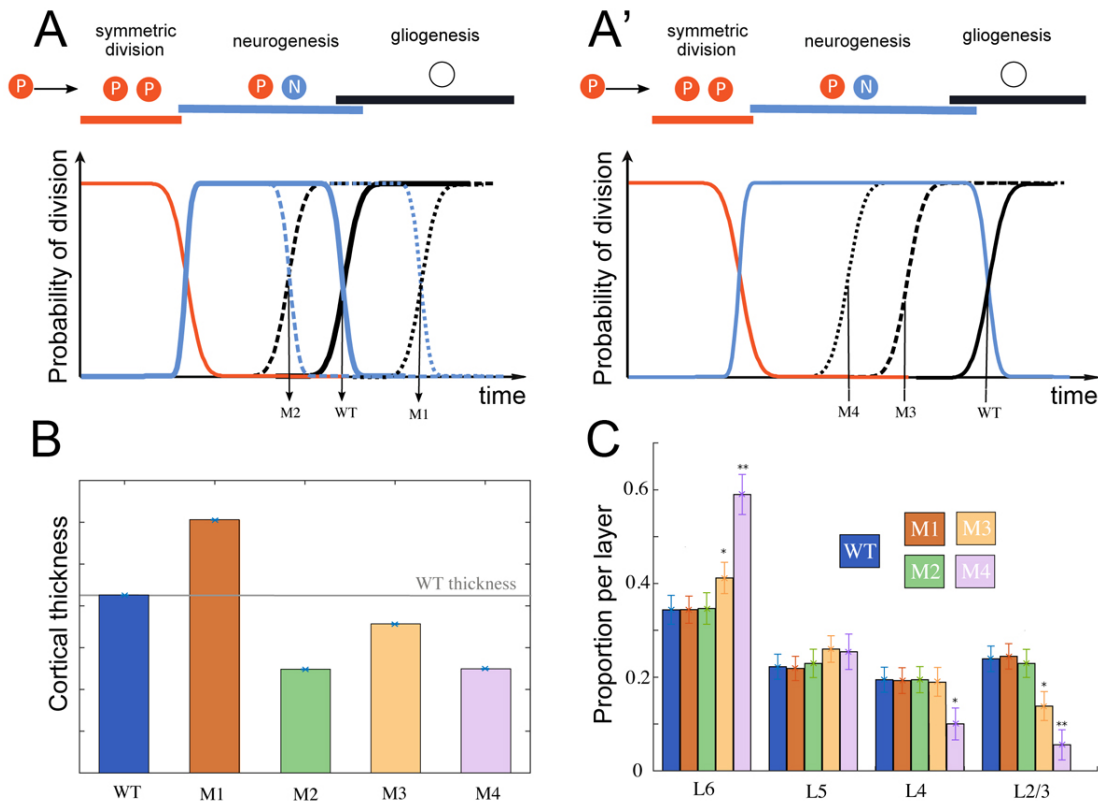


Figure S9. Role of neurogenesis timing in the thickness and layer proportions. (A) Timing of the neurogenesis in the WT model and 4 mutant models, M1 – M4. M1 and M2 differ of WT in the time progenitor switch from neurogenesis to gliogenesis, M3 and M4 have fixed neurogenesis duration but the onset of gliogenesis is advanced (see Supplementary Table 1 for parameters, the curves are illustrative here but not quantitative for legibility). (B) resulting cortical thicknesses, and (C) proportions of neurons in the different layers. Longer (resp. shorter) neurogenesis phase in the absence of precocious gliogenesis result (M1, resp. M2) in thicker (resp. thinner) cortices with no effect on the proportions of neurons in the different layers. Precocious gliogenesis reduces the cortex thickness (models M3 and M4) and imbalances the proportions of neurons in the different layers (decreased proportions in superficial layers).

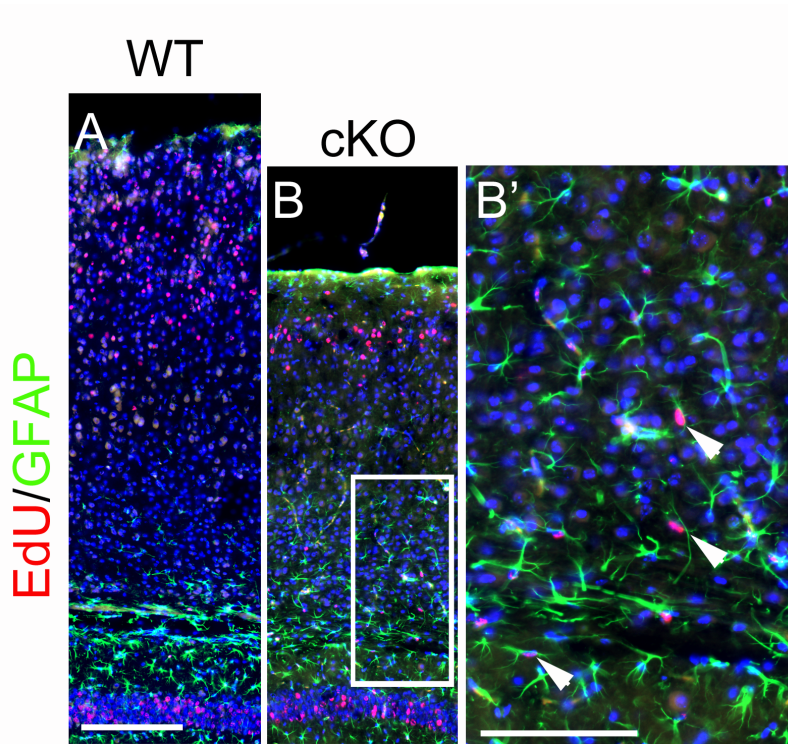


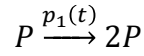
Figure S10 Precocious gliogenesis in *Lhx2* cKO cortices. Immunostaining for GFAP (green) and EdU (red) with DAPI staining (blue) on coronal sections of P15 WT and cKO cortices. EdU was injected at E17.5. (A) In WT, most of the EdU positive cells are located in the superficial layers. (B) In cKO, considerably fewer EdU positive neurons are in the superficial layers, and some EdU positive cells are found in the deep layers. (B') A higher magnification view of the inset in B. Many of the EdU positive cells in the deep layer in cKO cortices are GFAP positive glial cells. Scale bars, 100 μ m (A, B) and 50 μ m (B').

1.3 Theoretical calculation of the model

1.3.1 Specification of the Mode

The model we developed is based on reproducing the different divisions and differentiations that each progenitor cell undergoes during the developmental phase. We consider four main types of events, assumed to occur at random times with a rate that is function of time. In chronological order, these are:

- (i) The symmetric division of the progenitor cells that occur at early stages of cortical development, with an intensity $p_1(t)$



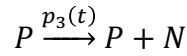
This is the unique phase associated with an increase of the number of progenitor cells. It constitutes the substrate upon which neurons and glia is formed, and therefore tightly regulates the size of the brain.

- (ii) Asymmetric division of a progenitor cell into IPC that subsequently divides and differentiates into two neurons



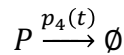
The neurons differentiate and are transported towards a layer that depends on the time of the division and differentiation.

- (iii) Asymmetric division of a progenitor cell into a progenitor and a neuron belonging to a specific layer depending on time (similarly to the division of the IP)



The probability $p_3(t)$ is the sum of the intensities of differentiation into the different layers $p_3^l(t)$ where l indicates the layer label ($l \in \{6, 5, 4, 2/3\}$).

- (iv) The last phase taking place in the process of cortical development is the loss of capacity to generate a neuron, that can either be related to the formation of glial cells or to apoptosis



where \emptyset indicates that a progenitor becomes inactive, in the sense

that it has lost its capacity to generate other progenitors and neurons: it gathers cell death and differentiation into glial cells.

1.3.2 Analytical Solution of the neurodevelopment problem

The system is simple enough to obtain be solved exactly as a function of the different functions $(p_1 \cdots p_4)$: we thus access to evaluations of the cortical surface and thickness as well as proportions of neurons in the different layers.

Maximal Number of Progenitors and Cortical Surface

Phases (i) and (iv) govern the number of active progenitor cells. Assuming that the initial number of progenitors P_0 at a time (denoted by convention $t = 0$) is known, we can therefore find the formula for the total number of active progenitors $P(t)$ at any time $t \geq 0$:

$$P(t) = P_0 \exp\left(\int_0^t [p_1(s) - p_4(s)] ds\right).$$

To fix ideas, considering the simplest case where p_1 (respectively, p_4) is constant during the period $t \in [0, T_1]$ of the symmetric division phase (respectively during the period $t \in [T_4^s, T_4^e]$ of loss of function of progenitor cells), we find for all time $t \geq 0$:

$$P(t) = P_0 \exp(p_1 [t \wedge T_1] - p_4 [t - T_4^s]_+)$$

where we use the notation $t \wedge T_1 = \min(t, T_1)$ and $x_+ = \max(x, 0)$. In particular, in the biological case in which $T_1 > T_4^s$, we find:

$$P(t) = \begin{cases} e^{p_1 t} & t \leq T_1 \\ e^{p_1 T_1} & T_1 \leq t \leq T_4^s \\ e^{p_1 T_1 - p_4 (t - T_4^s)} & t \geq T_4^s \end{cases}$$

The maximal value of the number of progenitors can easily be evaluated in all cases, and for instance in the case $T_1 > T_4^s$, the maximal number of progenitors is $P_{max} = P(T_1)$. This is hence an exponentially increasing function of the duration of the symmetric division phase. Even small fluctuations of the duration of the symmetric division phase have important effects on the cortical surface.

In that model, if it is found that the cortical surface is decreased (or increased) by a factor α , one can deduce in the simplest model that the duration of the symmetric division phase is

$$T_1' = T_1 + \frac{\log(\alpha)}{p_1}.$$

Number of Neurons in the Different Layers

Given the number of progenitors $P(t)$ and the neurogenesis intensities $p_3^l(t)$, we easily find that the number of neurons in layer l at time t is given by:

$$N_l(t) = \int_0^t P(s) p_3^l(s) ds$$

(a) Simple example: Gliogenesis arises after the end of neurogenesis:

Let us again provide a simple yet plausible example: if we assume that p_3^l is constant in time within a time window $[T_{3,l}^s, T_{3,l}^e]$ (of duration denoted $\delta t_3^l = T_{3,l}^e - T_{3,l}^s$) and moreover $T_1 \leq T_{3,l}^s < T_{3,l}^e \leq T_4^s$, we find that the neurons in layer l start appearing at time $T_{3,l}^s$ and evolve linearly in the time interval in which neurons of layer l are generated:

$$N_l(t) = P_{max} p_3^l (t - T_{3,l}^s)$$

for $T_{3,l}^s \leq t \leq T_{3,l}^e$. The total number of cells after cortical differentiation is hence given by $N_l = P_{max} p_3^l \delta t_3^l$. We conclude that the ratio between the number of neurons and the surface of the cortex is proportional to:

$$S = \sum_l p_3^l \delta t_3^l,$$

and the proportion of neurons in layer l given by $p_3^l \delta t_3^l / S$.

We thus note that in contrast to the very sensitive dependence of the cortical surface to the total time of the symmetric division, the cortical thickness is a linear function of the times of the different phases. Moreover, we note that the thickness and proportions of neurons in the different layers is independent of the duration of the

symmetric division phase and only depends on the parameters of the neurogenesis phase: relative durations and intensities of the generation of neurons in the different layers. In particular, provided that the neurogenesis intensity is known, we can easily find the duration of each phase given that we know the number of neurons in the different layers, which can indeed be evaluated experimentally. For instance if the proportions of the different neurons remain identical in the different layers but the surface is modified by a factor β , the only scenario, under the hypothesis that the whole phase of neurogenesis occurs after symmetric division and before gliogenesis, is that all durations δt_3^l are scaled by the coefficient β . But if the proportions of neurons in the different layers are changed, under the current assumptions, fine tuning of the duration of the differentiation in the different layers is necessary. We now consider the case where gliogenesis can occur as neurogenesis takes place.

(b) Symmetric division and gliogenesis can arise as neurogenesis takes place.

In the more biologically plausible situation in which neurogenesis takes place at the same time as symmetric division of progenitors and gliogenesis, we can again find analytic expressions for the number of layers in each neurons. For instance, one may assume (Model 4) that the duration of the neurogenesis is not affected, but gliogenesis takes place at an earlier time $T'_4 < T_4$. In order to compute explicitly the time T'_4 we can evaluate exactly the number of neurons under the assumption that the rates of differentiations are constant in time. While $t < T'_4$, the evaluations made in the case (a) apply: these provide the number of cells in the different layers generated prior to that time.

For instance, if $T_{3,l}^s < T_4 < t < T_{3,l}^e$ the number of neurons in layer l generated between T_4 and t is simply given by

$$N_l(t) - N_l(T_4) = p_3^l P_{max} \int_{T_4}^t e^{-p_4(s-T_4)} ds = P_{max} \frac{p_3^l}{p_4} [1 - e^{-p_4(t-T_4)}],$$

and if $T_{3,l}^s > T_4$, the number of neurons in layer l is given by:

$$N_l = P_{max} \frac{p_3^l}{p_4} [e^{-p_4(T_{3,l}^s-T_4)} - e^{-p_4(T_{3,l}^e-T_4)}].$$

If the proportions of cells in the different layers are decreased in an orderly manner, as is the case of the mutant considered, we can again solve the systems to find shrinkage of the neurogenesis phase and modifications in the gliogenesis phase.

1.3.3 Parameters fit

In order to specify the models in the case of constant division intensity, one only needs to adjust the start and end time of each phase. Based on the formulae obtained above, we can analytically choose parameters so that we reproduce a specific cortical surface, thickness and proportions of neurons in each layer. For the modifications of the scenario in the Mutant mice, we can reason as follows. We mentioned in the text an approximate halving of the number of neurons in superficial layers and a reduction of 40% in deeper layers. This points towards the following scenario

- i. The total number of progenitors created in the mutant mice is divided by two, which means that the progenitor symmetric division stops at a smaller time

$$T'_1 = T_1 + \frac{\log(0.6)}{p_1}. \text{ We denote by } \alpha = 0.6 \text{ the diminution of the number of}$$

neurons in the deeper layers.

- ii. In order to ensure that we obtain the proper reduction of the number of cells in the superficial layers, we consider that the neurogenesis starts competing with the loss of capacity to generate neurons at a time T^* occurring before the end of the generation of neurons in layer 4. We thus need to fix the rate at which neurons lose function and the time at which they start losing function. The rate μ is found by looking at the ratio between the number of neurons in the most superficial layers:

$$\gamma(\mu) = \frac{\alpha}{\mu(T_{2-3}^e - T_{2-3}^s)} \left[e^{-\mu(T_{2-3}^s - T^*)} - e^{-\mu(T_{2-3}^e - T^*)} \right]$$

and it is easy to see that this ratio reaches all values between 0 and 1 as μ goes from 0 to infinity, and this is a monotonically decreasing function. One therefore finds a unique μ satisfying this relationship for the proportions of neurons found in the most superficial layer. The last parameter to fix is T^* , the time at which gliogenesis starts. Again, we can solve this exactly in the model. Indeed, the ratio $\delta(y)$ of cells in layer 4 in the mutant and WT model is given by

$$\delta(y) = \alpha \left(y + \frac{1}{\mu'} (1 - e^{-\mu'(1-y)}) \right)$$

with $\mu' = \mu(T_{3,4}^e - T_{3,4}^s)$ and $y = \frac{T^* - T_{3,4}^s}{T_{3,4}^e - T_{3,4}^s}$. Since $y \mapsto \delta(y)$ is a strictly increasing map for $y \in [0,1]$ going from $\alpha/\mu'(1 - e^{-\mu'})$ at 0 to α at 1, we can therefore find a unique T^* as long as the proportions found experimentally are in this range, which is the case in our experiments in the main text.

1.4 Mathematical of neurogenesis based on progenitor potential drop

To fit the phenotype of *Nestin-cre; Lhx2* conditional knockout mice, we needed to accurately modify each time point of division transition. We were inspired by the published experimental data in the *Emx1-cre; Lhx2* conditional knockout mice, whereby when *Lhx2* is removed from neuronal progenitors one day in advance, progenitors change fate from lateral neocortex to piriform, leading to an expanded size of the olfactory cortex. Here, we move one step further. We modeled the switch from different type of divisions as an intrinsic property, so that the timing is generated by the cells themselves, and not prescribed by a timing function. To reproduce the fact that the progenitors undergo multiple typical divisions sequentially, we use an analogy with the dynamics of a noisy particle in a multi-well potential: as the particle progresses through this potential and falls in the consecutive wells, the progenitor cell transitions from proliferative to neurogenic to gliogenic divisions. This potential profile of progenitor cell is its intrinsic property. Progenitors are considered performing different types of divisions when they are trapped in the potential wells. Progenitors minimize locally their potential in the local wells. To allow progenitors to pass the transition state of the reaction hill, we added noise and broke symmetry including a constant force pushing the progenitor in the direction observed experimentally. Force is a positive constant value for each cell pushing the progenitors moving in one direction as progenitors lose the capacity with time. Noise is the stochastic parameter in the model. With a small noise, the division type of the progenitor evolves in one direction, like a ratchet. With a large noise, a progenitor can

switch back to its juvenile states and oscillate between two nearby states. Noise and force depend on the cell surrounding environment, such as the concentration of morphogens, which vary depending on cell position and timing. Using this new model, we demonstrate that only changing one parameter, force, is sufficient to reproduce the phenotype in *Nestin-cre; Lhx2* conditional knockout mice. Also this new model gives the possibility to explain the expanded size of the olfactory cortex observed in *Emx1-cre; Lhx2* conditional knockout mice.

1.4.1 Mathematical model of neurogenesis based on progenitor potential drop, expanding the original model to intrinsically generated timing only depending on a developmental “force” and noise

We have applied the model to explain the observation of a smaller and thinner cortex in the mutant mouse model *Nestin-cre; Lhx2* conditional knockout that *Lhx2* expression was depleted in the cortical progenitors from E11.5 (Hsu et al., 2015). We simulate the sequence of divisions of progenitors during cortical neurogenesis, considered the symmetric proliferative progenitor divisions, asymmetric neurogenic divisions and gliogenesis in the end. The probability of each division is a fixed curve as function of time. Here, we move one step further. We model the switch from different type divisions as a potential drop (figure 9-1).

$$U = (|x| - u)^2 (|x| > u) - \sum_{i=1}^4 \alpha_i \exp\left(-\frac{x - \beta_i}{\gamma_i}\right)^2 - x * slope$$

This potential profile of progenitor cell is its intrinsic property. Progenitors are considered as performing different types of divisions when they are trapped in the potential wells, in the sequence of (1) symmetric proliferative division into 2 progenitors; (2)-(5) asymmetric neurogenic division generating a layer 6/5/4/2/3 neuron and keep a progenitor; (6) gliogenesis (figure 9-2). Progenitors minimize their potential in the local wells. To allow progenitors to pass the transition state of the reaction hill, we add noise and force in the model. Force is a positive constant value for each cell pushing the progenitors moving towards one direction as cell maturation. Noise is the stochastic parameter in the model. With a small noise, the division types of the progenitor evolve with one direction, like a ratchet. With a large noise, a progenitor has the possibility to switch back to its juvenile states and intermingle the

two separate states. Noise and force are the parameters depending on the surrounding environment of cells, such as the concentration of morphogens, which vary with cell position and timing.

The state of the progenitor within this potential is thus given by the stochastic equation (Itô, or Langevin equation):

$$X_{t+1} = X_t - (U_{X_{t+dx}} - U_{X_t}) + \text{force} + \text{noise}$$

$$dX_t = (-\nabla U(X_t) + \text{Force})dt + \sigma dW_t$$

where U is the potential, ∇ is the gradient operator, Force is the constant positive force, σ controls the level of noise, considered to be a white noise (ie, W_t is a Brownian motion).

In this setting, contrasting with the model in publication I, we do not impose a timing. Instead, time is scaled depending on the step cost to transition between the potential wells, which is proportional to the activation energy, and inversely proportional to the driven force. Figure 9-3 plots how the number of progenitors and neurons in L6, L5, L4 and L2/3 evolves as a function of the neurogenesis time. Due to the noise, the transition time points between division states vary. Collectively, we observed a mix of division types, thus a rate (or probability) for each division type, as in the previous model, that varies in time (figure 9-4).

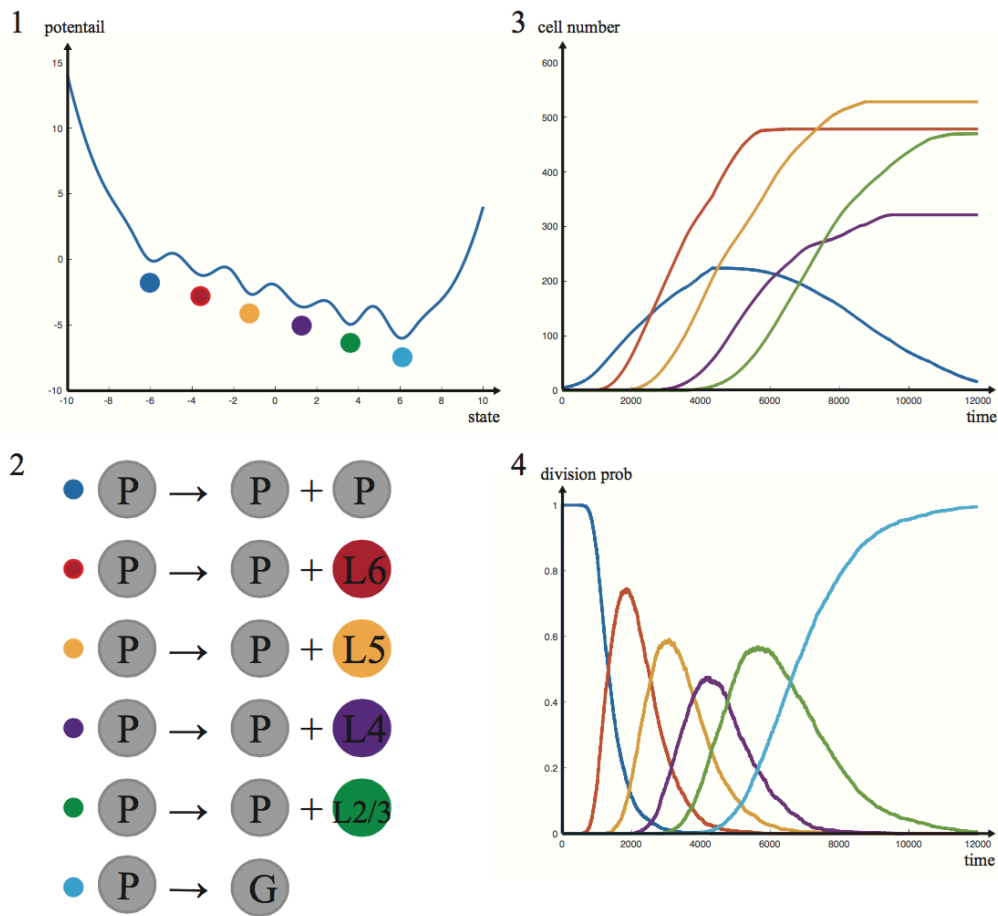


Figure 9. 1. An example of potential curve. Progenitors perform different types of division when trapped inside different wells. 2. Types of divisions progenitors perform. 3. Evolution of the number of RG progenitors (blue line) and number of neurons in each layer as a function of time (red for layer 6, yellow for layer 5, purple for layer 4 and green for layer 2/3). 4. The probability of different divisions and differentiations. In all MUT models, neurons die from E11 to E14 (black dashed line) and RGs precociously differentiate into 2 IPs (yellow dashed line). Three different mutant scenarios are schematically described below with the proportion and number of divisions performed by IPs as a function of time.

1.4.2 Fit to extensive data in WT (– in particular, extends to new data on piriform cortex and entorhinal cortex)

The potential curve is

$$U = (|x| - u)^2 (|x| > u) - \sum_{i=1}^4 \alpha_i \exp\left(-\frac{x - \beta_i}{\gamma_i}\right)^2 - x * slope$$

with parameters:

$$u = 7; \alpha_i = 4 (i = 1,2,3,4); \beta_1 = -6; \beta_2 = -2; \beta_3 = 2; \beta_4 = 6; \gamma_i = 2 (i = 1,2,3,4)$$

$$slope = 0.5$$

parameter for WT V1 data: noise = 0.025 and force = 0.002.

parameter for piriform data: noise = 0.07 and force = 0.003.

parameter for entorhinal cortex data: noise = 0.08 and force = 0.003.

1.4.3 Analysis of mutant model leads to predictions of abnormal timing of neurogenesis.

In the PNAS paper, we used the previous model based on division probability to explain the smaller and thinner cortex observed in Lhx2 conditional knockout mice (Hsu et al., 2015). To fit the phenotype of precocious neurogenesis, we adjusted the start and end time points of each division type. Here, with new potential model, we change only the force parameter but not the potential curve to reproduce the same division probability curve as the old model. Thus, the number of neurons evolves as the phenotype in mutant mice. With a larger driven force, the whole neurogenesis program is shifted forward including an early initiation of gliogenesis during the end neurogenesis phase (figure 10), which is exactly identical as what we imposed in the original model.

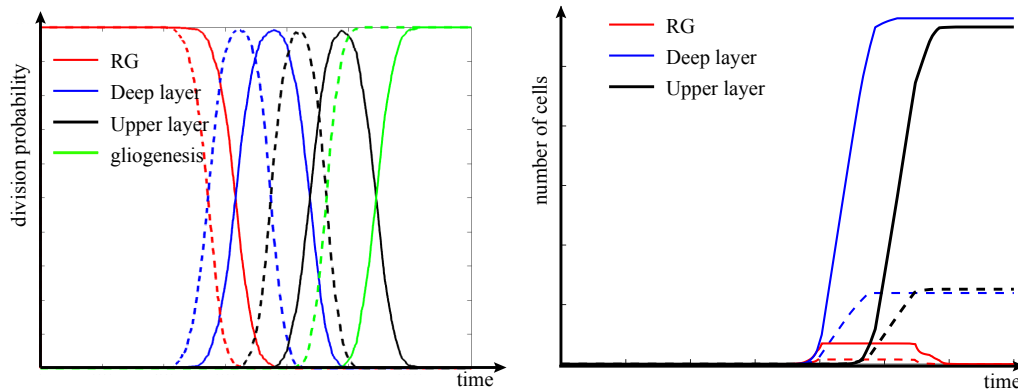


Figure 10. Influence on neurogenesis of the parameter ‘force’. Increase the parameter force significantly advances the whole program of neurogenesis. The shift is not with the same intervals. The early time point shifts less and the later time point, the starting point of gliogenesis, advances more. The number of RG and neurons in both deep and upper layer decreases.

In contrast, with a smaller driven force, the switch from symmetric to asymmetric division is delayed. The number of progenitor cells is precisely controlled by the duration and probability of symmetric divisions as an exponential function. Small delay of this switch is sufficient for causing a massive expansion of cortex size. This corresponds to the observation in the mutant mice overexpressing activated beta-catenin (Chenn & Walsh, 2002). In these mutant mice, the authors observe 25% less cell exits from symmetric division, which leads to a significant increase of number of progenitor cells thus an increased cerebral cortical surface area.

1.4.4 A simple gradient of force explains the differences in the phenotype of different brain areas according to their observed timing.

Pyramidal neurons in same layer are not generated synchronously across the entire neocortex. The onset and duration of layer formation differs along the rostral-caudal and lateral-medial axis in the neocortex. This difference is mainly due to progenitor cells being exposed to distinct morphogen gradient concentrations depending on the distance from cortical patterning center (Caviness, Nowakowski, & Bhide, 2009; Machon et al., 2007). This timing difference results in a cortical plate thickness

gradient: rostral-medial thick, caudal-lateral thin (Polleux, Dehay, & Kennedy, 1997). Here, we proposed a 2D model to reproduce this neurogenesis gradient. In the model, we considered all progenitor cells to share the same potential profile. The morphogen concentrations only modify the ‘force’ parameter. With high value of ‘force’, the progenitors accelerate the transition between potential wells. With the gradient of one parameter, we could reproduce the thickness difference in the different regions of the neocortex, meanwhile keeping the proportion of neuron number in each layer untouched (figure 11).

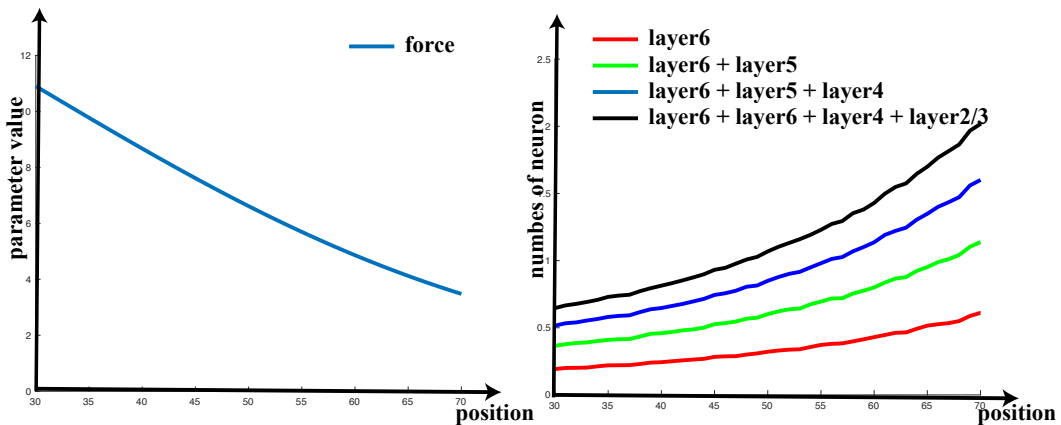


Figure11. A 2D model of neurogenesis gradient. With a special gradient of parameter ‘force’, this model can be extended to 2D to reproduce the cortex rostral-medial thick, caudal-lateral thin gradient.

Modification of the parameter ‘force’ to fit the thickness gradient in WT mice corresponds to the modification for mutant mouse models in last chapter. Lhx2 mRNA expression level shows a rostral-low/ caudal-high gradient at E11.5 in WT mice. This low concentration of lhx2 in the beginning of neurogenesis results in neurogenesis starting earlier in the rostral region. Same as lhx2 knockout mice, large ‘force’ has a consequence of precocious neurogenesis. This corresponds to the result described in 1.2.3.

1.4.5 Explaining in detail the timing of piriform cortex and entorhinal cortex generation.

The model could be expanded to explain the entorhinal cortex and piriform cortex generation. We collected data of neuron layer distribution at P7 of experiment of EdU injection at E11.5, E13.5, E15.5 and E17.5 in the entorhinal cortex. Entorhinal cortex shows similar layer organization and inside-out neuron generation order as the neocortex. However, the whole neurogenesis program is shifted early, starting before E11.5 and ending around E15.5. Also, neurons generated at the same time point disperse in two or three adjacent layers, requiring not only a large ‘force’ to accelerate the neurogenesis program, but also a larger noise to mix the neuron in different layers (Figure 12 Comparing neocortex-entorhinal).

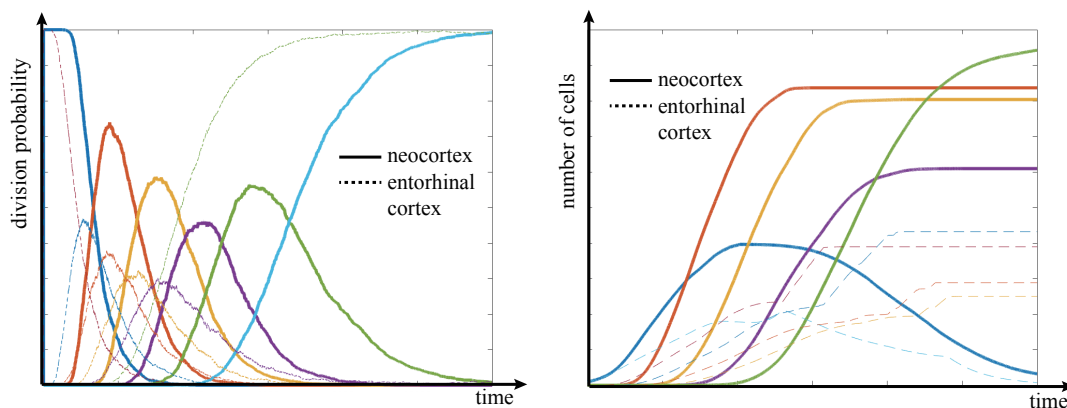


Figure 12. Difference between neocortex and entorhinal cortex. Increase the parameter force and noise significantly advances neurogenesis and change the ratio of neuron number in each layer, which describes perfectly the development of entorhinal cortex.

For the piriform cortex, neurons are organized in three layers. We consider only the progenitor division without regard to migration. There are two possible explanations of the three-layer phenotype: 1) progenitor cells pass by the symmetric division and the first three layers neurogenic division and stop in the fourth well; 2) progenitor

cells pass all through the neurogenesis program, but the layers are less well separated. We prefer the second hypothesis, as both upper and deeper neocortical layer markers are expressed, but in different manners in the three-layer piriform cortex. *Cux1*, as an upper layer marker in the neocortex, stains specific L4 and L2/3 but was detected in layers 2b and 3 in the piriform cortex. *Ctip2* is selectively expressed in neurons of L6 and L5 in the neocortex but was detected throughout the cell layers (Brunjes & Osterberg, 2015; Diodato et al., 2016). We collected cell number count at P21 of the piriform cortex. Compared to neocortex, there are 55% less cells in each column unit. Neurons are generated precociously. Most neurons are generated before E13. In addition, neurons generated at one time points are less well restricted to specific layers (Martin-Lopez et al., 2017). The piriform cortex and entorhinal cortex have different layer organization, however if we neglect the migration and only consider progenitor divisions, neuronal marker expressions are similar. They are both thinner and have less neuron number per column unit. The neurogenesis durations are shorter. The cause of this observation may be that both piriform and entorhinal cortex locate at the border of cerebral cortex and receive less accurate position information from patterning center.

Lhx2 is a timing and positioning cue in cortical development. We have described precocious neurogenesis observed in the mutant mice depleted of *Lhx2* from progenitor cells from E11.5 in *Nestin-cre; Lhx2* conditional knockout. If *Lhx2* is removed from neuronal progenitors one day in advance in the *Emx1-cre; Lhx2* conditional knockout mice, progenitors change fate from lateral neocortex to piriform, leading to an expanded size of the olfactory cortex. These two phenotypes caused by removing *Lhx2* expression with only one-day difference. Our model explains both observations. All progenitors share an identical potential profile.

2. Discussion

During the mammalian embryonic development, a specific pool of progenitors undergoes a precise sequence of divisions, differentiations and migrations leading to the emergence of the cells that constitute eventually the cerebral cortex. In this chapter, we first investigate theoretically the parameters governing the timing of the

spatio-temporal proliferation and differentiation of progenitor cells. To account for these observations and a variety of additional data from the literature, we have built a parsimonious mathematical model describing the sequence of divisions of progenitors during neurogenesis. The parameters of the model were fit with experimental data reported in the literature that we completed with data collected in our laboratories. We have applied this model to theoretically account for mutant mice phenotypes developed in our laboratories or by collaborators. The model simply emulates the sequence of divisions and differentiations as a function of time. It thus allows testing assumptions on the impact of neurogenesis timing on brain anatomies, which we did on mutant mice.

Small cortex phenotype: In collaboration with Dr. Chou (Academia Sinica, Taipei), we studied a new mutant mouse model where another homeodomain transcription factor, *Lhx2*, was eliminated in progenitors at a specific time. The mice displayed a significantly smaller and thinner cortex, with six cortical layers sequentially generated but abnormal proportions of neurons in each layer. The mathematical model allowed inferring the temporal modifications of the neurogenesis program, and pointed towards a shorter duration of progenitor proliferative divisions and of the neurogenesis phases, as well as an early loss of ability of progenitors to generate neurons, observations that were validated experimentally

In the second model, we considered the switch from different type of divisions as an intrinsic property, so that the timing is generated by the cells themselves. Much like the dynamics of a noisy particle in a multi-well potential, we model the progression of the progenitor cell transitions from proliferative to neurogenic to gliogenic divisions. In this metaphor, a constant force parameter pushes the particle through the potential, corresponding to the maturation of brain. Using this new model, only changing one parameter, force, is sufficient to reproduce the phenotype in *Nestin-cre; Lhx2* conditional knockout mice. Also, this new model allowed us to explain theoretically how different layer structures are generated in cortical areas, especially to explain the expanded size of the olfactory cortex observed in *Emx1-cre; Lhx2* conditional knockout mice.

This model is parsimonious; however, it is easy to implement more parameters in the

model. For example, we refined the model to include an additional population of progenitors, the IPs, and modeled their proliferative divisions and cell cycle, in collaboration with Dr. Pierani (IJM, U. Paris Diderot). This refinement was crucial to better understand mechanisms of neural loss compensation observed in a mutant mouse model which displayed an important neuronal death until mid-neurogenesis compensated for at the end of neurogenesis (same number of neurons but distinct repartition per layer: early born deeper layer neuron are compensated by superficial layer neuron). This is described in detail in the next chapter.

Our model can be also simply adapted to study cortical evolution. We have showed that the RGs cell number, which is crucial for the cortical surface expansion, is very sensitive to the duration of RGs symmetric proliferative division and gyrification of the brain (Barton & Harvey, 2000; Clark, Mitra, & Wang, 2001; Finlay & Darlington, 1995). The number of RGs increases exponentially when the end of proliferative division and beginning of neurogenic division is postponed. Also, in our model, the IPs have a very limited proliferation potential, with maximum two time symmetric division capacity. Increasing of the IPs proliferative division capacity has been proven to participate in the expansion of brain size in primates. During evolution the emergence of another type of progenitor, outer radial glial cells, has also been proposed to contribute to the expansion of cortical size during cortical evolution; the model could easily incorporate this population and reproduce their proliferative divisions and their generation of IPs (Betizeau et al., 2013; Fietz et al., 2010; Florio & Huttner, 2014).

Chapter III: Modeling the cell death and neurogenesis homeostasis

1. Introduction

1.1 Cell death during development

Neurogenesis, the process of cell division and differentiation leading to the formation of the brain, is a critical process for animal survival. The surface of the cortex, the number of neurons in each column and proportion of neurons in the distinct layers are precisely regulated during neurogenesis and failures may lead to often lethal abnormal brain phenotypes (macro or microcephalies, abnormal repartitions of neurons in the distinct layers). Programmed cell death (PCD) plays an important role in the development of the CNS. Cajal-Retzius cells, cortical plate transient neurons, the first wave of oligodendrocyte precursors and subplate cells are almost completely eliminated whereas cortical interneurons and glutamatergic projection neurons are subjected to partial elimination (figure 13) (Causeret, Coppola, & Pierani, 2018; Nijhawan, Honarpour, & Wang, 2000). PCD is not a negative process for neurogenesis, as it plays a potential role in optimization of synaptic connections and removal of unnecessary neurons (Burek & Oppenheim, 1999).

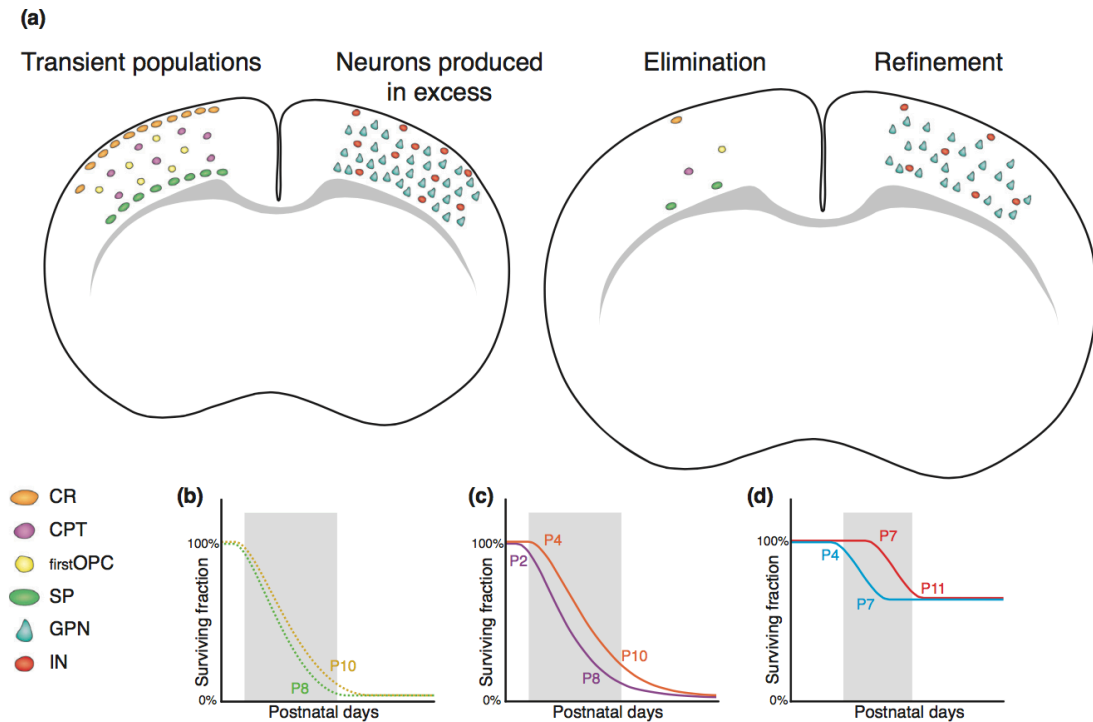


Figure 13. Cell populations subjected to postnatal developmental death. (a) Cajal-Retzius cells (CRs, orange), cortical plate transient neurons (CPTs, purple), the first wave of oligodendrocyte precursors (firstOPCs, yellow) and subplate cells (SPs, green) are almost completely eliminated whereas cortical interneurons (INs, red) and glutamatergic projection neurons (GPNs, blue) are subjected to partial elimination. (b)–(d) Extrapolated temporal windows of cell death and dynamics of disappearance of these populations are indicated with the same color code. Subtle differences might exist between populations, however they all undergo cell death within the first two postnatal weeks. Dashed lines for SPs and first OPCs indicate the absence of a precise time course. Adapted from Causeret et al., 2018.

Once a cell has made the decision of death, it activates molecules which trigger signaling cascades. PCD is a critical process and the slightest dysregulation in its cascades can have disproportionately far-reaching effects in an organism resulting in developmental defects if not embryonic lethality. In adults, PCD imbalance can be the reason behind a number of pathologies as will be described in later sections. For this reason, PCD is the subject of multiple modes of tight regulation mediated by the

means of gatekeeper molecules which are present at various stages of progression of PCD cascades.

PCD is normal and important process during nervous system development but is abnormal in brain and spinal cord disease and injury. Pathological cell death caused by traumatic brain injuries happens during embryonic development. Most of traumatic brain injuries are strongly related to alcohol intoxication (Weil & Karelina, 2017). Neuroinflammation and virus infection during pregnancy also possibly lead to neuronal loss. Necrosis can be resulted from acute oxidative stress. Apoptosis can be induced by DNA damage, cell surface receptor engagement and growth factor withdrawal (Martin, 2001).

1.2 Regulation of neuronal homeostasis after cell death by feedback from post-mitotic neurons

To regulate the number of neurons and proportion in each layer during development, the proliferation/differentiation of progenitor cells and the neuronal identity adopted by the progenitor cells are precisely regulated. This regulation includes intrinsic signals and extrinsic signals. Here, we mainly discuss the extrinsic signals from the environment influence the proliferation/differentiation of the progenitor cells during neurogenesis regulating the neuronal homeostasis after cell death. Many extrinsic signals are capable of influencing the progenitor proliferation and mitotic neuronal compartment such as cerebrospinal fluid, blood vessels, microglia cells, thalamic afferents and differentiated neurons (Taverna, Götz, & Huttner, 2014).

In 2001, Morrow and colleagues firstly suggested that post-mitotic neurons were able to modify the behavior of progenitors. Using progenitor culture techniques on slices, researchers have been able to show that progenitors in different developmental stages environments behave differently: the progenitors give rise to neurons during embryonic development while the same progenitor cell culture on postnatal cortex slices produced glial cells and not neurons. This first study suggests that differentiated neurons are able to regulate the behavior of progenitor cells via FGF2 and CNTF (Morrow, Song, & Ghosh, 2001). Another study subsequently showed that cortical neurons *in vitro* culture synthesized and secreted a neurotrophic cytokine cardiotrophin-1 important for the transition from neurogenesis to gliogenesis

(Barnabé-Heider et al., 2005). The first *in vivo* evidence that neurons have a feedback control function on progenitors dates back to 2009. Researchers have shown that loss of *Sip1* gene function in newly generated neurons induced early transition from deep layer to superficial layer neuron generation and also induced precocious gliogenesis. The fact that the only loss of Sip1 function in post-mitotic cells is sufficient to change the fate of progenitor cells, led the researchers to hypothesize that Sip1 regulates the expression of a secreted factor in young neurons that would have a function in determining the cell fate of the progenitor cells and the number of different subtypes of neurons generated by these progenitors (Seuntjens et al., 2009).

Other study by Toma, K. has supported the role of the post-mitotic compartment on the proliferation of progenitor cells. Using genetically engineered mice, researchers have shown that a massive death of deep-layered neurons in the early neurogenesis stage results in compensation of deep layer neurons at the expense of reduced upper layer neurons, keeping the proportion of deep and upper layer neuron number untouched. This study suggests that later born upper neuron generation is only started if deep layer neurons are generated and survive. There is therefore a feedback control from deep layer neurons in post-mitotic compartment that make it possible to generate neurons of the upper layers (Toma, Kumamoto, & Hanashima, 2014).

GABAergic interneurons also participate the regulation of cortical progenitor behavior. They secrete the neurotransmitter GABA during tangential migration into the cortex. GABA receptors are expressed by RG progenitors during development indicating a role of GABA regulation. The level of GABA regulates progenitor DNA synthesis (LoTurco, Owens, Heath, Davis, & Kriegstein, 1995). Another study has shown that GABA has different effects on these two types of progenitors: it promotes the division of APs and inhibits the division of BPs (Haydar, Wang, Schwartz, & Rakic, 2000).

1.3 Several predictions of mathematical model of compensation

In both mutants, only a part of the measurements of neurogenesis parameters is published. We therefore had to infer those missing parameters based on observed phenotypes and combining the experimental observations reported in both papers

within a single model and using the same set of parameters, and the resulting model reproduced all published data for both mutants. These parameters thus provide us with predictions that could be confirmed experimentally by measuring:

- (1) the number of IPs at E15.5 in Mut1, to check whether there is a significant increase compared to WT as predicted by the model
- (2) The IPs cell cycle duration, which is predicted to be shortened in Mut1
- (3) The slight deep to upper layer neuron generation switching time point, predicted to be delayed in Mut2.

2. Methods

In order to investigate the mechanisms supporting compensation in the face of embryonic cell death, we used a parsimonious mathematical model of the sequence of cell divisions from a progenitor population (Hsu et al., 2015). The model emulates the various phases of neurogenesis through time-dependent rates of divisions of progenitor cells during the neurogenesis phase. As highlighted in Freret-Hodara et al., 2016 using both a mathematical model and confirmed experimentally, regulation mechanisms in the mouse neocortex cannot rely only radial glial progenitors (RGs) divisions, but may involve a transient population of progenitors, the intermediate progenitors (IPs). Based on the original model, we consider detailed parameters of IPs including the IPs cell cycle duration, probability of IPs performing proliferative division and the numbers of IPs proliferative divisions before neurogenic division.

Based on classical biological evidence, both neurons and IPs are generated from an initial pool of RGs, through the following divisions or differentiations:

- (1) Symmetric proliferative divisions that produce two RGs.
- (2) Asymmetric divisions into one RG and one IP.
- (3) Asymmetric neurogenic divisions into one RG and a neuron.
- (4) Symmetric divisions into two IPs.

(5) Loss of capacity to generate neurons (e.g., gliogenesis).

Once an IP is generated, it will itself undergo 2 types of divisions or differentiations:

(6) Symmetric proliferative divisions to produce 2 IPs.

(7) Symmetric neurogenic divisions giving 2 neurons.

Proliferative divisions of IPs (6) are relatively rare, and we will thus limit their number to 2.

Neurons created by RGs (division 3 and 4) or by IPs (division 7) are assumed to migrate to upper or deep layers with a probability depending on their birthdate. Similarly, the rate at which each division occurs is a function of time. The system is thus fully defined once the time-dependent rate of each division is fixed. In order to evaluate those parameters for WT mice, we used data reported in the literature or that we measured (Gao et al., 2014; Hsu et al., 2015).

The initial number of RGs is not critical, as it only acts as a linear scaling parameter. In this study, we started with an initial progenitor pool of $RGE8 = 50$. The total number of RGs division within each $\Delta t = 0.1$ is inversely proportional to RG cell cycle TRG. Consistent with experiments (Manuel, Mi, Mason, & Price, 2015), we have considered that TRG varies in time, and linearly increases during cortical development (Takahashi et al. 1995; Calegari and Huttner 2003; Dehay et al. 2015; Manuel et al. 2015). With experimental data we collected from experiments and found in the literature of the mouse neocortex during development in wild-type, we fitted the shape of the potential curve of all progenitor cells and the force and noise of progenitor cells in the neocortex, based on the rate of divisions the potential generates.

(1) RG cell cycle duration

Cell cycle duration of RGs has been measured by several research groups (Federico Calegari, J.Neuroscience, 2005; Arai Y, Nature Communication 2011; Freret-Hodara B, Cereb Cortex. 2017). It varies in different brain areas and lengthens linearly through development (Mi et al., 2013). Also, the cell cycle duration depends on the type of divisions: around 20% longer for neurogenic divisions than proliferative

divisions (Federico Calegari, J.Neuroscience, 2005). We considered the average values from the literature. $CCDRG(E10.5)=11h$, $CCDRG(E14.5)=17h$. As the increase is linear, $CCDRG(t)=1.5t-4.75$.

(2) Probability of keeping proliferative symmetric divisions over differentiation into neurogenic asymmetric divisions

RGs perform proliferative symmetric divisions into two RGs to maintain the progenitor pool. The duration of this period influence the number of RGs exponentially, and this significantly changes the brain surface. From E11, RGs start neurogenic asymmetric divisions for neuron generation directly or through IPs. Neurogenic asymmetric divisions compete with RGs proliferative divisions. The percentage of RGs performing proliferative symmetric divisions decreases rapidly between E10-E12. It has been measured using the MADM method (Peng Gao, Cell, 2014): the percentage of RGs performing proliferative symmetric divisions is 85%, 40%, 20% at E10, E11, E12 respectively.

(3) Fit cell number of RG and N with time

Cell numbers of RGs (marker Pax6+), IPs (marker Tbr2+), neuron in deep layer neurons (marker Tbr1+ and Ctip2+) and upper layer neurons (marker Brn2+) per unit length (CPL) are counted and the lengths of apical membrane at the ventricle are measured E11.5, E15.5, E18.3 and P0 (Figure 14A).

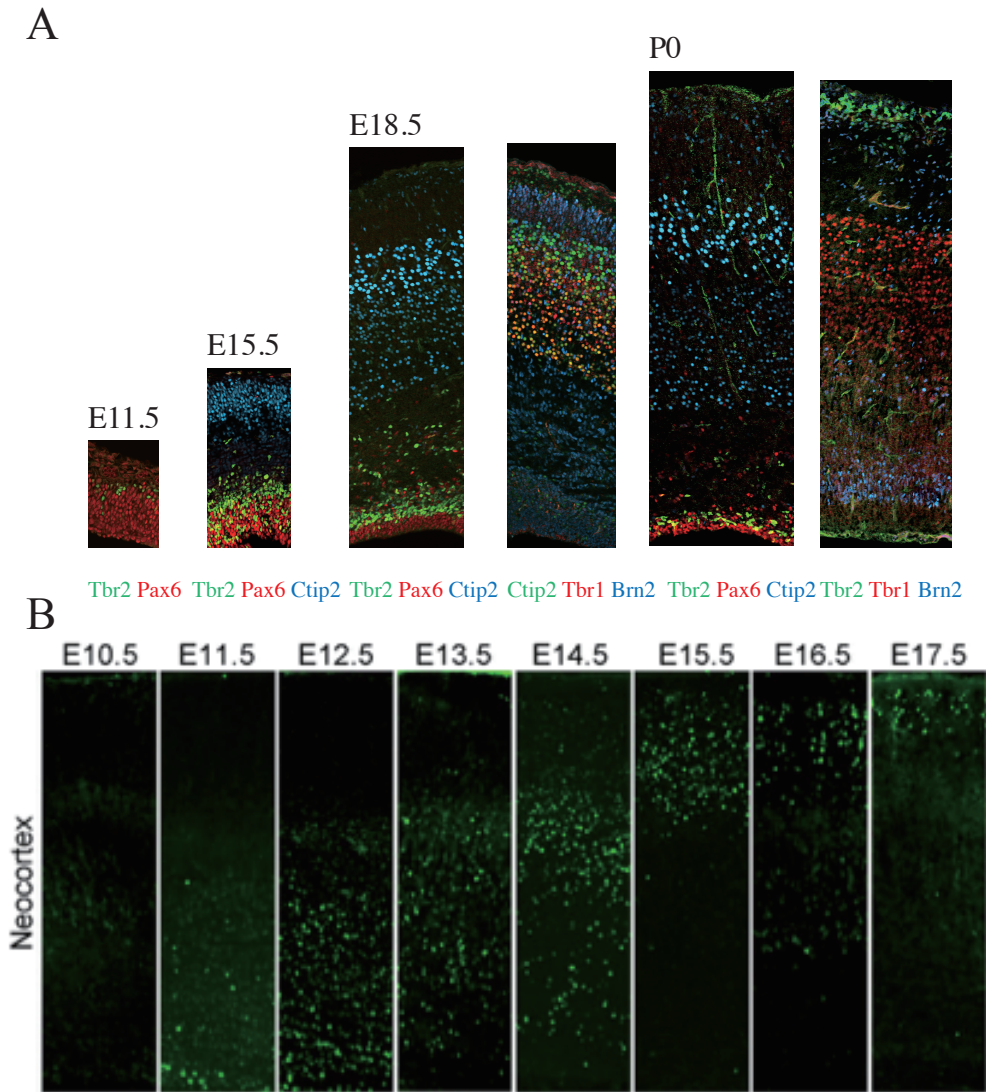


Figure 14. (A) Confocal scanning of coronal sections of the dorsal telencephalon at E11.5, E15.5, E18.5 and P0. Immunostaining with antibodies against Pax6 as marker to count RGs, Tbr2 as marker for IP), Ctip2 and Tbr1 as markers for deep layer neurons, Brn2 as markers for upper layer neurons. (B) BrdU was injected into pregnant mothers at E10.5, E11.5, E12.5, E13.5, E14.5, E15.5, E16.5 and E17.5 respectively. The distribution of BrdU positive cells are examined at P7. BrdU injected at E11.5 labeled neurons distributed in the subplate in WT mice. BrdU injected at E12.5 and E13.5 labeled neurons concentrated in deep layers. BrdU

injected at E14.5 labeled neurons concentrated in mainly deep layers but also upper layer. BrdU injected at after E15.5 labeled neurons concentrated in upper layers. (B) Images from Dr. Chou.

(4) Switch timing between making different layer neurons

Neuron layers are formed follow an inside-out sequence. The switch time points from making different layer neurons in the model are fitted with postnatal (P7) distribution of BrdU positive cells labelled during the neurogenesis period, respectively at E10.5, E11.5, E12.5, E13.5, E14.5, E15.5, E16.5 and E17.5 (figure 14B).

(5) Gliogenesis

RGs lose neurogenesis capacity by either symmetric neurogenic division into two neurons or gliogenesis. The first glia cells appear during development in the mouse cortex at E17 (Qian et al., 2000). A MADM study has shown that only one in six of neurogenic RGs ends into gliogenesis (Gao et al., 2014).

3. Results

3.1 Publication II



ORIGINAL ARTICLE

Enhanced Abventricular Proliferation Compensates Cell Death in the Embryonic Cerebral Cortex

Betty Freret-Hodara¹, Yi Cui^{1,2,3}, Amélie Griveau^{1,4}, Lisa Vigier¹, Yoko Arai^{1,5}, Jonathan Touboul², and Alessandra Pierani¹

¹Institut Jacques Monod, CNRS UMR 7592, Université Paris Diderot, Sorbonne Paris Cité, 15 Rue Hélène Brion, 75205 Paris Cedex, France, ²Center for Interdisciplinary Research in Biology (CIRB)—Collège de France and INRIA Paris, EPI MYCENAE, 11, Place Marcelin Berthelot, 75005 Paris, France, and ³Ecole Doctorale Cerveau Cognition Comportement (ED3C, ED n°158), Université Pierre et Marie Curie, 7 Quai Saint Bernard, 75005 Paris, France

⁴Present address: University of California San Francisco, Eli and Edythe Broad Center of Regeneration Medicine and Stem Cell Research, San Francisco, CA 94143-0525, USA

⁵Present address: INSERM U-1141, Robert Debré University Hospital, 48, Bld Séurier, 75019 Paris, FRANCE
Address correspondence to Alessandra Pierani, Institut Jacques Monod, Bâtiment Buffon 516B, 15 rue Hélène Brion, 75205 Paris Cedex 13, France.
Email: alessandra.pierani@ijm.fr

B.F.H. designed and performed the experiments, Y.C. and J.T. developed and analyzed mathematical models, A.G. analyzed the phenotype of mouse mutants at the initial stage of the project and provided advises, Y.A. designed cell cycle experiments and analyzed cell cycle data, L.V. helped for the animal maintenance. A.P supervised the project and analyzed data. B.F.H, Y.C., J.T., and A.P. wrote the article. All authors edited the article.

Abstract

Loss of neurons in the neocortex is generally thought to result in a final reduction of cerebral volume. Yet, little is known on how the developing cerebral cortex copes with death of early-born neurons. Here, we tackled this issue by taking advantage of a transgenic mouse model in which, from early embryonic stages to mid-corticogenesis, abundant apoptosis is induced in the postmitotic compartment. Unexpectedly, the thickness of the mutant cortical plate at E18.5 was normal, due to an overproduction of upper layer neurons at E14.5. We developed and simulated a mathematical model to investigate theoretically the recovering capacity of the system and found that a minor increase in the probability of proliferative divisions of intermediate progenitors (IPs) is a powerful compensation lever. We confirmed experimentally that mutant mice showed an enhanced number of abventricular progenitors including basal radial glia-like cells and IPs. The latter displayed increased proliferation rate, sustained Pax6 expression and shorter cell cycle duration. Altogether, these results demonstrate the remarkable plasticity of neocortical progenitors to adapt to major embryonic insults via the modulation of abventricular divisions thereby ensuring the production of an appropriate number of neurons.

Key words: abventricular proliferation, cell death, compensation, embryonic cerebral cortex, upper layer neurons

Introduction

Brain injuries due to neuronal death during embryonic development are caused by intrauterine infection/inflammation and hypoxia and represent major causes of cortical function

abnormalities and microcephaly (Rees et al. 2011). In the developing mouse cerebral cortex, excessive cell death due to gene mutations or cell ablation, including that of deep layer neurons (Toma et al. 2014), have mostly been correlated with a reduction

of cortical neurons (Rajaii et al. 2008; Borello et al. 2014). Conversely, it has also been reported that traumatic brain injury (TBI) (Conti et al. 1998) influence adult neurogenesis by increasing proliferation of neural stem and progenitor cells in the sub-ventricular zone (SVZ) of the lateral ventricle and in the dentate gyrus of the hippocampus (Gao et al. 2009; Sawada and Sawamoto 2013; Sun 2014). Furthermore, dying cells have been suggested to release signals that influence surrounding tissue by either triggering regeneration or promoting additional apoptosis in different model systems (Fuchs and Steller 2015). However, whether early neuronal death can be rescued in the developing cerebral cortex is still unknown.

In the neocortex, cortical neurons migrate out from the proliferative zones to form 6 neuronal layers in an inside-out manner so that early-born neurons form deep layers and late-born neurons upper layers (Angevine and Sidman 1961; Rakic 1972, 1974). The generation of a precise number and subtype of cortical neurons depends on a tight spatial and temporal control of distinct progenitor pools and their proliferation/differentiation rates. In the mouse cerebral cortex, 2 main types of neural progenitor cells exist during development, radial glial cells (RGs), and intermediate progenitor cells (IPs) (Haubensak et al. 2004; Englund et al. 2005; Götz and Huttner 2005). RGs divide at the apical side of the ventricular zone (VZ) and give rise to RGs, neurons, or IPs (Haubensak et al. 2004; Miyata et al. 2004; Noctor et al. 2004). IPs undergo self-consuming divisions in the SVZ generating the vast majority of cortical neurons. In mice, very few IPs go through 1 or 2 proliferative divisions before terminal mitosis (Noctor et al. 2004; Attardo et al. 2008; Arai et al. 2011; Wong et al. 2015). In mammals, the number of neurons, and, in particular, upper layers neurons, is amplified by an additional type of progenitor, the outer RGs (oRGs) (also known as basal RGs [bRGs]). Originally described as specific to ferrets and primates, oRGs (Fietz et al. 2010; Hansen et al. 2010; Pilz et al. 2013) are now known to be present in low numbers also in the intermediate zone (IZ) of the mouse (Shitamukai et al. 2011; Wang et al. 2011). Both cell intrinsic and extrinsic factors regulate the generation and proliferation properties of cortical progenitors (Dehay and Kennedy 2007; Taverna et al. 2014). While cell intrinsic changes of cell cycle parameters in neural progenitor cells primarily influence the production of neurons (Calegari et al. 2005; Dehay and Kennedy 2007; Lange et al. 2009; Pilaz et al. 2009; Arai et al. 2011), growing evidence also shows a contribution of the postmitotic compartment in controlling neurogenesis through a feedback signaling on progenitor cells (Seuntjens et al. 2009; Griveau et al. 2010; Teissier et al. 2012; Parthasarathy et al. 2014; Toma et al. 2014).

Here, we show that massive cell death in the postmitotic compartment during early cortical development promotes the generation of proliferative IPs and bRGs-like and, ultimately, leads to an increase in the number of upper layer neurons at the end of gestation recovering for the number of lost neurons in deep layers. These results indicate that compensatory mechanisms exist in the mouse developing cortex to rescue early neuronal loss and suggest that the proliferative properties of RGs and IPs are modulated by signals produced by dying cells or of cell density in the postmitotic compartment.

Materials and Methods

Ethics Statement

All animals were handled in strict accordance with good animal practice as defined by the national animal welfare bodies, 70

and all mouse work was approved by the Veterinary Services of Paris (Authorization number: 75-1454) and by the Animal Experimentation Ethical Committee Buffon (CEEA-40) (Reference: CEB-34-2012).

Mouse lines

Dbx1^{loxP-stop-loxP-DTA} mice (Bielle et al. 2005) were crossed with *Nestin:Cre* (provided by F. Tronche) to generate *Dbx1^{DTA};Nes:Cre* embryos. A functional DTA is expressed exclusively upon Cre-mediated recombination under the control of the Nestin promoter resulting in ablation of *Dbx1*-expressing cells in the CNS starting at E10.5. *Dbx1^{loxP-stop-loxP-DTA}* and *Nes:Cre* embryos were used as controls for all experiments. For Supplementary Figure 5 *Dbx1^{loxP-stop-loxP-DTA}* mice were crossed to *Nkx2.1:Cre* animals (Kessaris et al. 2006). In the telencephalon, this eliminated specifically *Dbx1*-expressing cells in the MGE and POA, thus *Dbx1*-derived cortical interneurons. All animals were maintained on a C57Bl/6J background. Embryos were genotyped by PCR using primers specific for the different alleles (Cre and DTA).

Tissue Preparation and Immunohistochemistry

For staging of embryos, midday of the vaginal plug was considered as embryonic day 0.5 (E0.5). Embryos were fixed by immersion in 4% PFA, PBS at 4 °C for 4 h or O/N for E14.5 and O/N for E18.5 brains and subsequently rinsed in PBS for 3 × 20 min. Brains were cryoprotected overnight in 30% sucrose, PBS, and embedded in O.C.T. compound (Sakura). Embedded tissues were sectioned on a cryostat with a 14 μm step for E14.5 and 18 μm for E18.5.

Immunohistochemistry on sections was performed as previously described (Pierani et al. 2001) or using an unmasking protocol (Arai et al. 2011). Primary antibodies used were chick anti-Tbr2 (Millipore, 1:500); goat anti-Brn2 (Santa Cruz, 1:250); rabbit antiactive Caspase 3 (Cell Signaling, 1:400), anti-Pax6 (Biolegend, 1:500), anti-PH3 (Millipore, 1:500) and anti-Tbr1 (Abcam, 1:500); rat anti-Ctip2 (Abcam, 1:300); mouse anti-Tuj1 (BabCo, 1:1000). Fluorescent secondary antibodies used were Cy3 donkey antimouse (Jackson ImmunoResearch Laboratories, 1:700), Cy5 donkey antigoat (Jackson ImmunoResearch Laboratories, 1:500), Alexa 488 donkey anti-chick (Jackson ImmunoResearch Laboratories, 1:1000). Nuclei were counterstained with 4',6-diamidino-2-phenylindole (DAPI) (Invitrogen, 1:2000). Terminal deoxynucleotidyl transferase-mediated biotinylated UTP nick end labeling (TUNEL) staining was performed using In Situ Cell Death Detection Kit according to the manufacturer's protocol (Roche [Sigma]). In situ hybridization was performed as previously described (Bielle et al. 2005). For DAB (3,3'-diaminobenzidine tetrahydrochloride) immunostaining subsequent to *Dbx1* mRNA in situ detection, the hybridization was processed in the absence of PK treatment. Anti-Tbr2 and antiactive caspase 3 antibodies were detected with a biotinylated secondary antibody using the Elite Vectastain ABC kit (Vector Laboratories).

Mathematical Models of Cell Divisions and Differentiations

We have introduced a model built upon the one introduced in Hsu et al. 2015. The model reproduces the sequence of divisions that a pool of progenitor cells undergoes during the neurogenesis phase. We have considered in this study 3 main cell types: 1) radial glia progenitors (RG cells), 2) intermediate progenitors (IPs), and 3) neurons. Experimentally, these correspond to 1)

Pax6⁺ cells in VZ, 2) Tbr2⁺ cells (thus pooling the different types of IP cells) (Noctor et al. 2004; Gal et al. 2006; Fietz et al. 2010; Hansen et al. 2010; Arai et al. 2011; Betizeau et al. 2013; Tyler and Haydar 2013; Florio and Huttner 2014), and 3) Ctip2⁺ and Tbr1⁺ cells for deeper layer neurons and Brn2⁺ cells for upper layer neurons.

All these cells are generated from an initial pool of progenitor cells, which may undergo the following divisions or differentiation:

1. Symmetric proliferative divisions to produce 2 progenitor cells.
2. Asymmetric divisions into a progenitor and an intermediate progenitor cell.
3. Asymmetric neurogenic divisions into a progenitor and a neuron.
4. Symmetric divisions into 2 intermediate progenitor cells.
5. Loss of capacity to generate neurons (e.g., gliogenesis). IPs may undergo 2 types of divisions or differentiation:
6. Symmetric proliferative divisions to produce 2 IPs (the number of such divisions from a given cell is limited to 1, or 2 depending on the mutant scenario considered).
7. Symmetric neurogenic divisions giving 2 neurons.

Neurons created are assumed to migrate to upper or deep layers with a probability depending on their birthdate. Similarly, the rate at which each division occurs is a function of time. We have chosen the following parameters reproducing closely the WT phenotype that we and others measured (Gao et al. 2014; Hsu et al. 2015).

We started with an initial progenitor pool of $RG_{EB} = 50$. The total number of RGs division within each $\Delta t = 0.1$ is inversely proportional to RG cell cycle T_{RG} . Consistent with experiments (Manuel et al. 2015), we have considered that T_{RG} varies in time, and linearly increases during cortical development (Takahashi et al. 1995; Calegari and Huttner 2003; Dehay et al. 2015; Manuel et al. 2015)

$$T_{RG} = 0.0625t + 0.1875d$$

In each simulation step Δt , the intensity of the divisions and differentiations of RGs are parameterized by the probabilities $Prob_i(t)$ ($i = 1, 2, 3, 4, 5$, numbered as in the above description list) depicted in Figure 8A:

$$Prob_1(t) = \frac{1}{2}(1 - \text{erf}(0.6(t - E11)));$$

$$Prob_2(t) = \frac{1}{4}(1 - \text{erf}(t - E12))(1 + \text{erf}(2.5(t - E14.5)));$$

$$Prob_3(t) = \frac{1}{12}(1 - \text{erf}(0.6(t - E11)))(1 + \text{erf}(3(t - E17.5)));$$

$$Prob_4(t) = \frac{1}{12}(1 - \text{erf}(3(t - E13)))(1 + \text{erf}(5(t - E15.5)));$$

$$Prob_5(t) = \frac{1}{2}(1 + \text{erf}(3(t - E16)))$$

The model is thus complete once we have set the probability of divisions and differentiation of IPs. In WT model, the probability that an IP performs one proliferative division (thus eventually generating 4 neurons) is constant in time and fixed consistently with the biological data to 10%. All other IPs directly perform a

symmetric neurogenic division, giving birth to 2 neurons. IPs have a fixed cell cycle duration $T_{IP} = 1.3d$ (27.6 h).

Newborn neurons choose to enter deep or upper layer depending on the timing of birth, which is described as $Prob_{deeper}(t)$ and $Prob_{upper}(t)$. The switching happens at E14.5.

$$Prob_{deeper}(t) = \frac{1}{4}(1 - \text{erf}(3(t - E11)))(1 + \text{erf}(3(t - E14.6)));$$

$$Prob_{upper}(t) = \frac{1}{4}(1 - \text{erf}(3(t - E14.4)))(1 + \text{erf}(3(t - E17.5)));$$

Theoretical Prediction of the Total Number of Neurons as a Function of IP Proliferation Rate

In Figure 4A, all divisions, and differentiations associated to RG are not influenced by the probability p of IPs undergoing 2 symmetric proliferative divisions. The total number of RGs, as well as the number of neurons N_{RG} and IP (IP_{RG}) generated directly from RGs are independent of p . IPs neurons are generated as in the following model:

$$IP_{RG} \begin{cases} \xrightarrow{10\%} 2IP \rightarrow 4N \\ \xrightarrow{p} 2IP \rightarrow 4IP \rightarrow 8N \\ \xrightarrow{90\% - p} 2N \end{cases}$$

From this relationship it is easy to compute the number of neurons generated from IPs:

$$N_{IP} = (10\% \times 4 + p \times 8 + (90\% - p) \times 2) \times IP_{RG} = (2.2 + 6p) \times IP_{RG}.$$

Since IP_{RG} is constant, N_{IP} is an affine function of p .

Parameters for the Mutant Models

The different mutant used for our simulations in Fig. 8 are based on the same model as the WT, but we varied the starting and end time of the compensation process t_{start} and t_{end} , varied the cell cycle duration of IPs (T_{IP}), the probability p of proliferative divisions of IPs and the number of divisions these cells undergo (N_{div}). The precise modalities and timing of the compensation are described in the results section, and the quantitative parameters for all models are provided in Table 1.

EdU Pulse and Cumulative Labeling and Staining

EdU injection was carried out using an intraperitoneal injection of 3.3 mg/kg EdU (Invitrogen), PBS into pregnant females. We performed a single-pulse EdU injection at E14.5 and analyzed at E18.5 (Fig. 3). For the calculation of each phase of the cell cycle we used the Nowakowski method, applied to E14.5 mouse cortices (Nowakowski et al. 1989; Takahashi et al. 1993,

Table 1 Parameters of the compensation mechanism for the mutant models of Figure 8

	t_{start}	t_{end}	T_{IP}	p	N_{div}
WT			27.6h	10%	1
MUT1	E11	E18	20.4h	23%	1
MUT2	E11	E14	20.4h	23%	2
MUT3	E11	E14 + 12 h	Proportional to cell death 20.4 h at E14.5	Proportional to cell death 23% at E14.5	2

1995; Calegari and Huttner 2003; Lange et al. 2009; Arai et al. 2011; Turrero Garcia et al. 2016) and performed EdU cumulative labeling by injections every 3 h up to 18 h after the first injection (Fig. 6E). Embryos were analyzed at 0.5, 6, 9, and 18 h. We quantified RGs (Tbr2⁻DAPI⁺) and IPs (Tbr2⁺DAPI⁺) that incorporated EdU at each time point in the VZ/SVZ. We considered that a negligible proportion of progenitors do not proliferate in the VZ and SVZ as we did not observe any neuronal contamination in the VZ and SVZ in the control as previously reported (Arai et al. 2011), but also in the mutant, using triple immunostaining with Pax6, Tbr2, and Tbr1/Ctip2 (data not shown and Supplementary Fig. 4A). Control RGs and mutant IPs reached a growth fraction (GF) of 1 within 18 h. Mutant RGs reached a GF of 0.95 at 18 h as non proliferating bRGs-like are also present in the VZ/SVZ of *Dbx1^{DTA};Nes:Cre* mutant embryos and represent a negligible percentage of around 5% of the counted cells. We calculated the length of G2 + M + G1 (X , $T_C - T_S$), as indicated by the time point at which the EdU labeling index reached the plateau (e.g., when all the progenitors were EdU⁺) and the proportion of the cell cycle in S-phase was indicated by the intercept of the cumulative EdU labeling curve with the y axis (Y). With the mathematical formulas $GF \times (T_S/T_C) = Y$ and $T_C - T_S = X$ (Arai et al. 2011) we deduced T_S and T_C . From the percentage of cells dividing (PH3⁺, Z) we deduced the $T_M = (Z \times T_C)/GF$.

Immunofluorescence Coupled With EdU Staining

Immunofluorescence and EdU staining were performed on 14 and 18 μ m coronal cryosections of the telencephalon prepared from PFA O/N-fixed E14.5 and E18.5 embryos, respectively. Immunofluorescence and EdU staining was performed as previously described (Arai et al. 2011) using the Edu labeling Kit from Invitrogen.

Images Acquisition

Images of immunofluorescence were acquired on a Zeiss LSM710 inverted confocal microscope and processed with the ZEN 2012 software and bright-field images of brain sections using a VHX-900F series Keyence microscope.

Statistical Analysis

For all experiments, results were obtained from at least 3 pairs of control and mutant embryos from at least 2 litters. All the quantifications were made on 100 μ m wide boxes spanning the entire VZ/SVZ (Figs 1C, 5, 6 and Supplementary Fig. 5), the IZ (Fig. 7), the entire cortical plate (CP) (Figs 1E, 2, 3 and Supplementary Fig. 3) and the IZ/CP (Fig 1C) in the dorso-lateral part of the rostral cortex. For each animal we selected 1 or 2 sections ($n = 3$ or $n = 6$). For all quantifications, normal distribution was confirmed and unpaired, 2-tailed t-test on group means was performed for statistical analysis, using the Microsoft Excel software.

Results

Generation of a Mouse Model for Early Embryonic Neuronal Death

To investigate the consequences of early cell death on cortical development, we analyzed *Dbx1^{DTA};Nes:Cre* (hereafter Mutant) embryos (Bielle et al. 2005). From the onset of neurogenesis (embryonic [E] day 11.5) to midneurogenesis (E14.5), the mutant developing cerebral cortex displayed a high number of dying

cells as measured by immunohistochemistry for active Caspase 3, and TUNEL staining compared with controls (Fig. 1A and Supplementary Fig. 1A). No differences in cell death were observed at E16.5 (Supplementary Fig. 1B). Neuronal death throughout the cortical primordium correlated with a specific ectopic expression of *Dbx1* mRNAs in the dorsal and lateral pallial SVZ and IZ in addition to its normal site of expression in the ventral pallium (VP) at the pallial-subpallial boundary (PSB) (Supplementary Fig. 2). This began at E11.5 upon death of *Dbx1*-derived Cajal-Retzius cells (Bielle et al. 2005). The majority of active Caspase 3⁺ cells appeared to be in the superficial half of the cortical wall and very few were detected in the deep half, close to the ventricle (Fig. 1B and Supplementary Fig. 2). In order to characterize which cells were dying in the mutant at E14.5, we used immunostaining for Tuj1, a marker of young neurons, and Tbr2, a marker of SVZ progenitors (Englund et al. 2005), to distinguish the postmitotic compartment, corresponding to the IZ and the CP, from the SVZ (Fig. 1B). The vast majority of activated Caspase 3⁺ cells was present in the Tuj1⁺ neuronal compartment with only few cells found in both the VZ and SVZ (Fig. 1B,C, Supplementary Fig. 1C and 2) suggesting that young neurons at E14.5 are undergoing cell death. We, thus, quantified the number of neurons in the CP in the dorso-lateral cortex using Tbr1, a marker of early-born deep layer neurons (Englund et al. 2005), and observed a significant decrease (~20%) in mutants compared with control cortices (Ctrl 100% \pm 0.7; Mut 82% \pm 3, $P < 0.05$) (Fig. 1D,E). Similar results were obtained using Ctip2, another marker of early-born neurons (Supplementary Fig. 1D). These results indicate that extensive cell death during the first half of corticogenesis leads to a decrease in the number of deep layer neurons at E14.5.

Overproduction of Upper Layer Neurons in Mutants at E14.5

We then investigated the consequences of early neuronal death on cortical development at later stages. Unexpectedly, we observed that the thickness of the dorso-lateral CP in the mutant was similar to the control at E18.5 (Fig. 2A,E). We quantified the numbers of deep and upper layers cortical neurons in the CP using Tbr1 and Ctip2 as markers of layers V–VI, and Brn2 of layers II–IV. We observed a 29% decrease in the number of Tbr1⁺ neurons (Ctrl 100% \pm 7; Mut 71% \pm 3, $P < 0.05$) (Fig. 2B,F) and a 37% reduction in that of Ctip2⁺ neurons (Ctrl 100% \pm 7; Mut 63% \pm 5, $P < 0.05$) (Fig. 2C,G). In contrast, the number of Brn2⁺ neurons was increased by 17% (Ctrl 100% \pm 0.4; Mut 117% \pm 0.5, $P < 0.001$) (Fig. 2D,H). These results reveal an overproduction of upper layer neurons occurring in the mutant cortex in response to early-born neuronal loss.

Since the peak of upper layer neuron generation is at E14.5, we studied finely the proliferation and differentiation properties of progenitor cells at this stage. To this end, we performed EdU (5-ethynyl-2-deoxyuridine)-birthdating using a single injection of EdU at E14.5 and immunostaining for EdU, Tbr1, Ctip2, and Brn2 at E18.5 (Fig. 3A–F). The vast majority of the EdU⁺ cells were located in the superficial portion of the CP, above prospective layer V Ctip2⁺ neurons, whereas only few EdU⁺ cells were detected in the deep portion of the CP (corresponding to prospective layer VI) in mutants as in controls (Fig. 3B,C). However, we observed that the superficial EdU⁺ portion of the CP appeared thicker in mutants suggesting an increase in the number of EdU⁺ cells in superficial layers compared with controls. We first analyzed whether the timing of deep and upper layers production was preserved by immunofluorescence for

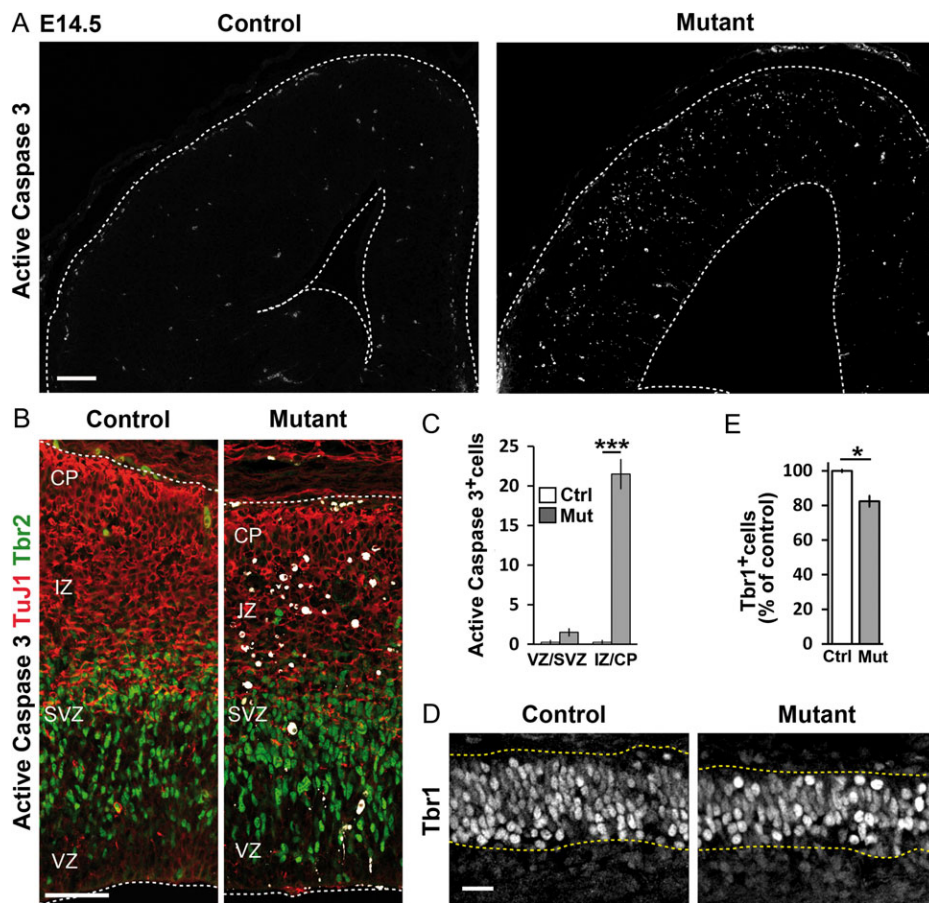


Figure 1. Mouse model for neuronal death from early to mid-corticogenesis. (A,B,D) Confocal images of coronal sections from control and *Dbx1^{DTA};Nes:Cre* (mutant) embryonic neocortex at e14.5. (A) Immunohistochemistry for active Caspase 3. (B) Immunohistochemistry for active Caspase 3 (white), Tbr2 (green), and TuJ1 (red). (C) Quantification of active Caspase 3⁺ cells in the ventricular zone/subventricular zone (VZ/SVZ) and in the intermediate zone/cortical plate (IZ/CP) per 100 μm of VZ. (D) Immunohistochemistry for Tbr1. (E) Quantification of Tbr1⁺ neurons in the cortical plate in a 100 μm wide box represented as percent of control. (C-E) Data are represented as mean ± standard error of the mean (SEM). Unpaired Student's t-test (n = 3). *P < 0.05 and ***P < 0.0001. Scale bars: 100 μm (A), 50 μm (B), and 20 μm (C).

EdU, Tbr1 and Ctip2. We observed no colabeling of either Tbr1 or Ctip2 with EdU in mutants and controls (Fig. 3C,D), indicating that mutant progenitor cells at E14.5 did not aberrantly generate layer VI and V neurons. We then quantified the number of EdU⁺ and EdU⁺Brn2⁺ neurons in the CP and detected that both were significantly increased in mutants (Fig. 3E,F). More than 80% of EdU⁺ cells were also Brn2⁺ in controls and mutants showing that proliferating progenitors at E14.5 primarily generate upper layer neurons in both but that in mutants the number of Brn2⁺ neurons born at E14.5 is enhanced. We further analyzed the distribution of EdU⁺ and/or Brn2⁺ cells within the CP by dividing it into 4 bins of equal thickness with bin 1 being the most superficial (Fig. 3E,F). Quantifications in each bin (Fig. 3G-I) indicated that, as in controls, the number of EdU⁺Brn2⁺ neurons progressively increased from bin 4 to 1 in mutants showing that the overall distribution is unaltered. While the number of EdU⁺Brn2⁺ neurons was unchanged in bin 1 and 4, we observed a higher number in bins 2 and 3 in mutants suggesting that no lagging neurons are detected in bin 4, and that the overproduced Brn2⁺ neurons accumulate in prospective layers IV and V, as determined with respect to Ctip2 labeling of layer V (see also Fig. 3C). Together these results indicate that an enhanced number of Brn2⁺ cells are generated at E14.5 and are able to migrate properly to the upper half of the CP in the mutant. However, we also observed that many Brn2⁺ cells were EdU⁻ (Fig. 3E,F), opening 73

the possibility that a precocious differentiation of these neurons was occurring in the mutant cortex. We, thus, performed EdU-birthdating at E12.5 and analyzed at E18.5. In both controls and mutants the vast majority of EdU⁺ neurons coexpressed Ctip2, and Tbr1, and were located in the deep portion of the CP, whereas none coexpressed Brn2⁺ (data not shown).

All together, these results demonstrate that in mutant cortices the temporal sequence in the generation of deep and upper layer neurons is unaltered, while an overproduction of Brn2⁺ neurons by progenitor cells at E14.5 is mediating the increase of the number of upper layers neurons observed at E18.5.

IP Proliferation as a Powerful Compensation Mechanism

The fact that the cortical thickness is recovered despite massive neuronal loss in mutants indicates the presence of a powerful adjustment mechanism for neurogenesis that compensates for the cell death by increasing the number of generated neurons. In order to test possible mechanisms by which this compensation may occur, we developed, and simulated a mathematical model describing the sequence of divisions and differentiation of a pool of progenitor cells as a function of time (see Materials and Methods).

In this model, the only divisions expanding the number of neurons are the asymmetric neurogenic divisions of RGs into a

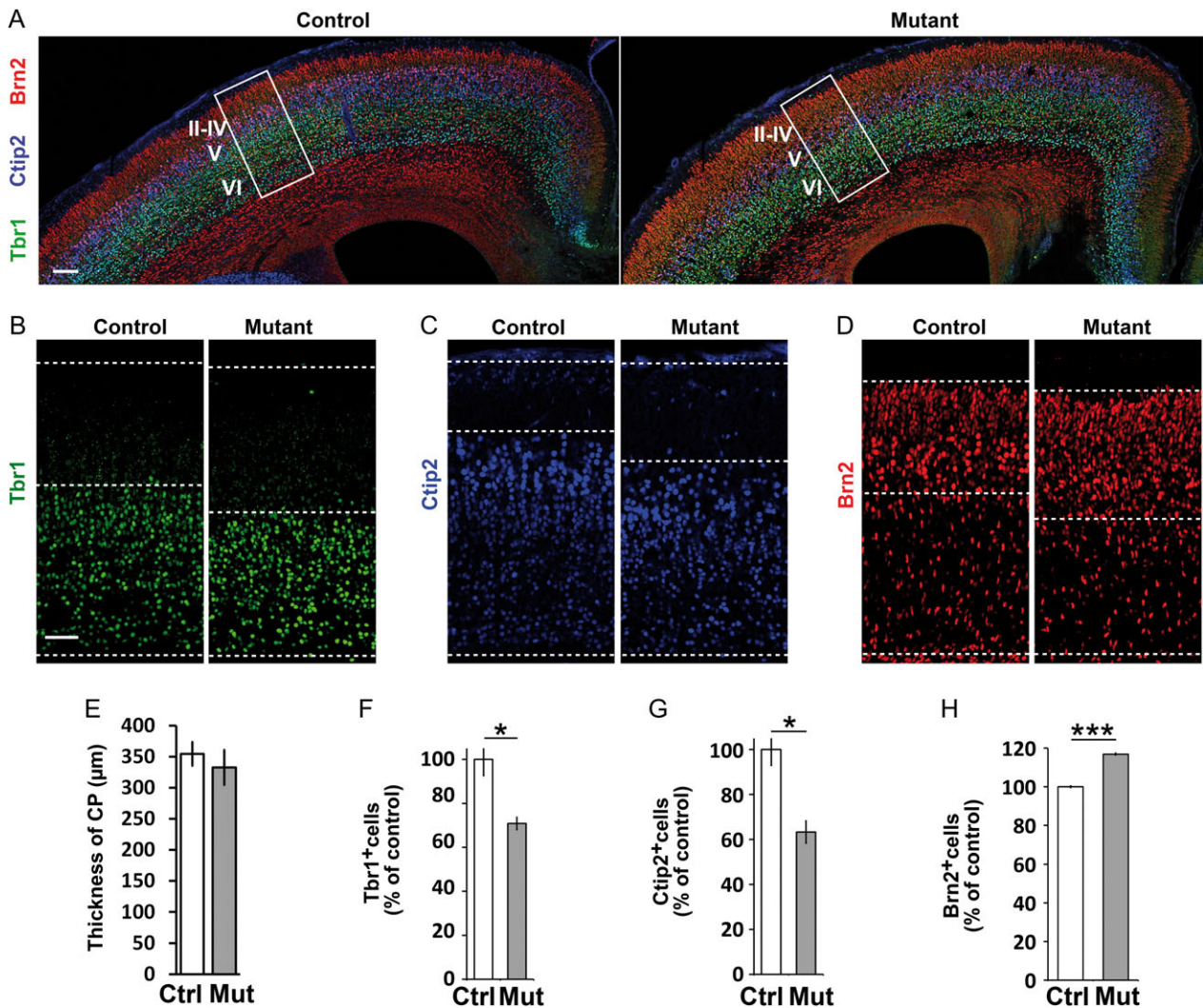


Figure 2. Increased number of upper layers neurons in mutants. (A–D) Confocal images of coronal sections from control and *Dbx1^{DTA};Nes:Cre* embryonic neocortex at e18.5. (A) Immunohistochemistry for Tbr1 (green), Ctip2 (blue) and Brn2 (red). (B–D) Enlarged view of the boxed regions shown in A. (E) Quantification of the CP thickness in a 100 μm-wide box. (F–G) Quantifications of the numbers of Tbr1⁺ (F), Ctip2⁺ (G) and Brn2⁺ (H) neurons within the cortical plate in a 100 μm-wide box represented as percent of control. Data are represented as mean ± SEM. Unpaired Student's t-test, (n = 3). *P < 0.05, ***P < 0.0001. Scale bars: 100 μm (A) and 50 μm (B,C,D).

neuron and a RG cell, and symmetric neurogenic divisions of IPs into 2 neurons. In order to compensate for a loss of neurons, the mutant mice should therefore adjust the number of these divisions. Increasing the number of asymmetric divisions of RGs could arise by shortening their cell cycle duration: the number of created neurons would increase as the inverse of the cell cycle duration. This compensation is thus limited in vivo by the fastest possible cell cycle. Concerning IPs, we expected that they dispose of a tremendous capacity to generate neurons by increasing the rate of symmetric proliferative divisions they perform. Indeed, this mechanism may increase exponentially fast the pool of IPs, thus the number of generated neurons. This capacity is largely underexploited in wild-type (WT) mice: it was reported that only 10% of IPs are undergoing (at least) one symmetric proliferative division before terminal mitosis based on time-lapse microscopy and sustained Pax6 expression which promotes symmetric proliferative divisions (Noctor et al. 2004; Arai et al. 2011; Wong et al. 2015).

We, thus, investigated in Figure 4 the role of both cell cycle duration and proliferative divisions of IPs in our mathematical 74

model, with parameters fitted to data we and others obtained in WT mice (Gao et al. 2014; Hsu et al. 2015). We observed that using the capability of IPs to divide recursively by increasing the proportion of IPs performing symmetric proliferative divisions we could indeed compensate for a massive loss of neurons (Fig. 4A). This compensation could only occur at the expense of an imbalance in the number of upper and deep layers neurons (Fig. 4B) since neurons would be generated later in the developmental program, after IPs symmetric divisions. Note that this disparity could be slightly counterbalanced by shortening IPs cell cycle duration without affecting the total number of neurons (Fig. 4C,D). In particular, a cell cycle duration of 27.6 h, as observed in WT mice (Arai et al. 2011), corresponds to a fraction of neurons in deep layers equal to 53% as measured experimentally in WT mice (Fig. 4D and Supplementary Fig. 3) (Hsu et al. 2015). Since IPs were not reported to show a high number of multiple symmetric divisions, in the model we limited to 2 the total number of symmetric proliferative divisions one IP may undergo. Even under this limitation, the increase in the number of generated

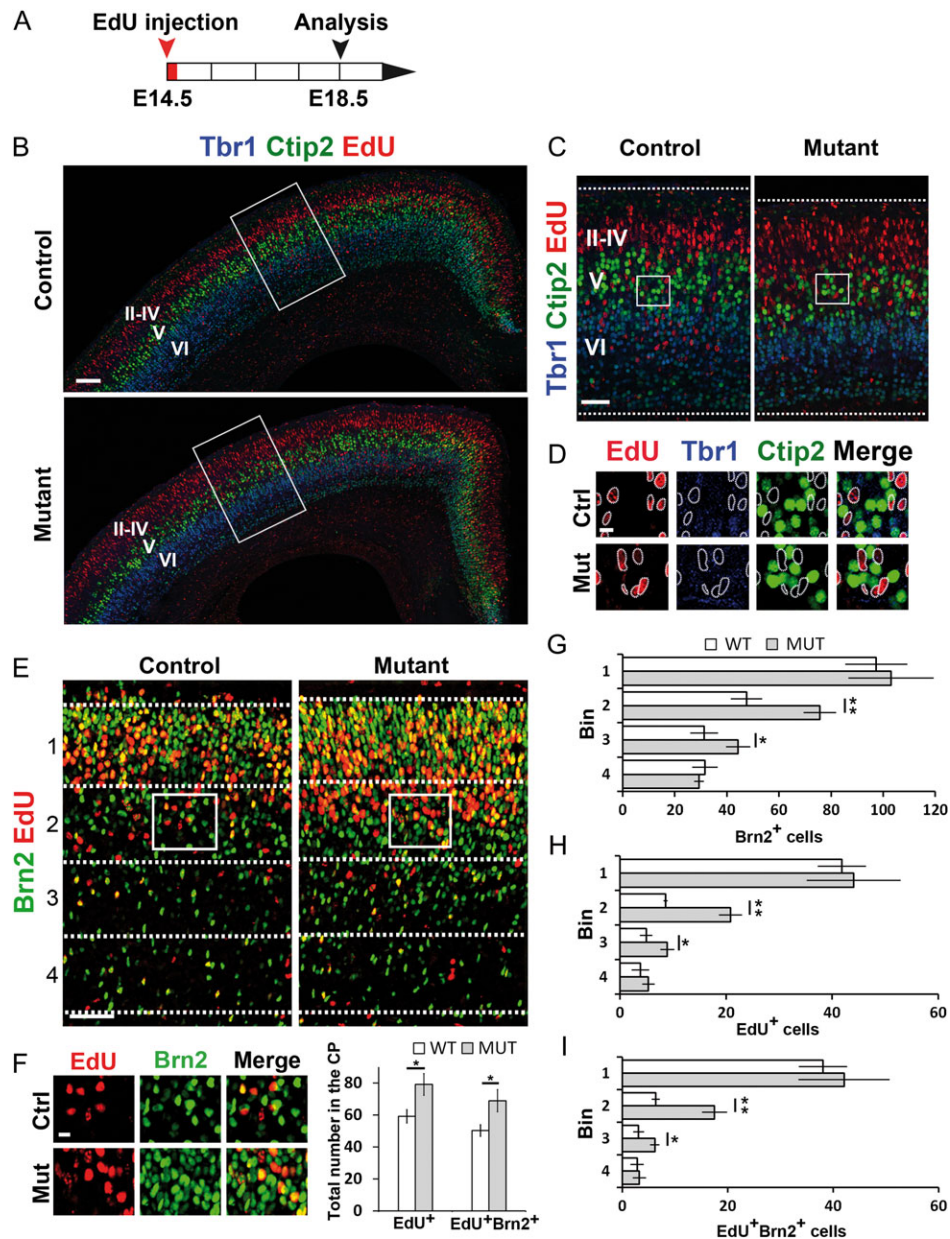


Figure 3. Overproduction of upper layer neurons at E14.5. (A) Experimental scheme. Embryos were collected at E18.5 after one single injection of EdU at E14.5. (B–F) Confocal images of coronal sections from control and *Dbx1^{DTA};Nes:Cre* embryonic neocortex at e14.5. (B–D) Immunohistochemistry for EdU (red), Ctip2 (green) and Tbr1 (blue). (C) Enlarged view of the boxed regions shown in (A). (D) Enlarged view of the boxed regions shown in C. (E) Immunohistochemistry for EdU (red) and Brn2 (green). (F) Enlarged view of the boxed regions shown in E and quantification of the total number of EdU⁺ and EdU⁺Brn2⁺ cells in the CP per 100µm of VZ. (G–I) Total cell numbers quantified by dividing the cortical plate into 4 equal-size bins. Graphs show mean ± SEM for each bin of Brn2⁺ cells (G) (Bin 1: Ctrl 97 ± 12, Mut 103 ± 16; Bin 2: Ctrl 48 ± 6, Mut 76 ± 6; Bin 3: Ctrl 31 ± 5, Mut 44 ± 5; Bin 4: Ctrl 32 ± 4.9, Mut 29 ± 2), EdU⁺ cells (H) (Bin 1: Ctrl 42 ± 5, Mut 44 ± 9; Bin 2: Ctrl 9 ± 0.4, Mut 21 ± 2; Bin 3: Ctrl 4.9 ± 1, Mut 9 ± 1; Bin 4: Ctrl 4 ± 2, Mut 5 ± 1) and EdU⁺Brn2⁺ cells (I) (Bin 1: Ctrl 38 ± 5, Mut 42 ± 9; Bin 2: Ctrl 6 ± 1, Mut 18 ± 2; Bin 3: Ctrl 3 ± 1, Mut 6 ± 1; Bin 4: Ctrl 3 ± 1, Mut 3 ± 1). Unpaired Student's t-test (n = 3). *P < 0.05, **P < 0.001. Scale bars: 100 µm (B), 50 µm (C and E), and 10 µm (D and F).

neurons was largely sufficient to already compensate for a substantial loss of neurons. We quantified in Figure 4A,B the effect of an increased fraction of IPs performing 2 symmetric divisions on the final number of neurons and on the proportion of neurons in deep and upper layers. In detail, we considered that in addition to the 10% of IPs performing one symmetric proliferative division as observed in WT mice, a proportion p of IPs perform 2 symmetric divisions. Theoretically, we showed (see [Materials and Methods](#)) that the number of neurons generated from RGs, N_{RG} , is independent on the probability of IPs

undergoing 2 symmetric proliferative divisions p (see Fig. 4A light blue area), while the number of neurons generated from IPs, N_{IP} , is an affine increasing function of p (see Fig. 4A pink area), consistent with the simulations of the model (blue line with error bars in Fig. 4A). Increasing p augmented the proportion of later-born upper layers neurons (Fig. 4B). Figure 4A shows the dramatic efficacy of the capacity of IPs making 2 symmetric proliferative divisions: as the proportion of IPs dividing twice increases to 90%, the number of neurons generated was more than tripled (going from 1.05×10^6 to 3.1×10^6 total

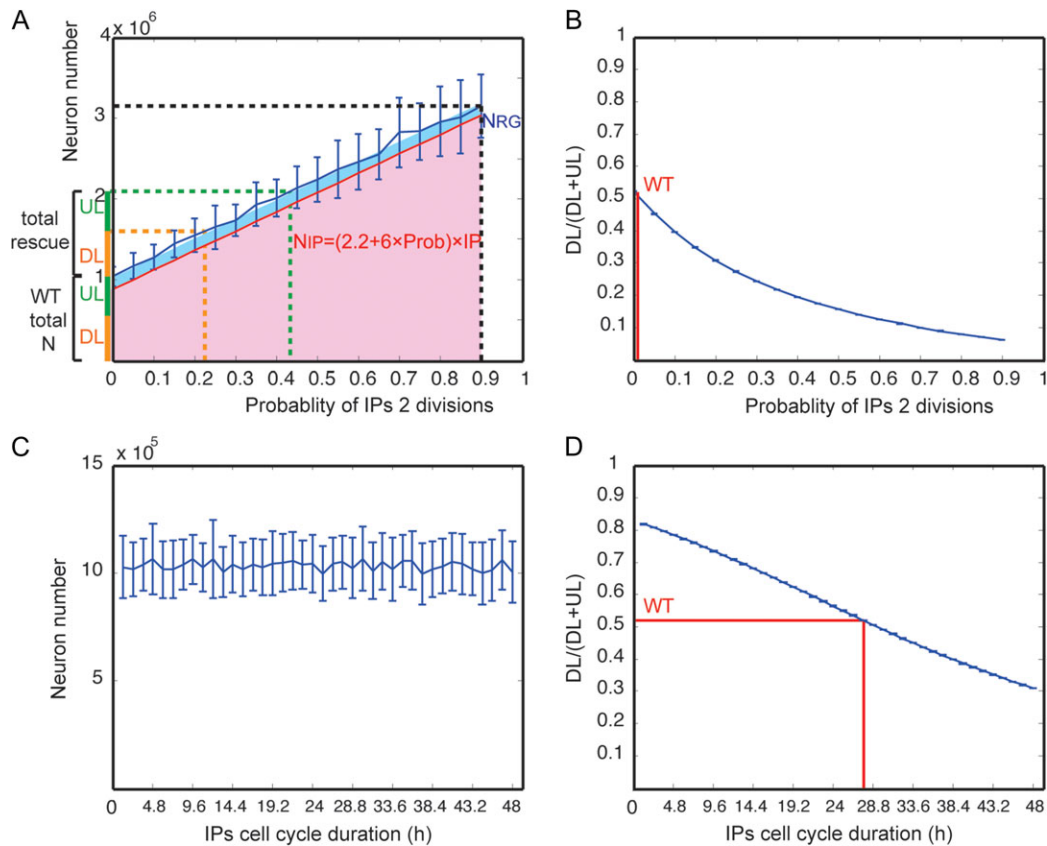


Figure 4. Theoretical predictions of neuron numbers in deeper and upper layers as a function of progenitor proliferation properties. (A, B) Variations according to the probability p of IPs performing 2 proliferative divisions: (A) the total number of neurons increases linearly with p as predicted theoretically (red line). Pink region: number of neurons generated by IPs; blue: neurons generated directly from RGs. Orange line: $p = 22\%$ compensates for a total loss of deep layer neurons. Green line: $p = 53\%$ compensates for a total loss of all neurons. (B) Newly generated neurons essentially contribute to superficial layers, leading to a decrease of the proportion of deep layer neurons. (C, D) Dependence on the IP cell cycle duration for $p = 0$. As expected, we find no variation of the number of neurons (C), but the ratio of deep layer neurons (D) decreases as cell cycle duration is increased since neurons are generated later. A cell cycle of 27.6 h corresponds to the WT ratio (red line). Data are represented as mean \pm standard deviation (SD) with 50 independent MATLAB simulations.

number of neurons). No more than 22% of IPs undergoing 2 symmetric proliferative divisions was sufficient to compensate for a complete loss of all deep layer neurons and 43% to compensate for a total loss of both deep and upper layer neurons.

These theoretical observations prompted us to investigate more closely the number of IPs performing symmetric proliferative division, as well as possible modifications of the cell cycle duration in RGs and IPs.

Decrease in the Number of RGs and Increase of Proliferating IPs in the Mutant VZ/SVZ

To examine whether the model prediction of a change in the proliferative properties of RGs and/or IPs indeed contributed to the increase of upper layer neurons at E18.5, we quantified the number of RGs ($\text{Pax6}^+\text{Tbr2}^-$) and IPs (Tbr2^+) in the mutant and control VZ/SVZ at E14.5 (Fig. 5A). We controlled that these were progenitors by coimmunolabeling with *Ctip2*, and found them all negative. We observed a decrease in the number of $\text{Pax6}^+\text{Tbr2}^-$ RGs in the mutant ($\text{Ctrl } 197 \pm 10$; $\text{Mut } 161 \pm 8$, $P < 0.05$; $n = 5$) and an increase in that of Tbr2^+ IPs ($\text{Ctrl } 122 \pm 6$; $\text{Mut } 155 \pm 11$, $P < 0.05$; $n = 5$) (Fig. 5A–C). Notably, 2 subtypes of IPs were identified in the cerebral cortex: neurogenic IPs and proliferative IPs (Noctor et al. 2004; Fietz et al. 2010; Arai et al. 2011; 76

Betizeau et al. 2013; Florio and Huttner 2014). Neurogenic IPs undergo only one round of division to produce 2 neurons, whereas proliferative IPs, defined as expressing both *Tbr2*, and *Pax6*, mainly in primates and recently in mice (Wong et al. 2015), undergo at least 1–2 rounds of proliferative divisions before producing neurons. In the mouse, only 10% of IPs was reported to be proliferative and our quantification of $\text{Pax6}^+\text{Tbr2}^+$ in control cortices at E14.5 confirmed these data (Fig. 5D). In mutant animals, we, however, observed a 2-fold increase in the number of IPs that express both *Pax6* and *Tbr2* ($\text{Ctrl } 10\% \pm 1$; $\text{Mut } 23\% \pm 4$, $P < 0.05$; $n = 5$) (Fig. 5D) suggesting that an increase in proliferative IPs might indeed occur in the mutant cortex. We, therefore, quantified the number of progenitors undergoing mitosis using phospho-Histone 3 (PH3) immunostaining (Fig. 6A). We considered as RGs all the cells in the VZ/SVZ that were $\text{DAPI}^+\text{Tbr2}^-$, since cells that do not express *Tbr2* are almost all Pax6^+ in both compartments and only a negligible number of Tbr2^- postmitotic neurons were found in the VZ/SVZ (Fig. 5A, Supplementary Fig. 4A) (Arai et al. 2011). No differences in the ratio of dividing RGs ($\text{PH3}^+\text{DAPI}^+\text{Tbr2}^-$) ($\text{Ctrl } 17\% \pm 4$; $\text{Mut } 15\% \pm 1$, $P < 0.05$; $n = 3$) were observed between mutants and control cortices at E14.5 (Fig. 6A,C). In contrast, we detected a 2-fold increase in the percentage of dividing IPs ($\text{PH3}^+\text{DAPI}^+\text{Tbr2}^+$) ($\text{Ctrl } 5\% \pm 1$; $\text{Mut } 9\% \pm 0.5$, $P < 0.05$; $n = 3$)

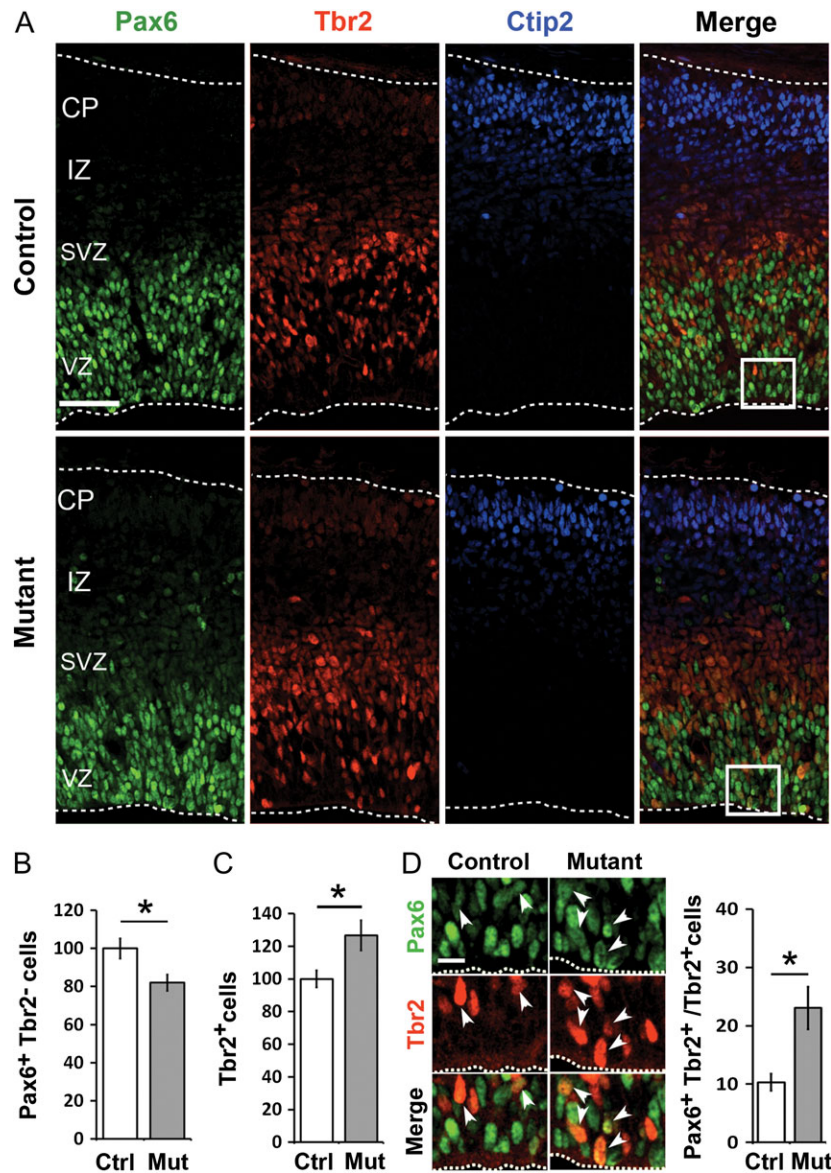


Figure 5. Decrease in the number of RGs and increase in that of IPs. (A, D) Confocal images of coronal sections from control and *Dbx1^{DTA};Nes:Cre* embryonic neocortex at e14.5. (A) Immunohistochemistry for Pax6 (green), Tbr2 (red) and Ctip2 (blue). (B, C) Quantifications of the total numbers of Pax6⁺Tbr2⁻ (B) and Tbr2⁺ (C) cells per 100 µm of VZ. (D) Enlarged view of the boxed regions shown in (A). White arrowheads show Tbr2⁺Pax6⁺ cells quantified in the graph as percentage of the total number of Tbr2⁺ cells. Quantifications were done within the entire thickness of the cortical wall in a 100µm-wide box. Data are represented as mean ± SEM. Unpaired Student's t-test (n = 5). *P < 0.05. Scale bars: 50 µm (A) and 10 µm (D).

(Fig. 6A,B,D). Altogether these results demonstrate that early death in the postmitotic compartment differentially affects cortical progenitors at mid-cortico-genesis with a reduction in the number of RGs, but not their proportion in mitosis, and an increase in dividing IPs, possibly proliferative IPs, that co-express Pax6. These results also support the mathematical model prediction that an increase in the proliferative capacity of IPs mediates the enhanced generation of upper layers neurons at mid-cortico-genesis.

IPs Display a Shorter Cell Cycle Length in Mutants

We next investigated the model prediction of variation in the cell cycle duration. It was already reported that progenitors have different cell cycle durations depending whether they go

through proliferative or neurogenic division (Lange et al. 2009; Pilaz et al. 2009; Arai et al. 2011). To investigate whether the increase of PH3⁺ IPs in the mutant was due to a change in their cell cycle length and/or specifically of the M-phase, we performed cumulative S-phase labeling using EdU injections at 3 h intervals to calculate the duration of the total cell cycle length (T_c) and of each cell cycle phase (Nowakowski et al. 1989). Pregnant females were sacrificed at different time points after the first injection at E14.5 (0.5, 6, 9, and 18 h) (Fig. 6E) and the rate of EdU incorporation (EdU labeling index) into RGs and IPs was analyzed by immunostaining for EdU and Tbr2 to differentiate between RGs (Tbr2⁻DAPI⁺) and IPs (Tbr2⁺DAPI⁺) (Fig. 6E). This revealed that the length of the G2+M+G1 (T_{C-T_S}), as indicated by the time point at which the EdU labeling index reached the plateau (Fig. 6E), was not significantly different for

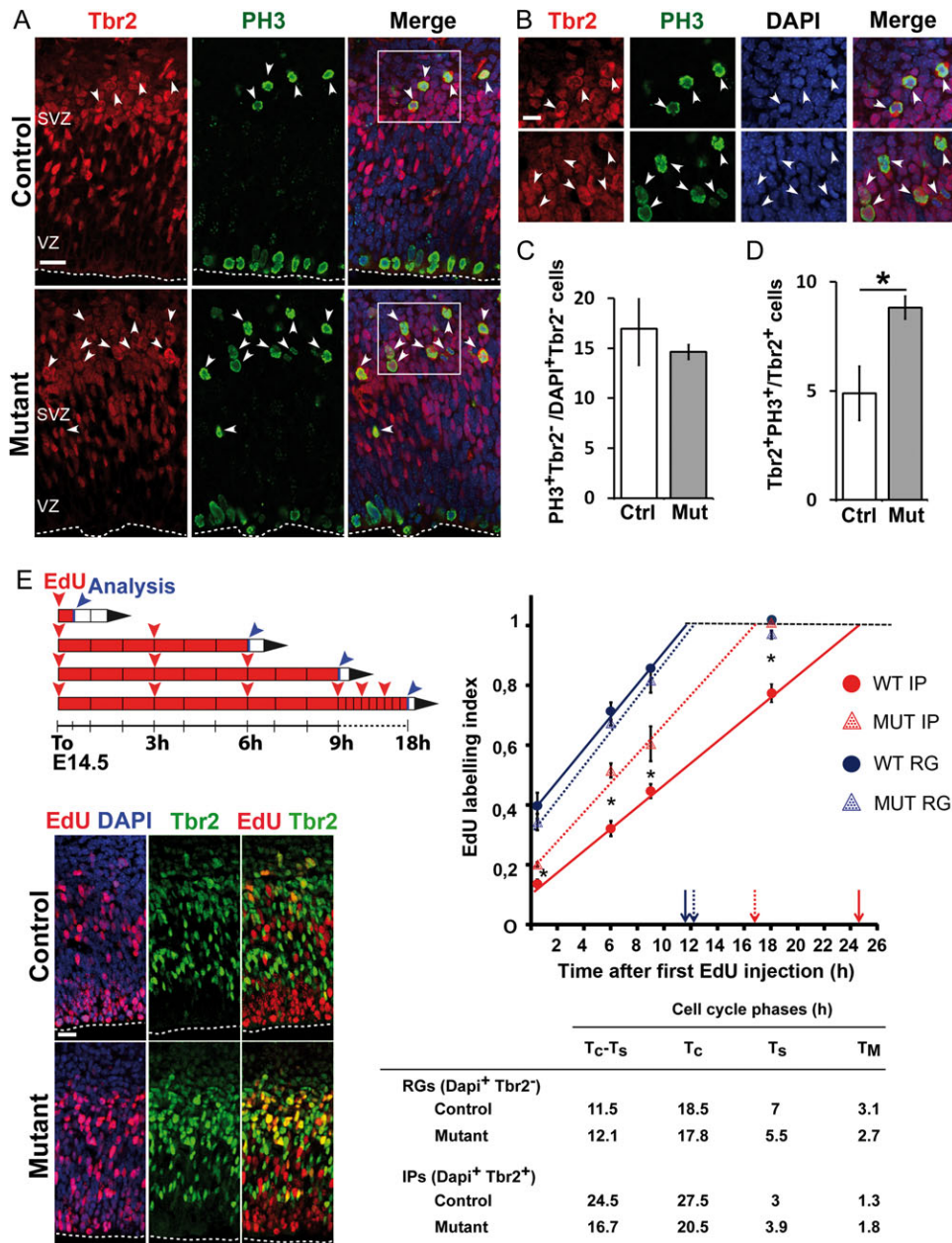


Figure 6. Intermediate progenitors increase their proliferation rate and shorten their cell cycle. (A, B, E) Confocal images of coronal sections from control and *Dbx1^{DTA};Nes:Cre* embryonic neocortex at e14.5. (A) Immunostaining for Tbr2 (red) and PH3 (green) counterstained for DAPI (blue). White arrowheads show dividing IPs. (B) Enlarged view of the boxed regions shown in A. (C–D) Quantification in a 100- μ m-wide box of the number of PH3⁺Tbr2⁻ RGS along the ventricle (C) and PH3⁺Tbr2⁺ IPs (D) abventriculantly. Data are represented as mean \pm SEM and percentages of DAPI⁺ and Tbr2⁺ for RGS and IPs, respectively. Unpaired Student's t-test ($n = 3$). * $P < 0.05$. (E) Experimental scheme of cumulative EdU injections from E14.5 every 3 h (on the left). Animals were sacrificed at 0.5, 6, 9, and 18 h after the first EdU injection. Immunohistochemistry for EdU (red) and Tbr2 (green) staining after cumulative EdU labeling for 6 h (on the left) counterstained for DAPI (blue). Calculation of cell cycle parameters (on the right). Proportion of EdU-labeled progenitors nuclei over the total number of nuclei (EdU labeling index) after cumulative EdU labeling for 0.5, 6, 9, and 18 h. The intercept of the cumulative EdU labeling curve with the y axis indicates the proportion of cells in S-phase. Color-coded arrows indicate the time point at which the labeling index reaches a plateau (T_C–T_S) (see [Materials and Methods](#)). The EdU labeling index was separately determined for RGS (Tbr2⁻EdU⁺) and IPs (Tbr2⁺EdU⁺) in WT and mutants. Data are represented as mean \pm SEM. Unpaired Student's t-test ($n = 3$). * $P < 0.05$. Calculated length of cell cycle phases (bottom right panel) of RGS (Tbr2⁻EdU⁺) and IPs (Tbr2⁺EdU⁺). T_C: total cell cycle; T_S: S-phase; T_M: M-phase. Scale bars: 20 μ m (A, E), 10 μ m (B).

RGs between controls (11.5 h) and mutants (12.1 h). However, for IPs, the T_C–T_S was shorter in mutants (16.7 h) compared with controls (24.5 h). For both progenitor types in control cortices, the cell cycle lengths were similar to the ones previously reported (Arai et al. 2011). Moreover, for RGS the proportion of cells in S-phase measured 30 min after EdU

injection (Ctrl: 38%, Mut: 32%), the total cell cycle length (Ctrl: 18.5 h, Mut: 17.8 h) (Fig. 6E) as well as the length of the S-phase (T_S) (Ctrl: 7 h, Mut: 5.5 h) was not significantly different between controls and mutants. In contrast, for IPs, the proportion of cells incorporating EdU was significantly increased for the mutant compared with the control (Ctrl: 11%, Mut:

19%) but the length of the S-phase was not (Ctrl: 3 h, Mut: 3.9 h). IPs also displayed a shortening of the T_C in mutants (Ctrl: 27.5 h, Mut: 20.5 h). Finally, the percentage of cells in M phase estimated using PH3 labeling showed that the length of the M-phase (T_M) was unaltered for both RGs and IPs (RGs, Ctrl: 3.1 h, Mut: 2.7 h; IPs, Ctrl: 1.3 h, Mut: 1.8 h) in the control compared with the mutant cortex (Fig. 6E,C,D). Since the G_2 phase has not been shown to change during development or between progenitor types (Arai et al. 2011), our results strongly suggest that the reduced cell cycle length of mutant IPs is due to a shortening of the G_1 phase (T_{G1}). These results show that at mid-corticogenesis mutant IPs also display a shortening of the cell cycle. As the model suggests, this acceleration in the cell cycle duration limits the imbalance between upper and deep layers, as visible from the decay of the proportion of deep layer neurons as cell cycle duration increases (Fig. 4D).

bRGs-Like Progenitors Number Increases in the Mutant Cortex

In the mouse neocortex, among the basal progenitor (BP) population, more than 90% are IPs and a small fraction are basal RGs (bRGs) (Miyata et al. 2004; Noctor et al. 2004; Shitamukai et al. 2011; Wang et al. 2011; Martinez-Cerdeno et al. 2012). bRGs are a population of progenitors that delaminate from the VZ, populate the SVZ and IZ and share the molecular markers of apical RGs (aRGs) (for review see (Lui et al. 2011; Florio and Huttner 2014)). These express Pax6, Sox2, and can also express Tbr2 (Wang et al. 2011). They undergo only asymmetric self-renewing neurogenic divisions but not symmetric proliferative divisions in the mouse (Shitamukai et al. 2011; Wang et al. 2011). In ferrets and primates, including humans, this population is largely expanded, represents the vast majority of BPs and has the capacity to undergo multiple rounds of

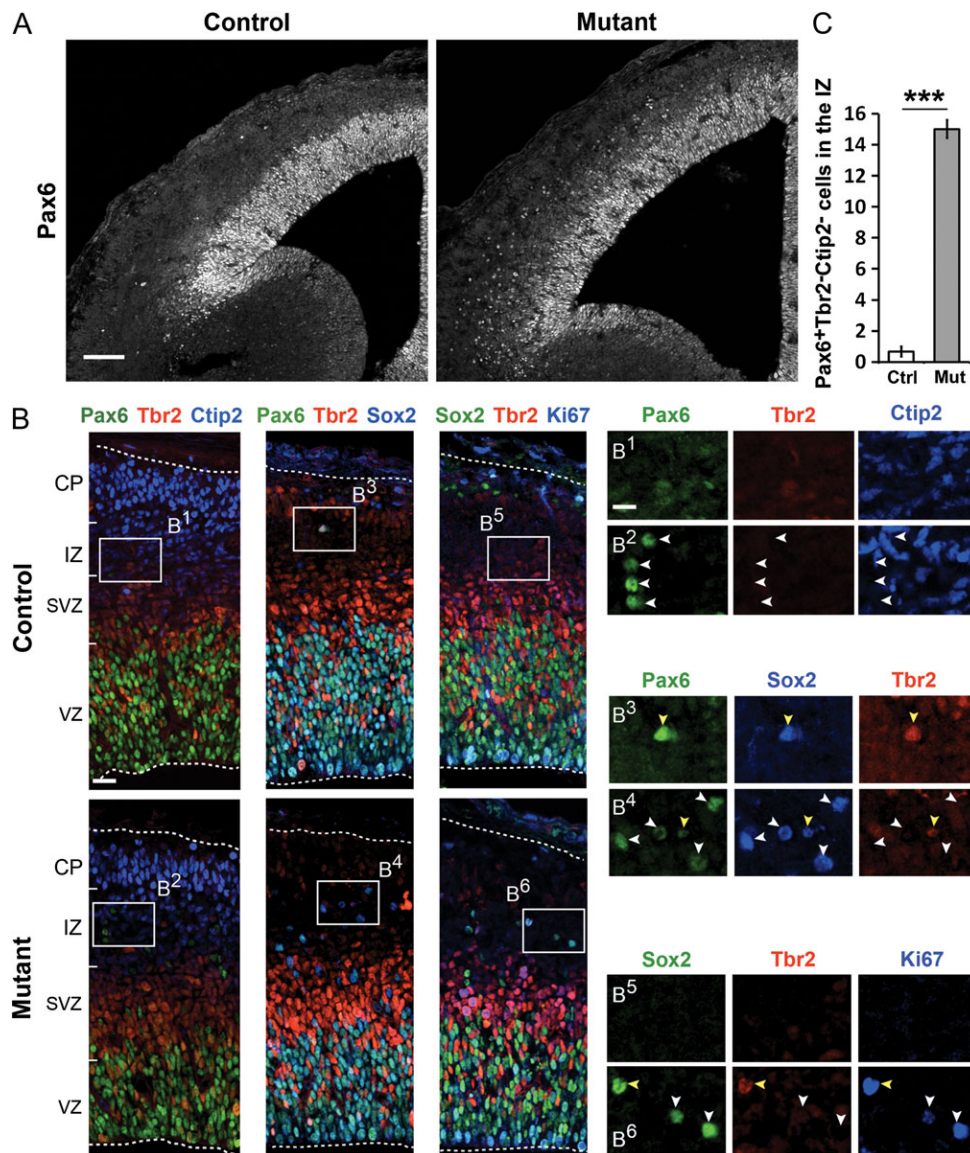


Figure 7. Enhanced number of bRGs-like in the intermediate zone of mutants. (A, B) Confocal images of coronal sections from control and *Dbx1^{DTA};Nes:Cre* embryonic neocortex at e14.5. (A) Immunohistochemistry for Pax6. (B) Immunohistochemistry for Pax6, Tbr2, Ctip2, Sox2, and Ki67. (B¹-B⁶) High magnifications of boxed regions in left panels. Yellow arrowheads indicate cells that colabeled with Tbr2 and white arrowheads cells that did not colabel with Tbr2. (C) Quantification of Pax6⁺Tbr2⁻Ctip2⁻ cells in the IZ. Data are represented as mean ± SEM. Unpaired Student's *t*-test (*n* = 3). ****P* < 0.0001. Scale bars: 100 μm (A), 20 μm (B), and 10 μm (B¹).

proliferative divisions before generating neurons (Fietz et al. 2010; Hansen et al. 2010; Betizeau et al. 2013; Pilz et al. 2013). Surprisingly when analyzing the expression of Pax6 in the cerebral cortex of mutants we observed a greater than 10-fold increase in the number Pax6⁺ cells located outside of the VZ, namely in the SVZ and IZ, compared with controls (Ctrl 0.7 ± 0.7 ; Mut 15 ± 0.6) (Figs 5A and 7A–C). These cells did not express neuronal markers such as Ctip2 (Fig. 7B, B¹, B²). A small fraction expressed Tbr2 at low levels and all coexpressed Sox2⁺ (Fig. 7B, B³, B⁴). Furthermore, we showed that all ectopic Sox2⁺ cells in the IZ expressed the Ki67 marker of cycling cells (Fig. 7B, B⁵, B⁶). These results show that also an excess of cycling bRGs-like is produced in the mutant cerebral cortex.

Predicting the Timing of Neurogenesis Compensation

The data obtained experimentally on the increase of proliferative IPs proportion and on the reduction of their cell cycle duration thus agrees with the qualitative predictions derived from the mathematical model.

The massive increase of bRGs-like cells observed experimentally also led us to consider this as a potential important element to incorporate into the model. We thus investigated further the capacity of bRG-like cells to generate neurons in the mutant mice. Unexpectedly, we found experimentally that none of the bRG-like cells in mutant mice appeared to go through the S-phase within an 18 h period as determined by sequential injections of EdU every 3 h, whereas few bRGs-like in control mice did incorporate EdU (Supplementary Fig. 4B). We, thus, conclude that bRG-like cells are unlikely to contribute substantially to the overproduction of upper layers neurons in mutant cortices at E14.5 and did not incorporate them in the model.

In order to infer the possible mechanisms of the compensation phenomenon based on the observation of the mutant mice phenotype, we developed a mathematical model of the mutant mice by fitting it with all quantifications measured experimentally. We considered that IPs can shorten their cycle duration down to 20.4 h and imposed that the ratio of IPs performing 2 symmetric divisions at E14.5 is at most 23%. In this model, the fine modalities and timing of the compensation mechanism are unknown. The free parameters were, thus, the ratio $p \leq 23\%$ of IPs performing 2 symmetric divisions, as well as the initiation and termination of proliferative divisions of IPs. We thus simulated a few hypotheses on the possible compensation scenarios for these free parameters which should be consistent with the data collected in our experiments (Fig. 8).

We first tested whether the compensation could occur when IPs can perform only one symmetric division. In such conditions (MUT 1 in Fig. 8A) simulations showed that even if the ratio of IPs performing one symmetric division jumped from 10% to 23% as soon as neuronal death occurs and remained steady until the end of the neurogenesis period, the total number of neurons generated would remain lower than in WT mice. We conclude that the compensation observed experimentally requires that a fraction of IPs must perform at least 2 symmetric divisions.

We then considered the effect of limiting the compensation mechanism to the period of neuronal death. To this end, we limited to 23% the ratio of IPs performing symmetric divisions consistently with the data and tested different hypotheses. First, if among these dividing cells we conserved 10% performing one symmetric division, as in the WT mice, and an extra 13% of IPs performing 2 symmetric divisions, this was not sufficient to compensate for neuronal loss (data not shown). We

found nevertheless that maintaining a fixed proportion $p \leq 23\%$ (actually exactly equal to 23%) of IPs performing 2 symmetric divisions during the whole phase of neuronal death leads to recover a number of neurons consistent with the WT mice (MUT2 in Fig. 8A). Of course, the scenario proposed in MUT2 is unrealistic. It is indeed not plausible that an instantaneous and synchronous response of all 13% of IPs occurs immediately at the onset of the neuronal death phase. Moreover, the 23% of IPs performing symmetric division only provides a compensation for a specific total loss of cells that cannot be predicted at the onset of the neuronal death phase. Indeed for a fixed ratio of IPs performing symmetric division, shall neuronal death period or rate increase (or decrease), this ratio would lead to undercompensation or overcompensation. However, MUT2 is particularly interesting in that it shows that even using the full compensation capacity of the symmetric division of IPs during the whole neuronal death period is barely enough to compensate, which strongly argues in favor of the need of an additional mechanism to compensate.

A realistic mechanism shall adapt to the number of dying cells. We, thus, designed an adaptive compensation mechanism that smoothly interpolates between WT and mutant levels as a function of the number of neurons dead in the near past (MUT3 in Fig. 8A). The experimental observation that the number of RGs is decreased while the number of IPs is increased motivated us to incorporate in our model the capacity of RGs to perform a self-consuming symmetric division into 2 IPs (Florio and Huttnner 2014). In this model, we assumed that the cell cycle duration, the probability of IP proliferation and the probability of symmetric division of RGs into IPs depended on the total number d of dead cells within the previous 12 h. In response to cell death, we assumed that the cell cycle accelerated, IPs made more proliferative divisions and RGs increased their rate of symmetric division to 2 IPs (see Materials and Methods). The parameters were adjusted to match the quantitative measurements observed both in WT and mutant mice. In detail, IP cell cycle duration was chosen to vary linearly from 27.6 h, when no cells have died in the previous half-day, to 20.4 h at the peak of cell death in the model. The probability of IPs performing only 1 symmetric division decreases as d increases from 0.1 to 1, while the probability p of IPs performing 2 proliferative divisions increases proportionally to d . The parameters were adjusted to interpolate between WT and mutant data, that is, for proliferating IPs from 10% in the absence of cell death to 23% at E14.5 in the mutant mice. With this model and by only fitting the type of response curve to cell death, we obtained a very good agreement of the model to the mutant phenotype (Fig. 8B). Indeed, with this model, the neuronal loss is precisely compensated, and the ratio between deep and upper layers neurons obtained is perfectly consistent with the mutant mice data. Moreover, the model provided finer information on the timing of the compensation mechanism compared with the development of the WT mice (Fig. 8B). Indeed, the simulations showed that the growth of the neuronal population is initially slower in MUT3 (Fig. 8B yellow solid lines) compared with the WT model (Fig. 8B yellow dashed lines) due to cell death. This results in a 20% decrease of the total number of neurons at E14.5 chiefly affecting deep layers, consistent with the data. At E14.5, we observed an increase of the neuronal generation rate that initiates the compensation process. This increase originates from the combined effect of 1) the termination of the neuronal death period and 2) the emergence of the neurons generated by proliferative IPs. Indeed, cell death triggers proliferation of IPs at E11.5, and each of these cells

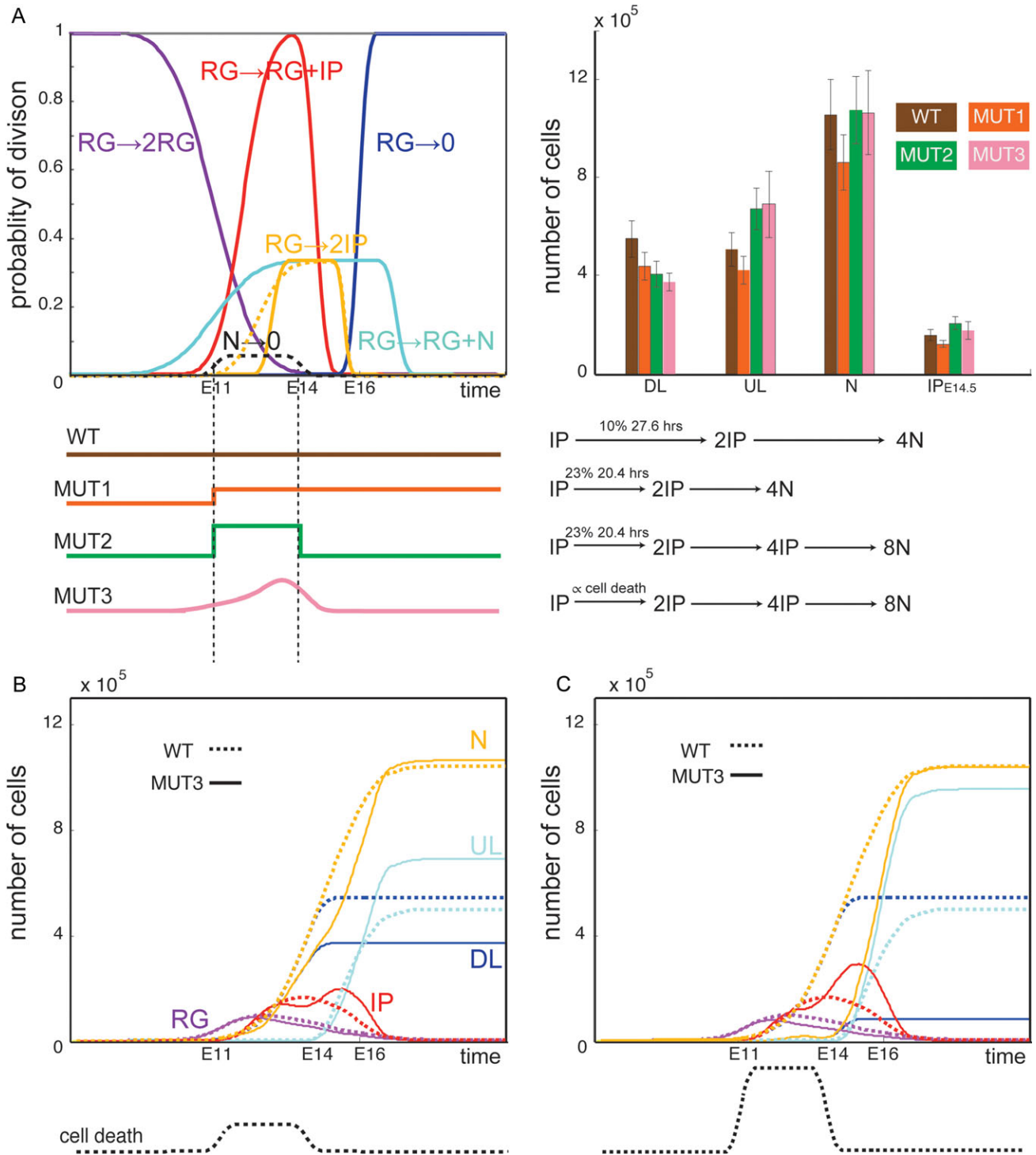


Figure 8. Different theoretical neurogenesis scenarios and their timing. (A) The probability of different divisions and differentiations. The WT model corresponds to plain lines. In all MUT models, neurons die from E11 to E14 (black dashed line) and RGs precociously differentiate into 2 IPs (yellow dashed line). Three different mutant scenarios are schematically described below with the proportion and number of divisions performed by IPs as a function of time. Top right panel: number of neurons in deep layer (DL), upper layer (UL) and the total number of neurons (N) at the end of neurogenesis, together with the total number of IPs at E14.5 for WT and the 3 mutant models. Data are represented as mean \pm STD with 50 independent MATLAB simulations. (B) Evolution in time of the number of cells during neurogenesis (RG in purple, IP in red, total neuron number in yellow, deep layers neurons in dark blue and upper layers neurons in light blue) for the WT model (dashed lines) and MUT3 (solid lines). (C) Same as (B) for a massive cell death level. Even if all neurons generated from E11 to E14 die, mutant MUT3 fitted to the data responds to this level of cell death by perfectly compensating for all neurons lost.

differentiates into 8 neurons after 3 cell cycles (thus slightly before E14.5). Moreover, this model also displays a 10% decrease of RGs at E14.5, which is due to precocious RG differentiation into 2 IPs, consistent with the decrease measured in mutant mice. This precocious differentiation together with the presence of proliferative IPs (each generating 4 IPs after 2 cell cycles) gives rise to a peak of IPs appearing between E14 and E16, which corresponds to the experimental observation of 20% more IPs at E14.5 in mutants. We thus conclude that this model precisely fits the experimental observations of the compensation mechanism in the mutant mice. It also strongly suggests that the self-consuming symmetric division of RGs into 2 IPs in response to cell death allows designing a realistic compensation scenario leading to a phenotype perfectly consistent with the mutant mice.

Notably, the interest of this model goes beyond the specific mutant studied experimentally ($Dbx1^{DTA};Nes:Cre$) and can be used to test for the neurogenic capacity of the system in response to different values of cell death intensity and cell cycle duration. Indeed, we observed that the model, with the parameters we chose for the mutant mice (MUT3), adjusts very nicely to different intensities of cell death. For instance, in Figure 8C we have considered the effect of a very high rate of neuronal death leading to a complete loss of neurons generated before E14 in the mutant model MUT3. Strikingly, we found that similarly to the mutant mice, a perfect compensation of the neuronal loss is reached, with of course a dramatic imbalance in the ratio between upper and deep layer neurons.

The analysis of the model thus led us to conclude that it is plausible, by adjusting only as a function of the number of dead cells in the past hours the probability of IPs to perform symmetric self-renewing division, the capacity of RGs to generate 2 IPs and the shortening of the cell cycle duration, to reproduce all experimental observations of the mutant phenotype in model MUT3, and that those parameters are sufficient to rescue the loss of neurons for a wide variation of cell death levels.

Discussion

We have shown that early neuronal loss triggers a compensation mechanism at mid-corticogenesis which promotes the expansion of abventricular progenitor pools, including IPs, and bRGs-like, in the mouse developing cerebral cortex. This leads to an increase in upper layers neurons and hence a rescue in final neuronal numbers. Mathematical modeling predicted that a minor increase in the probability of proliferative divisions of IPs is a powerful compensation lever of the system and that the compensation capacity is proportional to cell death. The expansion of abventricular proliferation and of upper layer neurons is associated with cortical evolution and mediates the complexification of cortical functions. Our results strongly argue in favor of the notion that amplification of pre-existing mechanisms rather than innovative acquisitions underlies cortical evolution and open the possibility of a crucial role exerted by the postmitotic compartment on the control of the amplification of abventricular proliferation in primates. They also suggest that through the manipulation of corticogenesis, neuronal content, although with an unbalance of deep versus upper layer neurons, can be recovered before birth after brain injury during embryonic life.

Mathematical Modeling of Compensation

Mathematical modeling was crucial to predict how compensation might occur in the mutant cortex through the amplification of self-renewing IPs as a primary determinant (Fig. 4). 82

Furthermore, we developed, and precisely fitted to the experimental data a mathematical model emulating the sequences of divisions and differentiation of the cell populations contributing to the generation of the neuronal populations. The model is based on specific parameters that essentially govern the time profile of cell divisions and differentiation on WT embryos and postnatal animals. These are estimated in the present study based on data collected in the literature or our own data. This thus provides a stochastic version of the system proposed by Finlay and collaborators (Workman et al. 2013; Cahalane et al. 2014) that includes more cell types and that is well fit to mice brains. The model is very flexible and allows adding more cell types when necessary. Here for instance, the present model refines the mathematical system proposed in Hsu et al. (2015) by adding a population of IPs which plays an essential role in the $Dbx1^{DTA};Nes:Cre$ mutants and predict the requirement of increase self-renewing proliferation of IPs and the decrease in their cell cycle length to mimic the observed phenotype. Moreover, it led us to quantify precisely the mathematical model in order to fit accurately to the data. The interest of the model is also that it can be used to predict the possible phenotypes in diverse situations. In particular, we presented in Figure 8C an hypothetical scenario in which massive cell death would lead to a total loss of neurons generated before E14.5 and we observed that IPs have the theoretical capacity to compensate this extreme loss of neurons. One important perspective of this work would be to model the signaling pathways that govern these probabilities of divisions and differentiations.

Progenitor Pools, Cell Cycle Regulation, and Cortical Evolution

We have shown that upon early death in the postmitotic compartment at mid-corticogenesis the RG pool is decreased but retains its proliferation rate, whereas that of abventricular progenitor pools, both IPs, and bRGs-like, is augmented. This suggests that a precocious differentiation of RGs into IPs occurs in mutants by mid-corticogenesis. The mutant IPs display the molecular signature of proliferative self-renewing IPs as a significant proportion maintains high Pax6 expression and their cell cycle length is reduced due to a shortening of the G1 phase. In the WT mouse only approximately 10% of IPs are proliferative and ~90% are neurogenic (Noctor et al. 2004; Arai et al. 2011; Shitamukai et al. 2011; Wong et al. 2015). Neurogenic IPs are thought to downregulate Pax6, and by contrast proliferative IPs to sustain Pax6 expression (Shitamukai et al. 2011; Wong et al. 2015). Sustained Pax6 expression has recently been shown to promote multiple rounds of symmetric division of IPs in the mouse cortex as suggested to enhance proliferation in primates (Fietz et al. 2010; Betizeau et al. 2013; Florio and Huttner 2014; Wong et al. 2015). Furthermore, the mechanism controlling the expansion versus differentiation of neural progenitors depends on cell cycle regulation. Total cell cycle duration is different between each progenitor type (Nowakowski et al. 1989; Lange et al. 2009; Pilaz et al. 2009; Arai et al. 2011) and it has been shown that G1 shortening is sufficient to promote the generation and expansion of IPs (Glickstein et al. 2009; Lange et al. 2009). Thus, both shortening of the G1 phase and high Pax6 expression as observed in $Dbx1^{DTA};Nes:Cre$ mutants are consistent with an increase in the self-renewing capacity of IPs.

During evolution of the cerebral cortex, increased neuronal number is achieved by augmenting the pool of neural stem and progenitor cells (Lui et al. 2011) and, in particular, by enhancing their proliferative capacity. In human and macaque, the vast

majority of IPs is proliferative and maintains Pax6 expression. Furthermore in macaque, there is a smaller difference in the total cell cycle length between RGs and IPs than that reported in the mouse, allowing them to proliferate faster (Arai et al. 2011; Betizeau et al. 2013). The combination of the increase in the number of IPs undergoing mitosis, possibly being proliferative IPs because of the Pax6, and Tbr2 co-expression, and their reduced cell cycle length, suggests that IPs in *Dbx1^{DTA};Nes:Cre* mutants resemble what has been observed in primates.

An additional modality by which the progenitor pool is enhanced during evolution is via another population of abventricular dividing precursors, namely bRGs. We found that the generation of this progenitor type is also augmented in *Dbx1^{DTA};Nes:Cre* mutant cortices, further arguing in favor of the presence in these mutants of the alteration of a global mechanism central to the control of abventricular proliferation and upper layers neuron numbers during evolution. This is evocative of the fact that mutants for genes involved in spindle orientation have been reported to display enhanced abventricular self-renewing progenitors, and in particular bRG-like precursors (Konno et al. 2008; Postiglione et al. 2011; Shitamukai et al. 2011; Kielar et al. 2014). Interestingly, all these mutants also have in common the temporal appearance of these progenitors at mid-corticogenesis and some rescue properties at later stages, which led to the conclusion that cell fate is not affected. The most prominent difference is that the overall neuronal content is recovered in *Dbx1^{DTA};Nes:Cre* mutants but the proportion of deep and superficial neurons is altered. In most mouse mutants for progenitor proliferation parameters both deep and upper layer neurons are affected in a similar manner, with parallel loss or increase in both as in mutants for precocious differentiation (Hsu et al. 2015) or increased proliferation (Teissier et al. 2012). It was actually recently proposed that the number of upper layers will be scaled to that of the previously born deep layers (Toma et al. 2014). This raises the interesting question of what determines whether or not scaling of deep and upper layer neurons occurs. One possibility is that a temporal shift in the onset of the genesis of abventricular progenitors is a crucial determinant that would control specifically the number of intracortical projection neurons (superficial layer neurons) independently on their subcortical projection neuron counterparts (deep layers neurons) in cortical development and evolution. The second possibility is that not all progenitor types have the same capacity to respond to scaling mechanisms and/or injuries. In favor of this, it has been previously shown that brain injuries can promote neurogenesis in different areas of the adult brain which normally undergo neurogenesis but also in areas which are non-neurogenic (Ekdahl et al. 2009; Gao et al. 2009; Sawada and Sawamoto 2013; Sun 2014). Quiescent neural progenitors, specifically, respond to brain injury in the adult hippocampus by increasing their proliferation rate, but not other progenitor types (Gao et al. 2009; Sawada and Sawamoto 2013; Sun 2014). It was also shown that compensation cannot occur when neural progenitors committed to generate upper cortical neurons are eliminated by environmental insults, such as X-irradiation (Selemon et al. 2013) and absent cells cannot be replaced adequately by the later generated neurons. During development of the neocortex in the mouse, we showed that early neuronal death specifically promotes the amplification of progenitors in the SVZ/IZ but not in the VZ supporting that specific pools of progenitors have the ability to counterbalance the injured brain.

Our data also highlights that recovery of neuronal number does not imply that of function as deep and upper layers

neurons serve very distinct roles by forming descending sub-cerebral tracks and cortico-cortical connections, respectively. Thus, measurements of brain volume or in general neuronal numbers, as often used in human pathology, is not a reliable criteria to determine abnormalities and specific progenitor types and neuronal populations should be carefully analyzed.

Mechanism Promoting the Feedback Control Regulating IPs and bRGs-Like Amplification

In *Dbx1^{DTA};Nes:Cre* mutants, either cell death per se and/or the absence of early-born neurons could lead to IPs and bRGs-like amplification and trigger a mechanism which compensates neuronal content at the end of corticogenesis.

Enhanced abventricular dividing progenitors in *Dbx1^{DTA};Nes:Cre* mutants could be induced by the presence of dying cells. Apoptotic cells have been shown to release signals influencing the proliferation of neighboring cells in various systems (Fuchs and Steller 2015). Major general cell death in the postmitotic compartment has been described in multiple mutants (Yang et al. 2004; Rajaii et al. 2008; Borello et al. 2014). However, none of these mutants displayed enhanced proliferation but rather a decrease in the number of progenitors and neurons in the cerebral cortex. Recently, Toma et al. (2014) demonstrated that the sequential acquisition of the competence to generate upper layer neurons requires a negative feedback from deep layers neurons and that an early ablation of postmitotic neurons prevents the generation of upper layer neurons. In this report no increase in the number of IPs or of superficial layer neurons was observed although massive cell death was present in the postmitotic compartment. Furthermore, we did not observe a temporal shift in the timing of generation of early and late-born neurons as observed by Toma et al. Together these data strongly argue against a general role of cell death itself in enhancing abventricular progenitor proliferation rate and fate as observed in *Dbx1^{DTA};Nes:Cre* mutants. It rather argues in favor of distinct mechanisms underlying the phenotypes in these 2 mutants and either independent on cell death or dependent on the death of a specific cell/progenitor population or on its timing and which will be distinct in each mutant.

The most likely cause of the phenotype in *Dbx1^{DTA};Nes:Cre* mutants is the lack of early-born neurons. These include first early-born preplate neurons, namely Cajal-Retzius cells by E11.5, and subsequently CP transient neurons (Bielle et al. 2005; Teissier et al. 2010) and deep layers neurons starting at E12.5 (this report). We can exclude that *Dbx1*-derived interneurons originating in the POA, which are also eliminated in these mutants, are responsible of the increase of abventricular self-renewing progenitors as this phenotype was not observed in *Dbx1^{DTA};Nkx2.1:Cre* (Supplementary Fig. 5). In these embryos specific ablation of *Dbx1* progenitors in the subpallium did not lead to cell death in the neocortical primordium (Supplementary Fig. 5). Moreover, specific ablation of *Dbx1*-derived CP transient neurons in *Dbx1^{DTA};E1-Ngn2:Cre* starting at E11.5 and sparing Cajal-Retzius cells (Teissier et al. 2010; Teissier et al. 2012), caused an opposite phenotype with precocious neurogenesis and a depletion of Tbr2⁺ progenitors and both deep and upper layer neurons. Consistently, the ablation of deep layer neurons reported by Toma et al. (2014) occurs after E11.5, also likely sparing Cajal-Retzius cell death. Together, these data argue in favor of Cajal-Retzius cell loss as a primary determinant of the phenotype observed in *Dbx1^{DTA};Nes:Cre* mutants.

Several reports have started to unravel the existence of a feedback control from the postmitotic compartment on progenitors (Seuntjens et al. 2009; Griveau et al. 2010; Teissier et al. 2012; Toma et al. 2014; Srivatsa et al. 2015) but the molecular mechanisms are still under investigation. In the developing neocortex, specific overexpression of Ntf3, a Sip1 target neurotrophin, in neurons promotes an overproduction of IPs at the expense of RGs and a shift from deep to upper layer neuron generation (Parthasarathy et al. 2014). It is, thus, possible that the lack of a feedback diffusible signal as a consequence of early neuron loss is also involved in inducing a switch from RGs to IPs in *Dbx1^{DTA};Nes:Cre*. However, this signal is unlikely to be mediated by Ntf3 since its decrease due to neuronal loss would result in an opposite effect and, thus, a decrease in the generation of IPs. Furthermore, Sip1 mutants display a temporal shift of both deep and upper layer generation whereas in *Dbx1^{DTA};Nes:Cre* the timing of deep and upper layer production is as in WT mice. Whether a feedback signal from the postmitotic compartment reaches progenitors via cell-cell contacts or diffusible molecules and whether is direct onto RGs or IPs or through other intermediaries remains to be determined.

Although recent papers have pointed out the role of early-born neurons in the control of neurogenesis, our results point for the first time to the existence of a rescuing mechanism which in the absence of this feedback control allows the cerebral cortex to compensate for early neuronal loss by overproducing abventricular progenitor pools and boosting the generation of upper layer neurons. It is tempting to speculate that during cortical evolution, the increased size of the germinal zones prevents this negative feedback from the postmitotic compartment to be effective and allows the progenitors to continue proliferating. Our results open the possibility that through the manipulation of corticogenesis, neuronal content can in some cases be recovered before birth even after major brain injury during embryonic life and provide a mouse model allowing to shed light on how this process could occur in physiological and pathological conditions.

Supplementary Material

Supplementary material can be found at: <http://www.cercor.oxfordjournals.org/>.

Notes

We acknowledge the ImagoSeine facility, member of the France BioImaging infrastructure supported by the French National Research Agency (ANR-10-INSB-04, "Investments for the future") for help with confocal microscopy and Animalliance for animal care. We thank F. Francis, S. Garel, S. Schneider Maunoury, M. Courgeon, and F. Causeret for critical reading of the manuscript, members of the Pierani's laboratory for discussion, F. Tronche and N. Kessarar for providing the *Nes:Cre* and *Nkx2.1:Cre* mouse lines, A. Prochiantz for helpful discussions and scientific and financial support, E. Coppola for help with the in situ hybridization experiments followed by antibody staining. Y. Arai was the recipient of a fellowship from ARC (Association pour la Recherche sur le Cancer) and FRM (Fondation pour la Recherche Médicale). A.P. is a CNRS (Centre National de la Recherche Scientifique) Investigator and member Team of the École des Neurosciences de Paris Ile-de-France (ENP). This work was supported by grants 84

from the Agence Nationale de la Recherche (ANR-2011-BSV4-023-01), FRM (INE20060306503), FRM («Equipe FRM DEQ20130326521»), Ville de Paris (2006 ASES 102), Association pour la Recherche sur le Cancer (ARC, Projet ARC n° SFI20111203674) and Fédération pour la Recherche sur le Cerveau (FRC) to A.P. *Conflict of Interest*: None declared.

References

- Angevine JBJr, Sidman RL. 1961. Autoradiographic study of cell migration during histogenesis of cerebral cortex in the mouse. *Nature*. 192:766–768.
- Arai Y, Pulvers JN, Haffner C, Schilling B, Nüsslein I, Calegari F, Huttner WB. 2011. Neural stem and progenitor cells shorten S-phase on commitment to neuron production. *Nat Commun*. 2:154.
- Attardo A, Calegari F, Haubensak W, Wilsch-Brauninger M, Huttner WB. 2008. Live imaging at the onset of cortical neurogenesis reveals differential appearance of the neuronal phenotype in apical versus basal progenitor progeny. *PLoS One*. 3:e2388.
- Betizeau M, Cortay V, Patti D, Pfister S, Gautier E, Bellemin-Ménard A, Afanassieff M, Huissoud C, Douglas Rodney J, Kennedy H, et al. 2013. Precursor diversity and complexity of lineage relationships in the outer subventricular zone of the primate. *Neuron*. 80:442–457.
- Bielle F, Griveau A, Narboux-Nême N, Vigneau S, Sigrist M, Arber S, Wassef M, Pierani A. 2005. Multiple origins of Cajal-Retzius cells at the borders of the developing pallium. *Nat Neurosci*. 8:1002–1012.
- Borello U, Madhavan M, Vilinsky I, Faedo A, Pierani A, Rubenstein J, Campbell K. 2014. Sp8 and COUP-TF1 reciprocally regulate patterning and Fgf signaling in cortical progenitors. *Cereb Cortex*. 24:1409–1421.
- Cahalane DJ, Charvet CJ, Finlay BL. 2014. Modeling local and cross-species neuron number variations in the cerebral cortex as arising from a common mechanism. *Proc Natl Acad Sci U S A*. 111:17642–17647.
- Calegari F, Haubensak W, Haffner C, Huttner WB. 2005. Selective lengthening of the cell cycle in the neurogenic subpopulation of neural progenitor cells during mouse brain development. *J Neurosci*. 25:6533–6538.
- Calegari F, Huttner WB. 2003. An inhibition of cyclin-dependent kinases that lengthens, but does not arrest, neuroepithelial cell cycle induces premature neurogenesis. *J Cell Sci*. 116:4947–4955.
- Conti AC, Raghupathi R, Trojanowski JQ, McIntosh TK. 1998. Experimental brain injury induces regionally distinct apoptosis during the acute and delayed post-traumatic period. *J Neurosci*. 18:5663–5672.
- Dehay C, Kennedy H. 2007. Cell-cycle control and cortical development. *Nat Rev Neurosci*. 8:438–450.
- Dehay C, Kennedy H, Kosik KS. 2015. The outer subventricular zone and primate-specific cortical complexification. *Neuron*. 85:683–694.
- Ekdahl CT, Kokaia Z, Lindvall O. 2009. Brain inflammation and adult neurogenesis: the dual role of microglia. *Neuroscience*. 158:1021–1029.
- Englund C, Fink A, Lau C, Pham D, Daza RAM, Bulfone A, Kowalczyk T, Hevner RF. 2005. Pax6, Tbr2, and Tbr1 are expressed sequentially by radial glia, intermediate progenitor cells, and postmitotic neurons in developing neocortex. *J Neurosci*. 25:247–251.

- Fietz SA, Kelava I, Vogt J, Wilsch-Bräuninger M, Stenzel D, Fish JL, Corbeil D, Riehn A, Distler W, Nitsch R, et al. 2010. OSVZ progenitors of human and ferret neocortex are epithelial-like and expand by integrin signaling. *Nat Neurosci.* 13:690–699.
- Florio M, Huttner WB. 2014. Neural progenitors, neurogenesis and the evolution of the neocortex. *Development.* 141:2182–2194.
- Fuchs Y, Steller H. 2015. Live to die another way: modes of programmed cell death and the signals emanating from dying cells. *Nat Rev Mol Cell Biol.* 16:329–344.
- Gal JS, Morozov YM, Ayoub AE, Chatterjee M, Rakic P, Haydar TF. 2006. Molecular and morphological heterogeneity of neural precursors in the mouse neocortical proliferative zones. *J Neurosci.* 26:1045–1056.
- Gao P, Postiglione MP, Krieger TG, Hernandez L, Wang C, Han Z, Streicher C, Papusheva E, Insolera R, Chugh K, et al. 2014. Deterministic progenitor behavior and unitary production of neurons in the neocortex. *Cell.* 159:775–788.
- Gao X, Enikolopov G, Chen J. 2009. Moderate traumatic brain injury promotes proliferation of quiescent neural progenitors in the adult hippocampus. *Exp Neurol.* 219:516–523.
- Glickstein SB, Monaghan JA, Koeller HB, Jones TK, Ross ME. 2009. Cyclin D2 is critical for intermediate progenitor cell proliferation in the embryonic cortex. *J Neurosci.* 29:9614–9624.
- Götz M, Huttner WB. 2005. The cell biology of neurogenesis. *Nat Rev Mol Cell Biol.* 6:777–788.
- Griveau A, Borello U, Causeret F, Tissir F, Boggetto N, Karaz S, Pierani A. 2010. A novel role for Dbx1-derived Cajal-Retzius cells in early regionalization of the cerebral cortical neuroepithelium. *PLoS Biol.* 8:e1000440.
- Hansen DV, Lui JH, Parker PR, Kriegstein AR. 2010. Neurogenic radial glia in the outer subventricular zone of human neocortex. *Nature.* 464:554–561.
- Haubensak W, Attardo A, Denk W, Huttner WB. 2004. Neurons arise in the basal neuroepithelium of the early mammalian telencephalon: a major site of neurogenesis. *Proc Natl Acad Sci U S A.* 101:3196–3201.
- Hsu LC, Nam S, Cui Y, Chang CP, Wang CF, Kuo HC, Touboul JD, Chou SJ. 2015. Lhx2 regulates the timing of beta-catenin-dependent cortical neurogenesis. *Proc Natl Acad Sci U S A.* 112:12199–12204.
- Kessarlis N, Fogarty M, Iannarelli P, Grist M, Wegner M, Richardson WD. 2006. Competing waves of oligodendrocytes in the forebrain and postnatal elimination of an embryonic lineage. *Nat Neurosci.* 9:173–179.
- Kielar M, Tuy FP, Bizzotto S, Lebrand C, de Juan Romero C, Poirier K, Oegema R, Mancini GM, Bahi-Buisson N, Olasso R, et al. 2014. Mutations in Eml1 lead to ectopic progenitors and neuronal heterotopia in mouse and human. *Nat Neurosci.* 17:923–933.
- Konno D, Shioi G, Shitamukai A, Mori A, Kiyonari H, Miyata T, Matsuzaki F. 2008. Neuroepithelial progenitors undergo LGN-dependent planar divisions to maintain self-renewability during mammalian neurogenesis. *Nat Cell Biol.* 10:93–101.
- Lange C, Huttner WB, Calegari F. 2009. Cdk4/CyclinD1 overexpression in neural stem cells shortens G1, delays neurogenesis, and promotes the generation and expansion of basal progenitors. *Cell Stem Cell.* 5:320–331.
- Lui JH, Hansen DV, Kriegstein AR. 2011. Development and evolution of the human neocortex. *Cell.* 146:18–36.
- Manuel MN, Mi D, Mason JO, Price DJ. 2015. Regulation of cerebral cortical neurogenesis by the Pax6 transcription factor. *Front Cell Neurosci.* 9:70.
- Martinez-Cerdeno V, Cunningham CL, Camacho J, Antczak JL, Prakash AN, Cziep ME, Walker AI, Noctor SC. 2012. Comparative analysis of the subventricular zone in rat, ferret and macaque: evidence for an outer subventricular zone in rodents. *PLoS One.* 7:e30178.
- Miyata T, Kawaguchi A, Saito K, Kawano M, Muto T, Ogawa M. 2004. Asymmetric production of surface-dividing and non-surface-dividing cortical progenitor cells. *Development.* 131:3133–3145.
- Noctor SC, Martínez-Cerdeño V, Ivic L, Kriegstein AR. 2004. Cortical neurons arise in symmetric and asymmetric division zones and migrate through specific phases. *Nat Neurosci.* 7:136–144.
- Nowakowski RS, Lewin SB, Miller MW. 1989. Bromodeoxyuridine immunohistochemical determination of the lengths of the cell cycle and the DNA-synthetic phase for an anatomically defined population. *J Neurocytol.* 18:311–318.
- Parthasarathy S, Srivatsa S, Nityanandam A, Tarabykin V. 2014. Ntf3 acts downstream of Sip1 in cortical postmitotic neurons to control progenitor cell fate through feedback signaling. *Development.* 141:3324–3330.
- Pierani A, Moran-Rivard L, Sunshine MJ, Littman DR, Goulding M, Jessell TM. 2001. Control of interneuron fate in the developing spinal cord by the progenitor homeodomain protein Dbx1. *Neuron.* 29:367–384.
- Pilaz L-J, Patti D, Marcy G, Ollier E, Pfister S, Douglas RJ, Betizeau M, Gautier E, Cortay V, Doerflinger N, et al. 2009. Forced G1-phase reduction alters mode of division, neuron number, and laminar phenotype in the cerebral cortex. *Proc Natl Acad Sci U S A.* 106:21924–21929.
- Pilz GA, Shitamukai A, Reillo I, Pacary E, Schwausch J, Stahl R, Ninkovic J, Snippert HJ, Clevers H, Godinho L, et al. 2013. Amplification of progenitors in the mammalian telencephalon includes a new radial glial cell type. *Nat Commun.* 4:2125.
- Postiglione MP, Juschke C, Xie Y, Haas GA, Charalambous C, Knoblich JA. 2011. Mouse inscuteable induces apical-basal spindle orientation to facilitate intermediate progenitor generation in the developing neocortex. *Neuron.* 72:269–284.
- Rajaii F, Bitzer ZT, Xu Q, Sockanathan S. 2008. Expression of the dominant negative retinoid receptor, RAR403, alters telencephalic progenitor proliferation, survival, and cell fate specification. *Dev Biol.* 316:371–382.
- Rakic P. 1972. Mode of cell migration to the superficial layers of fetal monkey neocortex. *J Comp Neurol.* 145:61–83.
- Rakic P. 1974. Neurons in rhesus monkey visual cortex: systematic relation between time of origin and eventual disposition. *Science.* 183:425–427.
- Rees S, Harding R, Walker D. 2011. The biological basis of injury and neuroprotection in the fetal and neonatal brain. *Int J Dev Neurosci.* 29:551–563.
- Sawada M, Sawamoto K. 2013. Mechanisms of neurogenesis in the normal and injured adult brain. *Keio J Med.* 62:13–28.
- Selemon LD, Ceritoglu C, Ratnanather JT, Wang L, Harms MP, Aldridge K, Begovic A, Csernansky JG, Miller MI, Rakic P. 2013. Distinct abnormalities of the primate prefrontal cortex caused by ionizing radiation in early or midgestation. *J Comp Neurol.* 521:1040–1053.
- Seuntjens E, Nityanandam A, Miquelajauregui A, Debruyne J, Stryjewska A, Goebbels S, Nave K-A, Huylebroeck D, Tarabykin V. 2009. Sip1 regulates sequential fate decisions by feedback signaling from postmitotic neurons to progenitors. *Nat Neurosci.* 12:1373–1380.

- Shitamukai A, Konno D, Matsuzaki F. 2011. Oblique radial glial divisions in the developing mouse neocortex induce self-renewing progenitors outside the germinal zone that resemble primate outer subventricular zone progenitors. *J Neurosci*. 31:3683–3695.
- Srivatsa S, Parthasarathy S, Molnár Z, Tarabykin V. 2015. Sip1 downstream effector ninein controls neocortical axonal growth, ipsilateral branching, and microtubule growth and stability. *Neuron*. 85:998–1012.
- Sun D. 2014. The potential of endogenous neurogenesis for brain repair and regeneration following traumatic brain injury. *Neural Regen Res*. 9:688.
- Takahashi T, Nowakowski RS, Caviness VS Jr. 1993. Cell cycle parameters and patterns of nuclear movement in the neocortical proliferative zone of the fetal mouse. *J Neurosci*. 13:820–833.
- Takahashi T, Nowakowski RS, Caviness VS Jr. 1995. The cell cycle of the pseudostratified ventricular epithelium of the embryonic murine cerebral wall. *J Neurosci*. 15:6046–6057.
- Taverna E, Gotz M, Huttner WB. 2014. The cell biology of neurogenesis: toward an understanding of the development and evolution of the neocortex. *Annu Rev Cell Dev Biol*. 30:465–502.
- Teissier A, Griveau A, Vigier L, Piolot T, Borello U, Pierani A. 2010. A novel transient glutamatergic population migrating from the pallial-subpallial boundary contributes to neocortical development. *J Neurosci*. 30:10563–10574.
- Teissier A, Waclaw RR, Griveau A, Campbell K, Pierani A. 2012. Tangentially migrating transient glutamatergic neurons control neurogenesis and maintenance of cerebral cortical progenitor pools. *Cereb Cortex*. 22:403–416.
- Toma K, Kumamoto T, Hanashima C. 2014. The timing of upper-layer neurogenesis is conferred by sequential derepression and negative feedback from deep-layer neurons. *J Neurosci*. 34:13259–13276.
- Turrero Garcia M, Chang Y, Arai Y, Huttner WB. 2016. S-phase duration is the main target of cell cycle regulation in neural progenitors of developing ferret neocortex. *J Comp Neurol*. 524:456–470.
- Tyler WA, Haydar TF. 2013. Multiplex genetic fate mapping reveals a novel route of neocortical neurogenesis, which is altered in the Ts65Dn mouse model of Down syndrome. *J Neurosci*. 33:5106–5119.
- Wang X, Tsai JW, LaMonica B, Kriegstein AR. 2011. A new subtype of progenitor cell in the mouse embryonic neocortex. *Nat Neurosci*. 14:555–561.
- Wong FK, Fei JF, Mora-Bermudez F, Taverna E, Haffner C, Fu J, Anastassiadis K, Stewart AF, Huttner WB. 2015. Sustained Pax6 expression generates primate-like basal radial glia in developing mouse neocortex. *PLoS Biol*. 13:e1002217.
- Workman AD, Charvet CJ, Clancy B, Darlington RB, Finlay BL. 2013. Modeling transformations of neurodevelopmental sequences across mammalian species. *J Neurosci*. 33:7368–7383.
- Yang X, Klein R, Tian X, Cheng HT, Kopan R, Shen J. 2004. Notch activation induces apoptosis in neural progenitor cells through a p53-dependent pathway. *Dev Biol*. 269:81–94.

3.2 Basic response mechanisms to cell death

Both mutant models studied in Freret-Hodara et al., 2016; Toma et al., 2014 induced early deep layer neuron loss, however opposite compensation consequences were reported in these two mutant mice. Diffuse chemically-induced cell death in *Neurog2:Cre; Rosa26^{DTA}* mice (mut1) (Toma et al., 2014) leads to around 30% reduced volume but deep layer and upper layer proportions untouched. Early neurons death between E11.5 to E14.5 caused by ablation of *Dbx1* expressing cells in *Nes:Cre; Dbx1^{DTA}* mice (mut2) (Freret-Hodara et al., 2016) yield normal neuron number per unit with abnormal neuron layer proportions, 30% reduction of deep layer neurons and 20% increase of upper layer neurons.

This difference may be due to at least two factors: (1) the duration of neuronal death, that may differ in the two models, and (2) the specific mechanisms of neuron death induction. Indeed, supporting the former view, we note that in mut1, tamoxifen was applied for three consecutive days, which requires 5-6 days after the first injection to be eliminated (Jahn et al., 2018). Therefore, we inferred that neuronal death would last till E16 after the switch time point from deep layer to upper layer neuron generation. Supporting the latter factor, we note that in mut1, cell death, induced by DTA, is a diffuse process throughout (from E11.5 to around E16) (figure 15 A and B). DTA is expressed in *Neurog2* positive cells, meaning only new born neurons are affected. Neurons that were generated before E11.5 are thus spared from apoptosis. In contrast, in mut2, DTA is not expressed directly in neurons, and neuron death is caused by the ablation of *Dbx1* expressing cells. Even though the tamoxifen is not cleaned, once *Dbx1* positive cells are eliminated, neuron death ends. In that situation, both newly generated neurons and already generated neurons have a probability to enter the apoptosis program (figure 15 A and B).

Based on these observations, we hypothesized that an identical compensation mechanism may account for both phenotypes, and that the observed differences are due to the way neural death was induced. To test this hypothesis, we developed a simple compensation mechanism based on neural death signals. Dead cells indeed send signals in their direct environment (Morrow et al., 2001), which triggers physiological reactions, in particular the mobilization of macrophages clearing the

dead cells, and thus interrupting their signalization within half a day. Based on these facts, we considered that the neurogenesis system may have access to a cumulated signal released by those cells dead within the past 12h.

Many complex cascades may be triggered by those signals and induce compensation mechanisms. In particular, we can infer from biological data that a high level of cell death signal will:

- (1) increase the probability of IPs proliferative symmetric divisions and inducing at least one of these divisions to occur, with a maximum of two divisions (Fietz et al., 2010; Martínez-Cerdeño, Noctor, & Kriegstein, 2006; Noctor et al., 2004);
- (2) delay the switch between upper- and deep-layer neurons generation. In the WT mice, this switch occurs at around E15, and for an effective compensation of early born neuronal death (therefore, from deep layers neuron), the switching time may be postponed depending on the level of cell death, by a maximum of 24h.

These two basic mechanisms, supported by the data, are the bare necessary elements to account for the biological observations at hand. We fitted the probability of IPs to perform two time divisions and the IPs cell cycle duration with the neuron number count data in mut2. We fitted the change of probability for neurons to choose deep layer and upper layer with the experimental data of mut1. Then we show here that their combination is sufficient to explain phenotypes in the WT, mut1 and mut2, and to predict what happens in a wide range of situations. In that, we show that these two mechanisms provide the brain with a powerful homeostasis mechanism able to restore normal brain phenotype in a response to a wide range of cell death levels, and it is only in extreme situations (massive death of early born neurons in mut2, or long-lasting neuronal death in mut1) that it breaks down.

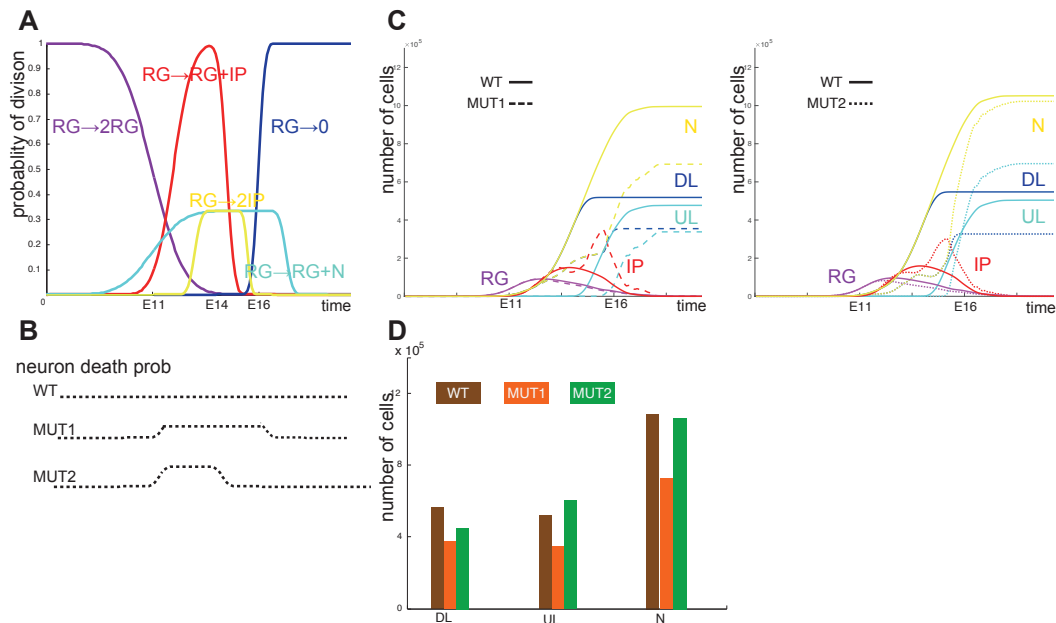


Figure 15. Reproduction of two experimental data with the one compensation model. (A) The probability of different divisions and differentiations. (B) Neurons die from E11 to E16 in mut1 and intense death from E11 to E14 in mut2. (C) Evolution in time of the number of cells during neurogenesis (RG in purple, IP in red, total neuron number in yellow, deep layer neurons in dark blue and upper layer neurons in light blue) for the WT model (solid lines), mut1 (dashed lines) mut2 (dotted lines). (D) Number of neurons in deep layer (DL), upper layer (UL) and the total number of neurons (N) at the end of neurogenesis for WT. Data are represented as mean \pm STD with 50 independent MATLAB simulations.

3.3 Compensation breakdown in mutant models

To test the model, we simulated the number of RGs, deep and upper layer neurons, as well as the transient population of IP cells, as a function of time and in response to a diffuse but long induction of cell death (as in mut1), or to an acute and brief induction of cell death (as in mut2). Figure 15B represents the simulated size of those populations of neurons as a function of the developmental time for the WT model (solid line), mut1 (dashed line) and mut2 (dotted line). The simulation results of

neuron number fit with the experimental observation (Figure 15 C). We observe that despite the acuity of cell death in mut2, the total cumulated number of dead neurons is significantly higher in mut1. The average of total neuron death number is 70% in mut1 compared to 35% in mut2 of total neuron number in WT. This observation therefore provides an account for the distinct phenotypes generated: the level of neuron loss in mut2 remains in the range of compensation capacity of IPs, particularly during the longer period of time remaining within the neurogenesis process. However, in mut1, the diffuse cell death lasting until E16 induces a severe loss that exceeds the compensation capacity of IPs during the remaining time after termination of cell death at E16, 2 days later than in to mut2. E16 is the middle-late stage of neurogenesis. At this stage, the IP population size starts decreasing due a decreased generation from RGs associated with the natural decrease in the RG population size as they are consumed by symmetric neurogenic divisions. Despite a remarkable peak of IPs at around E16, significantly larger than the size of the IP population in mut1, the capacity of the IP population in mut1 to compensate for neuronal loss after E16 is affected.

Early neuronal death (occurring between E11 and E14) reduces only number of deep layer neuron. After the response to signals generated by dead neurons, IPs start preforming two proliferative divisions before a final symmetric neurogenic division, and thus each IP can eventually give rise to 8 neurons over the course of 3 IPs cycles. Even though IPs cycle duration shortens from 24.5h in WT to 16.7 in mut2, it takes more than 2 days from neuron death to the beginning of compensation. As a result, IP numbers reach a peak between E15-E16 in both mutant models. If the switching time between the generation of deep or upper layer neurons was maintained unchanged, the ratio between deep and upper layer neuron number should decrease significantly in both mutants. The observation in Toma et al., 2014 of a conserved ratio therefore suggests that the transition of generating deep to upper layer neurons delayed in response to cell death signals. Since little is known about this adjustment, we assumed that this delay should be proportional to the signal. As deep and upper layer neurons shows different projection behavior and function, we limit this time point shift maximum 24h. This hypothesis is consistent with the observations in both mutants, particularly mut1 where neuronal death lasts until mid-late stage of neurogenesis

stage and the ratio between deep and upper layer neuron number maintained identical to the WT ratio, which could not occur if the switching time between upper- and deeper-layer neurons was unchanged and where upper layer neuron would largely dominate.

3.4 Homeostasis and compensation of mild to severe neuronal death

Despite the failure to compensate massive cell death observed in the two mutant mice models studied in the previous section, the combination of the two previously described mechanisms has powerful homeostatic capabilities. In particular, because of its multiplicative impact, even a small increase in IPs performing one additional proliferative division before neurogenic division is enough to compensate severe cell death occurring during early stages of development. These additional divisions delay the birthdate of neurons compensating for dead cells. The regulation of the switching time point from deep to upper layer neuron generation up to 24h can perfectly accommodate for this delayed emergence of cells. Altogether, these two basic mechanisms are sufficient to stabilize the WT brain phenotype for a wide range and patterns of cell death in early development stage. We tested this capacity quantitatively by continuously varying the amplitude and the duration of an increase in neural death. Figure 16 shows the total number of neurons generated (associated with cortical thickness) and the proportion of deep layer neurons as a function of new born neurons apoptosis probability and the occurrence timing. We observe that the total neuron number is maintained constant regardless of death probability when cell death occurs early enough (before E14), but the percentage of deep layer neuron shows some fluctuations, limited to a 10% range around the 50% WT proportion. Therefore, for cell death occurring between E11.5 to E14.5, even though the accumulated cell death reaches around 70% of deep layer neuron number in WT, these two compensation mechanisms adjust the total neuron number and the ratio in deep and upper layers precisely (figure 16 A).

However, when the cell death extends 2 more days till E16.5, the cumulative number of dead cells could reach a level equivalent to the total number of neurons generated in the WT model (figure 16 B). The compensation becomes ineffective when

apoptosis probability is large, and the upper layer⁺ neurons generated to compensate for the loss of neurons end up dominating. Once the cell death probability reaches 70%, the total number of neurons generated decreases significantly, therefore a thinner cortex is generated, consistent with what is observed in *mut1*. As for the layer organization, it remains essentially within a level of 10% even when apoptosis probability results in the death of a number of neurons corresponding to 85% of the total number of neurons in the WT model. From these results, we can infer that the level of cell death is between 70% to 85% of the total brain size in *mut1*. In this range, the ratio of deep over upper layer neurons is conserved as WT, but the total neuron number decreases significantly.

Then we tested how the end time point affects the compensation capacity with a fixed death rate. As expected, with low death cell rate causing around 50% neuronal loss, the simulations show perfect compensation regardless of the duration. When fixing death rate to the level associated with 85% neuron loss, the compensation behavior is related to cell death duration. Perfect compensation is only observed when cell death ends before E14. When the neuronal death is severe and persistent, these two mechanisms are not enough to sustain full compensation as shown in figure 16C.

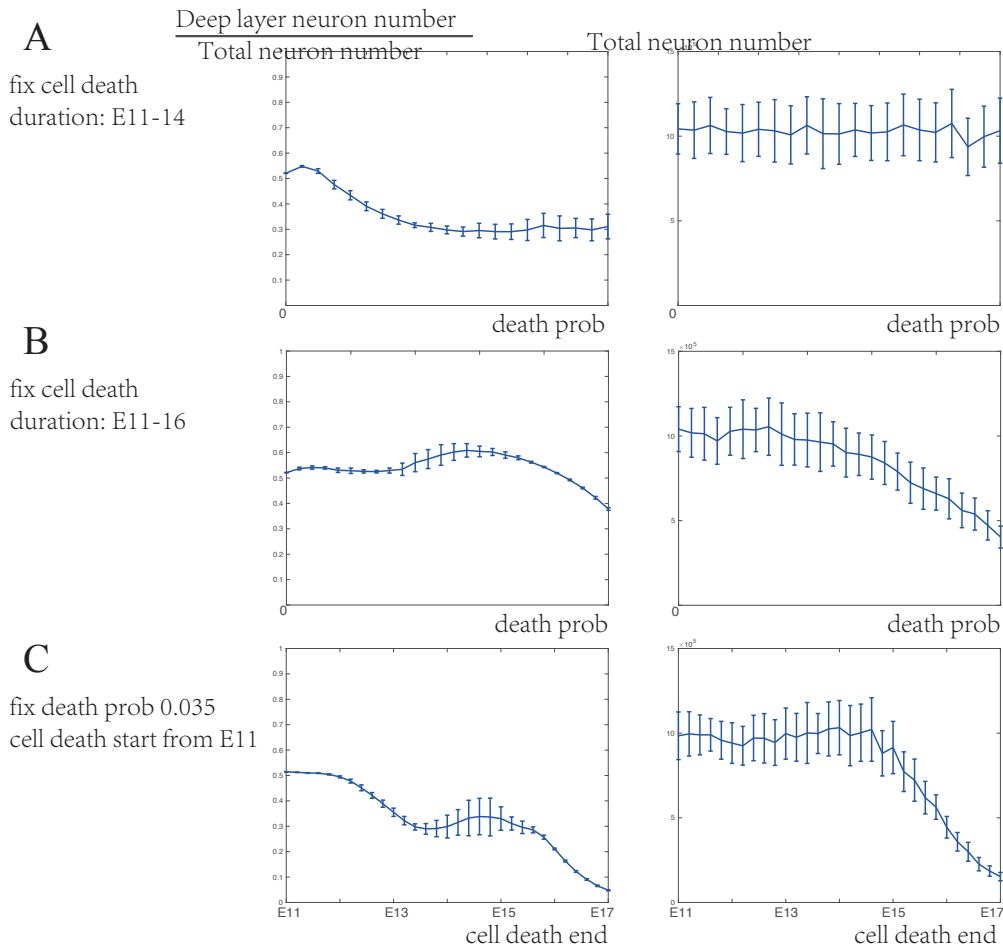


Figure 16. The compensation ranges of neuron death probability and death duration. (A,B) Variations according to the probability of cell death with a fixed cell death duration: (A) from E11 to 14, the number of neurons is fully compensated regardless of the death probability, while newly generated neurons essentially contribute to superficial layers, leading to a decrease of the proportion of deep layer neurons. (B) from E11 to 16, the proportion is kept because the death lasts until after the transition to upper layer neurons. With high death probability, the total neuron number is not fully compensated. (C) Variations according to the death end time point with a fixed and relative high cell death probability. The ratio of deep layer neurons is sensitive to cell death end point. The compensation of neuron number breaks down when the death ends after E14.5. Data are represented as mean \pm standard deviation (SD) with 50 independent MATLAB simulations.

Altogether we have shown that increasing the probability of IPs performing once more proliferative division before neurogenic division and postponing the shift from deep to upper layer maximum by 24 hours can allow the compensation of a large range of neuron death.

3.5 Programmed and abnormal cell death, homeostasis and its breakdown

In physiological conditions, multiple types of cells undergo cell death during the development of the cerebral cortex. Programmed cell death is an important mechanism contributing to homeostasis in embryonic development (Burek & Oppenheim, 1999). Reciprocally, unexpected apoptosis is also common, not only in pathological conditions, but also following incidents such as alcohol intoxication, temporary asphyxia or viruses. Mechanisms responding appropriately to these incidents, in a sense, are as essential as programmed cell death during cortical development.

The above analysis revealed the presence of at least two simple compensation mechanisms involved in this regulation: 1) A gradual increase in the number of the transient IP population through an increase of their probability to be generated and to perform an additional proliferative division before their neurogenic division, sufficient to recover neuron number even in intense cell death during early-mid development stage. 2) A gradual delay in the switching time between generating deep neurons and upper layer neuron, limited to 24h, regulates the layer ratio. These two mechanisms are sufficient to stabilize the WT brain phenotype for a wide range and patterns of cell death, breaking down only when levels of cell death are excessive and late.

Despite this apparent strong compensation capability, a number of conditions lead to significant microcephaly, some being lethal. Two important examples considered important public health issues are the Zika virus infection and the prenatal ethanol exposure. We discuss why the regulatory mechanisms described above breakdown in both cases.

Zika virus infection of pregnant women causes fetal developmental abnormalities and

disabilities. In particular, a causal link between Zika Virus infection during pregnancy and the development of microcephaly was established. This infection thus provides us with a choice situation where homeostasis mechanisms breakdown; microcephaly could indeed ensue from a late neuronal death, or the inability of the homeostasis mechanisms to operate. Data seem to favor the second hypothesis. Indeed, recent studies have shown that Zika Virus mainly targets progenitor cells. All mechanisms described in the present manuscript therefore no more apply: first, microcephaly does not seem to be a result of neuronal death, but rather a lower level of neurogenesis. No cell death signal is thus released to trigger a response. Moreover, our mechanisms rely on the capacity of progenitor cells to accelerate their cell cycle, modify the probabilities of specific divisions and delay deep to upper layer neurons generation time shift. By affecting directly the ability of progenitors, none of the regulatory mechanism can be triggered, in addition to the fact that Zika virus is not generating the same cell death signals that we hypothesized engender recovery. Contrasting with neuronal death during development that can be compensated by modifications of the programmed divisions of progenitor cells, the compensation mechanism we proposed is not operant when progenitors are affected (figure17) (Wen, Song, & Ming, 2017).

The central nervous system of the embryo is the main organ influenced by prenatal ethanol exposure during pregnancy. Mild to moderate microcephaly is a typical symptom in the fetal alcohol syndrome. When pregnant rats are treated with ethanol, a nearly twofold increase in caspase-3 expression in neuron layers compared to control rats is found during development stages, indicating prenatal alcohol exposure induces neuronal apoptosis in cerebral cortex (Sogut et al., 2017). According to the model, we could expect IP progenitors to increase the number of proliferative division to compensate neuron number after apoptosis. That is exactly the observation in experiment using rat model. There are more IPs and more proliferating IPs in the ethanol treatment rat (Miller, 1989). Also experiments show that prenatal ethanol exposure also delays the generation of neurons by 1 day from the generation of layer 5 (Miller, 1987; 1993).

However, in the prenatal ethanol exposure condition, the proliferation of neural progenitors is also impaired. This ethanol inducing hyper-differentiation of glutamatergic neuron prevents progenitor compensation. Neuron death together with

both RGs and IPs loss reduces brain size under prenatal ethanol exposure (figure 17).

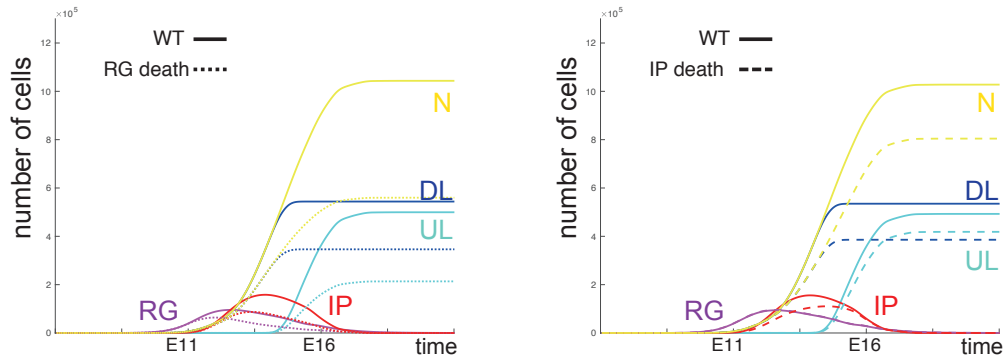


Figure 17. Progenitor death, both RGs and IPs, during development significantly reduces neuron number. Death of a small number RGs in the beginning of neurogenesis reduces the number of itself at later development stage, thus, half the number of neurons. The neuron number is less influenced by IPs death compared to RGs, but also irreparable by these two compensation mechanisms.

4. Discussion

4.1 Possible biological compensation mechanisms

We analyzed two experimental models of early neurons ablation leading to massive neuron loss phenotypes at E14.5. Both the experimental models of cell death show compensation after neuronal death, however the phenotypes observed at the term of neocortical neurogenesis are opposite. This surprising discrepancy may be multifarious, including a potential relationship with the procedure of cell death induction (that are indeed distinct in the two mutant models), or the superposition of various compensation mechanisms that would be favored in one or the other model, or combinations of those potential mechanisms.

Signal from deep-layer neurons and inflammation caused by cell death may be responsible for this phenotype. Postmitotic neurons exert a role on the proliferation and differentiation of progenitors (Griveau et al., 2010; Seuntjens et al., 2009; Srivatsa, Parthasarathy, Molnár, & Tarabykin, 2015; Teissier, Waclaw, Griveau, Campbell, & Pierani, 2011). Indeed, the feedback on the progenitors is dependent on the expression of Ntf3 inhibited by Sip1 in the postmitotic cells (Parthasarathy, Srivatsa, Nityanandam, & Tarabykin, 2014; Seuntjens et al., 2009). In the Nes:Cre;Dbx1DTA mutant, there is a decrease in RGs, an increase in IPs, a decrease in deep layer neurons and an increase in upper layers. It would be interesting to check if there is a deregulation of Ntf3 in this mutant. In both ablation mutant mice, there is significant cell death of cortical neurons. We therefore wondered whether it is the neuroinflammation induced by the cell death or if it is the absence of these neurons that modify the proliferation of progenitors. Neuroinflammation was indeed shown to increase neurogenesis in adulthood, for example in the subependymal zone that generates interneurons and in the hippocampus ventricles in adult (Akhtar & Breunig, 2015; Chirumamilla, Sun, Bullock, & Colello, 2002; Dash, Mach, & Moore, 2001). Several studies have also shown that the loss of neurons in the adult cerebral cortex can induce the division and differentiation of precursors (Magavi, Leavitt, & Macklis, 2000; Sawada & Sawamoto, 2013). Interestingly, embryonic and postnatal microglia cells appear to mediate the proliferation and differentiation of progenitors (Cunningham, Martínez-Cerdeño, & Noctor, 2013; Ekdahl, Kokaia, & Lindvall,

2009). In the *mut2*, microglia cells are present in greater numbers at sites where cell death is present.

4.2 A universal mathematical model of compensation

Despite all possible biological compensation mechanisms and various phenotypes observed, it is likely that a single, universal mechanism is at play in brain regulation of the number of neurons and proportion in each layer in a physiological ranges, and that the same mechanism participates to a robust compensation of minor neuronal loss that could occur during cortical development. To discover this unified model, we developed a mathematical model based on various data from the literature or that we collected. We first detailed the mathematical model on neurogenesis describing the progenitor divisions and differentiations we developed and described in chapter I. In the original model, we considered only one type of neuronal progenitor RGs.

To adapt the model to the neuronal loss mouse models, we introduced a new type of progenitor IPs. IPs are derived from RGs. IPs divide symmetrically either neurogenically producing two new neurons or, in amplification divisions, two of daughter IPs. Thus, we add several types of new divisions describing RGs differentiate into IPs and IPs 2 types of divisions or differentiation into 2 IPs and 2 neurons, which give the possibility to modulate the number of IPs, IPs division types and IPs cell cycle duration. These two simple compensation mechanisms alone were sufficient to explain phenotypes in both mutants. First, cell death recruits IPs by adding one time more symmetric division to proliferative IPs and increased probability of IP symmetric division. Second, the transition between upper- and deep-layer neurons generation is adjusted to compensate the delayed neurogenesis associated with the additional cells-cycles necessary for the first step. In WT the switch timing is around E15. To compensate early deep layer neuron loss, the end time point of deep layer neuron postponed, with a maximum 24h delay of the WT.

4.3 Compensation capacity of the model

The compensation mechanism we proposed is very powerful which could enable recovery from a large range of postmitotic neuron loss during early. Massive cell death occurred, but did not target the same neuronal populations: *mut1* targeted new

born neurons only, while in *mut2* increased cell death affected all existing neurons irrespective of their birthdate. We observed that by increasing the probability that IP neurons undergo one additional proliferative division, the system has the theoretical capacity to compensate this extreme loss of neurons. This hypothesis is a realistic mechanism. Indeed, studies have shown that modifications of IPs amplification across developmental stages in different cortical areas modulate laminar neurogenesis and contributes to the cytoarchitectonic differentiation of cortical areas (Pontious, Kowalczyk, Englund, & Hevner, 2008). It also has been shown that regulation IPs genesis and amplification plays a role in tangential expansion of the cerebral cortex during evolution (Martínez-Cerdeño et al., 2006).

However, these additional divisions induce a delay in the generation of neurons. The observed persistence of the ratio between upper and deeper layer neurons in *mut1* reveals that the transition between deeper and upper layer neurons should be delayed in response to cell death, and data support this view (Toma, Kumamoto, & Hanashima, 2014). We thus added to the model a progressive delay in the transition from deep to upper layer neuron generation, within a limit of one day. This delay was able to perfectly balance the proportion of neuron number in deep and upper layers in the circumstance of massive early neuron loss. In WT, this transition happens around E14.5, the peak of neurogenesis. Thus the proportion of neuron number is sensitive to this transition time point.

4.4 Prenatal ethanol exposure induced neuron loss triggers both of the compensation mechanisms

Microcephaly is a typical symptom in the fetal alcohol syndrome. Lower number of neurons has been observed in alcohol treated animals (Cheema, West, & Miranda, 2000; McAlhany, West, & Miranda, 2000). In particular, it was shown that ethanol-treated rats have one third fewer cells compared to controls in the S1 region (Miller & Potempa, 1990). According to our model of compensation, we predict that the progenitors should react to this neuron loss to keep the homeostasis, by 1) increasing the number of IPs and performing an additional proliferative division before IPs neurogenic division, 2) delaying the switching time to generating upper layer neurons, limited to 24h, regulates the layer ratio. The experimental observation

coincides with the prediction from the model. Both IPs total number and number of cells under mitosis in SVZ significantly increase in ethanol treated mice (Miller, 1989). Studies have also shown that ethanol delays the generation of corticospinal neurons by 1 day, from the generation of layer 5 (Miller, 1987; 1993). Thus, prenatal ethanol exposure is a perfect *in vivo* pathological evidence of the two compensation mechanisms we proposed in the model. However, a perfect compensation does not occur, inconsistent with the model. The literature in the fetal alcohol syndrome actually shows that it is not only neurons that are driven to apoptosis, but also RGs. Considering the vast literature on Zika virus and RG apoptosis, it seems that RGs cell death does not trigger any compensation mechanisms (Tang et al. 2016; Garcez et al. 2016; Cugola et al. 2016). Therefore, the impact of ethanol on the fetal developing brain decreases the pool of RGs and does not add to the signal triggering compensation. As a consequence, rescue mechanisms may compensate only for those neurons entered in apoptosis, but not to the loss of potential neurons that would have been generated by the progenitors that entered apoptosis in response to ethanol exposure.

Chapter IV: Role of homeoprotein Pax6 diffusion in cortical development

1. Introduction

Homeoproteins are a class of transcription factors with a highly conserved DNA binding domain, the homeodomain. This homeodomain is coded by a 180-nucleotide long sequence. Homeoproteins are active throughout development and in adulthood. Their membrane transduction properties were discovered over 30 years ago, opening an original field of research in the domain of vector peptides and signal transduction.

1.1 Role of homeoproteins during development

Homeoproteins as classical transcription factors playing a key role throughout development and in the adult. In *Drosophila* mutants of the homeodomain genes, dramatic modifications of the body plan of the organism were observed. In one of the striking examples of the transformations, the antenna on the head is replaced by the legs of the second thoracic segment, suggesting that homeoproteins play a key role in specifying cell identity and positioning during embryonic development (Gehring, 1967; D. L. Lewis et al., 1999; E. B. Lewis, 1978).

In mammalian central nervous system development, homeoproteins play a crucial role in the compartmentalization (figure 18). They participate in the formation, positioning and stabilization of the boundaries separating two adjacent compartments. On two sides of the boundaries, two different homeoproteins are expressed. The boundaries are established due to the mechanism of self-activation and reciprocal inhibitory activities at a transcription level of two homeoproteins (figure 18A) (Kiecker & Lumsden, 2005; Quiñinao et al., 2015). One of the well-studied examples is the midbrain/hindbrain boundary governed by the balance between *Otx2* and *Gbx2* (Joyner, Liu, & Millet, 2000; Simeone, 2000). However, for the realization of the neocortex, there is no sharp boundary of the expression of homeodomain transcription factors during development. Homeodomain transcription factors *Pax6* and *Emx2* form opposite gradients along the anterior-posterior and medial-lateral axes of the neocortex and these gradients of *Pax6* and *Emx2* are crucial for the position of the frontier between S1 and V1 (figure 18B) (O'Leary & Sahara, 2008).

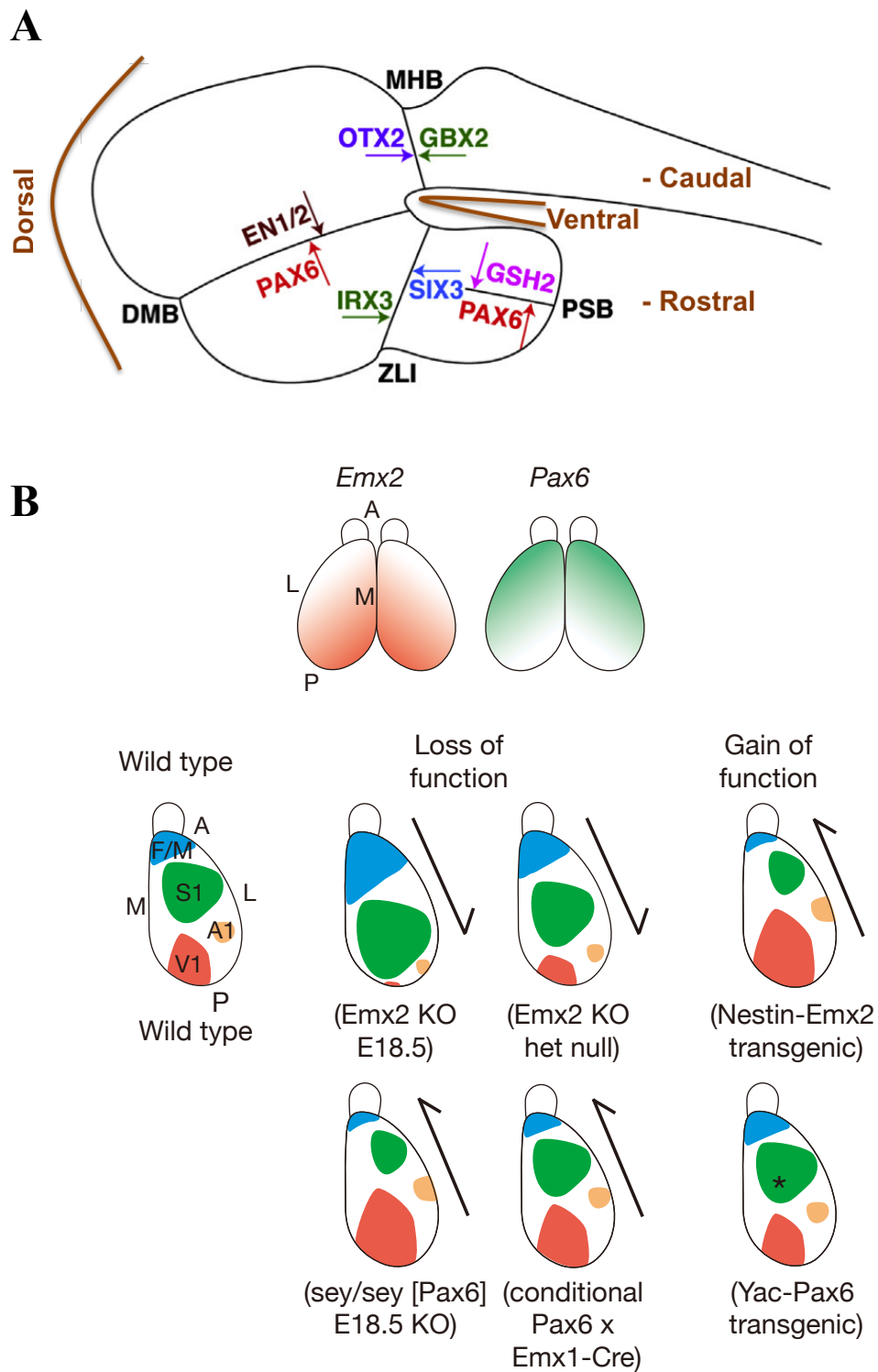


Figure 18. A. Example of boundaries defined by the expression of abutting homeoproteins with self-activating and reciprocal inhibiting properties. MHB

midbrain/hindbrain boundary, DMB diencephalon/midbrain, ZLI Zona limitans intrathalamica, PSB pallial-subpallial boundary. B. Emx2 and Pax6 graded expression in cortical progenitors. Emx2 is expressed in a high posterior - medial to low anterior-lateral gradient. Pax6 expression gradient is opposite that of Emx2. Boundary shift of adult mice mutant of TFs that regulate area patterning. Emx2^{-/-} and Emx2 heterozygote mutant mice show posterior shifts of S1/V1 boundary with expansion of S1 and shrinkage of V1. Gain-of-function of Emx2 under the control of the Nestin promoter shifts the boundary anteriorly. Small eye mutant (Pax6 hypomorph) mice, with less functional Pax6, have a smaller frontal/motor cortex and die before the S1/V1 boundary could be defined. YAC transgenic mice of Pax6 show a significant reduction in the size of S1. Adapted from O'Leary & Sahara, 2008; Prochiantz & Di Nardo, 2015.

1.2 Homeoprotein transfer

Homeoproteins, in addition to their cell autonomous activities, can transfer between cells and regulate transcription and translation in a non-cell autonomous way. Nearly 30 years ago, Alain Prochiantz's group discovered the ability of homeoproteins to translocate across biological membranes. The first observation of this unconventional role of homeoproteins was the internalization of the homeodomain of Antennapedia. As a negative control experiment, the homeodomain of Antennapedia was put in the external environment without modification of the membrane, the researchers also observed a change in the morphology of the neurons, similar as when the homeodomain was artificially internalized into cells. This observation suggested that the homeodomain may have the capacity of entering cell by itself (Joliot, Pernelle, Deagostini-Bazin, & Prochiantz, 1991). Then a 16 amino acids long minimal domain was identified to be necessary and sufficient for translocation and matches exactly the homeodomain third helix (Derossi, Joliot, Chassaing, & Prochiantz, 1994; Le Roux, Joliot, Bloch-Gallego, Prochiantz, & Volovitch, 1993).

Most of the homeoproteins continue to be expressed during the whole process of development and during adulthood. Like many other proteins, there is much about their function that we are yet to discover and they are constantly revealing new functions. More importantly, homeoprotein transfer has been shown to be involved in

many physiological roles. In the nervous system, in addition to their role in segmentation and compartmentalization, Engrailed has been shown the function of regulation the guidance of retinal ganglion cell axons (Brunet et al., 2005; Wizenmann et al., 2009). Later in the adult, Engrailed is expressed in dopaminergic neurons of the substantia, play a neuron protection role (Rekaik et al., 2015). Otx2 secreted from the choroid plexus can be internalized by the Parvalbumin interneurons of the visual cortex and regulate their plasticity (Bernard et al., 2016; Beurdeley et al., 2012; Spatazza et al., 2013).

1.3 Role of Pax6 during cortical development

The Pax6 protein contains different DNA binding domains: the paired domain at the amino terminal, a homeodomain and a transactivation domain. It is very highly conserved during evolution, presenting a rostro-lateral high to caudo-medial low gradient throughout the developing cortex. Its expression level and pattern are essential for normal corticogenesis. Pax6 functions both inside the cell as a transcription factor and also by transferring between neighboring cells non-cell autonomously. The transcriptional functions of Pax6 are well-studied analyzing the phenotype of mutant mice small eye mutant (Pax6^{Sey}) which is carrying a non-functional Pax6 protein (Hill et al., 1991).

Losing Pax6 expression in the developing cortex leads to a reduction of the brain size and a thinner cortical plate with appropriate neuron migration. The role of Pax6 together with Emx2 in regionalization of the telencephalon defining the borders between the V1 and S1 has been introduced in Chapter 1. Other than that, Pax6 is involved in the regulation of the neurogenic process. In Pax6^{Sey}, the neurogenesis of dorsal telencephalon of mutant mice is strongly impaired (Schmahl, Knoedlseder, Favor, & Davidson, 1993). Modification of Pax6 expression leads to impaired of RGs neurogenic program (Heins et al., 2002; Noctor et al., 2004). The Pax6 concentration inside progenitors controls the balance between progenitor proliferation to enlarge the progenitor pool and differentiation to generate new pyramidal neurons. Increasing Pax6 expression, progenitors precociously turn on the program for neuron differentiation, causing progenitors exit the cell cycle and start differentiating. In the developing cortex, the deletion of Pax6 leads to an increase of proliferation of

progenitors (Götz, Stoykova, & Gruss, 1998). In addition, when Pax6 is not functional, RGs delaminate from apical membrane prematurely and contribute to the non-apical increase of proliferating progenitors (Asami et al., 2011). Both increase and decrease the concentration of functional Pax6 lead to a small brain ultimately, but through very different mechanisms (figure 19) (Sansom et al., 2009).

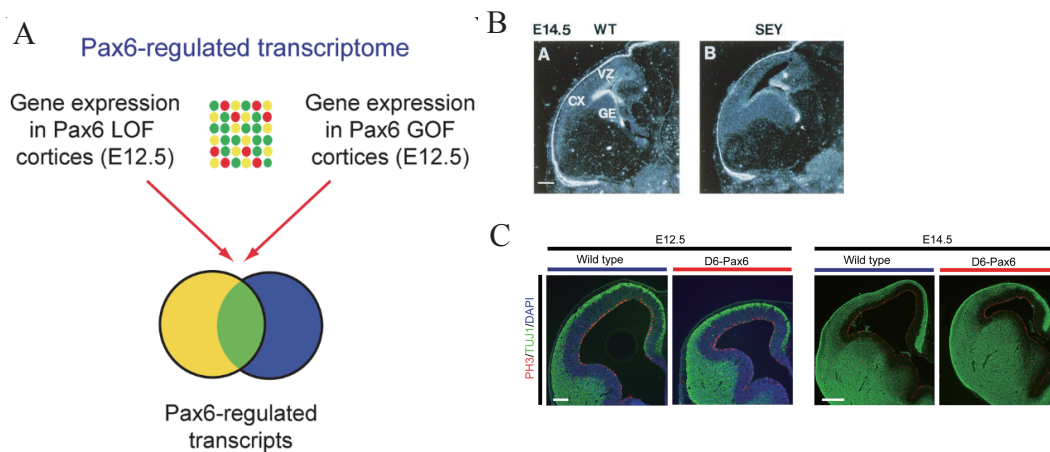


Figure 19. Pax6 regulates the balance between progenitor proliferation and neurogenesis. A. At E12.5 Pax6 regulate the downstream gene transcription in wild-type and Pax6 loss-of-function (LOF) cortices (*Sey/Sey*) and also between wild-type and Pax6 gain-of-function (GOF) cortices (*D6-Pax6*). B. Sagittal sections of E14.5 between wild-type and Pax6 loss-of-function (LOF) cortices (*Sey/Sey*). Decrease Pax6 expression results in a thinner cortex. C. Coronal sections of E12.5 between wild-type and Pax6 gain-of-function (GOF) cortices (*D6-Pax6*). Increased Pax6 expression results in a reduction in total cortical size at both at E12.5 and E14.5. Green, Tuj1; red, phospho-histone H3, staining for cells in M-phase at the ventricular surface; blue, DAPI. Adapted from Asami et al., 2011; Götz et al., 1998; Heins et al., 2002.

The non-cell autonomous role of Pax6 is also well studied in Prochiantz's lab using the single-chain antibodies against Pax6 (anti-Pax6 scFv) technique. Blocking Pax6 diffusion by the expression of anti-Pax6 scFv in the developing zebrafish leads to a

reduced eye field, demonstrating a non-cell autonomous role for Pax6 homeoprotein in eye development (Lesaffre, Joliot, Prochiantz, & Volovitch, 2007). Then Elizabeth Di Lull and colleagues investigated role for Pax6 transfer in oligodendrocyte precursor cell migration using embryonic chick neural tube. They found oligodendrocyte precursor cell migration is promoted by extracellular Pax6 (Di Lullo et al., 2011). Recently, another study in our lab shows that tangential migration of CRs is disturbed after blocking extracellular Pax6 by genetic approach. The distance CRs travelled is shortened and the direction is modified (Kaddour et al., 2018).

2. Materials & Methods

Animals

Single chain antibody against Pax6 mice (Bernard et al., 2016) and Wnt3aCre (Yoshida, Assimacopoulos, Jones, & Grove, 2006) transgenic mice were kept in a C57BL/6J background. Animals were genotyped by PCR using specific primers for each allele. C57BL/6J mice were provided by Janvier laboratory (France). The day of vaginal plug was considered to be E0.5. All animal procedures, including housing, were carried out in accordance with the recommendations of the European Economic Community (86/609/EEC), the French National Committee (87/848) and French bylaws (AGRG1240332A / AGRG1238724A / AGRG1238767A / AGRG1238729A / AGRGR1238753A). All mouse work was approved by the Veterinary Services of Paris (Authorization number: 75-1454) and by the Animal Experimentation Ethical Committee Buffon (CEEA-40) (Reference: CEB-34-2012).

Whole embryo culture and Electroporation

E11.5 embryos were dissected out from the uterus and placed in a petri dish containing Tyrode solution at room temperature. The Reichert's membranes that cover the embryo were carefully removed, and the more avascular part of the yolk sac and amnion were opened, taking care to maintain the integrity of the vitelline arteries and veins that connect the embryo to the placenta. After dissection, the embryos were pre-cultured for 2 h before electroporation and 24 h post electroporation in 2 ml culture medium, which contains 50% rat serum (Charles River Japan), 50%

DMEM/F-12 (1:1) medium, Penicillin-Streptomycin and D-glucose (2mg/ml). Autoclaved glass bottles containing the embryos were attached to a rotor housed in an incubator (B.T.C. Engineering Milton) and maintained at 37.5 °C with continuous gazing (95% O₂/5% CO₂), 50cc between 0-6 h, 75cc between 6-12 h, 100cc between 12-24 h and 125cc after 24 h (M. Takahashi & Osumi, 2010).

All gain- and loss-of-function constructs for electroporation are based on pCAGGS expression vector containing the composite CMV/chicken β -Actin promoter, engineered for bicistronic expression of GFP (pCAGGS-IRES-GFP). For loss-of-function experiments, single-chain antibody (scFv) sequences myc-tagged at their C terminus were taken from plasmids previously described (Lesaffre et al., 2007), and inserted into pCAGGS-IRES-GFP to give secreted versions of the single-chain antibody against Pax6 (pCGSaP6iGFP, coding for anti-Pax6 scFv). A mutant and inactive form of anti-Pax6 scFv (non-functional anti-Pax6 scFv) was constructed by mutating cysteine 43 into a serine, thus preventing the formation of a disulfide bond necessary for Pax6 recognition. Another inactive form of anti-Pax6 scFv (non-sec anti-Pax6 scFv) was constructed by removing the secretion signal. For gain-of-function experiments, HA-tagged Pax6-coding sequence, not including exon 5a, taken from pCHAPax6 (Lesaffre et al., 2007) was provided with the IgK signal peptide and inserted in a derivative of pCAGGS-IRES-GFP, pL6sechaPax6SRiGfp, coding for secPax6.

For electroporation, embryos were transferred into a chamber bordered by negative and positive electrodes (NEPA GENE). The plasmid vector solutions were prepared with EndoFree Plasmid Maxi Kit (Qiagen), diluted at a concentration of 1mg/ml with EndoFree TE and injected into both telencephalic vesicles. Square pulses (70 V; 50ms; 950ms intervals; 6 times) were delivered into the embryos using an electroporator (CUY21, NEPA GENE).

Immunohistochemistry and in situ hybridization

Embryos were fixed by immersion in 4% PFA in PBS for 2 h at 4°C, rinsed in PBS for 1 h and subsequently rinsed in PBS for 3 \times 20 min. Samples were cryoprotected overnight in 20% sucrose / PBS and embedded in O.C.T. (Sakura). Embedded tissues were sectioned on a cryostat with a 12 μ m step. Immunohistochemistry was

performed as previously described (Pierani et al., 2001) or using an unmasking protocol (Arai et al. 2011). Primary antibodies used were G10 mouse anti-Reelin (Calbiochem; 1:1000), rabbit anti-GFP (Molecular Probes; 1:1000), chicken anti-Tbr2 (Millipore, 1:500), rabbit anti-Pax6 (Biolegend, 1:500), rabbit anti-myc (Sigma; 1/400), mouse anti-PH3 (Millipore, 1:500), rabbit anti-Tbr1 (Abcam, 1:500), mouse anti-Tuj1 (BabCo, 1:1000) and goat anti-calretinin (Abcam; 1/250). Fluorescent secondary antibodies used were Cy3 donkey anti-mouse (Jackson ImmunoResearch Laboratories, 1:700), Cy5 donkey anti-goat (Jackson ImmunoResearch Laboratories, 1:500) and Alexa 488 donkey anti-chick (Jackson ImmunoResearch Laboratories, 1:1000). Nuclei were counterstained using fluoromount-G with DAPI (Thermo Fisher). *In situ* hybridization was performed as previously described (Pierani et al., 2001). *In situ* probes were mouse Reelin (Schiffmann, Bernier, & Goffinet, 1997).

Imaging and cell counting

Images were acquired using a Zeiss Spinning Disk W1 microscope and an inverted laser scanning confocal microscope (Zeiss 780) with an oil immersion 25x objective. Coronal cryostat sections of E11.5 embryos brains were used to quantify immunostaining. Quantification were done on images from rostral and caudal sections with at least 3 brains analyzed for each condition. For intact brains, the cortex was subdivided into medial and dorso-lateral regions. Cells were quantified using the cell-count tool of the Image J software.

Statistics

Prism 6 software (GraphPad, version 6.01) was used for statistical analysis. When data followed a normal distribution, paired comparisons were analyzed with t test, whereas multiple comparisons were analyzed using one-way ANOVA with post hoc Bonferroni correction. Data are presented as mean and \pm SEM throughout the manuscript. $p < 0.05$ was considered significant.

3. Results

3.1 Neutralizing extracellular Pax6 induces ectopic generation of neurons

In addition to its cell autonomous activity (Asami et al., 2011; Götz et al., 1998; Heins et al., 2002), Pax6 can be secreted and transferred to neighboring cells (Di Lullo et al., 2011), a direct non-cell autonomous activities shared by many HPs (Di Nardo, Fuchs, Joshi, Moya, & Prochiantz, 2018; Prochiantz & Di Nardo, 2015). We first verified the distance of extracellular Pax6 (ePax6) diffusion to test how many cells can be influenced by an endogenous Pax6 source. This was done by electroporating a plasmid encoding Ha-tagged Pax6 with a secretion signal peptide (secPax6) plus a GFP separated by an IRES sequence allowing for the identification of electroporated cells. Electroporation was done at E11.5 and analysis at E12.5 (Figure 20 a and b). Inside the electroporation region most cells co-expressed both GFP+ and Pax6 revealed by the Ha-tag+ (Figure 20 b and c). In contrast, abutting regions contain receiving cells that only express the tagged Pax6 (Figure 20 b and c) and are located at a distance of only 2-3 cell diameters from the nearby electroporated cells (Figure 20 b and c), demonstrating that ePax6, even with a secretion peptide, does not diffuse at long distances.

In addition, it was observed that the extracellular diffusion of ePax6 inhibits reelin expression, probably reflecting decrease in CR cell generation. Indeed, ePax6 overexpression in the Pallium Sub-pallium Boundary region (PSB) induced a decrease of 27% of Reelin-positive cells, compared to the non-electroporated hemisphere of the same cortex (Figure 20 d and e). No change was observed following the electroporation of a plasmid encoding GFP only (Figure 20 d and e), confirming that the effect observed is due to the overexpression of ePax6 in the PSB. This downregulation of Reelin expression was confirmed by *in situ* hybridization (Figure 20 d).

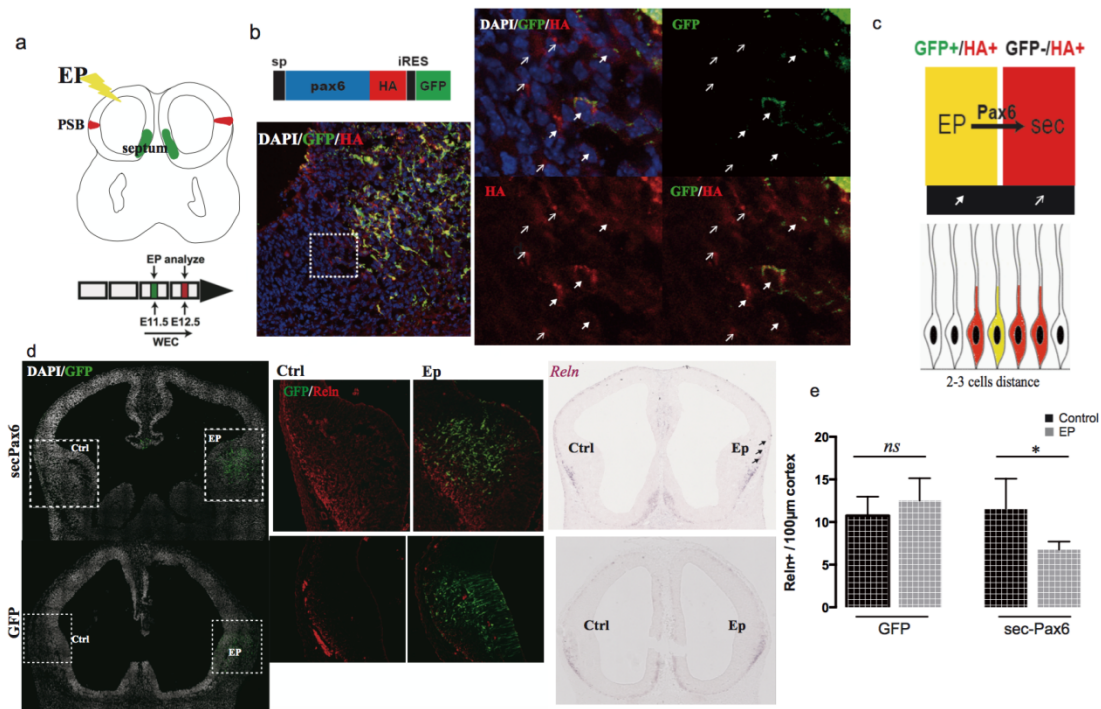


Figure 20. Diffusion of extracellular Pax6 and its function on CRs generation. A. a schematic diagram of electroporation and plan for whole embryo culture. B. the structure of sec-Pax6 plasmid and its diffusion. C. a schematic diagram of sec-Pax6 diffusion. D. Overexpression of extracellular Pax6 inhibits CRs generation at PSB. E. Quantification of CRs number both on control and electroporation sides under the condition of electroporation of GFP or sec-Pax6.

To study the effect of ePax6 on neurogenesis, we performed a loss of function experiment by expressing anti-Pax6 scFv was electroporated at the level of the dorsal telencephalon of E11.5 embryos, specifically targeting cortical progenitors in the VZ (Figure 21 a). We observed that ePax6 neutralization leads to a change in the type of neurons that VZ progenitors generate (Figure 21 b and c). Indeed, targeted progenitors (i) generate more post-mitotic neurons (35%, Tbr1+ cells) and (ii) switch from generating pyramidal neurons to Reelin+ neurons (nearly 60% more Reelin+ cells at the electroporation side compared to the control side in the same animal) (Figure 21 b and c, Figure 22 a). This increase in Reelin positive cells was not observed when the non-functional anti-Pax6 scFv mutated antibody or a non-sec anti-Pax6 scFv (deleted of its signal peptide for secretion) were electroporated in the dorsal telencephalon of E11.5 embryos (Figure 21 a b and c).

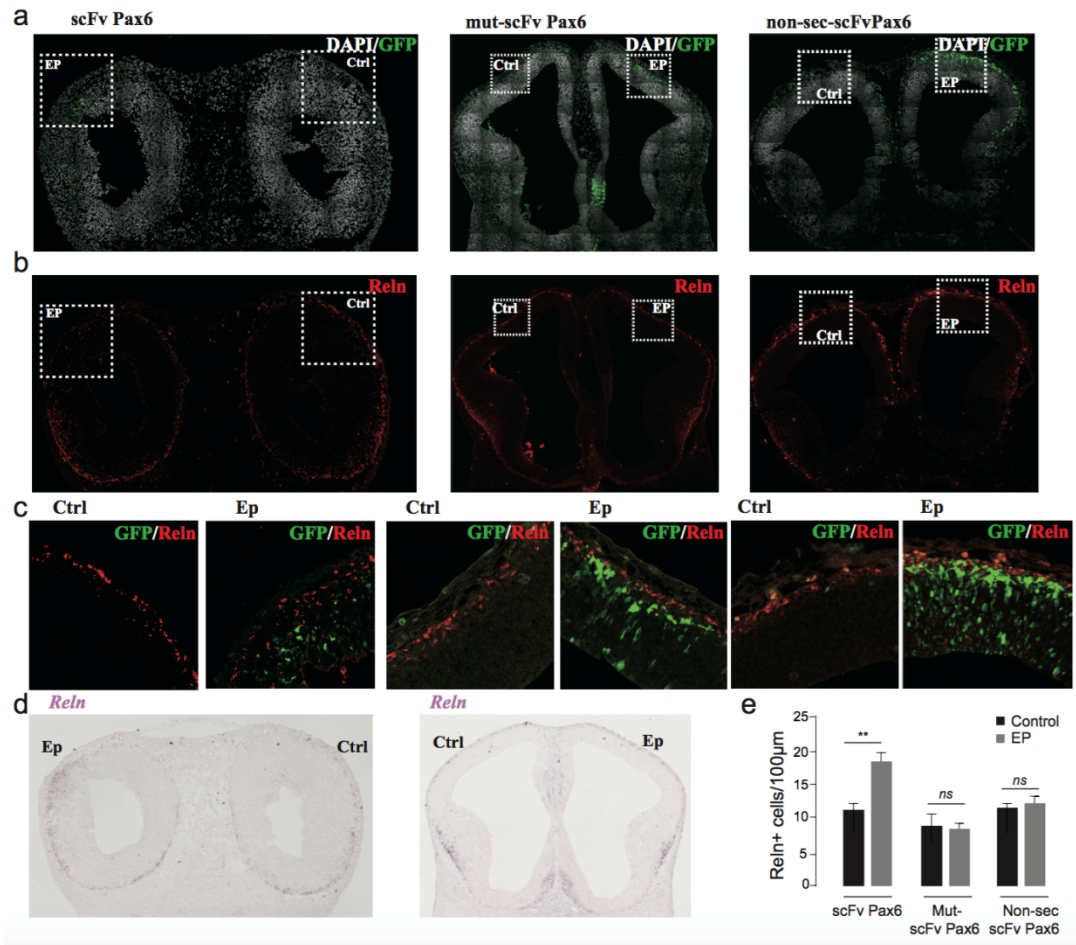


Figure 21. Blocking extracellular Pax6 induces CRs generation. A,B,C show the result of electroporation of anti-Pax6 scFv, mut anti-Pax6 scFv and non-sec anti-Pax6 scFv. Only the electroporation of anti-Pax6 scFv induce reelin expression. D. *in situ* hybridization result confirmed this result. E. quantification of reelin positive cells in each condition.

At early developmental stages, CR neurons are the only cells expressing the Reelin and Tbr1. We performed calretinin immunostaining, another neuronal marker, and observed that more than 20% of Reelin/GFP double-positive cells express Calretinin (Figure 22 b) supporting the idea that these ectopic neurons generated following ePax6 neutralization are CR neurons. A distinct possibility is that neutralizing ePax6 in VZ progenitors modulates the length of their cell cycle and generates more post mitotic neurons.

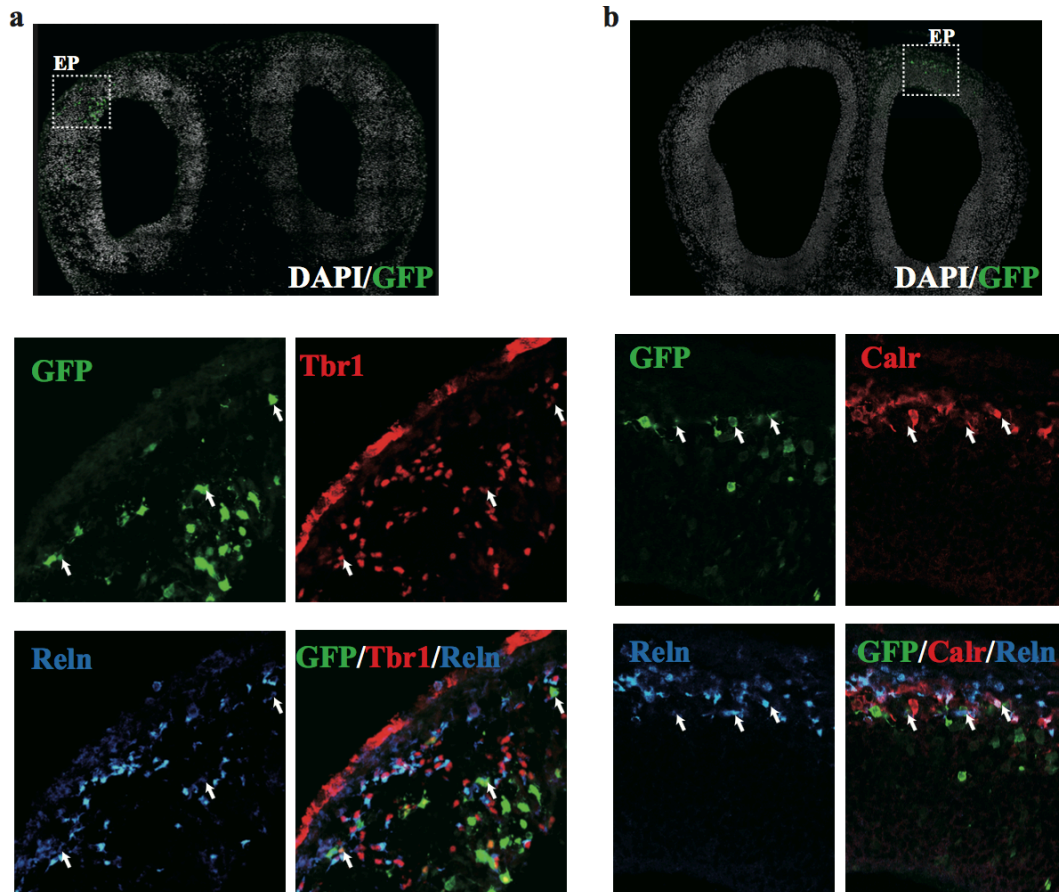


Figure 22. Blocking extracellular Pax6 induced cell expression other CRs markers, Tbr1 and Calretinin.

3.2 Induction of CR neurons generation by blocking ePax6 is time and region specific.

The role of ePax6 on neurogenesis was the investigated in different cortical regions and at different developmental time points. Electroporation of anti-Pax6 scFv was done in the dorsal telencephalon at E10.5 followed by 24 h culture of the embryos (Figure 23). We observed no significant differences in the numbers of Reelin⁺ cells generated in the electroporated side compared to the non-electroporated side and to controls electroporation with non-functional anti-Pax6 scFv. At E10.5, only a few post mitotic neurons are present and the VZ progenitors mainly perform symmetric proliferative divisions. Our results suggest that at E10.5, the cortex is not competent to generate Reelin⁺ cell or that ePax6 concentration at E10.5 is low compared to

E11.5 when Pax6 level shows a rostro-lateral high to caudo-medial low gradient across the cortex (Manuel et al., 2015).

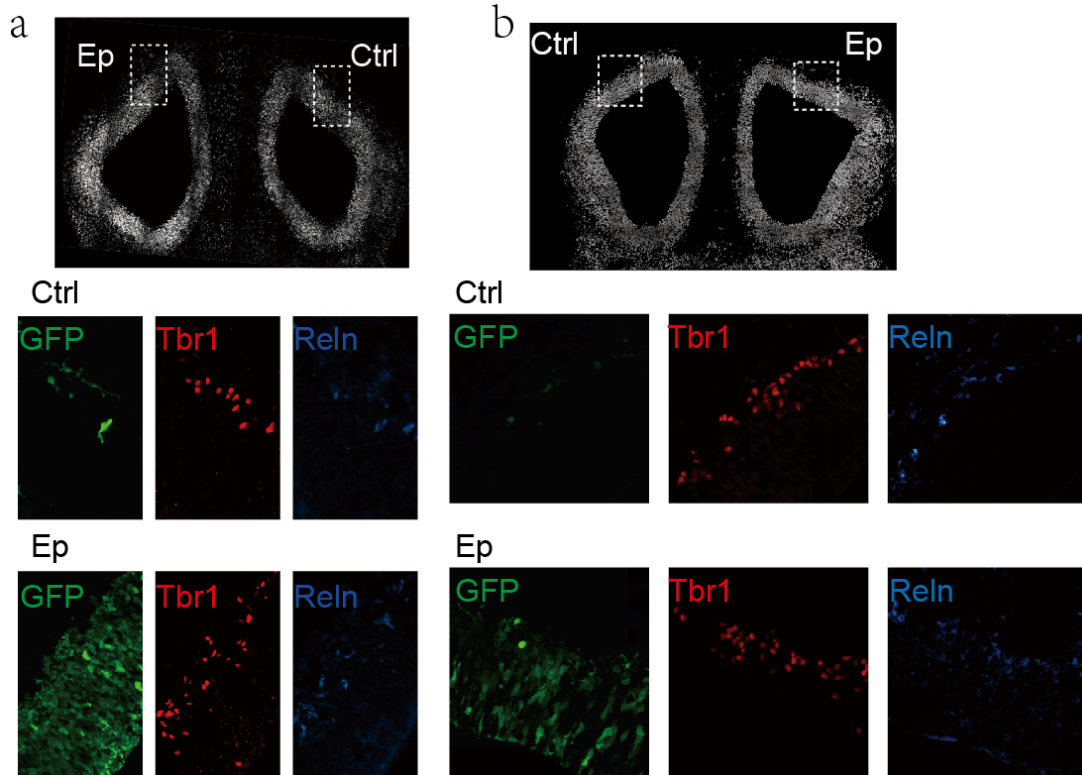


Figure 23. Induction of CR neurons generation by blocking ePax6 is timing specific. No CRs induction was observed when electroporate at E10.5

To test whether other regions of the cortex are able to generate neurons, we targeted the electroporation at the PSB and in the septum, two CR cell sources (Figure 24 a and b). In these regions, anti-Pax6 scFv electroporation did not modify the amount of Reelin+ cells (Figure 24 a and b), suggesting that not all of the cortex is competent to generate ectopic neurons and that this effect on neurogenesis may depend on the amount of ePax6.

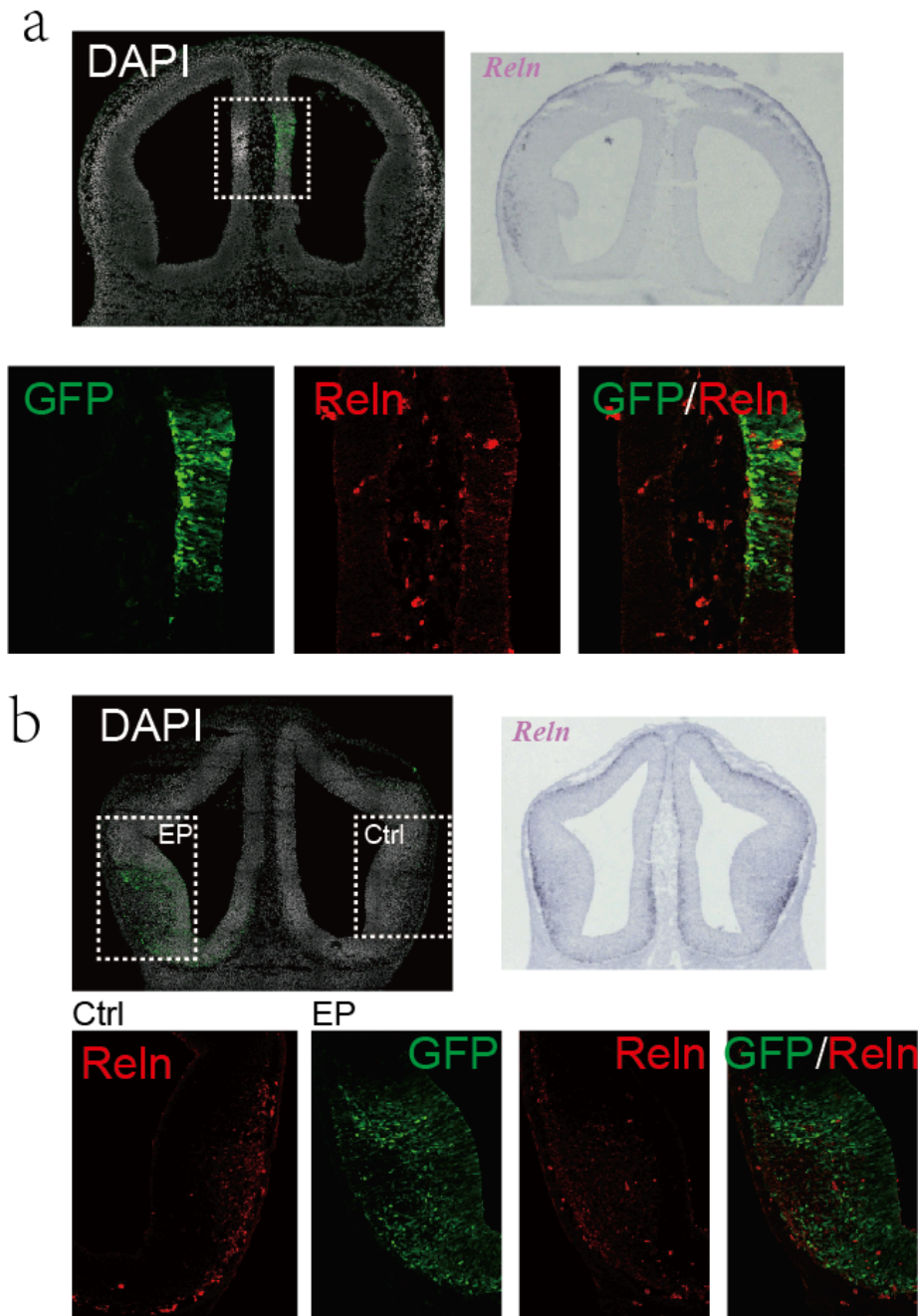


Figure 24. Induction of CR neurons generation by blocking ePax6 is region specific. No CRs induction was observed when electroporate targeted at the PSB and in the septum

To confirm these observations, we analyzed the non-cell autonomous effect of Pax6 on cells generated specifically at the level of the CH, another CR cell source, by

crossing mice bearing a transgene encoding anti-Pax6 scFv with the Wnt3aCre mouse line (Figure 25 a). This led to an ectopic generation of neuronal markers, Reelin and Tuj1, in the VZ of regions abutting the CH where the Myc-tagged antibody is produced (Figure 25 b, c). This ectopic generation of CRs in the VZ was not observed in rostral regions highlighting a region-dependant effect. The global effect on CR cells was quantified by ISH, demonstrating a decrease of Reelin positive cells in the caudo-medial and caudo-lateral cortex (figure 25 d). More specifically, if we look to the neighbor region of the CH, we observed an increase of reelin positive cells (figure 25 e, f). This long-distance effect of the ePax6 on neurogenesis could be explained by a defect in CR migration as already demonstrated (Kaddour et al., 2018) and/or a more highlighted effect when the ePax6 is lower.

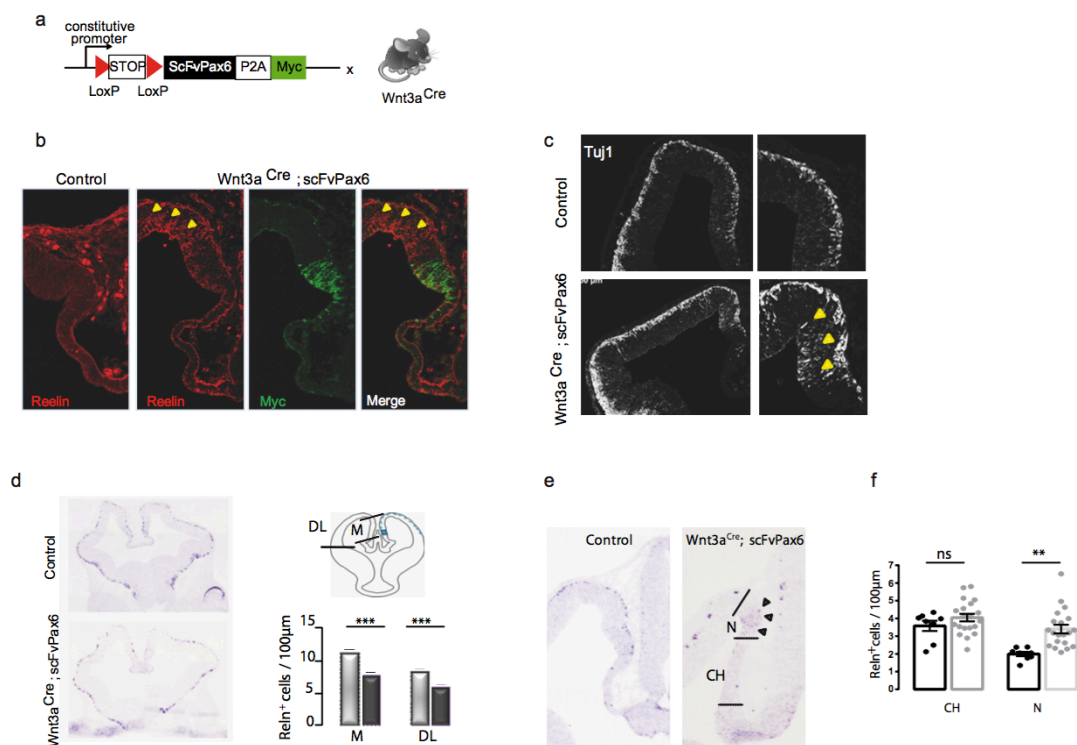


Figure 25. Confirmation of the electroporation result by genetic tool anti-Pax6 scFv with the Wnt3aCre mouse line. This ectopic generation of CRs in the VZ abutting the CH where the single chain antibody is produced.

4. Discussion

Our main conclusion from this work is that Pax6 is required in cortical development to regulate the progenitor's pool and the onset of expression of pyramidal neural-specific markers. This main effect during development has been already suggested in previous studies but for the first time here we demonstrate a non-autonomous activity of this transcription factor on proliferation and neurogenesis.

At the onset of neurogenesis, several TFs including Pax6 expressed in the cortical neuroepithelium function mainly to influence areal patterning and regulate progenitor cell proliferation (Bishop, Goudreau, & O'Leary, 2000; Bishop, Rubenstein, & O'Leary, 2002; Hevner et al., 2006; Muzio & Mallamaci, 2003; Muzio et al., 2002; Stenman et al., 2003). There is mounting evidence that TFs exert region-specific control of cortical progenitor cell cycle progression. Pax6 is one of a number of TFs that are expressed in distinct gradients across cortical areas (Georgala, Carr, & Price, 2011; Salomoni & Calegari, 2010; Sansom & Livesey, 2009) and several studies have implicated Pax6 in the temporal and spatial control of cell cycle duration in cortical progenitors and neuronal differentiation (Estivill-Torrus, Pearson, van Heyningen, Price, & Rashbass, 2002). In this study we modify extracellular Pax6 concentration by introducing either secret Pax6 which enrich extracellular Pax6 or secret single chain antibody against Pax6 which neutralize extracellular Pax6 in the developing mouse cortex, in order to study the non-cell autonomous function of homeoprotein Pax6 in neurogenesis (Bernard et al., 2016; Kaddour et al., 2018; Prochiantz & Di Nardo, 2015). We apply two methods to trigger the expression 1) *in vitro* electroporation following 24h whole embryo culture and 2) genetic strategy. We show that modifications of extracellular Pax6 concentration influence CRs generation and the neurogenesis process. Gain of function studies performed by electroporation of the scFv Pax6 at PSB, the source of CRs, of E11.5 embryos revealed a decrease of the number of post mitotic neurons expressing reelin. In contrary, loss of extracellular Pax6 in the dorsal telencephalon induced the opposite effect with an enhancement of neurons in the electroporated region. In fact, gain of function studies, in PAX77 mice, which express Pax6 protein in its normal pattern but at approximately double the wild type level, there is a reduction in the number of proliferating progenitors in the rostral and central cortex, the areas where levels of Pax6 expression are normally highest

(Manuel et al., 2007). It was also shown that loss of Pax6 during early cortical development in mice *in vivo* led to a temporary increase in the production of post-mitotic neurons (Estivill-Torrus et al., 2002). Moreover, electroporation of the anti-Pax6 scFv in the same region at an earlier stage (E10.5) showed no difference in the number of neurons generated as well as the electroporation of the PSB or the medial cortex of E11.5 brains. Thus, both gain and loss of extracellular Pax6 function studies revealed powerful context-specific effect of ePax6 on neurogenesis resulting from influence the cell cycle exit of progenitors and cell fate. This might in addition with cell cycle duration change of progenitor cells.

To verify this region specific effect of the ePax6, we expressed the anti-Pax6 scFv specifically in the CH of E11.5 embryos. We looked specifically to the medial cortex where the antibody is expressed and diffused to its neighbor region. Surprisingly, we observed ectopic generation of neurons expressing *reelin* and *Tuj1* in the VZ of CH neighbor region but the number of neurons does not change in the CH. Moreover, at the level of the CH, extracellular Pax6 expression increases mitosis in apical progenitors (pH3 marker) and decrease the IP pool (*Tbr2* marker). Modulation of the amount of progenitor's pools could explain a precocious neurogenesis observed in the neighbor region. It was shown that loss of Pax6 during early cortical development in mice *in vivo* led to a shortening of the cell cycle of progenitors coupled with higher proportions of asymmetrical divisions (Estivill-Torrus et al., 2002; Walcher et al., 2013; Warren et al., 1999). Forced expression of Pax6 impairs progenitor cell proliferation *in vitro* (Cartier et al., 2006; Hack, Sugimori, Lundberg, Nakafuku, & Götz, 2004; Heins et al., 2002). Several studies thus indicate that the function of Pax6 on cortical progenitor cell cycle duration modification is associated with its expression levels, which is region dependent. In fact, during early corticogenesis (E12.5), when the Pax6 gradient is steepest, areas of highest expression correlate with regions where the cell cycle duration is longest. Loss of Pax6 causes shortening of the cell cycle only in these areas (Mi et al., 2013). In our study, the effect on cell proliferation and neurogenesis is not observed in a region where Pax6 expression is the highest. These results could be due to the lower level of ePax6 comparing to its endogenous form. Taken together, these studies indicate the temporal-spatial specific function of ePax6 on regulating progenitor cell division and daughter cell fate.

Bibliography

- Aboitiz, F., Montiel, J., Morales, D., & Concha, M. (2002). Evolutionary divergence of the reptilian and the mammalian brains: considerations on connectivity and development. *Brain Research Reviews*, 39(2-3), 141–153.
- Akhtar, A. A., & Breunig, J. J. (2015). Lost highway (s): barriers to postnatal cortical neurogenesis and implications for brain repair. *Frontiers in Cellular Neuroscience*, 9, 216.
- Alcántara, S., Pozas, E., Ibañez, C. F., & Soriano, E. (2005). BDNF-modulated spatial organization of Cajal–Retzius and GABAergic neurons in the marginal zone plays a role in the development of cortical organization. *Cerebral Cortex*, 16(4), 487–499.
- Alfano, C., Magrinelli, E., Harb, K., Hevner, R. F., & Studer, M. (2014). Postmitotic control of sensory area specification during neocortical development. *Nature Communications*, 5, 5632.
- Allendoerfer, K. L., & Shatz, C. J. (1994). The subplate, a transient neocortical structure: its role in the development of connections between thalamus and cortex. *Annual Review of Neuroscience*, 17(1), 185–218.
- Anderson, S. A., Eisenstat, D. D., Shi, L., & Rubenstein, J. (1997). Interneuron migration from basal forebrain to neocortex: dependence on *Dlx* genes. *Science*, 278(5337), 474–476.
- Arai, Y., & Pierani, A. (2014). Development and evolution of cortical fields. *Neuroscience Research*, 86, 66–76.
- Arai, Y., Pulvers, J. N., Haffner, C., Schilling, B., Nüsslein, I., Calegari, F., & Huttner, W. B. (2011). Neural stem and progenitor cells shorten S-phase on commitment to neuron production. *Nature Communications*, 2, 154.
- Asami, M., Pilz, G. A., Ninkovic, J., Godinho, L., Schroeder, T., Huttner, W. B., & Götz, M. (2011). The role of *Pax6* in regulating the orientation and mode of cell division of progenitors in the mouse cerebral cortex. *Development*, dev. 074591.
- Azzarelli, R., Guillemot, F., & Pacary, E. (2015). Function and regulation of *Rnd* proteins in cortical projection neuron migration. *Frontiers in Neuroscience*, 9, 19.
- Barber, M., Arai, Y., Morishita, Y., Vigier, L., Causeret, F., Borello, U., et al. (2015). Migration speed of Cajal–Retzius cells modulated by vesicular trafficking controls the size of higher-order cortical areas. *Current Biology*, 25(19), 2466–2478.
- Barnabé-Heider, F., Wasylnka, J. A., Fernandes, K. J., Porsche, C., Sendtner, M., Kaplan, D. R., & Miller, F. D. (2005). Evidence that embryonic neurons regulate the onset of cortical gliogenesis via cardiotrophin-1. *Neuron*, 48(2), 253–265.

- Barton, R. A., & Harvey, P. H. (2000). Mosaic evolution of brain structure in mammals. *Nature*, 405(6790), 1055.
- Bernard, C., Vincent, C., Testa, D., Bertini, E., Ribot, J., Di Nardo, A. A., et al. (2016). A mouse model for conditional secretion of specific single-chain antibodies provides genetic evidence for regulation of cortical plasticity by a non-cell autonomous homeoprotein transcription factor. *PLoS Genetics*, 12(5), e1006035.
- Berry, M., Rogers, A. W., & Eayrs, J. T. (1964). Pattern of cell migration during cortical histogenesis. *Nature*, 203(4945), 591–593.
- Betizeau, M., Cortay, V., Patti, D., Pfister, S., Gautier, E., Bellemin-Ménard, A., et al. (2013). Precursor diversity and complexity of lineage relationships in the outer subventricular zone of the primate. *Neuron*, 80(2), 442–457.
- Beurdeley, M., Spatazza, J., Lee, H. H., Sugiyama, S., Bernard, C., Di Nardo, A. A., et al. (2012). Otx2 binding to perineuronal nets persistently regulates plasticity in the mature visual cortex. *Journal of Neuroscience*, 32(27), 9429–9437.
- Bielle, F., Griveau, A., Narboux-Nême, N., Vigneau, S., Sigrist, M., Arber, S., et al. (2005). Multiple origins of Cajal-Retzius cells at the borders of the developing pallium. *Nature Neuroscience*, 8(8), 1002.
- Bishop, K. M., Goudreau, G., & O'Leary, D. D. (2000). Regulation of area identity in the mammalian neocortex by Emx2 and Pax6. *Science*, 288(5464), 344–349.
- Bishop, K. M., Rubenstein, J. L., & O'Leary, D. D. (2002). Distinct Actions of Emx1, Emx2, and Pax6 in Regulating the Specification of Areas in the Developing Neocortex. *Journal of Neuroscience*, 22(17), 7627–7638.
- Borello, U., & Pierani, A. (2010). Patterning the cerebral cortex: traveling with morphogens. *Current Opinion in Genetics & Development*, 20(4), 408–415.
- Broca, P. (1861). Remarques sur le siège de la faculté du langage articulé, suivies d'une observation d'aphémie (perte de la parole). *Bulletin Et Memoires De La Societe Anatomique De Paris*, 6, 330–357.
- Brodman, K. (1909). Vergleichende Lokalisationslehre der Grosshirnrinde in ihren Prinzipien dargestellt auf Grund des Zellenbaues.
- Brunet, I., Weint, C., Piper, M., Trembleau, A., Volovitch, M., Harris, W., et al. (2005). The transcription factor Engrailed-2 guides retinal axons. *Nature*, 438(7064), 94.
- Brunjes, P. C., & Osterberg, S. K. (2015). Developmental markers expressed in neocortical layers are differentially exhibited in olfactory cortex. *PloS One*, 10(9), e0138541.

- Burek, M. J., & Oppenheim, R. W. (1999). Cellular interactions that regulate programmed cell death in the developing vertebrate nervous system, 145–179.
- Cahalane, D. J., Charvet, C. J., & Finlay, B. L. (2014). Modeling local and cross-species neuron number variations in the cerebral cortex as arising from a common mechanism. *Proceedings of the National Academy of Sciences*, 111(49), 17642–17647.
- Cai, L., Hayes, N. L., & Nowakowski, R. S. (1997). Local homogeneity of cell cycle length in developing mouse cortex. *Journal of Neuroscience*, 17(6), 2079–2087.
- Calegari, F., & Huttner, W. B. (2003). An inhibition of cyclin-dependent kinases that lengthens, but does not arrest, neuroepithelial cell cycle induces premature neurogenesis. *Journal of Cell Science*, 116(24), 4947–4955.
- Calegari, F., Haubensak, W., Haffner, C., & Huttner, W. B. (2005). Selective lengthening of the cell cycle in the neurogenic subpopulation of neural progenitor cells during mouse brain development. *Journal of Neuroscience*, 25(28), 6533–6538.
- Campbell, K. (2003). Dorsal-ventral patterning in the mammalian telencephalon. *Current Opinion in Neurobiology*, 13(1), 50–56.
- Cartier, L., Laforge, T., Feki, A., Arnaudeau, S., Dubois Dauphin, M., & Krause, K. H. (2006). Pax6-induced alteration of cell fate: Shape changes, expression of neuronal α tubulin, postmitotic phenotype, and cell migration. *Journal of Neurobiology*, 66(5), 421–436.
- Causseret, F., & Pierani, A. (2016). Patterning of higher-order cortical areas is developmentally regulated by the distribution of Cajal-Retzius cells. *Medecine Sciences: M/S*, 32(4), 317.
- Causseret, F., Coppola, E., & Pierani, A. (2018). Cortical developmental death: selected to survive or fated to die. *Current Opinion in Neurobiology*, 53, 35–42.
- Caviness, V. S., Jr, Nowakowski, R. S., & Bhide, P. G. (2009). Neocortical neurogenesis: morphogenetic gradients and beyond. *Trends in Neurosciences*, 32(8), 443–450.
- Ceci, M. L., López-Mascaraque, L., & de Carlos, J. A. (2010). The influence of the environment on Cajal–Retzius cell migration. *Cerebral Cortex*, 20(10), 2348–2360.
- Cheema, Z. F., West, J. R., & Miranda, R. C. (2000). Ethanol induces Fas/Apo [apoptosis]-1 mRNA and cell suicide in the developing cerebral cortex. *Alcoholism: Clinical and Experimental Research*, 24(4), 535–543.
- Chenn, A., & Walsh, C. A. (2002). Regulation of cerebral cortical size by control of cell cycle exit in neural precursors. *Science*, 297(5580), 365–369.

- Chirumamilla, S., Sun, D., Bullock, M. R., & Colello, R. J. (2002). Traumatic brain injury induced cell proliferation in the adult mammalian central nervous system. *Journal of Neurotrauma*, 19(6), 693–703.
- Clark, D. A., Mitra, P. P., & Wang, S. S.-H. (2001). Scalable architecture in mammalian brains. *Nature*, 411(6834), 189.
- Cugola, F.R. et al., 2016. The Brazilian Zika virus strain causes birth defects in experimental models. *Nature*, 534(7606), p.267.
- Cunningham, C. L., Martínez-Cerdeño, V., & Noctor, S. C. (2013). Microglia regulate the number of neural precursor cells in the developing cerebral cortex. *Journal of Neuroscience*, 33(10), 4216–4233.
- D'arcangelo, G., Miao, G. G., Chen, S.-C., Scares, H. D., Morgan, J. I., & Curran, T. (1995). A protein related to extracellular matrix proteins deleted in the mouse mutant reeler. *Nature*, 374(6524), 719.
- Dash, P. K., Mach, S. A., & Moore, A. N. (2001). Enhanced neurogenesis in the rodent hippocampus following traumatic brain injury. *Journal of Neuroscience Research*, 63(4), 313–319.
- Dehay, C., & Kennedy, H. (2007). Cell-cycle control and cortical development. *Nature Reviews Neuroscience*, 8(6), 438.
- Derossi, D., Joliot, A. H., Chassaing, G., & Prochiantz, A. (1994). The third helix of the Antennapedia homeodomain translocates through biological membranes. *Journal of Biological Chemistry*, 269(14), 10444–10450.
- Di Lullo, E., Haton, C., Le Poupon, C., Volovitch, M., Joliot, A., Thomas, J.-L., & Prochiantz, A. (2011). Paracrine Pax6 activity regulates oligodendrocyte precursor cell migration in the chick embryonic neural tube. *Development*, 138(22), 4991–5001.
- Di Nardo, A. A., Fuchs, J., Joshi, R. L., Moya, K. L., & Prochiantz, A. (2018). The Physiology of Homeoprotein Transduction. *Physiological Reviews*, 98(4), 1943–1982.
- Diodato, A., De Brimont, M. R., Yim, Y. S., Derian, N., Perrin, S., Pouch, J., et al. (2016). Molecular signatures of neural connectivity in the olfactory cortex. *Nature Communications*, 7, 12238.
- Donato, F., Jacobsen, R. I., Moser, M.-B., & Moser, E. I. (2017). Stellate cells drive maturation of the entorhinal-hippocampal circuit. *Science*, 355(6330), eaai8178.
- Ekdahl, C. T., Kokaia, Z., & Lindvall, O. (2009). Brain inflammation and adult neurogenesis: the dual role of microglia. *Neuroscience*, 158(3), 1021–1029.

- Estivill-Torres, G., Pearson, H., van Heyningen, V., Price, D. J., & Rashbass, P. (2002). Pax6 is required to regulate the cell cycle and the rate of progression from symmetrical to asymmetrical division in mammalian cortical progenitors. *Development*, 129(2), 455–466.
- Falconer, D. S. (1951). Two new mutants, 'trembler' and 'reeler', with neurological actions in the house mouse (*Mus musculus* L.). *Journal of Genetics*, 50(2), 192–205.
- Fietz, S. A., Kelava, I., Vogt, J., Wilsch-Bräuninger, M., Stenzel, D., Fish, J. L., et al. (2010). OSVZ progenitors of human and ferret neocortex are epithelial-like and expand by integrin signaling. *Nature Neuroscience*, 13(6), 690.
- Finlay, B. L., & Darlington, R. B. (1995). Linked regularities in the development and evolution of mammalian brains. *Science*, 268(5217), 1578–1584.
- Fischl, B., & Dale, A. M. (2000). Measuring the thickness of the human cerebral cortex from magnetic resonance images. *Proceedings of the National Academy of Sciences*, 97(20), 11050–11055.
- Florio, M., & Huttner, W. B. (2014). Neural progenitors, neurogenesis and the evolution of the neocortex. *Development*, 141(11), 2182–2194.
- Franco, S. J., & Müller, U. (2013). Shaping our minds: stem and progenitor cell diversity in the mammalian neocortex. *Neuron*, 77(1), 19–34.
- Freret-Hodara, B., Cui, Y., Griveau, A., Vigier, L., Arai, Y., Touboul, J., & Pierani, A. (2016). Enhanced abventricular proliferation compensates cell death in the embryonic cerebral cortex. *Cerebral Cortex*, 27(10), 4701–4718.
- Garcez, P.P. et al., 2016. Zika virus impairs growth in human neurospheres and brain organoids. *Science*, 352(6287), pp.816–818
- Gao, P., Postiglione, M. P., Krieger, T. G., Hernandez, L., Wang, C., Han, Z., et al. (2014). Deterministic progenitor behavior and unitary production of neurons in the neocortex. *Cell*, 159(4), 775–788.
- Gehring, W. (1967). Clonal analysis of determination dynamics in cultures of imaginal disks in *Drosophila melanogaster*. *Developmental Biology*, 16(5), 438–456.
- Georgala, P. A., Carr, C. B., & Price, D. J. (2011). The role of Pax6 in forebrain development. *Developmental Neurobiology*, 71(8), 690–709.
- Götz, M., Stoykova, A., & Gruss, P. (1998). Pax6 controls radial glia differentiation in the cerebral cortex. *Neuron*, 21(5), 1031–1044.

- Griveau, A., Borello, U., Causeret, F., Tissir, F., Boggetto, N., Karaz, S., & Pierani, A. (2010). A novel role for Dbx1-derived Cajal-Retzius cells in early regionalization of the cerebral cortical neuroepithelium. *PLoS Biology*, 8(7), e1000440.
- Haberly, L. B., Hansen, D. J., Feig, S. L., & Presto, S. (1987). Distribution and ultrastructure of neurons in opossum piriform cortex displaying immunoreactivity to GABA and GAD and high-affinity tritiated GABA uptake. *Journal of Comparative Neurology*, 266(2), 269–290.
- Hack, M. A., Sugimori, M., Lundberg, C., Nakafuku, M., & Götz, M. (2004). Regionalization and fate specification in neurospheres: the role of Olig2 and Pax6. *Molecular and Cellular Neuroscience*, 25(4), 664–678.
- Hafting, T., Fyhn, M., Molden, S., Moser, M.-B., & Moser, E. I. (2005). Microstructure of a spatial map in the entorhinal cortex. *Nature*, 436(7052), 801.
- Hansen, D. V., Lui, J. H., Parker, P. R., & Kriegstein, A. R. (2010). Neurogenic radial glia in the outer subventricular zone of human neocortex. *Nature*, 464(7288), 554.
- Hatakeyama, J., Bessho, Y., Katoh, K., Ookawara, S., Fujioka, M., Guillemot, F., & Kageyama, R. (2004). Hes genes regulate size, shape and histogenesis of the nervous system by control of the timing of neural stem cell differentiation. *Development*, 131(22), 5539–5550.
- Haydar, T. F., Wang, F., Schwartz, M. L., & Rakic, P. (2000). Differential modulation of proliferation in the neocortical ventricular and subventricular zones. *Journal of Neuroscience*, 20(15), 5764–5774.
- Heins, N., Malatesta, P., Cecconi, F., Nakafuku, M., Tucker, K. L., Hack, M. A., et al. (2002). Glial cells generate neurons: the role of the transcription factor Pax6. *Nature Neuroscience*, 5(4), 308.
- Hevner, R. F., Hodge, R. D., Daza, R. A., & Englund, C. (2006). Transcription factors in glutamatergic neurogenesis: conserved programs in neocortex, cerebellum, and adult hippocampus. *Neuroscience Research*, 55(3), 223–233.
- Hevner, R. F., Neogi, T., Englund, C., Daza, R. A., & Fink, A. (2003). Cajal–Retzius cells in the mouse: transcription factors, neurotransmitters, and birthdays suggest a pallial origin. *Developmental Brain Research*, 141(1-2), 39–53.
- Hill, R. E., Favor, J., Hogan, B. L., Ton, C. C., Saunders, G. F., Hanson, I. M., et al. (1991). Mouse small eye results from mutations in a paired-like homeobox-containing gene. *Nature*, 354(6354), 522.

- Holcman, D., Kasatkin, V., & Prochiantz, A. (2007). Modeling homeoprotein intercellular transfer unveils a parsimonious mechanism for gradient and boundary formation in early brain development. *Journal of Theoretical Biology*, 249(3), 503–517.
- Hsu, L. C.-L., Nam, S., Cui, Y., Chang, C.-P., Wang, C.-F., Kuo, H.-C., et al. (2015). Lhx2 regulates the timing of β -catenin-dependent cortical neurogenesis. *Proceedings of the National Academy of Sciences*, 112(39), 12199–12204.
- Jahn, H. M., Kasakow, C. V., Helfer, A., Michely, J., Verkhatsky, A., Maurer, H. H., et al. (2018). Refined protocols of tamoxifen injection for inducible DNA recombination in mouse astroglia. *Scientific Reports*, 8(1), 5913.
- Jessell, T. M. (2000). Neuronal specification in the spinal cord: inductive signals and transcriptional codes. *Nature Reviews Genetics*, 1(1), 20.
- Joliot, A., Pernelle, C., Deagostini-Bazin, H., & Prochiantz, A. (1991). Antennapedia homeobox peptide regulates neural morphogenesis. *Proceedings of the National Academy of Sciences*, 88(5), 1864–1868.
- Joyner, A. L., Liu, A., & Millet, S. (2000). Otx2, Gbx2 and Fgf8 interact to position and maintain a mid–hindbrain organizer. *Current Opinion in Cell Biology*, 12(6), 736–741.
- Jun, J. A., & Sidman, R. L. (1961). Autoradiographic study of cell migration during histogenesis of cerebral cortex in the mouse. *Nature*, 192(4804), 766.
- Kaddour, H., Coppola, E., Di Nardo, A., Wizenmann, A., Volovitch, M., Prochiantz, A., & Pierani, A. (2018). Extracellular Pax6 regulates tangential Cajal-Retzius cell migration. *bioRxiv*, 269480.
- Kasatkin, V., Prochiantz, A., & Holcman, D. (2008). Morphogenetic gradients and the stability of boundaries between neighboring morphogenetic regions. *Bulletin of Mathematical Biology*, 70(1), 156–178.
- Kiecker, C., & Lumsden, A. (2005). Compartments and their boundaries in vertebrate brain development. *Nature Reviews Neuroscience*, 6(7), 553.
- Kowalczyk, T., Pontious, A., Englund, C., Daza, R. A., Bedogni, F., Hodge, R., et al. (2009). Intermediate neuronal progenitors (basal progenitors) produce pyramidal–projection Neurons for all layers of cerebral cortex. *Cerebral Cortex*, 19(10), 2439–2450.
- Lange, C., & Calegari, F. (2010). Cdks and cyclins link G1 length and differentiation of embryonic, neural and hematopoietic stem cells. *Cell Cycle*, 9(10), 1893–1900.

- Lange, C., Huttner, W. B., & Calegari, F. (2009). Cdk4/cyclinD1 overexpression in neural stem cells shortens G1, delays neurogenesis, and promotes the generation and expansion of basal progenitors. *Cell Stem Cell*, 5(3), 320–331.
- Le Roux, I., Joliot, A. H., Bloch-Gallego, E., Prochiantz, A., & Volovitch, M. (1993). Neurotrophic activity of the Antennapedia homeodomain depends on its specific DNA-binding properties. *Proceedings of the National Academy of Sciences*, 90(19), 9120–9124.
- Lefèvre, J., & Mangin, J.-F. (2010). A reaction-diffusion model of human brain development. *PLoS Computational Biology*, 6(4), e1000749.
- Lesaffre, B., Joliot, A., Prochiantz, A., & Volovitch, M. (2007). Direct non-cell autonomous Pax6 activity regulates eye development in the zebrafish. *Neural Development*, 2(1), 2.
- Lewis, D. L., DeCamillis, M. A., Brunetti, C. R., Halder, G., Kassner, V. A., Selegue, J. E., et al. (1999). Ectopic gene expression and homeotic transformations in arthropods using recombinant Sindbis viruses. *Current Biology*, 9(22), 1279–1287.
- Lewis, E. B. (1978). A gene complex controlling segmentation in *Drosophila*, 205–217.
- Lodato, M. A., Woodworth, M. B., Lee, S., Evrony, G. D., Mehta, B. K., Karger, A., et al. (2015a). Somatic mutation in single human neurons tracks developmental and transcriptional history. *Science*, 350(6256), 94–98.
- Lodato, S., Shetty, A. S., & Arlotta, P. (2015b). Cerebral cortex assembly: generating and reprogramming projection neuron diversity. *Trends in Neurosciences*, 38(2), 117–125.
- LoTurco, J. J., Owens, D. F., Heath, M. J., Davis, M. B., & Kriegstein, A. R. (1995). GABA and glutamate depolarize cortical progenitor cells and inhibit DNA synthesis. *Neuron*, 15(6), 1287–1298.
- Lukasiewicz, A., Savatier, P., Cortay, V., Kennedy, H., & Dehay, C. (2002). Contrasting effects of basic fibroblast growth factor and neurotrophin 3 on cell cycle kinetics of mouse cortical stem cells. *Journal of Neuroscience*, 22(15), 6610–6622.
- Luskin, M. B., & Shatz, C. J. (1985). Studies of the earliest generated cells of the cat's visual cortex: cogeneration of subplate and marginal zones. *Journal of Neuroscience*, 5(4), 1062–1075.
- Machon, O., Backman, M., Machonova, O., Kozmik, Z., Vacik, T., Andersen, L., & Krauss, S. (2007). A dynamic gradient of Wnt signaling controls initiation of neurogenesis in the mammalian cortex and cellular specification in the hippocampus. *Developmental Biology*, 311(1), 223–237.

- Magavi, S. S., Leavitt, B. R., & Macklis, J. D. (2000). Induction of neurogenesis in the neocortex of adult mice. *Nature*, 405(6789), 951.
- Manuel, M. N., Mi, D., Mason, J. O., & Price, D. J. (2015). Regulation of cerebral cortical neurogenesis by the Pax6 transcription factor. *Frontiers in Cellular Neuroscience*, 9, 70.
- Manuel, M., Georgala, P. A., Carr, C. B., Chanas, S., Kleinjan, D. A., Martynoga, B., et al. (2007). Controlled overexpression of Pax6 in vivo negatively autoregulates the Pax6 locus, causing cell-autonomous defects of late cortical progenitor proliferation with little effect on cortical arealization. *Development*, 134(3), 545–555.
- Marie, P., Karam, A., Guillaume, P., Sylvie, S.-M., & Frédérique, C. (2018). A multiscale mathematical model of cell dynamics during neurogenesis in the mouse cerebral cortex.
- Martin, L. J. (2001). Neuronal cell death in nervous system development, disease, and injury. *International Journal of Molecular Medicine*, 7(5), 455–478.
- Martin-Lopez, E., Ishiguro, K., & Greer, C. A. (2017). The Laminar Organization of Piriform Cortex Follows a Selective Developmental and Migratory Program Established by Cell Lineage. *Cerebral Cortex*, 1–16.
- Martínez-Cerdeño, V., Noctor, S. C., & Kriegstein, A. R. (2006). The role of intermediate progenitor cells in the evolutionary expansion of the cerebral cortex. *Cerebral Cortex*, 16(suppl_1), i152–i161.
- Mayhew, T. M. (1991). Anatomy of the cortex: Statistics and geometry. *Journal of Anatomy*, 179, 203.
- McAlhany, R. E., Jr, West, J. R., & Miranda, R. C. (2000). Glial-derived neurotrophic factor (GDNF) prevents ethanol-induced apoptosis and JUN kinase phosphorylation. *Developmental Brain Research*, 119(2), 209–216.
- Mi, D., Carr, C. B., Georgala, P. A., Huang, Y.-T., Manuel, M. N., Jeanes, E., et al. (2013). Pax6 exerts regional control of cortical progenitor proliferation via direct repression of Cdk6 and hypophosphorylation of pRb. *Neuron*, 78(2), 269–284.
- Migliore, M., & Shepherd, G. M. (2005). An integrated approach to classifying neuronal phenotypes. *Nature Reviews Neuroscience*, 6(10), 810.
- Miller, M. W. (1987). Effect of prenatal exposure to alcohol on the distribution and time of origin of corticospinal neurons in the rat. *Journal of Comparative Neurology*, 257(3), 372–382.
- Miller, M. W. (1989). Effects of prenatal exposure to ethanol on neocortical development: II. Cell proliferation in the ventricular and subventricular zones of the rat. *Journal of Comparative Neurology*, 287(3), 326–338.

- Miller, M. W. (1993). Migration of cortical neurons is altered by gestational exposure to ethanol. *Alcoholism: Clinical and Experimental Research*, 17(2), 304–314.
- Miller, M. W., & Potempa, G. (1990). Numbers of neurons and glia in mature rat somatosensory cortex: effects of prenatal exposure to ethanol. *Journal of Comparative Neurology*, 293(1), 92–102.
- Misson, J. P., Takahashi, T., & Caviness, V. S., Jr. (1991). Ontogeny of radial and other astroglial cells in murine cerebral cortex. *Glia*, 4(2), 138–148.
- Miyashita-Lin, E. M., Hevner, R., Wassarman, K. M., Martinez, S., & Rubenstein, J. L. (1999). Early neocortical regionalization in the absence of thalamic innervation. *Science*, 285(5429), 906–909.
- Molyneaux, B. J., Arlotta, P., Menezes, J. R., & Macklis, J. D. (2007). Neuronal subtype specification in the cerebral cortex. *Nature Reviews Neuroscience*, 8(6), 427.
- Morrow, T., Song, M.-R., & Ghosh, A. (2001). Sequential specification of neurons and glia by developmentally regulated extracellular factors. *Development*, 128(18), 3585–3594.
- Murray, J. D. (1988). How the leopard gets its spots. *Scientific American*, 258(3), 80–87.
- Muzio, L., & Mallamaci, A. (2003). *Emx1*, *emx2* and *pax6* in specification, regionalization and arealization of the cerebral cortex. *Cerebral Cortex*, 13(6), 641–647.
- Muzio, L., Di Benedetto, B., Stoykova, A., Boncinelli, E., Gruss, P., & Mallamaci, A. (2002). Conversion of cerebral cortex into basal ganglia in *Emx2*^{-/-} *Pax6*/*Sey*/*Sey* double-mutant mice. *Nature Neuroscience*, 5(8), 737.
- Nadarajah, B., & Parnavelas, J. G. (2002). Modes of neuronal migration in the developing cerebral cortex. *Nature Reviews Neuroscience*, 3(6), 423.
- Nadarajah, B., Brunstrom, J. E., Grutzendler, J., Wong, R. O., & Pearlman, A. L. (2001). Two modes of radial migration in early development of the cerebral cortex. *Nature Neuroscience*, 4(2), 143.
- Nijhawan, D., Honarpour, N., & Wang, X. (2000). Apoptosis in neural development and disease. *Annual Review of Neuroscience*, 23(1), 73–87.
- Noctor, S. C., Flint, A. C., Weissman, T. A., Dammerman, R. S., & Kriegstein, A. R. (2001). Neurons derived from radial glial cells establish radial units in neocortex. *Nature*, 409(6821), 714.
- Noctor, S. C., Martínez-Cerdeño, V., Ivic, L., & Kriegstein, A. R. (2004). Cortical neurons arise in symmetric and asymmetric division zones and migrate through specific phases. *Nature Neuroscience*, 7(2), 136.

- O'Leary, D. D., & Nakagawa, Y. (2002). Patterning centers, regulatory genes and extrinsic mechanisms controlling arealization of the neocortex. *Current Opinion in Neurobiology*, 12(1), 14–25.
- O'Leary, D. D., & Sahara, S. (2008). Genetic regulation of arealization of the neocortex. *Current Opinion in Neurobiology*, 18(1), 90–100.
- Orford, K. W., & Scadden, D. T. (2008). Deconstructing stem cell self-renewal: genetic insights into cell-cycle regulation. *Nature Reviews Genetics*, 9(2), 115.
- Paridaen, J. T., & Huttner, W. B. (2014). Neurogenesis during development of the vertebrate central nervous system. *EMBO Reports*, 15(4), 351–364.
- Parnavelas, J. G., Barfield, J. A., Franke, E., & Luskin, M. B. (1991). Separate progenitor cells give rise to pyramidal and nonpyramidal neurons in the rat telencephalon. *Cerebral Cortex*, 1(6), 463–468.
- Parthasarathy, S., Srivatsa, S., Nityanandam, A., & Tarabykin, V. (2014). Ntf3 acts downstream of Sip1 in cortical postmitotic neurons to control progenitor cell fate through feedback signaling. *Development, dev.* 114173.
- Penfield, W. (1961). Activation of the Record of Human Experience: Summary of the Lister Oration delivered at the Royal College of Surgeons of England* on 27th April 1961. *Annals of the Royal College of Surgeons of England*, 29(2), 77.
- Perthame, B., Quiñinao, C., & Touboul, J. (2015). Competition and boundary formation in heterogeneous media: Application to neuronal differentiation. *Mathematical Models and Methods in Applied Sciences*, 25(13), 2477–2502.
- Picco, N., García-Moreno, F., Maini, P. K., Woolley, T. E., & Molnár, Z. (2018). Mathematical Modeling of Cortical Neurogenesis Reveals that the Founder Population does not Necessarily Scale with Neurogenic Output. *Cerebral Cortex*, 28(7), 2540–2550.
- Pierani, A., Moran-Rivard, L., Sunshine, M. J., Littman, D. R., Goulding, M., & Jessell, T. M. (2001). Control of interneuron fate in the developing spinal cord by the progenitor homeodomain protein Dbx1. *Neuron*, 29(2), 367–384.
- Pilaz, L.-J., Patti, D., Marcy, G., Ollier, E., Pfister, S., Douglas, R. J., et al. (2009). Forced G1-phase reduction alters mode of division, neuron number, and laminar phenotype in the cerebral cortex. *Proceedings of the National Academy of Sciences*, 106(51), 21924–21929.
- Polleux, F., Dehay, C., & Kennedy, H. (1997). The timetable of laminar neurogenesis contributes to the specification of cortical areas in mouse isocortex. *Journal of Comparative Neurology*, 385(1), 95–116.

- Pontious, A., Kowalczyk, T., Englund, C., & Hevner, R. F. (2008). Role of intermediate progenitor cells in cerebral cortex development. *Developmental Neuroscience*, 30(1-3), 24–32.
- Prochiantz, A., & Di Nardo, A. A. (2015). Homeoprotein signaling in the developing and adult nervous system. *Neuron*, 85(5), 911–925.
- Qian, X., Shen, Q., Goderie, S. K., He, W., Capela, A., Davis, A. A., & Temple, S. (2000). Timing of CNS cell generation: a programmed sequence of neuron and glial cell production from isolated murine cortical stem cells. *Neuron*, 28(1), 69–80.
- Quiñinao, C., Prochiantz, A., & Touboul, J. (2015). Local homeoprotein diffusion can stabilize boundaries generated by graded positional cues. *Development*, 142(10), 1860–1868.
- Rakic, P. (1972). Mode of cell migration to the superficial layers of fetal monkey neocortex. *Journal of Comparative Neurology*, 145(1), 61–83.
- Rakic, P. (1974). Neurons in rhesus monkey visual cortex: systematic relation between time of origin and eventual disposition. *Science*, 183(4123), 425–427.
- Rakic, P. (1988). Specification of cerebral cortical areas. *Science*, 241(4862), 170–176.
- Rekaik, H., de Thé, F.-X. B., Fuchs, J., Massiani-Beaudoin, O., Prochiantz, A., & Joshi, R. L. (2015). Engrailed homeoprotein protects mesencephalic dopaminergic neurons from oxidative stress. *Cell Reports*, 13(2), 242–250.
- Salomoni, P., & Calegari, F. (2010). Cell cycle control of mammalian neural stem cells: putting a speed limit on G1. *Trends in Cell Biology*, 20(5), 233–243.
- Sansom, S. N., & Livesey, F. J. (2009). Gradients in the brain: the control of the development of form and function in the cerebral cortex. *Cold Spring Harbor Perspectives in Biology*, 1(2), a002519.
- Sansom, S. N., Griffiths, D. S., Faedo, A., Kleinjan, D.-J., Ruan, Y., Smith, J., et al. (2009). The level of the transcription factor Pax6 is essential for controlling the balance between neural stem cell self-renewal and neurogenesis. *PLoS Genetics*, 5(6), e1000511.
- Sauer, F. C. (1935). Mitosis in the neural tube. *Journal of Comparative Neurology*, 62(2), 377–405.
- Sawada, M., & Sawamoto, K. (2013). Mechanisms of neurogenesis in the normal and injured adult brain. *The Keio Journal of Medicine*, 62(1), 13–28.
- Schiffmann, S. N., Bernier, B., & Goffinet, A. M. (1997). Reelin mRNA expression during mouse brain development. *European Journal of Neuroscience*, 9(5), 1055–1071.

- Schmahl, W., Knoedlseder, M., Favor, J., & Davidson, D. (1993). Defects of neuronal migration and the pathogenesis of cortical malformations are associated with Small eye (Sey) in the mouse, a point mutation at the Pax-6-locus. *Acta Neuropathologica*, 86(2), 126–135.
- Schuurmans, C., & Guillemot, F. (2002). Molecular mechanisms underlying cell fate specification in the developing telencephalon. *Current Opinion in Neurobiology*, 12(1), 26–34.
- Seuntjens, E., Nityanandam, A., Miquelajauregui, A., Debruyne, J., Stryjewska, A., Goebbels, S., et al. (2009). Sip1 regulates sequential fate decisions by feedback signaling from postmitotic neurons to progenitors. *Nature Neuroscience*, 12(11), 1373.
- Shipley, M. T., & Ennis, M. (1996). Functional organization of olfactory system. *Journal of Neurobiology*, 30(1), 123–176.
- Shitamukai, A., Konno, D., & Matsuzaki, F. (2011). Oblique radial glial divisions in the developing mouse neocortex induce self-renewing progenitors outside the germinal zone that resemble primate outer subventricular zone progenitors. *Journal of Neuroscience*, 31(10), 3683–3695.
- Simeone, A. (2000). Positioning the isthmic organizer: where Otx2 and Gbx2 meet. *Trends in Genetics*, 16(6), 237–240.
- Singh, A. M., & Dalton, S. (2009). The cell cycle and Myc intersect with mechanisms that regulate pluripotency and reprogramming. *Cell Stem Cell*, 5(2), 141–149.
- Slater, J. L., Landman, K. A., Hughes, B. D., Shen, Q., & Temple, S. (2009). Cell lineage tree models of neurogenesis. *Journal of Theoretical Biology*, 256(2), 164–179.
- Sogut, I., Uysal, O., Oglakci, A., Yucel, F., Kartkaya, K., & Kanbak, G. (2017). Prenatal alcohol-induced neuroapoptosis in rat brain cerebral cortex: protective effect of folic acid and betaine. *Child's Nervous System*, 33(3), 407–417.
- Spatazza, J., Lee, H. H., Di Nardo, A. A., Tibaldi, L., Joliot, A., Hensch, T. K., & Prochiantz, A. (2013). Choroid-plexus-derived Otx2 homeoprotein constrains adult cortical plasticity. *Cell Reports*, 3(6), 1815–1823.
- Srinivasan, S., & Stevens, C. F. (2017). A quantitative description of the mouse piriform cortex. *bioRxiv*, 099002.
- Srivatsa, S., Parthasarathy, S., Molnár, Z., & Tarabykin, V. (2015). Sip1 downstream Effector ninein controls neocortical axonal growth, ipsilateral branching, and microtubule growth and stability. *Neuron*, 85(5), 998–1012.

- Stenman, J., Ruth, T. Y., Evans, R. M., & Campbell, K. (2003). Tlx and Pax6 co-operate genetically to establish the pallio-subpallial boundary in the embryonic mouse telencephalon. *Development*, 130(6), 1113–1122.
- Striegel, D. A., & Hurdal, M. K. (2009). Chemically based mathematical model for development of cerebral cortical folding patterns. *PLoS Computational Biology*, 5(9), e1000524.
- Sur, M., & Rubenstein, J. L. (2005). Patterning and plasticity of the cerebral cortex. *Science*, 310(5749), 805–810.
- Takahashi, M., & Osumi, N. (2010). The method of rodent whole embryo culture using the rotator-type bottle culture system. *Journal of Visualized Experiments: JoVE*, (42).
- Takahashi, T., Nowakowski, R. S., & Caviness, V. S. (1995). The cell cycle of the pseudostratified ventricular epithelium of the embryonic murine cerebral wall. *Journal of Neuroscience*, 15(9), 6046–6057.
- Takiguchi-Hayashi, K., Sekiguchi, M., Ashigaki, S., Takamatsu, M., Hasegawa, H., Suzuki-Migishima, R., et al. (2004). Generation of reelin-positive marginal zone cells from the caudomedial wall of telencephalic vesicles. *Journal of Neuroscience*, 24(9), 2286–2295.
- Tang, Q., Burgalossi, A., Ebbesen, C. L., Ray, S., Naumann, R., Schmidt, H., et al. (2014). Pyramidal and stellate cell specificity of grid and border representations in layer 2 of medial entorhinal cortex. *Neuron*, 84(6), 1191–1197.
- Tang, H. et al., 2016. Zika virus infects human cortical neural progenitors and attenuates their growth. *Cell stem cell*, 18(5), pp.587–590.
- Taverna, E., Götz, M., & Huttner, W. B. (2014). The cell biology of neurogenesis: toward an understanding of the development and evolution of the neocortex. *Annual Review of Cell and Developmental Biology*, 30, 465–502.
- Teissier, A., Waclaw, R. R., Griveau, A., Campbell, K., & Pierani, A. (2011). Tangentially migrating transient glutamatergic neurons control neurogenesis and maintenance of cerebral cortical progenitor pools. *Cerebral Cortex*, 22(2), 403–416.
- Thompson, D. W. (1942). On growth and form. *On Growth and Form*.
- Tissir, F., Ravni, A., Achouri, Y., Riethmacher, D., Meyer, G., & Goffinet, A. M. (2009). DeltaNp73 regulates neuronal survival in vivo. *Proceedings of the National Academy of Sciences*, 106(39), 16871–16876.
- Toma, K., Kumamoto, T., & Hanashima, C. (2014). The timing of upper-layer neurogenesis is conferred by sequential derepression and negative feedback from deep-layer neurons. *Journal of Neuroscience*, 34(39), 13259–13276.

- Trousse, F., Poluch, S., Pierani, A., Dutriaux, A., Bock, H. H., Nagasawa, T., et al. (2014). CXCR7 Receptor Controls the Maintenance of Subpial Positioning of Cajal–Retzius Cells. *Cerebral Cortex*, 25(10), 3446–3457.
- Tsao, A., Sugar, J., Lu, L., Wang, C., Knierim, J. J., Moser, M.-B., & Moser, E. I. (2018). Integrating time from experience in the lateral entorhinal cortex. *Nature*, 1.
- Turing, A. M. (1952). The chemical basis of morphogenesis. *Phil. Trans. R. Soc. Lond. B*, 237(641), 37–72.
- Tyler, W. A., & Haydar, T. F. (2013). Multiplex genetic fate mapping reveals a novel route of neocortical neurogenesis, which is altered in the Ts65Dn mouse model of Down syndrome. *Journal of Neuroscience*, 33(12), 5106–5119.
- Valverde, F., De Carlos, J. A., & López-Mascaraque, L. (1995). Time of origin and early fate of preplate cells in the cerebral cortex of the rat. *Cerebral Cortex*, 5(6), 483–493.
- Van der Loos, H., & Woolsey, T. A. (1973). Somatosensory cortex: structural alterations following early injury to sense organs. *Science*, 179(4071), 395–398.
- Villar-Cerviño, V., Molano-Mazón, M., Catchpole, T., Valdeolmillos, M., Henkemeyer, M., Martínez, L. M., et al. (2013). Contact repulsion controls the dispersion and final distribution of Cajal-Retzius cells. *Neuron*, 77(3), 457–471.
- Walcher, T., Xie, Q., Sun, J., Irmeler, M., Beckers, J., Öztürk, T., et al. (2013). Functional dissection of the paired domain of Pax6 reveals molecular mechanisms of coordinating neurogenesis and proliferation. *Development*, 140(5), 1123–1136.
- Wang, Xiaoqun, Tsai, J.-W., LaMonica, B., & Kriegstein, A. R. (2011). A new subtype of progenitor cell in the mouse embryonic neocortex. *Nature Neuroscience*, 14(5), 555.
- Warren, N., Caric, D., Pratt, T., Clausen, J. A., Asavaritikrai, P., Mason, J. O., et al. (1999). The transcription factor, Pax6, is required for cell proliferation and differentiation in the developing cerebral cortex. *Cerebral Cortex*, 9(6), 627–635.
- Weil, Z. M., & Karelina, K. (2017). Traumatic brain injuries during development: Implications for alcohol abuse. *Frontiers in Behavioral Neuroscience*, 11, 135.
- Wen, Z., Song, H., & Ming, G.-L. (2017). How does Zika virus cause microcephaly? *Genes & Development*, 31(9), 849–861.
- White, J., & Dalton, S. (2005). Cell cycle control of embryonic stem cells. *Stem Cell Reviews*, 1(2), 131–138.
- Williams, B. P., & Price, J. (1995). Evidence for multiple precursor cell types in the embryonic rat cerebral cortex. *Neuron*, 14(6), 1181–1188.

- Wizenmann, A., Brunet, I., Lam, J. S., Sonnier, L., Beurdeley, M., Zarbalis, K., et al. (2009). Extracellular Engrailed participates in the topographic guidance of retinal axons in vivo. *Neuron*, 64(3), 355–366.
- Wolpert, L. (1969). Positional information and the spatial pattern of cellular differentiation. *Journal of Theoretical Biology*, 25(1), 1–47.
- Woolsey, T. A., & Wann, J. R. (1976). Areal changes in mouse cortical barrels following vibrissal damage at different postnatal ages. *Journal of Comparative Neurology*, 170(1), 53–66.
- Workman, A. D., Charvet, C. J., Clancy, B., Darlington, R. B., & Finlay, B. L. (2013). Modeling transformations of neurodevelopmental sequences across mammalian species. *Journal of Neuroscience*, 33(17), 7368–7383.
- Wu, S.-X., Goebbels, S., Nakamura, K., Nakamura, K., Kometani, K., Minato, N., et al. (2005). Pyramidal neurons of upper cortical layers generated by NEX-positive progenitor cells in the subventricular zone. *Proceedings of the National Academy of Sciences*, 102(47), 17172–17177.
- Yoshida, M., Assimacopoulos, S., Jones, K. R., & Grove, E. A. (2006). Massive loss of Cajal-Retzius cells does not disrupt neocortical layer order. *Development*, 133(3), 537–545.